

PA 1252229

PCT/IL 2005 / 000090

25 JAN 2005

REC'D 07 FEB 2005

WIPO

PCT

THE UNITED STATES OF AMERICA

TO ALL TO WHOM THESE PRESENTS SHALL COME:

UNITED STATES DEPARTMENT OF COMMERCE

United States Patent and Trademark Office

December 02, 2004

THIS IS TO CERTIFY THAT ANNEXED HERETO IS A TRUE COPY FROM THE RECORDS OF THE UNITED STATES PATENT AND TRADEMARK OFFICE OF THOSE PAPERS OF THE BELOW IDENTIFIED PATENT APPLICATION THAT MET THE REQUIREMENTS TO BE GRANTED A FILING DATE UNDER 35 USC 111.


APPLICATION NUMBER: 60/539,097

FILING DATE: January 27, 2004

**PRIORITY DOCUMENT
SUBMITTED OR TRANSMITTED IN
COMPLIANCE WITH
RULE 17.1(a) OR (b)**

**By Authority of the
COMMISSIONER OF PATENTS AND TRADEMARKS**




M. K. HAWKINS
Certifying Officer

PROVISIONAL APPLICATION FOR PATENT COVER SHEET

This is a request for filing a **PROVISIONAL APPLICATION FOR PATENT** under 37 CFR 1.53 (b)(2).

Docket Number		27479		Type a plus sign (+) inside this box ->	+
INVENTOR(s) / APPLICANT(s)					
LAST NAME	FIRST NAME	MIDDLE INITIAL	RESIDENCE (CITY AND EITHER STATE OR FOREIGN COUNTRY)		
BELKIN	Shimshon		Kiryat Ono, Israel		
PEDAHZUR	Rami		Moshav Bei Meir - D.N. Harei Yehuda, Israel		
ROSEN	Rachel		Modi'in, Israel		
BENOVICI	Itai		Jerusalem, Israel		
SHACHAM-					
DIAMAND	Yosi		Zichron-Ya'acov, Israel		
RABNER	Arthur		Beit Yehoshua, Israel		
OKSMAN	Mark		Bat-Yam, Israel		
TITLE OF THE INVENTION (280 characters max)					
CELL DETECTION SYSTEM, BACTERIAL PANEL FOR DETECTION OF ANALYTES AND INTEGRATION OF SAME					
CORRESPONDENCE ADDRESS					
G. E. EHRLICH (1995) LTD. c/o ANTHONY CASTORINA 2001 JEFFERSON DAVIS HIGHWAY SUITE 207					
STATE	VIRGINIA	ZIP CODE	22202	COUNTRY	USA
ENCLOSED APPLICATION PARTS (check all that apply)					
<input checked="" type="checkbox"/> Specification	Number of Pages	174	<input checked="" type="checkbox"/> Applicant is entitled to Small Entity Status		
<input checked="" type="checkbox"/> Drawing(s)	Number of Sheets	9	<input checked="" type="checkbox"/> Other (specify)		
			7 CLAIMS		
METHOD OF PAYMENT OF FILING FEES FOR THIS PROVISIONAL APPLICATION FOR PATENT (check one)					
<input type="checkbox"/> A check or money order is enclosed to cover the filing fees			FILING FEE AMOUNT (\$)		
<input checked="" type="checkbox"/> The Commissioner is hereby authorized to charge filing fees and credit Deposit Account Number:			50-1407		
			\$ 80.-		

The invention was made by an agency of the United States Government or under a contract with an agency of the United States Government.

☒ No

☐ Yes, the name of the US Government agency and the Government contract number are: _____

Respectfully submitted,

SIGNATURE _____

January 25, 2004

Date

25,457

TYPED or PRINTED NAME SOL SHEINBEIN

REGISTRATION NO.
(if appropriate)

☐ Additional inventors are being named on separately numbered sheets attached hereto

USE ONLY FOR FILING A PROVISIONAL APPLICATION FOR PATENT

Burden House Statement: This form is estimated to take 2 hours to complete. Time will vary depending upon the needs of the individual case. Any comments on the amount of time you are required to complete this form should be sent to the Chief Information Officer, Patent and Trademark Office, Washington DC 20231. DO NOT SEND FEES OR COMPLETED FORMS TO THIS ADDRESS. SEND TO: Box Provisional Application, Assistant Commissioner for Patents, Washington, DC 20231.

CELL DETECTION SYSTEM, BACTERIAL PANEL FOR DETECTION OF
ANALYTES AND INTEGRATION OF SAME

Inventors: Shimshon BELKIN, Rami PEDAHZUR, Rachel ROSEN, Itai
BENOVICI, Yosi SHACHAM-DIAMAND, Arthur RABNER and
Mark OKSMAN

This application comprise two disclosure documents as follows:

1. Whole cell based toxicity detection integrated system (pages i-xi and 1-118); and
2. A Bacterial panel for toxicity detection (pages 1-53) which also includes the claims.

Table Of Contents

Abstract	i
Table Of Contents	ii
List Of Signs	iv
List Of Figures	ix
List Of Tables	xi
1 Introduction	1
1.1 The Research Objectives	1
1.2 The Integrated System Research And Development Status	2
1.3 Organization Of The Work	3
2 Scientific And Technical Review	4
2.1 Background	4
2.2 Biosensors And Biochips Based Technologies For Hazard Materials Detection	4
2.3 Integrated Bio-Electronics Systems For Chemicals Detection	6
2.4 Fluorescence Based Technologies	7
3 Integrated System	9
3.1 The Integrated System Overview	9
3.2 The Biochip And Biochip Support Accessories	11
3.2.1 The Biochip - Introduction	11
3.2.2 Biochips Classification	13
3.2.3 The Simple Chip (SC)	13
3.2.4 The Integrated Pumps Micro Fluidic Chip (IPMFC)	14
3.2.5 The Externally Pumped Micro Fluidic Chip (EPMFC)	17
3.2.6 The Biochips Manufacturing Issues	21
3.2.7 The Reaction Chambers Functionality	21
3.3 Electro-Optics System	23
3.3.1 Spectrum Characterizations of The GFP Based Optical Reporter	24
3.3.2 Fluorescence Filters Set Selection	26
3.3.3 Light Emitting Devices For The Bio-Fluorescence Generation	27
3.3.4 Light Sensing And Quantification Devices	30
3.3.5 Modeling Of The Bio-Fluorescence Electro-Optical System	33
3.3.6 Optical Setups For Light Collection	40
3.3.7 Performance Comparison Of The Optical Setups	49
3.4 Temperature Control	52
3.4.1 Selection Of TEC & Heat Sink For IBIS4 CMOS IS Cooling	52
3.4.2 Selection Of The Cooling Configuration For Bio-House & LED Assembly	54
3.5 Electronics	55
3.5.1 The Suction Activation And Control Electronics	57
3.5.2 Temperature Control Electronics	58
3.5.3 The LEDs Driver	59
3.5.4 Light Quantification Devices Control And Data Acquisition	59
3.5.5 PC Communication	59
3.5.6 Expansion Connector	60
3.5.7 The Xcaliber Integrated ARM9 and Programmable Logic Device	60
3.6 Mechanical Design And Integration	62
3.7 The Software And Algorithms	65
3.7.1 Graphical User Interface (GUI)	65

3.7.2	Slow Biological Signal Compression Algorithm	67
3.7.3	The Simple Algorithm For Known Chemical Concentration Calculation	71
3.8	The Calibration Of The Integrated System	73
3.8.1	Bio-Fluorescence Signal Uncertainties Mapping	73
3.8.2	Excitation Light Preparation Procedure For TAU-WTA Integrated System	74
3.8.3	The TAU-WTA Calibration Procedure For The Biological Experiment	75
3.8.4	Temperature Stability	77
4	Biological Characterizations	81
4.1	Biological Signal Definition	81
4.2	Biological Signal Quantification	83
4.2.1	Bio-Signal Quantification on TAU-WTA Integrated System	83
4.2.2	Bio-Signal Characterization Using Victor-2 Fluoremeter	86
4.3	Emission - Excitation Dependency	94
4.3.1	The Halogen Lamp Based Excitation / Emission Intensity Experiment.....	94
4.3.2	The Excitation / Emission Intensity Experiment Performed On TAU-TMS	97
4.3.3	Emission / Excitation Dependency - Summary And Conclusion	101
4.4	Kinetics Experiments On The TAU-TMS	102
4.4.1	Fresh Biosensors Kinetics Experiments On The TAU-TMS	102
4.4.2	Dried Biosensors Kinetics Experiments On The TAU-TMS	103
4.5	The Biocompatible Glues Research	104
4.6	The Human Cells Emission Intensity As Function Of The Concentration ..	105
4.6.1	Increasing Integrated System Sensitivity By Growing Cells On The Beads	107
5	Discussions	109
6	Summary And Conclusions	111
7	References	113
	Appendices	116
	Appendix-A The Light Emitting Devices Comparison.....	116
	Appendix-B Photometry Technologies Comparison.....	117
	Appendix-C Minimal Light Intensity For The IBIS4 CMOS Image Sensor	117
	Appendix-D Abbreviations List	118

List Of Signs

Sign	Description	Sign	Description
Excitation energy absorption			
A_{mol}	Molecular absorption	ϵ	Molar absorption coefficient ($M^{-1}cm^{-1}$ units)
c	Light velocity	l	Path-length traversed by the light (cm units)
Electro-Optical Spectrum Equivalent Parameters			
$EmQE$	The ratio between the absorbed excitation photons and generated emission photons that depends on the wavelength		
$T_{Fem4ems}$	The transmittance parameter for emission photons by the emission filter	$T_{Fem4exc}$	The transmittance parameter for excitation photons by the emission filter
QE_{ems}	Effective QE of the light quantification device to the emission spectrum	QE_{exc}	Effective QE of the light quantification device for the excitation spectrum
$N_{GFP-i}(\lambda)$	Normalized emission spectrum received for the index i that specifies the excitation wavelength	$K(\lambda)$	Constant correlating between the normalized value and the emission intensity measured in a photon/sec units
Light Quantification Device			
QE	Quantum efficiency of the light sensing device	FF	Fill Factor of the light sensing pixel
N_{ph}	Number of photons collected by the pixel	QO	Quantified output from light sensing device
$bits$	Quantization levels: 2^{bits}	T_{rd-px}	Time for one pixel readout
T_{int}	Photo-electrons integration time	N_X	Size of the image sensor array window in X-dimension
$T_{blanking}$	Time between two successive rows readout necessary for calibration of the pre-amplifier	$N_{int-rows}$	Distance in rows between the readout and reset row pointers of the image sensor array
QO_{DC-e}	Quantified output from light sensing device in total darkness	F_{DC}	Parameter dividing the dynamic range of the light quantification device between the dark current and light
$T_{int-max-ws}$	Maximum integration time for the weak light signal	$T_{int-max-ss}$	Maximum integration time for the strong light signal

Sign	Description	Sign	Description
Bio-Fluorescence Layered Model			
H	Heights of the reaction chamber	W	The aperture of the reaction chamber
B_{cube}	The number of biosensors in cube with 1mm rib	B_{1D-1mm}	The number of biosensors in one dimension
B_{RC}	The number of bacteria inside the reaction chamber	N_{layers}	The number of layers dividing the reaction chamber
B_{layer}	The number of bacteria in single layer of the reaction chamber	ρ	Concentration of the biosensors inside the reaction chamber's volume
Δh	The width of one layer	d	Lens aperture
H_{2i}	Distance between the center of the layer i to the top of the reaction chamber	p_i	The distance between the lens and the OCM of the layer i
n_{RC}	Reaction chamber environment refraction index	n	Free space refraction index
β_{Qi}	The internal numerical aperture of the reaction chamber for the equivalent bacteria in layer i	β'_{Qi}	The numerical aperture of the reaction chamber in free space for the equivalent bacteria in layer i
α_{Qi}	The numerical aperture of rays emitted by the layer i of equivalent bacteria and collected by lens	$\alpha\beta_{Qi}$	The minimum angle between the numerical apertures α_{Qi} and β'_{Qi}
$S_{\alpha\beta i}$	The area corresponding to the solid angle	R_i	The radius corresponding to solid angle
$\Omega_{\alpha\beta i}$	The solid angle corresponding to the $\alpha\beta_{Qi}$ angle	F_{GFP}	The fraction bio-emission energy redirected to the light quantification device
d_b	Bacteria dimension of cube form	$A_{GFP-max}$	The absorption of excitation rays by biosensors of layer i saturated by GFP molecules
n_{GFP}	The percentage of the bacteria saturation by the GFP molecules	A_{GFP-i}	The absorption of excitation rays by the GFP molecules of layer i
I_{ems}	Intensity emitted by GFP molecules (photons/sec units)	$I_{ems-max-i}$	Intensity emitted by biosensors saturated by GFP molecules of layer i
λ	Wavelength	E_{ph}	Single photon energy
λ_{exc}	Wavelength of excitation rays	h	Plank constant
P_{fiber}	Excitation power measured from optical fiber	I_{exc}	GFP molecules excitation intensity in photons/sec units
T_{exc}	Transmission of the reaction chamber medium to the excitation rays	T_{ems}	Transmission of the reaction chamber medium to the emission rays

Sign	Description	Sign	Description
Geometrical Optics			
f	Focal length	$r1, r2$	Radiuses of the thin lens
p	Object distance	q	Image distance
h_i, h_o	Object and image heights	S_{px}	The area of the pixel
$S_{ems-det}$	The area of emission projected on the light sensing device	$S_{exc-det}$	The area of excitation projected on the light sensing device
T_{lens}	Lens transmission	$F/\#$	F number of the lens
Optical Setups Performance Evaluation			
$I_{ems-max-no-lens-det}$	Emission intensity collected by the light-sensing device for no-lens optical setup	$I_{exc-no-lens-det}$	Excitation intensity collected by the light-sensing device for no-lens optical setup
$I_{ems-max-no-lens-px}$	Emission intensity sensed by the pixel of the light-sensing device for no-lens optical setup	$I_{exc-no-lens-px}$	Excitation intensity sensed by the pixel of the light-sensing device for no-lens optical setup
$R_{ems/exc-no-lens}$	The ratio between the emission and excitation intensities sensed by pixel for no-lens optical setup	$R_{ems/exc-vlens}$	The ratio between the emission and excitation intensities sensed by pixel for video-lens optical setup
D	The aperture of the video-lens	FL	Focal length of the video-lens
T_{vlens}	Transmission of the video-lens	T_{mlens}	Transmission of the mLens
$I_{ems-max-vlens-det}$	Emission intensity collected by the light-sensing device for video-lens optical setup	$I_{exc-vlens-det}$	Excitation intensity collected by the light-sensing device for video-lens optical setup
$I_{ems-max-vlens-px}$	Maximum emission intensity sensed by the pixel of the light-sensing device for video-lens optical setup	$I_{exc-vlens-px}$	Excitation intensity sensed by the pixel of the light-sensing device for video-lens optical setup
$I_{ems-max-mlens-det}$	Maximum emission intensity collected by the light-sensing device for mLens optical setup	$I_{exc-mlens-det}$	Excitation intensity collected by the light-sensing device for mLens optical setup
$I_{ems-max-mlens-px}$	Maximum emission intensity sensed by the pixel of the light-sensing device for video-lens optical setup	$I_{exc-mlens-px}$	Excitation intensity sensed by the pixel of the light-sensing device for video-lens optical setup
$K_{angle}(\theta)$	The factor of emission filter efficiency as function of the incident angle	$R_{ems/exc-mlens}$	The ratio between the emission and excitation intensities sensed by pixel for mLens optical setup

Sign	Description	Sign	Description
$I_{ems-max-mlens-blocking-det}$	Maximum emission intensity collected by the light-sensing device for mLens optical setup with spatial filter	$I_{exc-mlens-blocking-det}$	Excitation intensity collected by the light-sensing device for mLens optical setup with spatial filter
D_{block}	Diameter of the blocking spot		
$K_{exc-trs}$	Transmission of the spatial filter for excitation rays	$K_{ems-trs}$	Transmission of the spatial filter for emission rays
I_{unc-px}	Signal uncertainty quantified by pixel in photoelectrons/sec unit		
$Un2B$	Uncertainty to Background Ratio	$S2Un$	Signal to Uncertainty ratio
Temperature Control			
ΔT	Temperature difference	Q_c	Total heat power
T_h	TEC hot side temperature	T_a	Ambient temperature
$V_{TEC-max}$	Maximum TEC voltage	$I_{TEC-max}$	Maximum TEC current
$Q_{TEC-max}$	Maximum TEC power dissipation	HSR	Heat Sink Resistance
LED current driver			
I_{LED}	Current supplied to the LED	R_{SET}	Resistor regulating the global maximum current of LED driver chip
Biological Signal Quantification And Light Sensing			
$QO_{LB-H2O-GFP-DC}$	Quantified output of light sensing device for LB and GFP emission; unfiltered excitation light and dark current	$QO_{LB-H2O-DC}$	Quantified output of light sensing device for LB, unfiltered excitation light and dark current
QI_{GFP}	Calculated quantified intensity contributed by fluorescence emission from GFP molecules	$QO_{int-sig}$	Quantified integrated signal by pixel of light quantification device
I_{GFP}	Intensity contributed by fluorescence emission from GFP molecules	QO_{Exc}	Quantified output of the unfiltered excitation energy
$I_{exc-Fem4exc}$	Excitation intensity after attenuation by the emission filter (photons/sec)	I_{LB}	Intensity contributed by fluorescence emission from LB
K_{bs-px}	Coefficient fitting between the excitation energy and bio-emission intensity projected on the pixel of light quantification device	$K_{bs-exc-ems-optics-mlens}$	Coefficient that depends on reaction chamber geometry; biosensors concentration; filters and medium transmission; mLens based optics geometry and photon energy at wavelength

Sign	Description	Sign	Description
Victor 2 Readout And Calculations - in Relative Florescence Units (RFU)			
$QO_{iExc}(t)$	The readout corresponding to empty test tube i	QO_{Exc}	Average readout from empty test tubers
QU_{Exc}	Excitation uncertainty	QU_{Exc+LB}	Excitation and LB intensity uncertainty
$QO_{iExc+LB}(t)$	The readout corresponding to test tube i filled with LB	$QI_{iLB}(t)$	Calculated LB contribution
$QO_{iExc+LB+GFP}(t)$	The readout corresponding to test tube i filled with LB and biosensors	$QI_{iGFP}(t)$	Calculated GFP molecules emission intensity
$QU_{GFP}(0)$	Uncertainty of GFP molecules emission intensity		
Growing human cells on the beads for the sensitivity increase			
D	Diameter of the bead	L	Number of the bead layers
N_{even}	Number of beads in even layer	N_{odd}	Number of beads in odd layer
N_{total}	The total number of beads in the reaction chamber	S_{bead}	The surface area of the single bead
S_{total}	The total surface area	R	The ratio of total beads area to monolayer's area

List Of Figures

Figure 3.1-1: The GFP Optical Reported Based Genetically Engineered Whole Cell Biosensor...	9
Figure 3.1-2: The Integrated System Block Diagram.....	10
Figure 3.2-1: Kiwi Biochip Layout (Top View)	14
Figure 3.2-2: The Schematics Of Electronics For High Current – Short Pulse Supply	15
Figure 3.2-3: Micro-Pumps Activation Mechanism.....	15
Figure 3.2-4: The Serial Channels Schematics.....	17
Figure 3.2-5: External Pumping Scheme.....	18
Figure 3.2-6: The EPMFC-ver3-2 3D Drawings.....	19
Figure 3.2-7: The EPMFC-ver4 – Side Cut View	20
Figure 3.2-8: The EPMFC-ver4 Final Production Step Process	20
Figure 3.2-9: Reaction Chambers Divided To The Functional & Sample Groups	21
Figure 3.2-10: Various Functional Groups.....	22
Figure 3.3-1: Bio-Fluorescence Based Electro-Optical Setup Concept	23
Figure 3.3-2: Excitation Spectrum Of The GFP Optical Reporter Based Biosensor	25
Figure 3.3-3: Emission Spectrum Of GFP Optical Reporter Based Biosensor	25
Figure 3.3-4: Excitation And Emission Filters Transmission Spectrums	26
Figure 3.3-5: The 4x3 Matrix Of SMT LEDs – Top View	27
Figure 3.3-6: The 4x3 Matrix Of SMT LEDs – Side View.....	28
Figure 3.3-7: The 5mm LED With Optical Fibers Solution.....	29
Figure 3.3-8: IBIS4 Simplified Schematics.....	31
Figure 3.3-9: Electro-Optical System Model	33
Figure 3.3-10: Spectrums To Parameter Conversion Schematics	34
Figure 3.3-11: The Ray Tracing Model For Emission Scattering Characterization.....	36
Figure 3.3-12: Emission Scattering Solid Angle	37
Figure 3.3-13: The Thick Lens Parameters Schematics	40
Figure 3.3-14: The Direct Coupling Optical Setup	41
Figure 3.3-15: The Bio-Emission Cross-Talks Problem	41
Figure 3.3-16: Projection Of The Excitation Light Parallel Rays	42
Figure 3.3-17: Optical Setup Based On The Video-Lens.....	43
Figure 3.3-18: Distraction Of The Excitation Parallel Rays	44
Figure 3.3-19: The Physical Layout Of m-Lens Matrix Based Optical System	44
Figure 3.3-20: The Single mLens Optical Path	45
Figure 3.3-21: The Astigmatism Created By The Top Reaction Chamber Layers	45
Figure 3.3-22: The Optical Power Collection Schematics	45
Figure 3.3-23: Excitation Parallel Rays Optical Path.....	46
Figure 3.3-24: The Emission Filter In Front Of mLens Design	47
Figure 3.3-25: Blocking The Excitation Rays	47
Figure 3.3-26: Spatial Filtering Of The Excitation Rays	48
Figure 3.3-27: Spatial Filtering Of The Excitation Rays And Emission Doubling.....	48
Figure 3.3-28: The Emission Rays Blocking	48
Figure 3.4-1: Calculation Of Cold Side Heat Pumping Parameters	53
Figure 3.5-1: The Block Diagram Of The Electronics Card	55
Figure 3.5-2: Electronics For The Suction Activation And Control	57
Figure 3.5-3: The Temperature Control Circuit Schematics	58
Figure 3.6-1: Excitation, Bio-House And Light Sensing Mechanical Modules Schematics	62
Figure 3.6-2: The Integrated System Electro-Opto Mechanical Assembly Scheme.....	63

Figure 3.7-1: The Main GUI Window	65
Figure 3.7-2: A Chart With Biological Signal Kinetics And ROI Contents.....	67
Figure 3.7-3: The Modules Of The Slow Biological Signal Compression Algorithm (Filled By Yellow)	68
Figure 3.7-4: The Processing Tools For Slow Biological Signal Curve.....	69
Figure 3.7-5: Function Descriptors Table Data Base.....	69
Figure 3.7-6: Biochemical Reaction Amplitude Versus Toxicant Concentration	71
Figure 3.7-7: The Wrapper Of The Chemical Concentration Calculation Algorithm.....	72
Figure 3.7-8: The Core Of The Chemical Concentration Calculation Algorithm	72
Figure 3.8-1: LED Optical Intensity Versus Temperature.....	78
Figure 3.8-2: ACS-1394 Camera Used In TAU-TMS Integrated System.....	79
Figure 3.8-3: ACS-1394 Camera Dark Readout After Power On	80
Figure 4.2-1: The Process Of Bio-Fluorescence Integrated Signal Formation.....	83
Figure 4.2-2: The Victor2 Kinetics Experiment Setup	87
Figure 4.2-3: The Kinetics Of E-Coli-REC-A \leftrightarrow NA interaction In LB Medium.....	87
Figure 4.2-4: The Kinetics Of LB Medium Fluorescence	88
Figure 4.2-5: The Kinetics Of Excitation Background.....	88
Figure 4.2-6: The Kinetics Of Biochemical Reaction At The First Hour.....	89
Figure 4.2-7: The Kinetics Of Biochemical Reaction During Period Of 60-150 minutes.....	90
Figure 4.2-8: The Kinetics Of Biochemical Reaction During Period Of 10 Hours.....	91
Figure 4.2-9: The Bio-Signal Amplitude Kinetics, $n_{GFP}(t)$,During The First Hour.....	92
Figure 4.2-10: The Bio-Signal Amplitude Kinetics, $n_{GFP}(t)$,During The First 15 0Minutes.....	92
Figure 4.3-1: Halogen Lamp Based Setup For Emission-Excitation Dependency Experiment	94
Figure 4.3-2: Excitation Power As Function Of Current Supplied To The Halogen Lamp	95
Figure 4.3-3: Combined Picture From: (1-5) Reaction Chambers Captures Under Different Excitation Intensities, (6) Reaction Chamber Captured Under Ambient Light.....	96
Figure 4.3-4: The Halogen Lamp Based Emission/Excitation Experiment.....	97
Figure 4.3-5: The 14 Pictures Captured During Emission / Excitation Experiment on TAU-TMS	100
Figure 4.3-6: The Emission Versus Excitation Intensity Linearity.	101
Figure 4.4-1: The Kinetics Experiment With The Fresh Biosensors	102
Figure 4.5-1: Influence Of The Glues On The Biochemical Reaction	104
Figure 4.6-1: Emission From Human Cells - 1500 cells/well.....	105
Figure 4.6-2: Emission Intensity As Function Of Human Cells Concentration	106
Figure 4.6-3: Human Cell Grown On The Beads Fills The Reaction Chamber Volume	107

List Of Tables

Table 3.2-1: The Biochips Types Are Used In Research	13
Table 3.2-1: The List Of Changes/Improvements Required For IPMFC.....	16
Table 3.3-1: Spectrum Equivalent Parameters	50
Table 3.3-1: Optical Systems Minimal Sensitivities Comparison	50
Table 3.3-1: Sensitivity Comparison For The mLens Based System With Spatial Filter.....	51
Table 3.4-1: The Modules Requiring Temperature Control In The Integrated System	52
Table 3.4-2: The IBIS4 CMOS IS Thermal Related Coefficients	52
Table 3.7-1: The Functions That Could Be Generated By Re-function Module	70
Table 4.1-1: The Typical Bio-Signal Characterization Experiments	82
Table 4.3-1: The Halogen Lamp Based Emission/Excitation Experiment Results Processing	96
Table 4.3-2: Mapping of TAU-TMS LEDs Intensities Versus Level	98
Table 4.3-3: Processing Of The Emission / Excitation Ratio Experiment Results	99
Table 4.6-1: Human Cells – 1500 cell/well results processing	106
Table 4.6-1: The Issues For Advanced Research	111

1 Introduction

The introduction section overviews the objectives of the Water Toxicity Analysis (WTA) integrated system. It also covers the history and status of WTA integrated system R&D in general and specifically at the Tel-Aviv University (TAU). Finally, the organization of this thesis book is described.

1.1 The Research Objectives

Bio-terrorism is one of the biggest threats of today's society. There are various ways to commit attacks of this kind, intentional water poisoning is among them. Unfortunately, this is a very actual today due to attempts of fanatic groups to tremor and frighten the free world. In order to save people lives and protect their well being a system for early water poisoning detection and warning is required.

Today there is a substantial shortfall in the detection capabilities of potential water poisoning. The gap is derived from the inability to obtain a sufficiently sensitive and early warning upon the occurrence of such events.

The efforts to develop a "lab-on-a-chip" are conducted currently mainly through university research projects, government agencies, and military research institutes. The reasons: (i) it is innovative technology with more questions than answers; (ii) the biological and chemical part requires time until stable usable results could be provided; (iii) the form of application to use these technologies has not matured yet.

A group of researchers from Tel-Aviv University (TAU) in collaboration with biologist from the Hebrew University Of Jerusalem (HUJI) proposed a solution for near real-time acute water toxicity detection. The proposed solution is based on portable integrated system incorporating electronic device and a disposable biochip with a battery of toxicants-sensing biological cells. The cells are genetically engineered to activate biochemical reaction and emit a readily detectable signal upon sensing toxicants; this signal is sensed and quantified by the electronic circuitry. The quantified signal is interpreted to the amplitude of the biochemical reaction. The amplitude of biochemical reaction is used for the water toxicity analysis algorithms.

The goal of the research in Tel-Aviv University is the development of a portable integrated system allowing water toxicity analysis. The integrated system includes a biochip, biochip 'house', external liquid suction mechanism, light sensing and quantification device, fluorescence excitation light generation device, temperature control mechanism, electro-

optical-mechanical module, electronics for activation of all the above listed modules, software for the control of all the above mentioned modules and biological data analysis methods.

The integrated system will support a complete field deployable solution: (1) the biosensors are preserved in dormant state; (2) the tested water is placed into the sample ports of the biochip; (3) the biochip is inserted into the integrated system; (4) the integrated system operates the suction mechanism withdrawing the tested water into the reaction chamber; (5) the electro-optical system excites the fluorescence process and sensing the bio-emission magnitude; (6) the software interprets the fluorescence magnitude to the bio-signal; (7) the water toxicity algorithms working on the bio-signal data and returns the water test results.

The real challenge in this work is the development of the biochip and the manufacturing process for the biosensor dehydration on it. The biosensors should be stored on the biochip in dormant state. After rehydration, the biosensors viability varies in range of 10% - 30%. Therefore an additional challenge is the development of sophisticated electro-optical module sensitive enough working with rehydrated whole cell based biosensors. The temperature control, electronics, mechanics and software are also real engineering challenges in the integrated system development.

The main goal of the research presented in this work is focusing on "development of the integrated system supplying quantified biological signals to the water toxicity analysis algorithms".

1.2 The Integrated System Research And Development Status

The investigation of the integrated system has been done in two stages. The integrated system named "Tel-Aviv University - Toxicity Measurement System" (TAU-TMS) was developed at the first stage. It supplied the solution for working with fresh whole cell biosensors, however wasn't sensitive enough to work with rehydrated biosensors. The biochip used in TAU-TMS is overviewed in the "Section 3.2.4".

The excitation part of the electro-optical module presented at the "Section 3.3.3.1: Matrix Of SMT LEDs". The light quantification device is shortly described in the "Section 3.8.4.2: Image Sensor Temperature".

At the second stage of the research the sensitivity increase goal has been set. The integrated system must be sensitive enough to the biological signal generated by the rehydrated biosensors. In order to meet the goal the new technology was developed as part of the TAU - "Water Toxicity Analysis" (TAU-WTA) integrated system. The TAU-WTA

incorporates the new biochip and electro-optical-mechanical designs. Those modules are described and analyzed in this work.

1.3 Organization Of The Work

This work is organized to cover the following sections: (i) scientific overview; (ii) integrated system; (iii) biological characterizations; (iv) discussions; and (v) summary and conclusions.

In Section 2 the scientific and technical review are presented. The various optical emission forms from living organisms are discussed. The methods of biosensors engineering are also listed. Finally, the integrated bioelectronics systems under investigation and those that are available on the market are overviewed.

In Section 3 the integrated system aspects that have been investigated at Tel-Aviv University are presented in details. It includes the theoretical modeling, calculations and practical implementations. The block diagram and essence of the integrated system operation sequence are presented in Section 3.1. The biochips that are used with TAU-TMS and TAU-WTA and their activation accessories are described in Section 3.2. All electro-optical and bio-optical aspects of the integrated system are described in Section 3.3. It includes the characterization of the optical devices that were used in the integration system, modeling of bio-emission, various optical setups and performance evaluation for each setup. The temperature control for the light generation, light sensing and biochip modules is shortly overviewed in Section 3.4. The design of the electronics, mechanics and software are presented in the sections 3.5, 3.6 and 3.7 correspondingly. Algorithms for slow biological signal compression and the known chemical concentration detection are also presented in the software section. The calibration of the integrated system is very important in order to get the reliable results. The issue is discussed in Section 3.8.

A lot of integrated system design considerations are based on the biological characterizations presented in Section 4. The very important issue is "Biological Signal" definition done in Section 4.1. The kinetics experiments with quantification of the biological signal on the Victor2 industrial fluorometer are described in Section 4.2. The experiments proving the linear dependency of the bio-emission from excitation intensity are presented in Section 4.3. The kinetics experiments conducted on the TAU-TMS – Section 4.4 showing that the integrated system is sensitive enough to work with fresh biosensors. The research of the biocompatible adhesives is concerned in Section 4.5. The experiment that was performed with human cells is found in Section 4.6.

In Section 4 we are discussing the status of the integrated system investigation. The discussions regarding achievements and difficulties could be found there.

The summary and conclusions regarding current research are done in the Section 6. It maps the issues required for advanced investigation in order to improve the integration system sensitivity and reliability, and doorway to the research commercialization.

2 Scientific And Technical Review

2.1 Background

Rapid classification of chemical and biological hazards has become increasingly important. One approach to solving the problem is using biosensors incorporated into biochips. The biosensors and biochips technologies are overviewed in Section 2.2. In addition to the sensors we include also a description of the biological material encapsulation and the biochip packaging.

The biochip requires support hardware and software. There are electronics, optics and mechanics components for control, support and data analysis. In fact, the biochip based system is actual a multi-disciplinary integrated system. Commercially available and experimental integrated systems for detection of hazard in water are overviewed in Section 2.3.

The whole cell based toxicity detection integrated system presented in this work is based on bio-fluorescence signal interpretation by light sensing device. The fluorescence based signal analysis technologies are widely used in many scientific and engineering applications. Therefore, other applications based on bio-fluorescence will be covered in Section 2.4. The fluorescence excitation light and emission quantification technologies will be also reviewed.

2.2 Biosensors And Biochips Based Technologies For Hazard Materials Detection

There are many methods for biosensors and biochips implementation. The methods have wide performance range, for example by their sensitivity, specificity, dynamic behavior and integrability. They also differ in their cost, size and portability.

A popular method of molecular recognition is based on immobilized antibodies capturing the appropriate analytes in liquids under test[1]. This method has high selectivity. However, highly specific methods are limited to a small number of analytes that is limited by the sensor array size and variability. Similar method for molecular recognition is the use of proteins with affinity to selected metals [2]. Binding of the metal to the protein induces a change in its

fluorescence intensity, lifetime, or anisotropy. The fluorescence intensity and lifetime can be conventionally measured through simple optics or remotely by optical fiber.

Global parameters, such as bioavailability, toxicity and genotoxicity¹, cannot be probed with high-specificity methods, such as molecular recognition. In a completely different approach, a live, intact cell could be used as the biological sensing entity [3]. The technology based on intact cells is titled "Whole Cell Based Biosensors" and it is used for that manner in our research. The methods of using whole cells biosensors are very relevant for detection of pollutants in the environment, as we will show in this work.

A simple way to describe the operation of genetically modified whole cell biosensors is to assume two key components: a. the promoter and b. the reporter. Both promoter and reporters are segment in the cells DNA that due to a certain property causes the reporter, which is another DNA segment to act, and via a complex bio-chemical reaction in the cell to produce fluorescence protein reporters, which we will call in this work for short "reporters" (not to be confused with the biological definition of reporters in such systems, in our case reporter genes, which is quite different). The reporter is an integrated part of the whole cell biosensors since it provides us a "communication line" to the nanometer size world of the cell internal machinery [4]. Reporter genes produce not only florescent proteins such as green florescent protein (GFP). They can produce bacterial luciferase, firefly luciferase, β -galactosidase, β -glucuronidase, catechol 2,3-dioxygenase and even ice nucleaton protein, InaZ. Each reporter protein has unique properties and can be used for sensors application with advantages and disadvantages in comparison with others.

GFP has become a popular reporter proteins for gene activity in bacteria. It requires complicated electro-optical setup for fluorescence light excitation, in addition to the detection system. Other reporter proteins may demonstrate bio-luminescence requiring just a light-sensing device for the biological response quantification. This approach has been demonstrated to function while integrated with solid-state semiconductor light-quantification devices [5].

Neuronal biosensors and microphysiometers should be also mentioned amongst the list of non-optical bio-reporters [6]. Neuronal cells bind with toxins, drugs and odors. The microelectrodes attached to the cells monitoring response to bounded substances. The monitored electrical signal is substance-specific and concentration-dependent. The micro-

¹ Damage to genetic material

physiometer is a device for sensing the extra-cellular pH changes. The biosensor's functional response is reflected by pH change that is monitored by potentiometric sensor.

The use of genetically modified microorganisms as whole cell biosensors has enhanced the need for reliable methodologies for long-term cell encapsulation. There are few proposed methods. One method is the sol-gel technology that supplies high chemical and biological stability and excellent transparency [7]. Therefore it is considered as a favorable for encapsulating matrices for optical sensors.

2.3 Integrated Bio-Electronics Systems For Chemicals Detection.

Currently, the developed technology platform that is presented in this work is unique. However, there are other technologies that offer methods to detect toxic material in water. The more mature technologies rely on chemical analysis of the tested sample, in order to identify specific toxic chemicals or biological elements, from a closed list of materials. They can not identify unknown hazard materials, beyond whatever is defined in their closed list.

The portable system developed in the Naval Research Laboratory is based on antibody capture sensors [1]. It allows detection of three bacteria and three protein toxins.

The experimental system developed in the University of Maryland School of Medicine in collaboration with University of Michigan has a sub-ppb sensitivity for Cu(II) and immunity from interference from other cations abundant in sea water [2]. The presence of copper in the seawater is the result of the effluents from shipyards activities. Cu(II) is toxic at sub-part per billion levels to commercially important shellfish.

Toshiba Corporation also announced that it has developed essential technology for an advanced biosensor chip capable of wide-ranging applications [8]. Experimental biosensors using the technology can detect proteins in blood much quicker and in a more efficient way than present chemical-based detection methods. Such system can measure glucose in blood with up to 500 times the sensitivity of current biosensors. That new biosensor comprises of a sensor chip that interacts with the sample and detection section that records the result.

PointSource Inc. has developed a cost-efficient testing apparatus that will allow for continuous, real time monitoring of the water supply for the presence of dangerous pathogens [9]. The patented system relies on a laser beam to identify microorganisms in water. A side stream of water, which assumed to be representative of the water in general, passes through a laser beam. As it passes through the beam, light is scattered. The system gathers the light and, using a mathematical technique, can determine what kind of particle it is by its shape, size and internal composition.

The two main technologies to identify cyanide in water are: (i) Colorimeters test kits include reagents that, when added to a water sample, react with the available cyanide ion to form a colored solution. A vial containing this solution is inserted into the hand-held colorimeter that measures the intensity of the sample's color and reports the cyanide concentration [10], [11]. (ii) Ion selective electrodes function as a sensor that, when inserted into a water sample, a data readout device reports the concentration of free cyanide [12], [13].

The Watersafe corporation [14] product family addresses the spectrum of water contaminants with a one-step, 10-minute test that bring the accuracy of laboratory procedures within everyone's reach. One kit tests for bacteria, lead, pesticides, nitrates, nitrites, chlorine, pH, and hardness.

Universal Detection Technology Inc. develops Anthrax 'Smoke Detector' [15]. The device continuously monitors the air for Anthrax spores; it uses a microwave to "pop" the spores, thus releasing a chemical from inside the spores called dipicolinic acid, which is unique to bacterial spores. This dipicolinic acid instantaneously reacts with the chemical sensor in the solution. The sensor triggers an intense green luminescence when viewed under ultraviolet light. The intensity of the luminescence corresponds to the concentration of bacterial spores in the sample.

2.4 Fluorescence Based Technologies

Fluorescence-based technologies are widely used in scientific and technological applications. For most of the fluorescent technologies optical filters are required. The right filter set selection can dramatically increase the sensitivity to the signal of interest [16].

Various solid-state devices like photomultiplier, photodiodes, CCD and CMOS image sensors, sense the fluorescence emission. The CMOS image sensor technology is the newest and most promising one among the rest [17]. It provides cost effective solution for multi-source fluorescence emission imaging.

Any fluorescence based technology requires an excitation light source. In most cases, laser, arc lamp, or halogen lamp are used. Recently, there is a significant progress in green and blue LED technologies. In particular the GaN based uLED chip technology is strongly promoted [18]. The uLED chip could supply the excitation energy to thousands of the biochemical reactors, located on the same biochip, simultaneously. Therefore the tremendous quantity of analytes could be processed in parallel.

The monolithic integration of vertical cavity surface emitting lasers (VCSELs) with PIN photo-detectors is a very promising method for fluorescence-based imaging [19]. It allows miniaturization and dramatically increases of simultaneous bio-chemical reactions monitoring. However, it requires special semiconductor processing and integration methods.

The excitation background is always the limiting factor that determines the sensitivity of the fluorescence based detection system. This is the case even when the optical filter set is optimized. One of the methods to significantly sensitivity increase is the flashing fluorescence, leaving the excitation background constant [20].

Optical fibers are commonly used in communications applications. And they become more and more used also in biomedical engineering. For fluorescence-based applications the excitation energy could be guided to the fluorescent material as well as transfer the emission signal to the detector [21].

One of the most actual biotechnology activities today is human genotype decryption. Recently, the research in this field moves from genomics to proteomics. The new approaches in proteomics chip allow signal acquisition from hundreds of reaction chambers simultaneously [22]. This accelerates the data collection process and also allows reducing significantly the sample volumes. The most common method is based on protein binding by profiled fluorescent biomarkers. The binding changes the fluorescence intensity allowing analyzing the sample contents.

The researchers at Beth Israel Deaconess Hospital combined surgical imaging system with NIR fluorophores [23]. The combination allows standard color imaging with functional imaging simultaneously and in the real time. The functional imaging includes the blood flow monitoring and perfusion. The combined imaging system provides a direct view of both cardiac anatomy and function during surgery.

3 Integrated System

3.1 The Integrated System Overview

The whole cell based toxicity detection integrated system is based on the following three general components: (i) the biochip; (ii) the biosensors that are incorporated into the biochip; (iii) the "Biological Signal Generation and Measurement" (BSG&M) device, which interfaces the biochip.

(i) The biochip includes a substrate with the reaction chambers, test water sample and suction ports, and micro-fluidic channels connecting between the chambers and the ports. The whole cell based biosensors are pre-placed into the biochip reaction chambers. The tested water are transferred by the suction action from the sample port into the reaction chambers and initiate the interaction between the chemicals dissolved in the water and the biosensors. This interaction induces a biochemical reaction that generates the "Green Fluorescent Protein" (GFP) molecules. The chip includes an optical path where the excitation light should reach the biological material and the photoluminescence would exit.

(ii) The biosensors are genetically engineered cells that fluoresce due an interaction with pre-determined or general set of chemicals (Fig. 3.1-1).

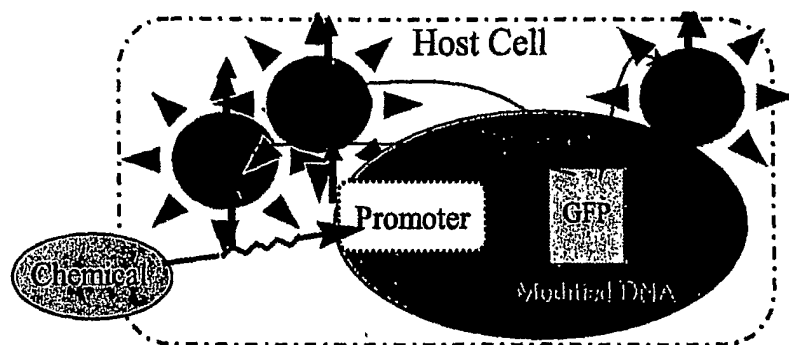


Figure 3.1-1: The GFP Optical Reported Based Genetically Engineered Whole Cell Biosensor

The biosensor is based on the host cell. The *Escherichia coli* (*E. coli*) bacteria is used as a host cell in our research. The cells include plasmids, which are an important component of the genetically engineered biosensors. The plasmid harbors a specific gene promoter fused to a GFP reporter gene. The promoter tailored to particular chemical to be responsive to it exposure. The promoter responds by the mobilization of the cell defense system, which "turns-on" the GFP reporter gene. The GFP reporter gene generates the GFP molecules. The

rate of the GFP molecules generation is quantifiable and is used as a measure of the biochemical interaction efficiency or the "Bio-Signal".

(iii) The BSG&M device is an integrated electro-optical, mechanical, thermal and electronics module. It is a major part of the integrated system (Fig. 3.1-2).

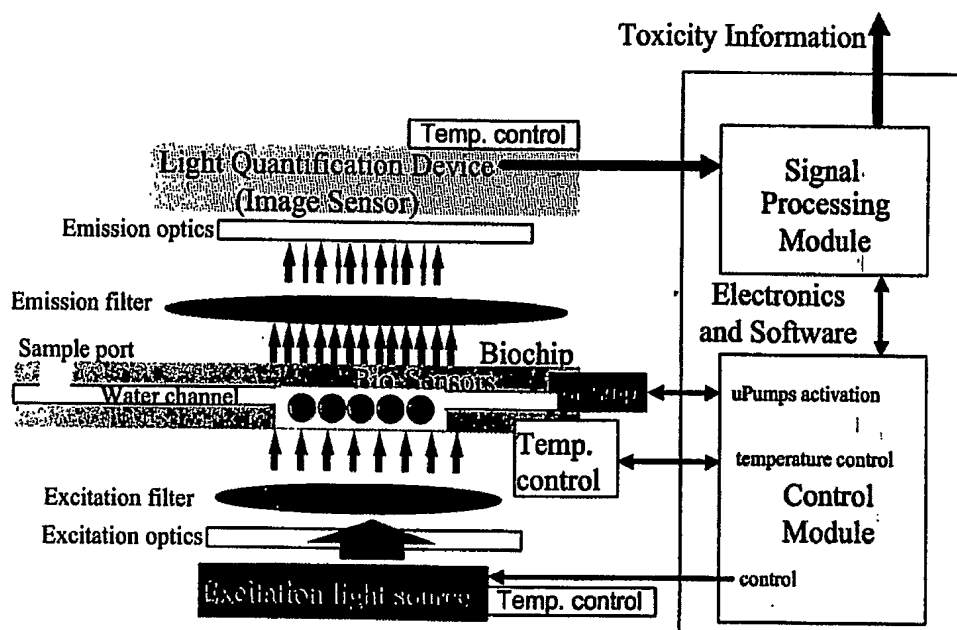


Figure 3.1-2: The Integrated System Block Diagram

All the modules are presented in the sketch of the system's block diagram (Fig. 3.1-2), except the biochip that not belongs to the BSG&M device. The BSG&M modules and their functions are listed below:

- The electronics system that includes the "Control" and "Signal Processing" modules:
- The control Module performing the following functions: (a) Micro-Pumps activation for drawing the tested water onto the reaction chambers; (b) temperature control; and (c) excitation light switching on/off and intensity regulation.
- The Signal Processing Module receives the information interprets it to the biological signal for the further processing. The information is: (a) quantified light received from a number of sources; (b) experiment initial conditions; (c) temperature readout.
- The electro-optical modules including: (a) an excitation light source – it excites the GFP molecules to emit measurable optical signal; (b) fluorescent filters set – used for separation between the excitation energy and emission optical signal; (c) optics that is used to point the excitation energy to the GFP molecules and the emitted optical

signal to the light quantification device; and a (d) light quantification device – in our research the CMOS Image Sensor is used for different light energies digitization.

- The temperature control modules are that provide the operation stabilization for: (a) biosensors – biological activity depends on the environmental temperature; (b) excitation light source – the intensity of the semiconductor device optical emission is depends on the ambient temperature; (c) light quantification device – the temperature fluctuations will vary the dark current and dark current noise, which will damage the reliability of the quantified light energy.
- The Mechanical packaging is a state of the art design integrating all above listed modules. It also includes a chassis and an external box for the integrated system mechanical protection.

3.2 The Biochip And Biochip Support Accessories

3.2.1 The Biochip - Introduction

The biochip is the core element of the integrated system. It performs the following functions: (a) preservation of the immobilized (dormant) biosensors, (b) biochemical reactions activation, and (c) provides the optical path for the excitation and the emission.

The micro-fluidic part of the biochip includes sample ports, reaction chambers, suction ports and micro-fluidic channels. The biosensors are pre-placed into the reaction chambers. The water with the dissolved chemicals is placed into the sample ports. The channels are connects between the sample ports, reaction chamber and the suction ports. The negative pressure that is applied to the suction ports pumps the tested water into the reaction chambers. Once the water reaches the cells the interaction between the biosensors and the chemicals begins.

The design of the micro-fluidic part of the biochip should meet the following requirements:

- The biosensors are pre-placed into the reaction chamber under vacuum. The sealing of the biochip must sustain the vacuum inside the chambers. The quantity of the pre-placed biosensors, of the same type, should be the same among the utilized reaction chambers. Deviations between the number of cells in the chambers may lead to signal variations.
- The pre-placed biosensor should not be an obstacle to the flow of liquid.

- The pre-placed biosensors should stay intact in the chamber during the liquid flow phase.
- Each chamber should receive the same amount of water under test. The pumped liquid must feel the reaction chamber above a certain minimum level.

A few materials were used for biochips implementation: silicon, adhesives, various types of polymers and glass.

3.2.2 Biochips Classification

The biochips have been developed according to the integrated system requirements. The integrated system requirements could be classified according to the various criteria, e.g. simplicity, robustness, cost, precision, etc. The classification of the biochips that have been used in our research is presented in the table below:

Table 3.2-1: The Biochips Used In the Research

#	Class	Description	Application
1	Simple Chip (SC)	A plate with reaction chambers.	Preliminary testing of the integrated system; manual cell deposition
2	Integrated Pumps - Micro Fluidic Chip. (IPMFC)	A plate with reaction chambers, liquid sample ports, on chip micro-pumps and micro-fluidic channels connecting between them.	Experiments in which the biosensors are pre-placed into the reaction chamber. The tested water is placed into the sample port. The pumping process is drawing the water into the reaction chamber and activates the reaction. In case of the EPMFC an external suction mechanism is required.
3	Externally Pumped - Micro Fluidic Chip. (EPMFC)	Plate with the reaction chambers, liquid sample and suction ports and micro-fluidic channels connecting between them.	

The biochip require an external peripheral circuit for the suction activation. In the case of the IPMFC an electrical current pulse is required for the "on chip" pumps activation. For the EPMFC the negative pressure is created externally and is applied to the suction ports via a special interface.

3.2.3 The Simple Chip (SC)

Silicon and plastic substrates were used for the simple chip (SC) configuration. The reaction chambers were drilled or etched into the substrate. The bottom holes were sealed with a transparent plastic. The biological and chemical materials are mixed in an external tube and initiate the reaction. Next, the solution is injected into the reaction chambers. After the water deposition the chambers could be sealed to prevent water evaporation. This keeps the cells viability for a long time. The SC is placed into a special housing on the integrated system that generates, measures and interprets the optical signal.

3.2.4 The Integrated Pumps Micro Fluidic Chip (IPMFC)

The integrated pumps micro fluidic chip technology (IPMFC) includes the micro-pumps and the reaction chamber, channels and sample ports. This technology does not require the external suction mechanism and is rather compact, suitable for portable systems. On other hand, the micro-pumps require activation electronics that complicates the integrated system and the biochip itself.

The integrated biochip was produce using Micro Electro Mechanical System (MEMS) technology [24]. The biochip implemented for our research, titled "Kiwi", includes 12 reaction chambers, 12 on chip micro-pumps, and 4 sample ports. Each sample port supplies water to the 3 reaction chambers. The water is pumped to each reaction chamber separately. The layout of the "Kiwi" biochip is presented in the figure 3.2-1.

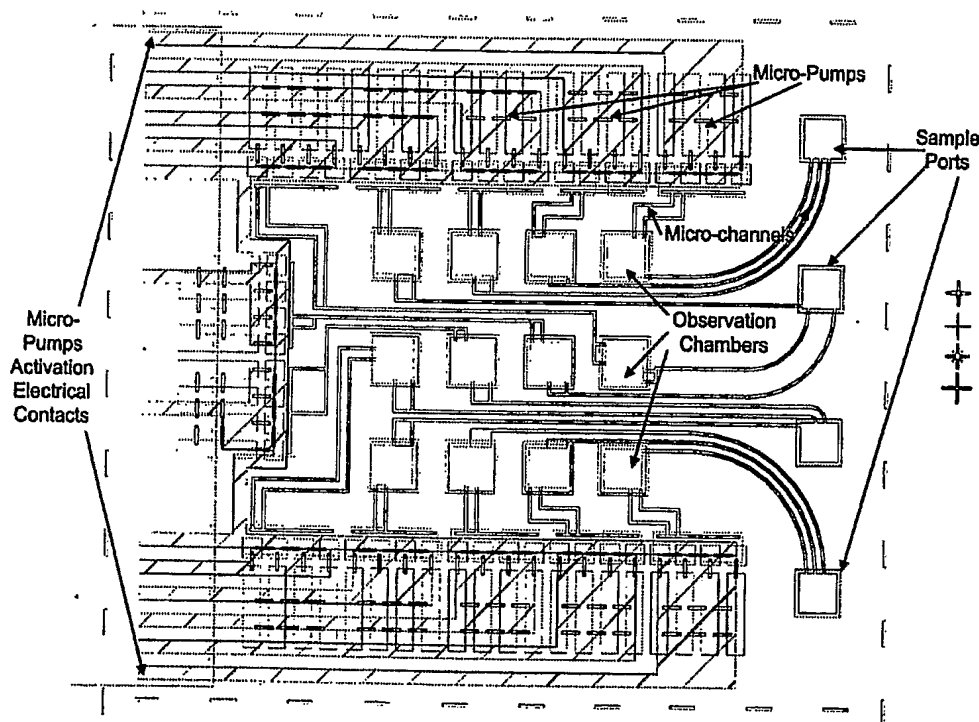


Figure 3.2-1: The "Kiwi" Biochip Layout (Top View)

The reaction chambers are marked in the drawing above as "Observation Chambers". The electrical current for the micro-pumps activation is supplied through the segment marked "Micro-Pumps Activation Electrical Contacts".

The electrical circuit for high current short pulses supply presented on the schematics below:

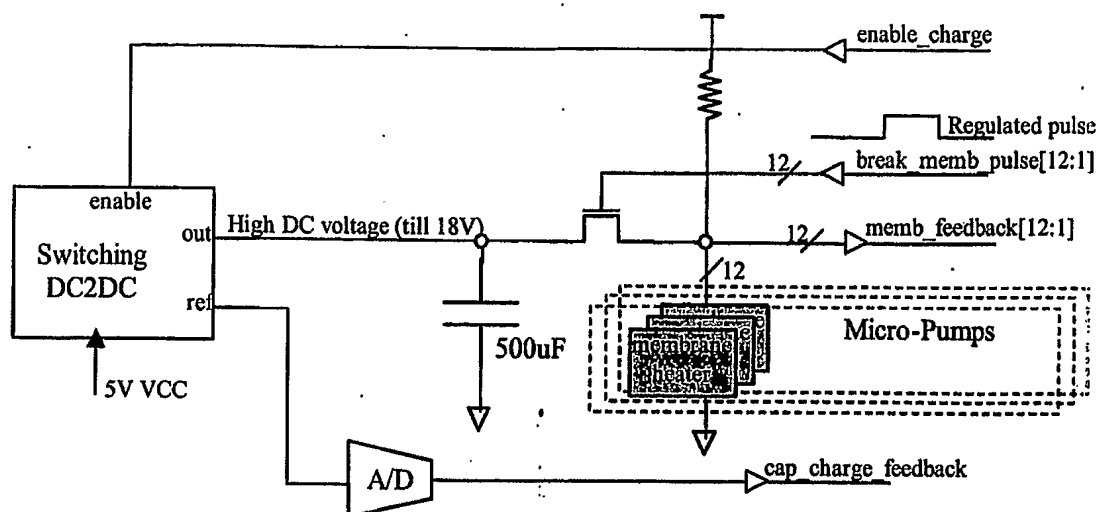


Figure 3.2-2: The Schematics Of Electronics For High Current – Short Pulse Supply

A DC to DC switching converter charges the 500 μ F capacitor in the enabled state.. The enabling performs an “enable_charge” which is interpreted as a low signal. The charged capacitor voltage is 18V. All the micro-pumps are connected to the capacitor through MOS transistor gates. The short regulated pulse is applied to one of the gates through “break_memb_pulse” lines. The opening of the gate discharges the capacitor through the corresponding micro-pump resistance (membrane heater). Typical resistance of the micro-pumps is 2 Ohms. For typical resistance of 2ohm, a current of 9A is supplied. Usually, a pulse of 20 μ s is sufficient to activate the micro-pumps. The status of the capacitor charge is received through a “cap_charge_feedback” line. The implemented digital feedback applies an “enable_charge” signal that recharges the capacitor to an appropriate level.

The mechanical structure of micro-pump and its activation mechanism presented in the following figure:

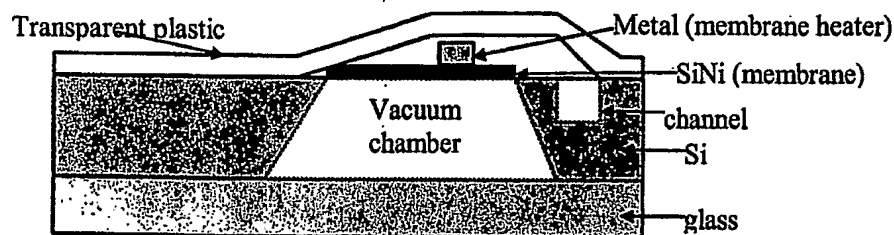


Figure 3.2-3: Micro-Pumps Activation Mechanism

The micro-pump includes a "vacuum chamber" covered by membrane made from *silicon-nitride deposited by chemical vapor deposition*. The "membrane heater" is deposited on the membrane. The short current pulse through the membrane heater provides a heat shock to the membrane that punctures the membrane. The negative pressure differential between the micro-pump and the sampling ports drive the liquid content of the sample port towards the reaction chamber.

The heat shock that breaks the membrane destroys also the membrane heater. Therefore, an activation status could be acquired through "*memb_feedback*" lines. In case that the activation fails, the membrane is left undamaged and the heater resistance remains the same and the output of the "*memb_feedback*" is '0'; otherwise it is '1'.

3.2.4.1 The "Kiwi" Biochip Status

The "Kiwi" test biochip is a state of the art technology. The on chip micro-pumps reduce the complexity of the integrated system. However, the manufacturing process is very complicated and expensive since it is made on Si and includes few masks steps. The main tradeoff is between complexity and chip area. The micro-pumps simplifies the system, however, they increases the chip are by more than 100% since the micro-pumps are is of the same order of magnitude as the cell chambers.

In this work we describe mostly results using external micro-pumps (EPMFC) due to the limited number of available chips with integrated pumps (IPMFC). The main design and manufacturing faults of the various methods were mapped and presented at the table below:

Table 3.2-2: The List Of Changes/Improvements Required For IPMFC

#	Fault	Reason	Way To Improve
1	Incomplete filling of the reaction chambers	The sample port volume was too small.	Enlarge the sample port volume by a factor (~X40) by increasing its area and depth. This requires having the micro-fluidics system to be placed at the bottom side of the chip.
2	Blocked fluidic channels	Manufacturing process	Improvement of manufacturing process, mainly the adhesion step.
3	Weak suction	Vacuum fleeing	Improvement of manufacturing process, mainly the adhesion and sealing processes.
4	The micro-pump fails to be activated.	The metal heater resistance is to high	Reducing the resistance, stabilization of manufacturing process
5	Miscellaneous	Mainly manufacturing process	Improvement of manufacturing process

3.2.5 The Externally Pumped Micro Fluidic Chip (EPMFC)

The externally pumped micro fluidic chip (EPMFC) technology has been developed at the Tel-Aviv University micro-technologies laboratories, faculty of engineering. Allowing the same functionality, as the IPMFC, the EPMFC has been re-designed to with the following highlights:

- Design simplification – the absence on chip micro-pumps and activation mechanism dramatically simplifies the design of the biochip
- Manufacturing process simplification – in contrast to the conventional microelectronics manufacturing process that are used for the IPMFC, the EPMFC could be manufactured using simple plastic processes such as “Hot Embossing” or “Injection Molding”
- Polymer based substrate – allows to reduce significantly the cost of manufacturing, especially in medium and large quantities.
- Low cost prototyping – using simple mechanical machining technology is suitable for the EPMFC prototyping. This allows short cycle time between prototyping steps.
- The area utilization for the reaction chambers – most of the area could be utilized for the reaction chambers. This will reduce the chip size, increase the yield and probably, will reduce the cost.

A few prototype versions have been developed. The goal was to find the optimal configuration of the reaction chambers and the micro-fluidics geometry. This configuration must comply with the requirements presented at Section 3.2.1: “The Biochip - Introduction”.

The real challenge was to balance the micro-pumping system in a sense that we wish to pump an equal amount of liquid into each one of the reaction chambers. Different topologies were designed and investigated. Among them the “Serial Channels” topology was found to be the most successful. The principle of the “Serial Channels” topology “ is displayed on the following figure:

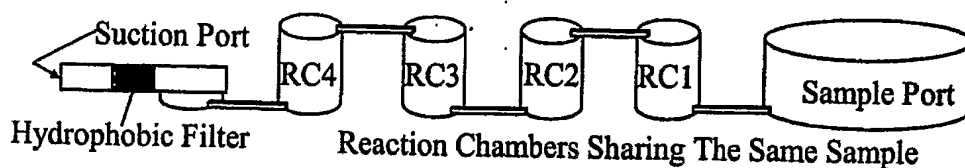


Figure 3.2-4: The Serial Channels Schematics

The "Serial Channels" topology has a single path for the drawn sampled water. Therefore, we assume that all the reaction chambers will be completely and equally filled. The hydrophobic filter is placed in order to stop the water flow, however, it not necessary due to nL precision of the suction mechanism.

3.2.5.1 The External Suction Mechanism

An external suction mechanism is required for pumping of the tested water from the sample port of the biochip into the reaction chambers. The mechanism required to allow precise dosing with a resolution in the range of 100 nL. In order to comply with that requirements the mechanism described on the schematics below was implemented:

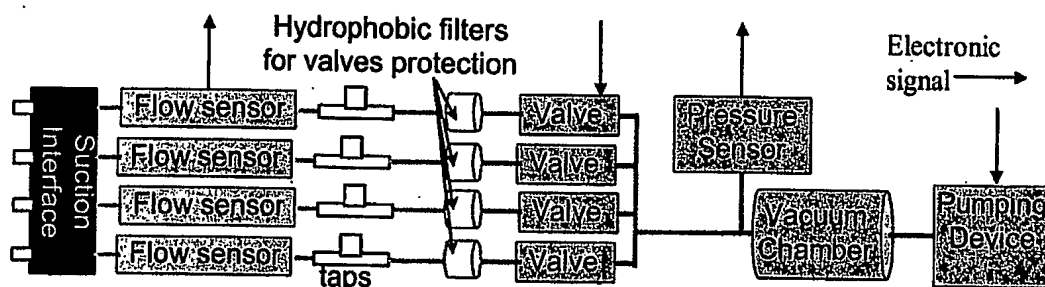


Figure 3.2-5: External Pumping Scheme

The external pumping mechanism performs the following operations: (a) Generation of the negative pressure in the vacuum chamber by activating the pumping device; (b) Control of the negative pressure level by sensing it by the pressure sensor; (c) Fast switching valves ON/OFF (delay of 5ms); (d) Regulation of the flow by taps and sensing the flow by the flow sensors; (e) Suction Interface fits to the suction ports of the biochips.

The external suction module is compatible with all the EPMFC biochips versions.

3.2.5.2 The Test Biochip For Reaction Observation (EPMFC-ver3-2)

The micro-fluidic chip was developed using the serial channels concept and was titled "EPMFC-ver3-2". (See the figure below):

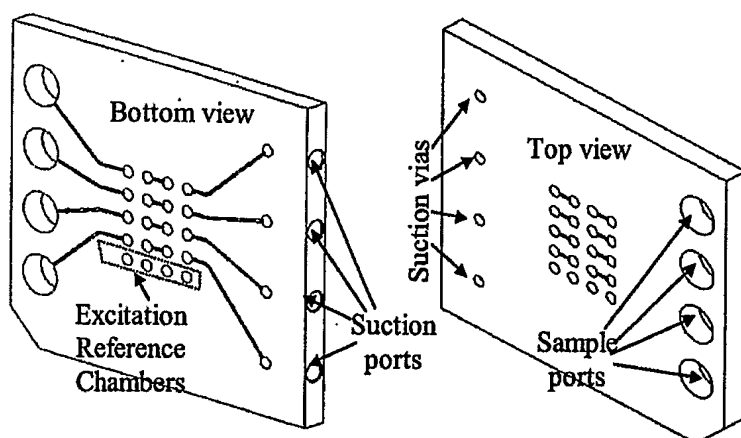


Figure 3.2-6: The EPMFC-ver3-2 3D Drawings

The EPMFC-ver3-2 includes 4 groups, each suction group included sample port, 4 reaction chambers and suction port. The channels connect the chambers serially. The reaction chambers are interconnected both from the top and from the bottom. The top and the bottom sealings use adhesive transparent plastic. The suction ports are prepared for the horizontal insertion of the pumping insertion ports (The "nipples"). The external suction mechanism implementation is described in Section 3.2.5.1. The fifth row of the holes is used as the excitation light reference, which is measured by the image sensor.

The EPMFC-ver3-2 allowed us to observe the off-chip initialized reaction. Its serial channels methodology allowed to pump equal volume of the tested solution into the all reaction chambers.

The other goal of the EPMFC-ver3-2 was to evaluate the precise mechanical machining technology and materials for prototyping. The channels with dimensions of 200x50um were prepared by gnawing. The materials that demonstrated good biocompatibility, optical and machining requirements were PVC and DelrinTM.

3.2.5.3 A Biochip With On Chip Initialized Reaction (EPMFC-ver4)

The final biochip configuration must meet all the requirements, listed in Section 3.2.1. That biochip will allow (i) pre-placing and immobilizing of the biosensors, (ii) the biochip hermetical sealing and (iii) on demand water test activation.

In order to meet the requirements a design with medium level liquid injection is suggested (see the figure below)

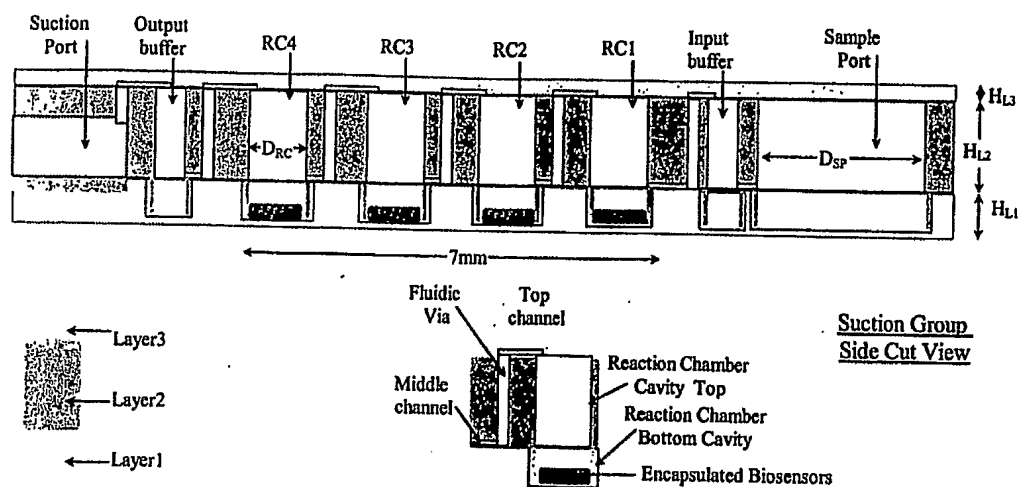


Figure 3.2-7: The EPMFC-ver4 - Side Cut View

The design is based on three layers of transparent polymer substrate. The whole cell biosensors are dehydrated inside cavities in the first layer (layer1). The drying process also crystallizes the nutrients that encapsulates the dehydrated biosensors. A crystallized membrane is created which will be melted during the process of the biosensors rehydration.

The third layer (layer3) is used for the top cover of the channels and for the top sealing. It fused with the second layer (layer2). The second layer includes the cavities for reaction chambers and buffers, and the fluidic channels for the medium level injection.

The EPMFC-ver4 chip allows us to perform the whole cell based biosensors dehydration, and sealing. That is supported by the special design presented on the figure below:

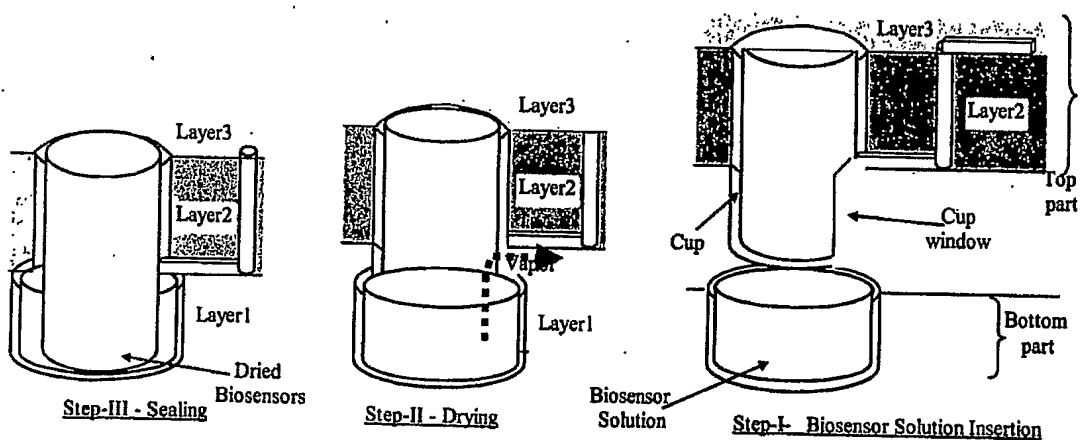


Figure 3.2-8: The EPMFC-ver4 Final Production Step Process

The second layer includes the cup structure. It is used to ensure complete sealing of the reaction chamber. The top part is placed above the bottom part on the distance of $\frac{1}{2}$ cup heights. The dehydration process is activated. The cup window allows evaporation of the water during biosensors dehydration process. At the end of the dehydration process a mechanical pressure is applied on the top of the biochip. The pressure pushes the top part towards the bottom and the manufacturing process is completed. The vacuum is preserved in the reaction chamber that allows sustaining the biosensors in the dormant state.

3.2.6 The Biochips Manufacturing Issues

Currently the chips are made either by Si micro machining or by mechanical machining. Both methods are expensive and suit small volume prototype production. In the future we anticipate that the biochip will be produced by hot-embossing technology [25]. The option to use the "Injection Molding" technology was also examined. Injection molding requires the production of master mold that are more complicated than what is required for the hot embossing.

3.2.7 The Reaction Chambers Functionality

The matrix of the reaction chambers is physically and logically divided to few groups. The physical division creates the suction groups titled "S.Group". The "S.Group" is compounded from the reaction chambers sharing the same sample and suction port. The logical division creates the functional groups, named "F.Group". The functional and suction groups are presented on the example of EPMFC-ver3:

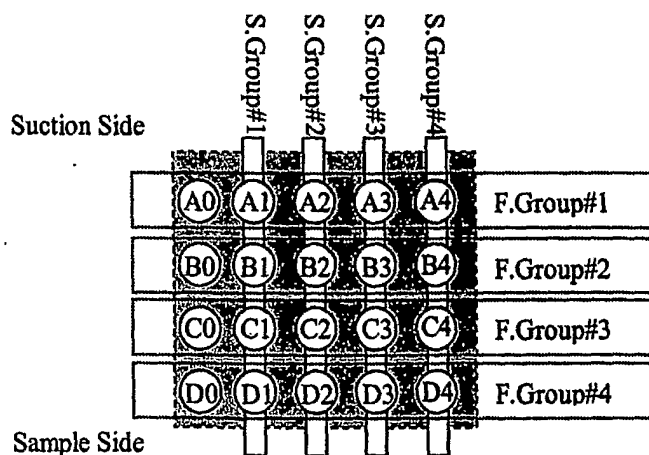


Figure 3.2-9: Reaction Chambers Divided To The Functional & Sample Groups

The "F.Group" includes the reaction chambers implementing together specific task as shown on the figure below:

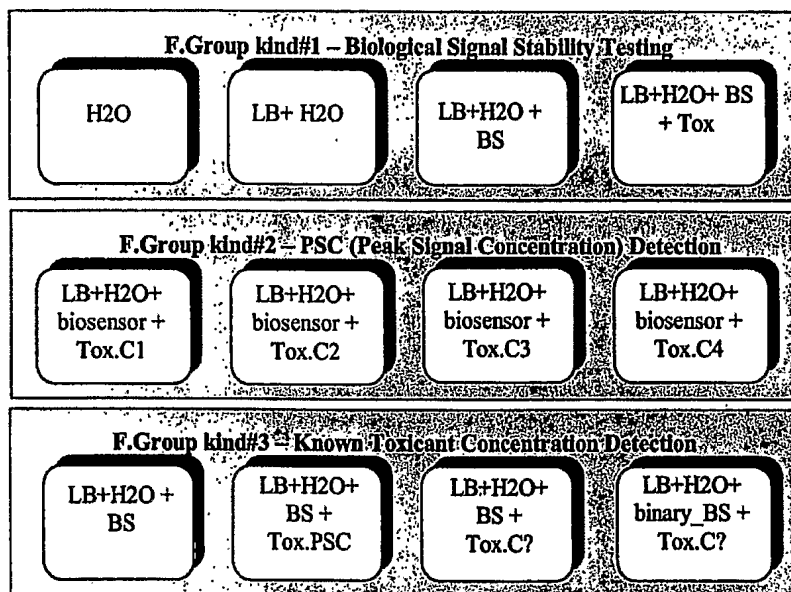


Figure 3.2-10: Various Functional Groups

The "F.Group-kind#1" is used to separate quantization of the light sources projected on the light sensing device. The separation between the projected light sources required for calculation of the biological signal. This is described in details in the "Section 4.2.1: Bio-Signal Quantification on TAU-WTA Integrated System".

The "F.Group-kind#2" is used for discovering chemical concentration inducing maximal biological signal. The concentration providing maximal biological signal named "Peak Signal Concentration" (PSC). The measurements of the biological signal as function of chemical concentration are required for water analysis algorithms. The utilization example of the F.Group-kind#1 and F.Group-kind#2 is described in the "Section 4.2.2: Bio-Signal Characterization Using Victor-2 Fluoremeter".

The F.Group-kind#3 is used for detection of concentration of known chemical. The algorithm example for F.Group-kind#3 utilization is described at the "Section 3.7.3: The Simple Algorithm For Known Chemical Concentration Calculation".

3.3 Electro-Optics System

This section covers all electro-optical aspects of the integrated system (a) characterization of the electro-optical devices used in the integrated system setup; (b) model of the reaction chamber bio-fluorescence; and (c) the electro-optical setups and their performance evaluation. The concept of the bio-fluorescence based electro-optical system is schematically shown on the figure below:

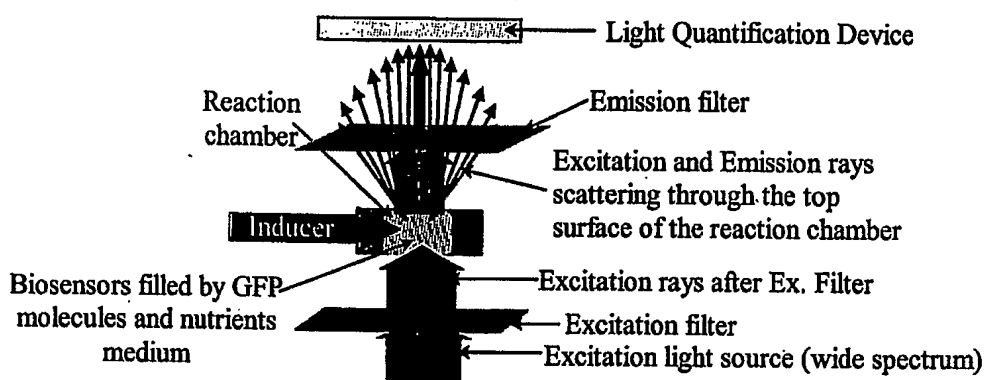


Figure 3.3-1: Bio-Fluorescence Based Electro-Optical Setup Concept

The excitation light source spectrum may overlap some of the emission spectrum. Therefore, it must be suppressed to avoid signal saturation and excess noise. The excitation filter removes the overlapping excitation spectrum, thus only the emitted light reaches the detector. The filtered excitation rays are partly absorbed by the biosensor and the nutrients medium. The unabsorbed rays pass through the reaction chamber and are attenuated by about 4 orders of magnitude by the emission filters before it reaches the light detectors. The GFP molecules and the fluorescent medium absorb the excitation rays and fluoresce. The fluorescent light that is collected by the emission optics is redirected to the light quantification device that converts the light to electrical signal. The portion of the quantified light contributed by the unfiltered excitation rays will be referred to as the "excitation background". The additional portion that is contributed by the nutrient medium will be referred to as the "nutrient background". There are methods to reduce the background signals, however the background fluctuations contribute noise that can not be completely eliminated. Therefore, the background uncertainties will be referred to as the "background noise".

The bio-fluorescence intensity is proportional to the quantity of the generated GFP molecules. This quantity depends on the efficiency of the biochemical reaction occurred due

to the interaction between the inducer and the biosensors. The sensitivity of the system depends on its ability to distinguish between the bio-fluorescent emission from the background noise. Typical electro-optical systems, and our biochip included, should minimize the background noise as much as possible.

3.3.1 Spectrum Characterizations of The GFP Based Optical Reporter

The characterization of optical reporter is required for: (a) the selection of the excitation device with an appropriate spectrum of the emission; (b) the selection of the fluorescence filters that are set for the excitation and the elimination of the bio-emission spectra overlap; and (c) the selection of the light quantification device that should be sensitive to the bio-emission spectrum. The characterization includes two parts. The first is a spectrum of the emission quantum efficiency or "excitation spectrum". The second part is the emission spectrum itself.

The characterizations were performed at Tel-Aviv University – Faculty of Medicine – Laboratory of Medical Physics. The following tools were used: (a) spectra-fluoremeter by SLM Instruments Inc. with illumination band pass filters of 1nm step; (b) personal computer for spectrometer control and results registration; and (c) GFP reporter based induced biosensors melted in water in transparent test tube. The received excitation and the emission spectrums are presented below:

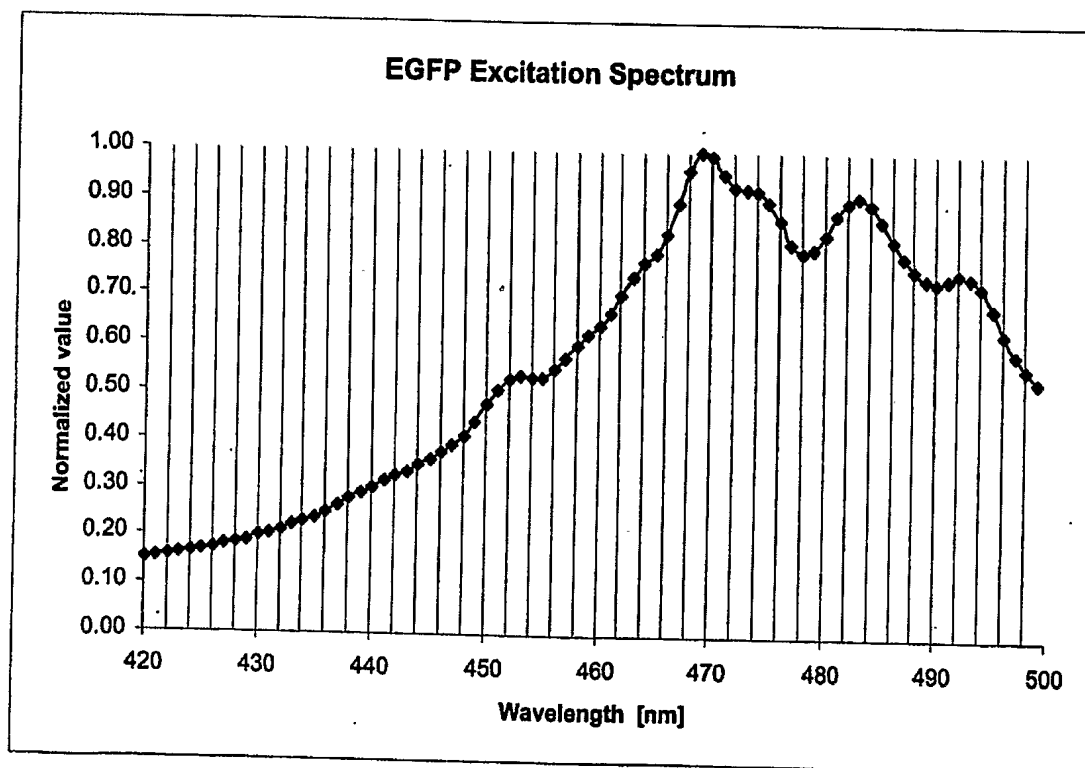


Figure 3.3-2: Excitation Spectrum Of The GFP Optical Reporter Based Biosensor

The y-axis of the graph is normalized to the maximum bio-emission intensity measured at the wavelength of 510 nm. The peak emission was received for 469 nm excitation wavelength. This is the wavelength with the maximal quantum efficiency of the GFP molecule.

The spectra of the GFP molecule emission as function of the excitation wavelength is presented below:

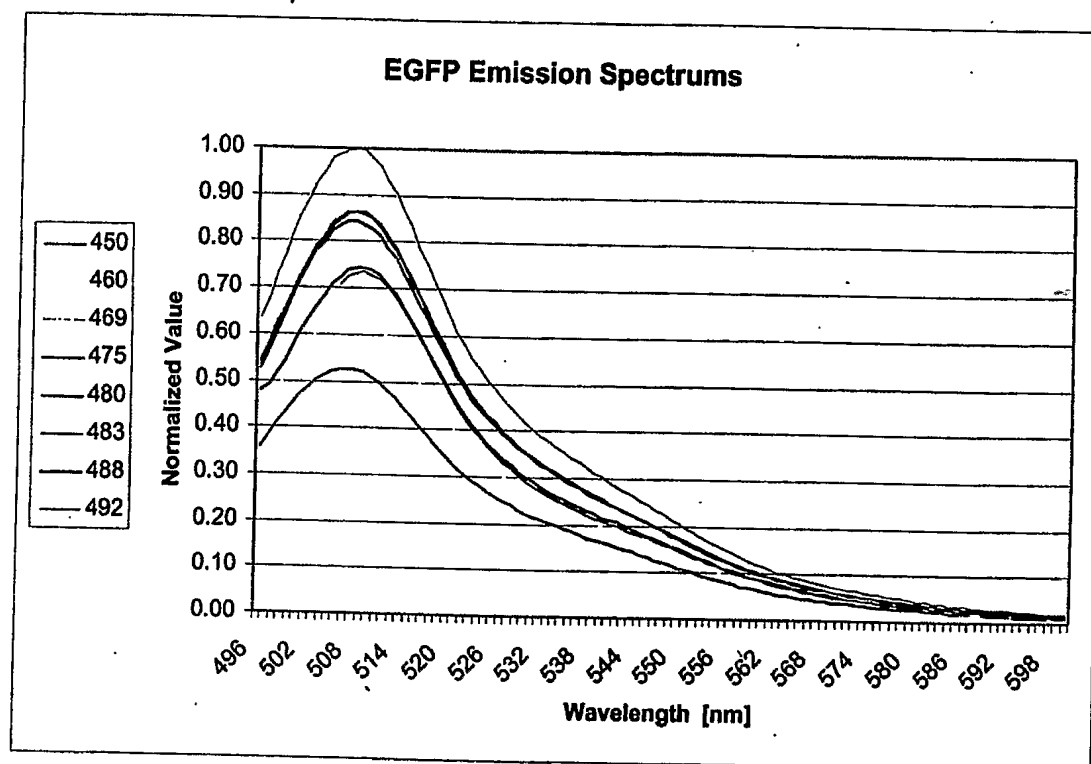


Figure 3.3-3: The Emission Spectra Of GFP Optical Reporter Based Biosensor

From the emission spectra we conclude that the maximal emission quantum efficiency is for the 469nm excitation. The emission spectrum is independent from the excitation wavelength. Most of the emission energy is spread in the range of {500:550nm}. The integrated emission intensity received for uniform excitation light source is in the range of {450:490nm} could be expressed by the following equation:

$$I_{ems} = K(\lambda) \cdot \sum_{i=450}^{i=490} \left(\int_{500}^{550} N_{GFP-i}(\lambda) d\lambda \right) \quad (3.3-1)$$

$N_{GFP-i}(\lambda)$ is a normalized emission spectrum received for the index i that specifies the excitation wavelength. $K(\lambda)$ is a constant correlating between the normalized value and the emission intensity measured in a photon per seconds.

3.3.2 Fluorescence Filters Set Selection

Following the GFP based optical reporter spectrum results the following filters were selected: (i) excitation filter - hq470/40x by Chroma Inc.; and (b) emission filter - hq425/40m by Chroma Inc.. The filters transmission spectrums were measured on the spectrometer and presented below:

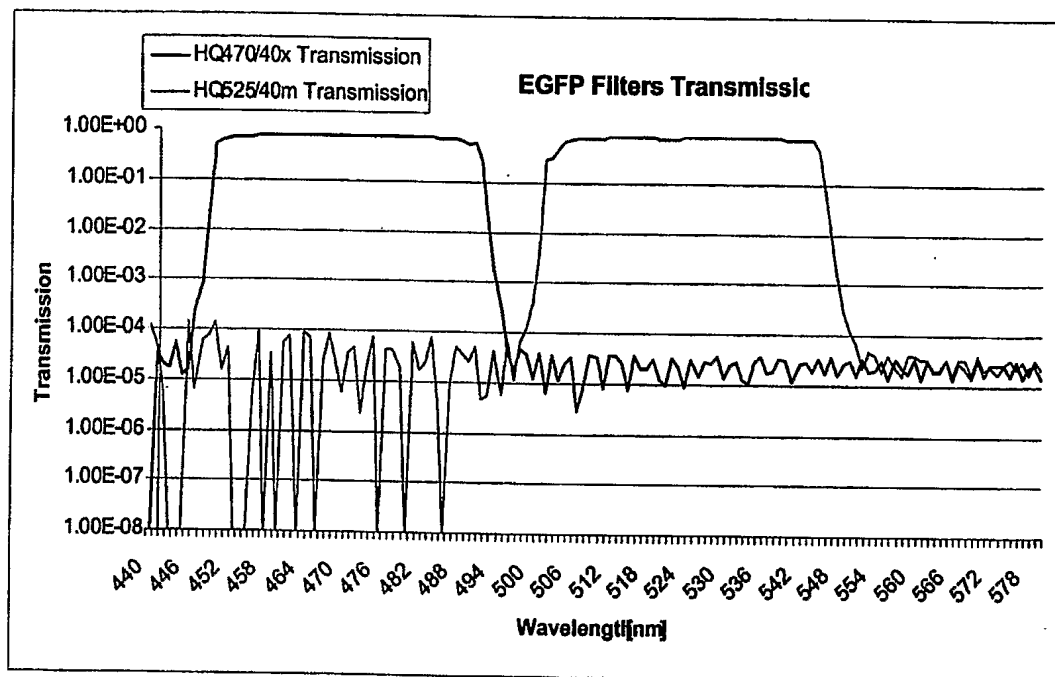


Figure 3.3-4: Excitation And Emission Filters Transmission Spectrums

As observed, the emission filter attenuates the excitation optical power by ~4 orders of magnitude. The excitation filter also reduces the excitation intensity that overlaps with the emission spectrum by 4 orders of magnitude. This bio-fluorescent emission depends on the excitation rays absorption. The optics collecting the bio-emission is important too. Actually, the bio-emission intensity reaching the light quantification device is weaker than the excitation in about 3-5 orders of magnitude. It means that the quantification intensities ratio between emission and excitation will be in range of {0.1:10}.

The filters described in that section are interference type. This type is effective for the rays perpendicular to the filter surface. However, they are less efficient for oblique incidence

of light. This filter attenuation versus incident angle was experimentally measured using standard laser source.

3.3.3 Light Emitting Devices For The Bio-Fluorescence Generation

The light-emitting device provides the energy for exciting the GFP molecules. The device must meet the following criteria: (a) maximum energy in the excitation spectrum; (b) the rays must be parallel to each other and perpendicular to the fluorescence filters plane; (c) the intensity could be regulated and strong enough to use integration time less than 10sec for the emission quantification; (d) compact dimensions in order to build the array of excitation elements or alternatively provide the uniform area lighting; and (e) the peak of the excitation energy is around 470nm.

The comparison of various light emitting devices is presented at Appendix-A. Two candidates were selected: (i) packaged LED die with reflector (SMT LED); and (ii) 5mm LED with Optical Fibers adaptor. Those devices were utilized for building a matrix of excitation light sources. The details are presented in the following sections.

3.3.3.1 Matrix Of SMT LEDs

The matrix of SMT LEDs was implemented in the TAU-TMS integrated system. The SMT470 LED by Epitex[26] was used. The individual LED located under the reaction chamber of the Kiwi biochip as shown on the figure below:

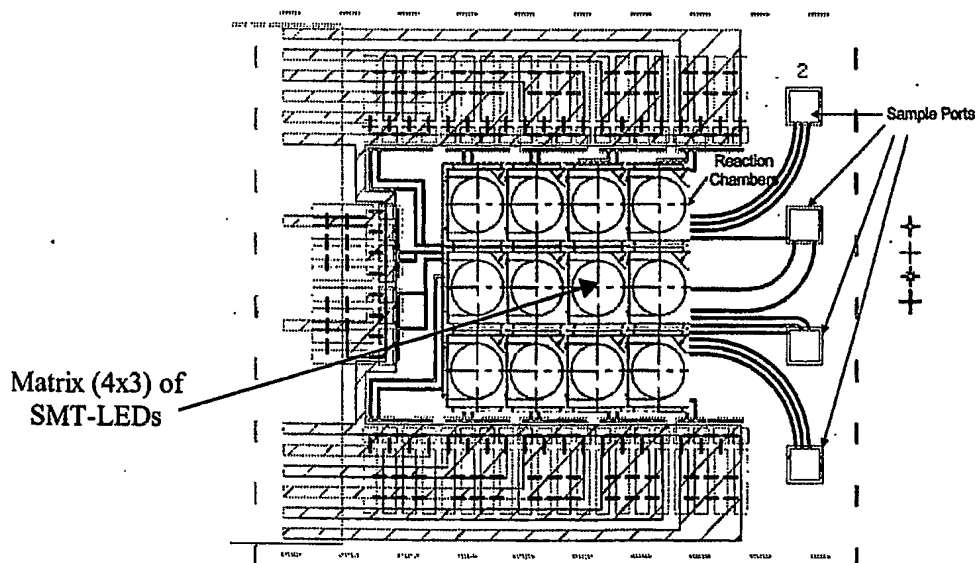


Figure 3.3-5: The 4x3 Matrix Of SMT LEDs – Top View

The cut view of the structure represents in details the electro-optical excitation module. It shown on the figure below:



Figure 3.3-6: The 4x3 Matrix Of SMT LEDs – Side View

The configuration presented above is problematic due to a wide view angle of the SMT LED and a thick excitation filter² (3.5mm). The following main problems are encountered:

- The rays from specific LED escape to neighbor reaction chambers (the problematic ray#1). Therefore, the reaction chambers in the center receive more excitation energy.
- The interference filters are not effective for oblique ray angles. The excitation light that is marked on the figure above as problematic ray#2 are partly filtered by the excitation and emission filters. The detector integrate any light, so again false biological signal will be registered.

The biological emission is proportional to the supplied excitation energy. In order to compare the biological signals received from the different reaction chambers the excitation energies should be know. The difference of the excitation energy supplied to the reaction chambers is hard to measure. The complex equipment and experiments are required for that. Therefore solution with isolated excitation light sources was suggested. It has been implemented for TAU-WTA integrated system and described in the next sub-section.

² The excitation filter is interference kind and made from thousands levels of coating. The thickness has inverse proportion to the cost

3.3.3.2 Super Bright LEDs With Optical Fibers

In order to isolate the reaction chambers from the foreign excitation sources and to generate straight excitation rays a "5 mm LED" based solution have been implemented in TAU-WTA integrated system. The "5mm LED" is built of LED die and lens. The lens rectifies the rays to view angle of 15°. The rectified rays are passing through the excitation filter, which cuts the bio-emission overlap spectrum. The most of the "5mm LED" energy concentrated in the ring, cause there is a blind spot in the center of the LED die. This allows us to place harbors for the optical fibers on the perimeter of the ring as shown on the figure below:

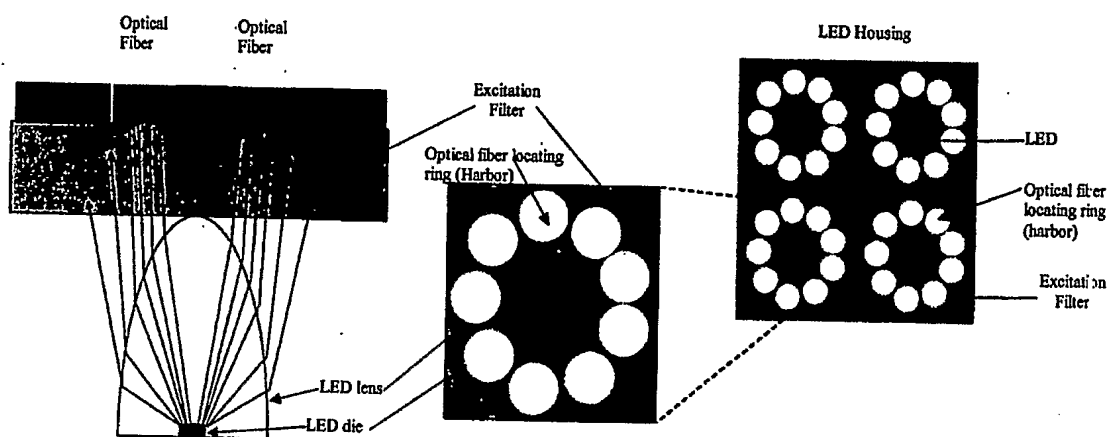


Figure 3.3-7: The 5mm LED With Optical Fibers Solution

The matrix of 2x2 LEDs is used to supply 20 excitation sources – 5 sources from each LED. The 5 of 9 optical fibers harbors are used. The rest 4 of 9 are optically blocked. The extra of 4 harbors is used for selection of 5 harbors providing the closest optical powers.

One of the most important parameters is the narrow angle of the excitation light emission. The almost parallel rays enters the optical fibers that carries the excitation rays to the reaction chambers. This method overcomes problems noted in the matrix of SMT LEDs case.

For a forward current of 30mA the optical power of the 5mm LED, attenuated by the excitation filter, is 5mW. The 1mm diameter optical fiber harbored to the ring utilizes about 50uW. In case of the TAU-TMS, the 500uW excitation light was supplied to the area of 4mm, which equal to 125uW/mm². The required integration time for bio-emission registering was 1sec. In current case of the TAU-WTA the 50uW supplied to the area of $\pi \cdot (1/2)^2 = 0.79 \text{ mm}^2$ or

63uW/mm²; the pixel sensitive area of the IBIS4 CMOS image sensor is x4 less. That's mean that integration time must be about 8 times longer, which is 8 sec.

3.3.4 Light Sensing And Quantification Devices

Alight sensing and quantification device is required for the digitization of the bio-emission and other light sources intensities. In other words the photometry device is required. Our applications specific requirements are: (a) sensing light from the matrix of sources in the same time; (b) self saturation time not less than 60sec; and (c) the price less than 50\$ in high quantities.

The various photometry technologies were compared in Appendix-B. The most suitable device for our requirements is based on the CMOS Image Sensor technology. It could sense the bio-fluorescence emission from a dense matrix of the reaction chambers with enough sensitivity and for the low price. The light sensing and quantification parts are integrated into the same device. This makes it more attractive due to the simple control and readout mechanism.

The ACS-1394 fire-wire camera based on the ACS-1024 CMOS Image Sensor by Photonics Vision Systems (PVS) was used for TAU-TMS integrated system. Unfortunately the PVS company was closed due to the difficulties during the last global economy stagnation period. More information about the ACS-1394 camera could be found in the "Section 3.8.4.2: Image Sensor Temperature".

The termination of the PVS support forced us to select a new CMOS Image Sensor supplier. After the comprehensive investigation of the available CMOS Image Sensor development companies, the Fill-Factory Ltd. (Belgium) has been selected. The IBIS4 CMOS Image Sensor has been choused. The additional reason for selection of the Fill-Factory, as supplier was excellent support and cooperation. The IBIS4 Evaluation Board firmware, software and schematics were received. That allowed us reducing efforts in own hardware and software developments. The IBIS4 CMOS Image Sensor is shortly described in the next section.

3.3.4.1 Light Quantification Using IBIS4 CMOS IS By Fill Factory

The detailed description of the IBIS4 CMOS IS by Fill Factory could be found under <http://www.fillfactory.com/htm/products/htm/ibis4/ibis4.htm> link. The patented technology [27] of the Fill-Factories increases the light conversion sensitivity and lowering the dark current.

Lets discuss how light quantification is performed by means of the IBIS4 image sensor. In order to better present the methodology the simplified schematics of the IBIS4 architecture was prepared:

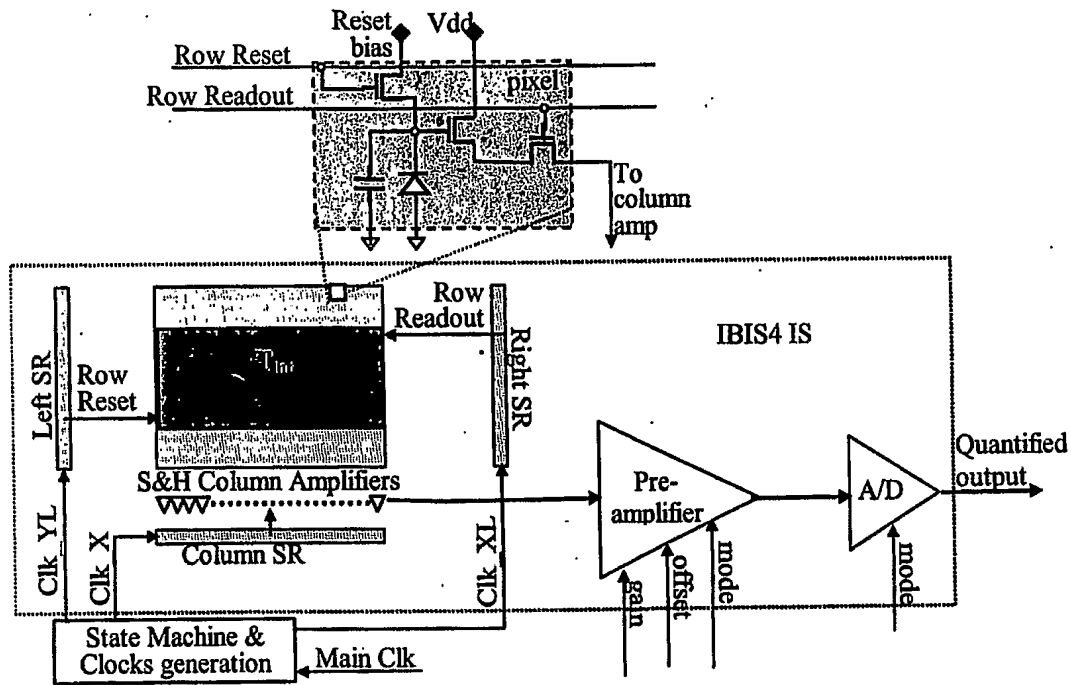


Figure 3.3-8: IBIS4 Simplified Schematics

The light sensing part of the CMOS image sensor is the matrix of pixels. Each pixel consist of capacitor pre-charged to Reset bias voltage, photodiode discharging the capacitor as response to photons absorption and 3 MOS transistors for pixel reset, signal sensing and leading to column amplifier. Such pixel structure named 3T due to three MOS transistors.

There are two vertical (Y) shift registers: left and right. The left points to the row that is pre-charged to reset bias voltage (reset row operation). The right points to the row which pixels are sampled by S&H Column Amplifier. The distance between two pointers determines the integration time, which could be calculated according to the following equation:

$$T_{int} = N_{int-rows} \cdot (T_{rd-px} \cdot N_X + T_{blanking}) \quad (3.3-2)$$

Where $N_{int-rows}$ is the distance in rows between the readout and reset row pointers, T_{rd-px} is the time for one pixel readout, N_X is the size of the window in X-dimension and the last $T_{blanking}$ is the time between two successive rows readout necessary for calibration of the pre-amplifier. The T_{rd-px} is a direct function of the Main Clock generating Clk_X . The $T_{blanking}$ is consisting from several operations duration that are synchronized by Main Clock too.

The column shift register selects the S&H column amplifier. The S&H column amplifier is routing the charge to the pre-amplifier input. The pre-amplifier has tunable gain and offset in order to fit the input signal range of the analog to digital converter. In addition the weak light could be amplified by the increasing the gain.

The IBIS4 image sensor has unique feature named "Double Slope Mode" [28] for dynamic range extension. However this feature wouldn't be used in this work. For the current research both pre-amplifier and A/D are operated in linear mode. The gain (3) and offset (2V) are adjusted. Therefore the quantified output will be proportional to the number of photons collides with pixel. The dependency is expressed below:

$$N_{ph}(T_{int}) = \frac{6e4 \cdot ((QO(T_{int}) - QO_{DC_e-}(T_{int}))/2^{bits})}{QE \cdot FF} \quad (3.3-3)$$

Where N_{ph} is a number of photons collected by the pixel, QO is a quantified output, $bits$ is the A/D quantization, QE is a quantum efficiency of the Image Sensor and FF is a Fill-Factor. The QO_{DC_e-} is a quantified output of the integrated dark current measured at the complete dark condition. The dark current depends on the temperature. For room temperature of 21°C the dark current is 344[pA/cm²] or 1055[e-/s] or 19[mV/s]. The quantified output of the dark current for the temperature of 21°C is:

$$QO_{DC_e-}(T_{int}) = \frac{1055[e-/sec] \cdot T_{int}[sec]}{6e4[e-]} \cdot 2^{bits} \quad (3.3-4)$$

The long integration time is necessary for the weak signals. However it is limited due to the pixel saturation by the dark current. The dark current is reduces the dynamic range of the light signal. Lets define parameter F_{DC} dividing the dynamic range between the dark current and light signal. The allocated gray levels for the dark current quantification are:

$$QO_{DC_e-_{max}} = F_{DC} \cdot 2^{bits} \quad (3.3-5)$$

And the maximum allowed integration time is:

$$T_{int-max-ws} = \frac{6e4[e-]}{1055[e-/sec]} \cdot F_{DC} \quad (3.3-6)$$

The other parameter that should be considered is dark current non-uniformity which is 15% RMS of dark current level. This increases uncertainty for the weak signals. The minimal light intensity calculation is presented in the Appendix-C. Minimal signal intensity of 1,485[photons/sec] at the room temperature is required.

For high intensity signals I_s [photons/sec] the long exposure will saturate the pixels. The exposure should be limited by the maximal integration time $T_{int-max-ss}$:

$$T_{int-max-ss} = \frac{6e4[e-]}{I_s \cdot QE \cdot FF} \quad (3.3-7)$$

3.3.5 Modeling Of The Bio-Fluorescence Electro-Optical System

The optical system intended to project the bio-emission on the light-sensing device and to eliminate the other light sources. In order to correctly design the optical part of the integrated electro-optical system, the characterizations of the bio-emission and other light sources are required. The characterization could be done experimentally, which is complicated or by modeling. The bio-fluorescence model of the electro-optical system presented below:

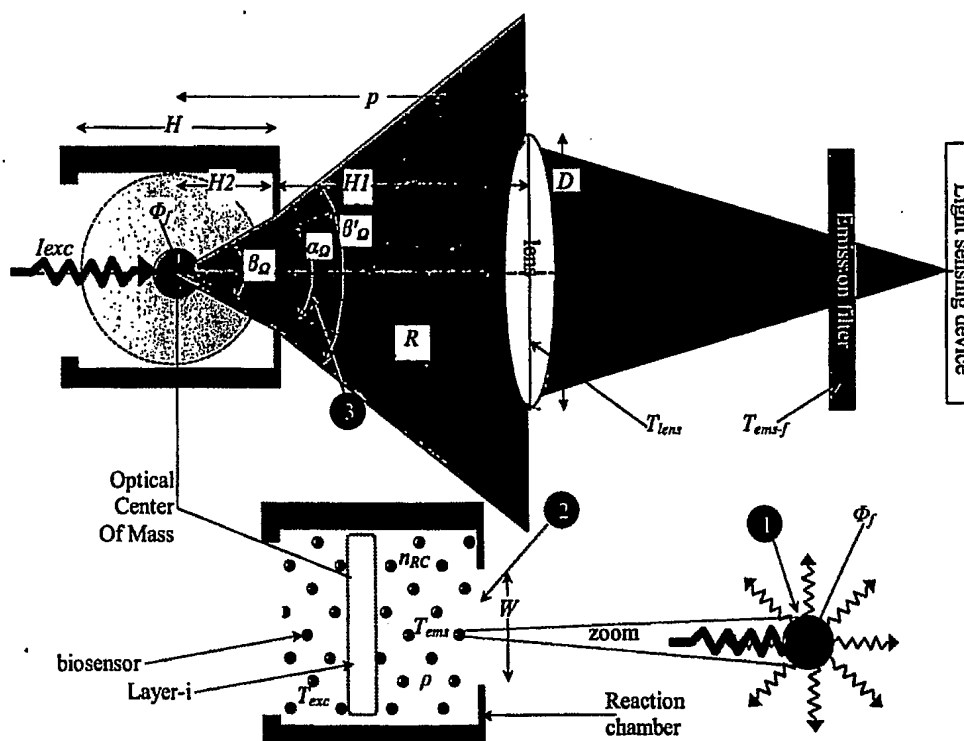


Figure 3.3-9: Electro-Optical System Model

The model consists of the following components: (a) a reaction chamber divided to layers; (b) an equivalent bacteria which is superposition of the all bacteria in the layer; (c) beam with excitation light rays absorbed by the biosensors (marked as I_{Exc}); (d) absorbed excitation photons generates the bio-emission. The bio-emission spreads through the aperture W of the reaction chamber. The numerical aperture is marked as β'_a and it depends on the depth of the layer; (e) lens projecting the emission on the light-sensing device. The lens collecting

emission spreads with numerical aperture of α_0 , which depends on the layer depth too; and (f) the emission filter attenuating the excitation light in some orders of magnitude and transferring most of the emission light; (g) light sensing device quantifying the light.

The section will cover the following aspects: (i) optical parameters calculations like efficiency and transmittance of the system components; (ii) ray tracing; (iii) optical transmittance and absorption of the excitation inside the reaction chamber.

3.3.5.1 Optical Parameters Calculation

The spectrum characteristic of the optical components is presented by a vector. The index of the vector is a wavelength and the member corresponding to the index is a value. The optical components represented by vector will require the complex matrix calculations. In order to simplify the calculations the spectrum will be represented by the mean effective parameter. The schematic process for this transformation shown below:

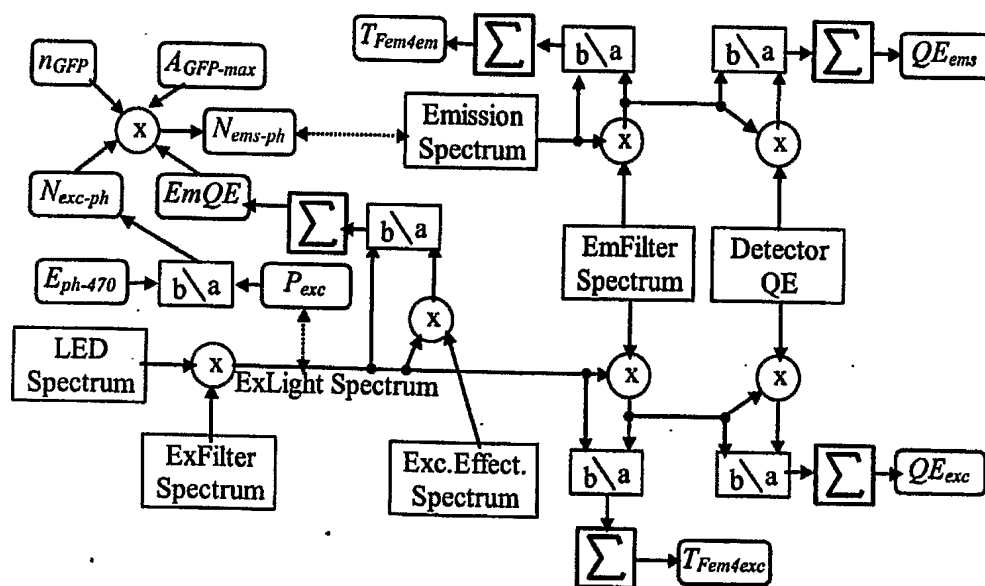


Figure 3.3-10: Spectrums To Parameter Conversion Schematics

The schematics above includes the following components:

- Input Spectrums: (a) LED spectrum; (b) excitation and emission filter spectrums; (c) fluorescence excitation efficiency, or emission quantum efficiency spectrum; (d) fluorescence emission spectrum; (e) Quantum Efficiency (QE) of the light quantification device.
- Resulted Coefficients: (a) Emission Quantum Efficiency ($EmQE$) – the ratio between the absorbed excitation photons and generated emission photons that depends on the

wavelength; (b) $T_{Fem4exc}$ – the transmittance parameter for excitation photons by the emission filter; (c) $T_{Fem4ems}$ – the transmittance parameter for emission photons by the emission filter; (d) QE_{ems} – effective QE of the light quantification device to the emission spectrum; (e) QE_{exc} – effective QE of the detector for the excitation spectrum

- The variables: (a) $A_{GFP-max}$ – the ratio between the area of equivalent bacteria saturated by the GFP molecules to the excitation beam area; (b) n_{GFP} – the percentage of the bacteria saturation by the GFP molecules

3.3.5.2 The Ray Tracing

The biosensors under the concentration ρ are uniformly distributed inside the reaction chamber as shown on the Figure 3.3-9. The reaction chamber has a form of cylinder, of the heights H and diameter W . The bio-emission is the result of the excitation photons absorption. The bio-emission photons are scattering into the all directions – 4π solid angle. Part of the bio-emission photons absorbed by the reaction chamber walls. Other part, with numerical aperture β_Ω , is pass through the reaction chamber outside. The lens collects the emission photon rays with numerical aperture less than α_Ω . The light collected by the lens attenuated by $(1 - T_{lens})$ and redirected to the light sensing device.

The medium inside the reaction chamber is liquid. Its refraction coefficient is n_{RC} . The rays that scattering out of the reaction chamber are traveling in a free space with refraction coefficient n . The rays are redirected to the angle β'_Ω , according to the Snell law:

$$n \cdot \sin(\beta_\Omega/2) = n_{RC} \cdot \sin(\beta'_\Omega/2) \quad (3.3-8)$$

Therefore the external scattering angle of the rays passing through the reaction chamber aperture will be:

$$\beta'_\Omega = 2 \cdot \sin^{-1}((n/n_{RC}) \cdot \sin(\beta_\Omega/2)) \quad (3.3-9)$$

The model simplifies the calculations by division of the reaction chambers on the layers. The biosensors inside the layer are concentrated into the single equivalent biosensor. The equivalent biosensor locates in the middle of the layer. The middle of the layer is named "Optical Center Of Mass". This is illustrated in the Figure 3.3-9.

The division of the reaction chamber on the layers, equivalent biosensors in the OCM, and the ray scattering simulated below:

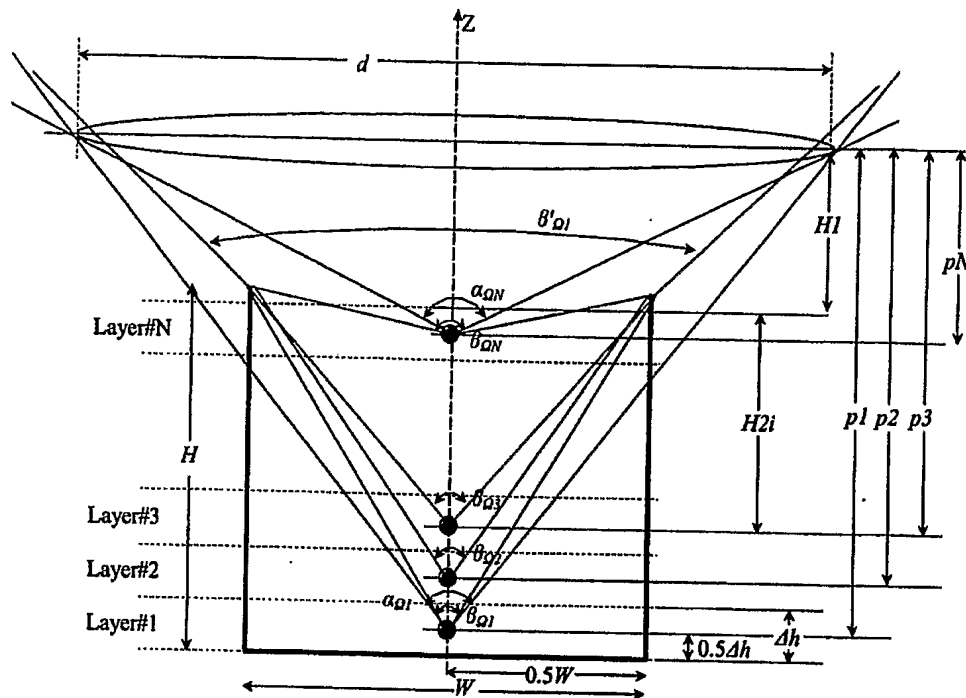


Figure 3.3-11: The Ray Tracing Model For Emission Scattering Characterization

First, the number of layers for the above model has to be determined. Lets assume that the biosensors are distributed inside the cube with 1mm rib. The number of the biosensors in this cube is B_{cube} . Using the assumption of uniform 3-dimensional distribution, the number of the biosensors in one dimension:

$$B_{1D-1mm} = \sqrt[3]{B_{cube}} \quad (3.3-10)$$

Now lets assume that this dimension is Z (look at the Figure 3.3-11) and all biosensors are located in the OCM of the X-Y planes. The number of such planes, or layers, is:

$$N_{layers} = B_{1D-1mm} \cdot (H/1mm) \quad (3.3-11)$$

The width of the one layer is:

$$\Delta h = H/N_{layers} \quad (3.3-12)$$

The OCM of the layer $i \in (1 : N_{layers})$ is at the height:

$$H_{2i} = H - \Delta h \cdot (i - 0.5) \quad (3.3-13)$$

The scattering angle of emission rays as function of the layer i is:

$$\beta_{\Omega i} = 2 \cdot \text{tg}^{-1}(W/2H_{2i}) \quad (3.3-14)$$

Following the equation (3.3-9) the emission rays angle outside the reaction chamber is:

$$\beta'_{\Omega} = 2 \cdot \sin^{-1}((n/n_{RC}) \cdot \sin(\text{tg}^{-1}(W/2H_{2i}))) \quad (3.3-15)$$

The distance between the lens and OCM of the layer i is:

$$p_i = H_1 + H_{2i} \quad (3.3-16)$$

The lens with aperture³ d , located at the distance p_i from the OCM of the layer i , collects the rays with numerical aperture:

$$\alpha_{\Omega i} = 2 \cdot \text{tg}^{-1}(d/2p_i) \quad (3.3-17)$$

Lets defined the angle $\alpha\beta_{\Omega i}$ as:

$$\alpha\beta_{\Omega i} = \min(\alpha_{\Omega i}, \beta'_{\Omega i}) \quad (3.3-18)$$

The rays emitted from the OCM of layer i that inside the angle inside the angle $\alpha\beta_{\Omega i}$ are redirected to the light-sensing device, as shown on the figure below:

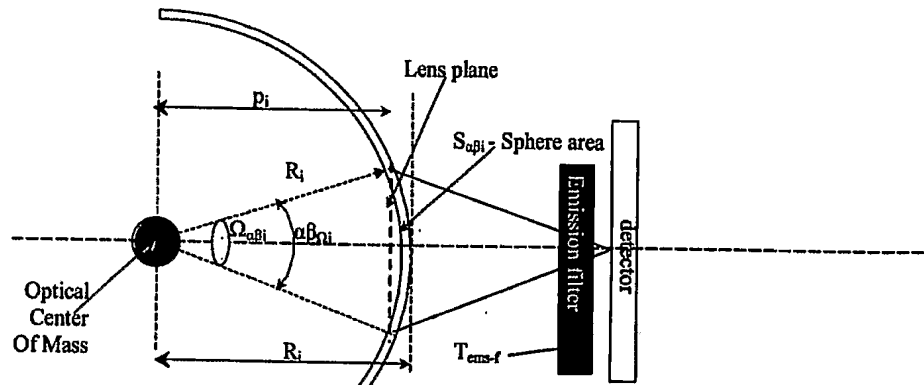


Figure 3.3-12: Emission Scattering Solid Angle

Generally, the bio-emission rays are scattered uniformly toward the all directions. Therefore, the fraction of the bio-emission energy is redirected to the detector to the total energy is:

$$F_{GFP} = \frac{\Omega_{\alpha\beta i}}{4\pi} \quad (3.3-19)$$

The solid angle $\Omega_{\alpha\beta i}$ corresponding to the angle $\alpha\beta_{\Omega i}$ is expressed by:

$$\Omega_{\alpha\beta i} = \frac{S_{\alpha\beta i}}{R_i^2} = \frac{\int_0^{2\pi} \int_0^{0.5\alpha\beta_{\Omega i}} R_i \sin(\theta) d\phi \cdot \int_0^{0.5\alpha\beta_{\Omega i}} R_i d\theta}{R_i^2} = 2\pi(1 - \cos(0.5\alpha\beta_{\Omega i})) \quad (3.3-20)$$

³ Generally, the video-lens aperture is expressed as $f/\#$ (f-number). The approximated formula of the f-number is: $f/\# = f/d$. Therefore in case of the video lens the front lens diameter is: $d = f/(f/\#)$

3.3.5.3 Absorption Of The Excitation Energy And Bio-Emission Generation

In the previous sub-sections describing the model the ray tracing and optical parameter calculations were presented. In order to complete the model characterizing the optical features of the bio-emission, here we show how it's generated.

The factors T_{exc} & T_{ems} are indicates the optical transmittance⁴ of the reaction chamber medium for the excitation and emission spectrums. Their values could be extracted experimentally.

The energy of the photon at the wavelength λ is:

$$E_{ph}(\lambda) = \frac{h \cdot c}{\lambda} \quad (3.3-21)$$

Therefore, the energy⁵ of the excitation photon at the wavelength of $\lambda_{exc} = 470\text{nm}$ is $3.8\text{e-}19[\text{J}]$. Lets assume that filtered excitation energy supplied by the optical fiber. The optical power P_{fiber} is measured with the optical power meter from the output of the optical fiber. The photon flux [photons/sec] of the excitation energy is expressed as:

$$I_{exc} = \frac{P_{fiber}}{E_{ph}(\lambda_{exc})} \quad (3.3-22)$$

The excitation optical power I_{exc} is applied to the reaction chamber cylinder. The reaction chamber cylinder is defined according to diameter W and height H . The energy is absorbed by the medium⁶ of the reaction chamber and by the biosensors. The bio-emission is occurs when the excitation photons are absorbed by GFP molecules distributed inside the biosensor.

Therefore the bio-emission is proportional to the (x-y) projection area⁷ of the GFP molecules. The maximal (x-y) projection area occurred for the biosensor saturated by the GFP molecules. It is also depends on the concentration of the biosensors inside the reaction chamber. In other words it depends on the number of bacteria in the layer $i - B_{layer}$ is:

$$B_{layer} = \frac{B_{RC}}{N_{layers}} \quad (3.3-23)$$

Where B_{RC} is a number of biosensors in the reaction chamber. For the cube form of the biosensor, with the rib d_b , the maximum absorption by the GFP molecules of the layer i is:

⁴ The transmittance is defined per unit length of the beam path

⁵ The photon energy is expressed in J or W/s units

⁶ This is expressed by T_{exc} transmission parameter

⁷ The (x-y) projection area is perpendicular to the excitation photons beam

$$A_{GFP-max-i} = \frac{d_b^2 \cdot B_{layer}}{\pi \cdot (W/2)^2} \quad (3.3-24)$$

The maximal absorption is occurs for the biosensor completely saturated⁸ by the GFP molecules. The efficiency of the bio-chemical reaction is proportional to the percentage of the biosensor saturation by the GFP molecules. The percentage of the saturation in layer i is signed as n_{GFP-i} . Therefore the absorption by the GFP molecules in the layer i is expressed as:

$$A_{GFP-i} = A_{GFP-max-i} \cdot n_{GFP-i} \quad (3.3-25)$$

Assuming that n_{GFP-i} is the same for the all layers, the n_{GFP} variable will be used. The value of the n_{GFP} could be in range [0:1]. The meaning of $n_{GFP} = 0$ is that GFP molecules were not generated at all. If $n_{GFP} = 1$, the whole cell biosensor is saturated by GFP molecules and the absorption is maximal - $A_{GFP-max-i}$.

The excitation energy beam is attenuated by the medium of the reaction chamber and by the biosensors. We will assume that attenuation due to the reaction chamber medium is dominant and therefore the attenuation expressed as:

$$I_{exc-i} = I_{exc-i-1} \cdot T_{exc}(\Delta h) = I_{exc} \cdot T_{exc}^{i-1}(\Delta h) \quad (3.3-26)$$

Now the maximal bio-emission, scattering in 4π solid angle, could be expressed as:

$$I_{ems-max-i} = A_{GFP-max-i} \cdot I_{exc-i} \cdot EmQE \quad (3.3-27)$$

Where the $EmQE$ is the emission quantum efficiency represented in the "Section 3.3.5.1". The bio-emission intensity as function of the bio-chemical reaction efficiency is expressed as:

$$I_{ems-i} = I_{ems-max-i} \cdot n_{GFP} \quad (3.3-28)$$

The direction of photon emitted by GFP molecule is random. Therefore the emission scattering solid angle is 4π . Just small portion of emission will reach the pixel of the light quantification device. This portion depends on optical setup between the reaction chamber and light quantification device. The various optical setups will be described and analyzed in the "Section 3.3.6".

⁸ The meaning of complete saturation is filling the (x-y) plane area by GFP molecules projections

3.3.6 Optical Setups For Light Collection

The main function of the light collection optics is to project the bio-emission light on the light-sensing device surface. The rays of the excitation light should be attenuated as more as possible. The following methods were tested for that goal: (i) direct coupling between the reaction chambers to the light-sensing device; (ii) video-Lens transforming the biological signal from all reaction chambers to the light-sensing device simultaneously; (iii) mLens – the small lens with diameter $\times 2$ larger than the reaction chamber. It projects the bio-emission from the reaction chamber to the light-sensing device. The number of the mLens is equal to the number of the reaction chambers.

The model of the bio-fluorescence integrated system was presented in the previous section. Now let's compare the model performance as function of the optical setup for the bio-emission light collection. In value $n_{GFP} = 1$ will be used for during the comparison.

Before we will discuss the optical setups let's remember the relevant geometrical optics theory. Schematics of the thick lens imaging is presented below:

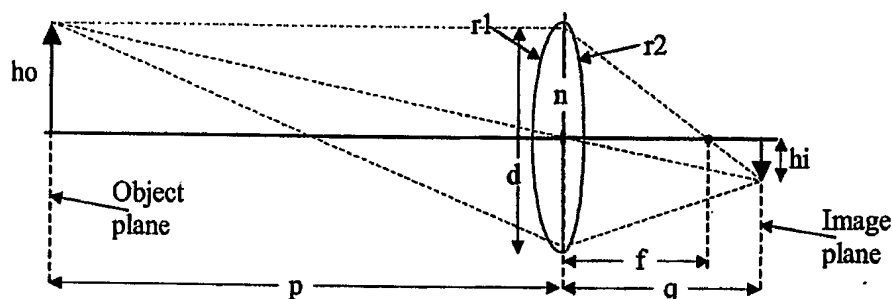


Figure 3.3-13: The Thick Lens Parameters Schematics

The focal length of the lens depends on radii of the left and right surface (r_1 , r_2) and the n number of the material:

$$\frac{1}{f} = (n-1) \left(\frac{1}{r_1} - \frac{1}{r_2} \right) \quad (3.3-29)$$

The object (p) and image (q) distances combinations are depends on the focal:

$$\frac{1}{p} + \frac{1}{q} = \frac{1}{f} \quad (3.3-30)$$

The object could be larger then the physical area of the detector. Therefore in order to project the complete object on the detector the magnification is required:

$$m = h_i/h_o = -q/p \quad (3.3-31)$$

The excitation and emission light that have been projected to the detector spreads over S_{em-det} and $S_{exc-det}$ areas correspondingly. In case that the projection area of the bio-emission is the same as source area it expressed by:

$$S_{ems-det} = \pi \cdot (W/2)^2 \quad (3.3-32)$$

The light-sensing device is divided by pixels of area S_{px} . We are interested to find the excitation and emission energy per single pixel in the “Region Of Interest” (ROI³). Using the assumption that the energy distributed uniformly per detector the energies per pixel are:

$$I_{exc-px} = I_{exc-det} \cdot (S_{px}/S_{exc-det}) \quad (3.3-33)$$

$$I_{ems-max-px} = I_{ems-max-det} \cdot (S_{px}/S_{ems-det}) \quad (3.3-34)$$

3.3.6.1 Direct Coupling Between The Reaction Chamber And Light Quantification Device

The setup of such configuration is presented on the figure below:

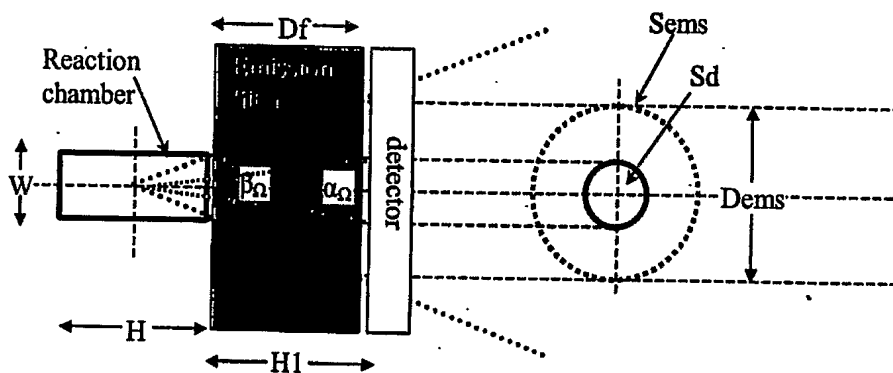


Figure 3.3-14: The Direct Coupling Optical Setup

The emission filter is separating between the reaction chamber and light quantification device (detector). The emission filter must be as thin as possible otherwise two problems appear: (i) most of the bio-emission energy is lost; (ii) the cross-talks of the bio-emission between the reaction chambers are occurs. The last presented on the figure below:

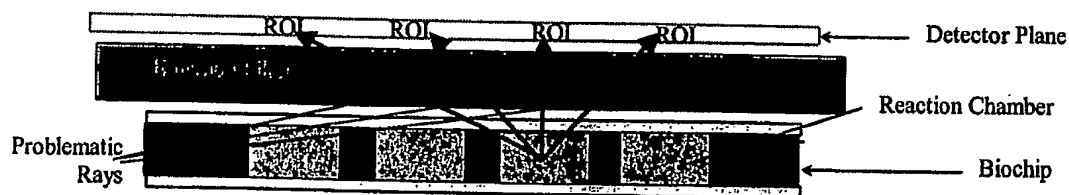


Figure 3.3-15: The Bio-Emission Cross-Talks Problem

⁹ ROI – Region Of Interest is the projection of the reaction chamber object on the imager

In case of the thick filter the beehive structure could be constructed to eliminate the crosstalk. The bio-emission intensity of the layer i is:

$$I_{ems-max-no-lens-det-i} = I_{ems-max-i} \cdot T_{ems}(H_{2l}) \cdot \frac{\Omega_{aff}}{4\pi} \cdot T_{Fem4ems} \quad (3.3-35)$$

While the T_{ems} is the transmission of the emission rays inside the reaction chamber medium and $T_{Fem4ems}$ is transmittance of the filter for emission. Both coefficients were presented in the "Section 3.3.5.1: Optical Parameters Calculation". The total emission energy reaching the detector is the superposition of contributions of the all layers:

$$I_{ems-max-no-lens-det} = \sum_{i=1}^{i=N_{layers}} I_{ems-max-no-lens-det-i} \quad (3.3-36)$$

The rays of the excitation light are parallel and projected on the detector surface as shown on the figure below:

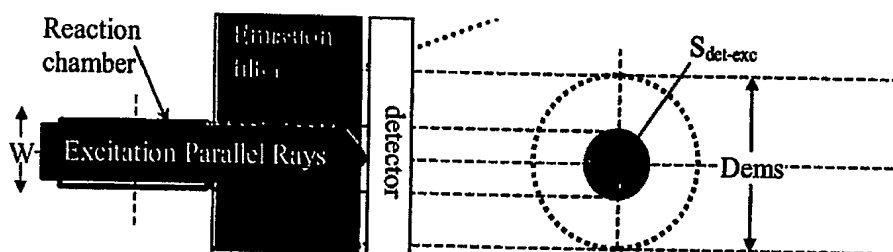


Figure 3.3-16: Projection Of The Excitation Light Parallel Rays

The scattering area of the excitation rays is:

$$S_{exc-det} = \pi \cdot (W/2)^2 \quad (3.3-37)$$

The excitation energy after the reaction chamber is $I_{exc-N_{layers}}$. The emission filter attenuates most of the excitation energy. The unfiltered and unabsorbed excitation energy reaching the detector is expressed as:

$$I_{exc-no-lens-det} = I_{exc-N_{layers}} \cdot T_{Fems4exc} \quad (3.3-38)$$

The Quantum Efficiency (QE) of the detector is depends on the wavelength. Therefore there is a different sensitivity of the detector to excitation and emission energies. The QE_{ems} and QE_{exc} are QE of emission and excitation correspondingly and expressed at the "Section 3.3.5.1". The intensities projected per single pixel of detector calculated according the equations: (3.3-33) & (3.3-34). The ratio between the emission and excitation intensities is:

$$R_{ems/exc-no-lens} = \frac{I_{ems-max-no-lens-px} \cdot QE_{ems}}{I_{exc-no-lens-px} \cdot QE_{exc}} \cdot n_{GFP} \quad (3.3-39)$$

3.3.6.2 The Video-Lens

The TAU-TMS integrated system optical part is based on the video-lens. The video-lens supplies the simplest solution for fluorescence imaging. It simultaneously projects the bio-emission from all reaction chambers to the image sensor. There is no problem with the crosstalk. In addition the video-lens with low f-number can collect a significant part of bio-emission energy. However, the integrated system cannot be miniaturized due to the video lens dimensions. The optical setup based on that video-lens is shown on the figure below:

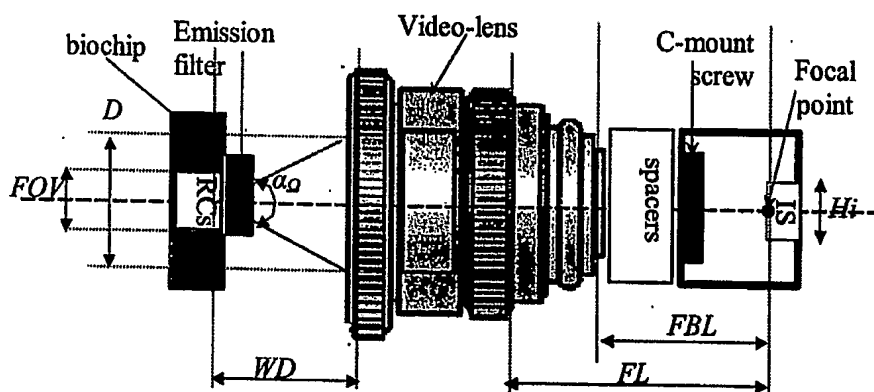


Figure 3.3-17: Optical Setup Based On The Video-Lens

The spacers used with the video-lens in order to provide the required magnification between the object - FOV and image - Hi . The video-lens is placed at the working distance (WD) from the biochip. The maximal aperture of the lens is $D = FL/(f/\#)$. Now all the parameters are known for the model presented in the "Section 3.3.5". The video-lens transmission is T_{vlens} . The contribution of the layer i to the bio-emission reaching the detector calculated according to:

$$I_{ems-max-vlens-det-i} = I_{ems-max-i} \cdot T_{ems}(H_{2i}) \cdot \frac{\Omega_{afi}}{4\pi} \cdot T_{vlens} \cdot T_{Fems4ems} \quad (3.3-40)$$

The total emission energy reaching the detector is:

$$I_{ems-max-vlens-det} = \sum_{i=1}^{i=N_{layers}} I_{ems-max-vlens-det-i} \quad (3.3-41)$$

The video-lens with the spacers tuned on the finite distant object. The parallel excitation rays are distracted as shown below:

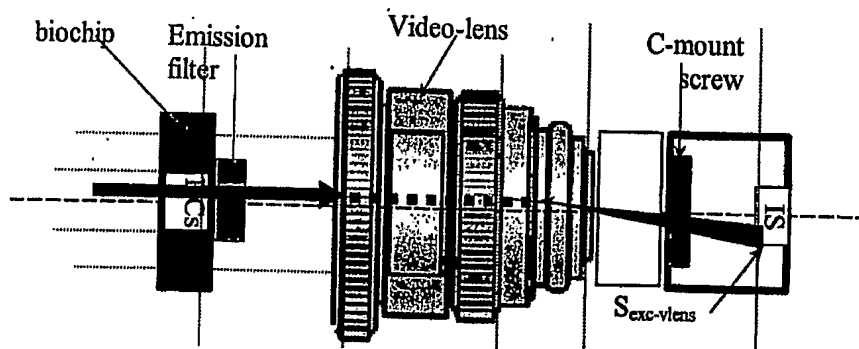


Figure 3.3-18: Distraction Of The Excitation Parallel Rays

The calculation of the parallel rays projection on the detector is a complicated task. However it could be received by simple picture capture. For the system performance estimation we will assume that there is no distraction. Therefore the simple equation could be used:

$$I_{exc-vlens-det} = I_{exc-N_{layers}} \cdot T_{vlens} \cdot T_{Fem4exc} \quad (3.3-42)$$

The ratio between the emission and excitation intensities sensed by the pixel is:

$$R_{ems/exc-vlens} = \frac{I_{ems-max-vlens-px} \cdot QE_{ems}}{I_{exc-vlens-px} \cdot QE_{exc}} \cdot n_{GFP} \quad (3.3-43)$$

3.3.6.3 The Matrix Of mLenses

The optical system with mLenses is used for the miniaturization of the integrated system and elimination of the bio-emission cross-talk problem. The side view of the optical system implemented in TAU-WTA integrated system presented below:

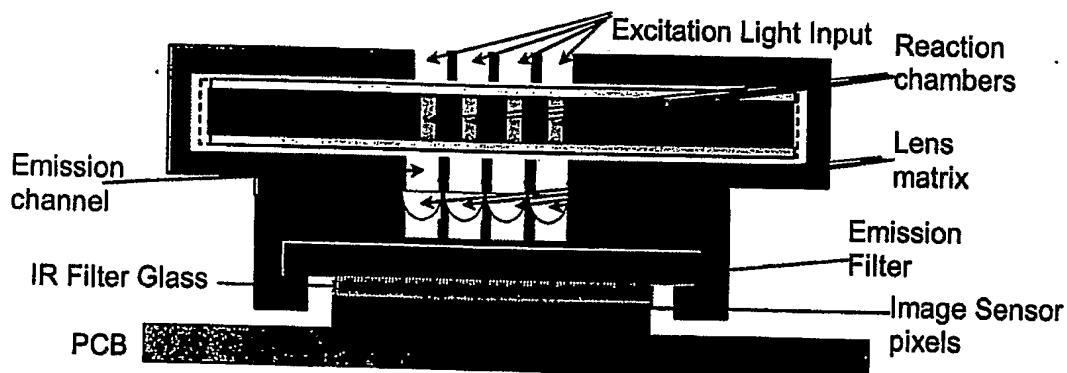


Figure 3.3-19: The Physical Layout Of m-Lens Matrix Based Optical System

The matrix of 4x4 mLens was implemented in the TAU-WTA integrated system. The optical design presented below for the single lens:

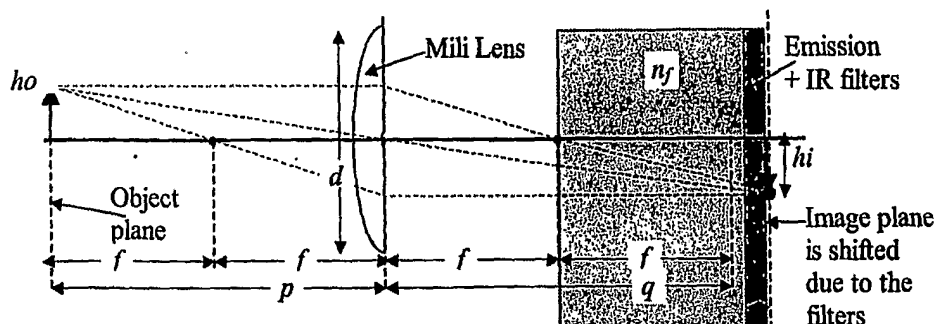


Figure 3.3-20: The Single mLens Optical Path

The object plane is the reaction chamber internal layer close to the bottom surface. The focus will be valid just for the bottom layers of the reaction chamber. Lets present the astigmatism due to the other layers:

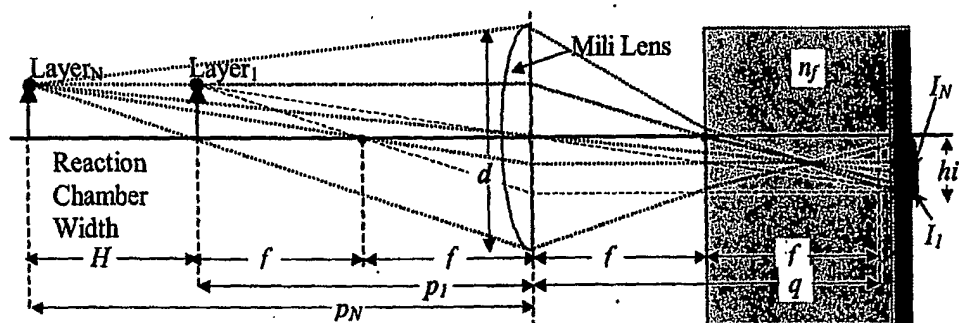


Figure 3.3-21: The Astigmatism Created By The Top Reaction Chamber Layers

As could be seen from the picture above the clear image from the top layer couldn't be accepted. However the energy is still redistributed over the region of interest on the detector.

The schematics of the optical power collection presented below.

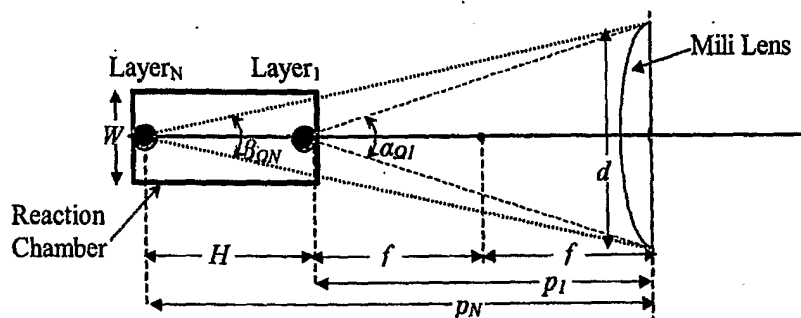


Figure 3.3-22: The Optical Power Collection Schematics

The contribution of the layer i to the emission projected on the detector is:

$$I_{ems-max-mlens-det-i} = I_{ems-max-i} \cdot T_{ems}(H_{21}) \cdot \frac{\Omega_{eff}}{4\pi} \cdot T_{mlens} \cdot T_{Fem4ems} \quad (3.3-44)$$

The total emission energy reaching the detector is:

$$I_{ems-max-mlens-det} = \sum_{i=1}^{i=N_{layers}} I_{ems-max-mlens-det-i} \quad (3.3-45)$$

3.3.6.3.1 The mLens Optical System Inefficiency To Excitation Rays

The optical-mechanical configuration presented on the Figure 3.3-19 eliminates the bio-emission cross-talks. However it has a design leakage. The optical path of the parallel rays passing the mLens is shown on the figure below:

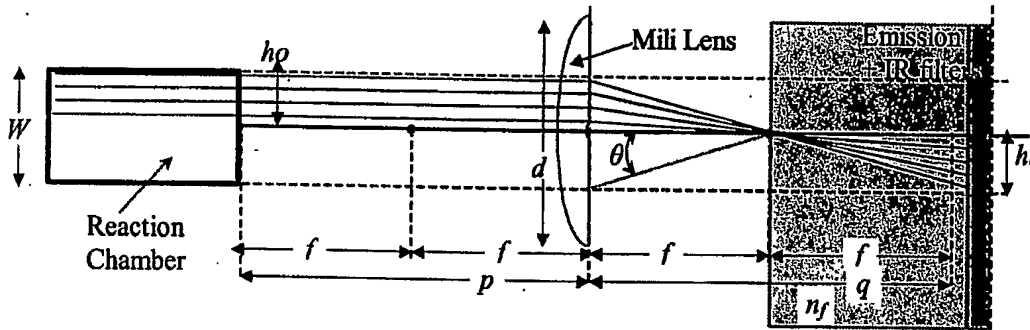


Figure 3.3-23: Excitation Parallel Rays Optical Path

The mLens focusing the parallel excitation rays and then they spread on the detector over the distance $2h_i$ that equal to W . Therefore the projection area on the detector is:

$$S_{det-exc} = \pi \cdot (W/2)^2 \quad (3.3-46)$$

We have to note that the after the lens the rays are not perpendicular to the emission filter. Therefore the emission filter attenuation for the excitation light is decreases. The filter attenuation as function of the incidence angle is an issue for the further research. Currently the excitation reference will be captured and subtracted. For the calculations the factor $K_{angle}(\theta) > 1$ will be used. The excitation intensity reaching the detector is:

$$I_{exc-mlens-det} = I_{exc-N_{layers}} \cdot T_{mlens} \cdot T_{Fems4exc} \cdot K_{angle}(\theta) \quad (3.3-47)$$

The ratio between the emission and excitation intensities measured by the pixel is:

$$R_{ems / exc-mlens} = \frac{I_{ems-max-mlens-px} \cdot QE_{ems}}{I_{exc-mlens-px} \cdot QE_{exc}} \cdot n_{GFP} \quad (3.3-48)$$

In the subsequent section we will show how to handle the problem of the emission filter ineffectiveness to the redirected excitation rays.

3.3.6.3.2 Placing The Emission Filter In Front Of mLens

Placing the emission filter in front of mLens solves the filter inefficiency problem. However it reduce the effectiveness of the emission cross-talk elimination. This solution is applicable for mLens with long focal length and thin emission filter, as shown below:

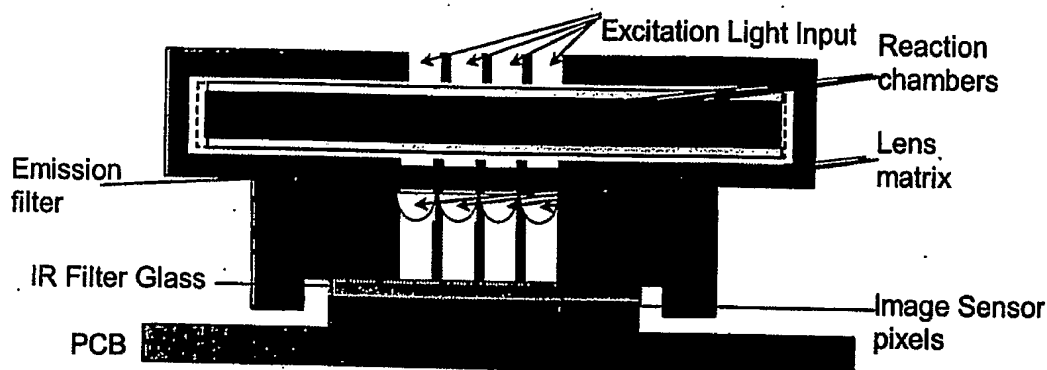


Figure 3.3-24: The Emission Filter In Front Of mLens Design

The schematics of suggested solution is illustrated on the Figure 3.3-25 below:

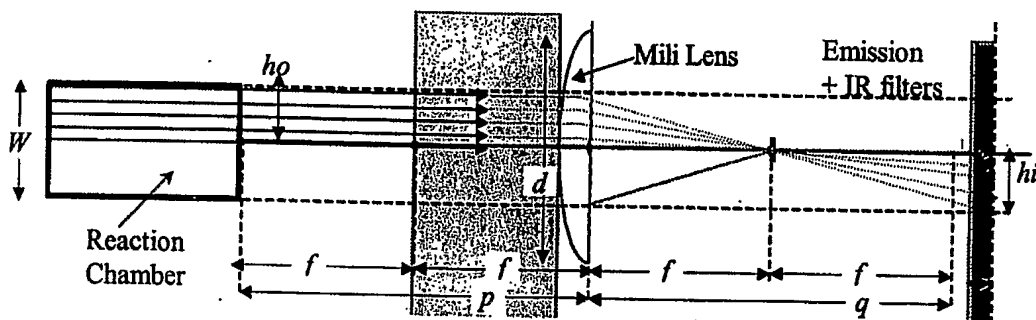


Figure 3.3-25: Blocking The Excitation Rays

In this case the unfiltered excitation intensity reaching the detector will be:

$$I_{exc-mLens-det} = I_{exc-N_{layers}} \cdot T_{mLens} \cdot T_{Fem4exc} \quad (3.3-49)$$

The suggested method is handles the emission filter inefficiency problem on behaves of the cross-talk elimination. In the next section we are suggesting solution figuring out the both design leakages.

3.3.6.3.3 The Elimination Of The Excitation Rays By Spatial Filtering

As was already mentioned in the "Section 3.3.6.3.1" the parallel excitation rays are redirected to the focal point by the mLens. Therefore the excitation rays could be spatially filtered. The spatial filter could be implemented by placing a light blocking spot exactly in the focal point, as shown on the figure below:

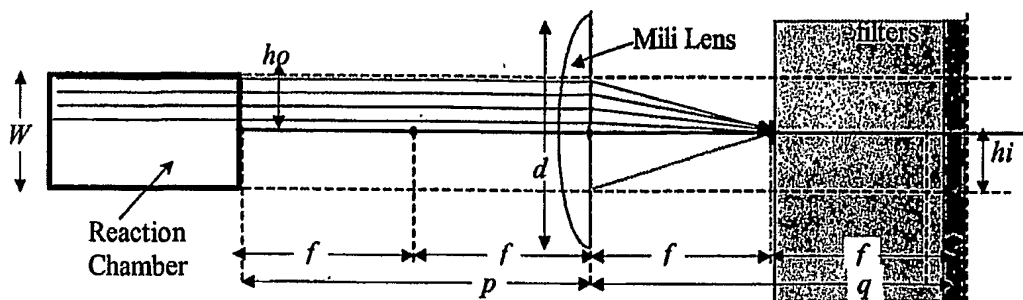


Figure 3.3-26: Spatial Filtering Of The Excitation Rays

Instead of the blocking spot, mirror could be used. The excitation rays will be returned back through the lens and redirected to parallel rays. The parallel rays will pass again through the reaction chamber and will double the emission.

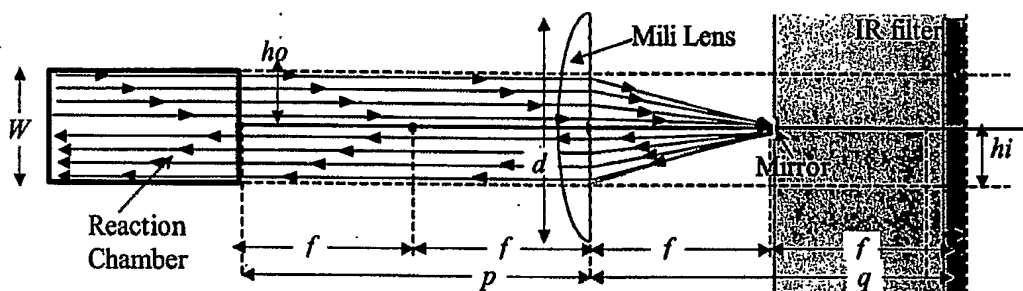


Figure 3.3-27: Spatial Filtering Of The Excitation Rays And Emission Doubling

The optical system is never ideal. In addition, the excitation rays are diffracted and would not be directed exactly into the blocking spot. Therefore part of the excitation energy is still will be transmitted to the detector. That could be found experimentally as function of the blocking spot size. Lets define the parameter $K_{exc-irs}(D_{block})$ that indicates the attenuation of the spatial filter. The excitation energy reaching the detector:

$$I_{exc-m lens-blocking-det} = I_{exc-N_{layers}} \cdot T_{mlens} \cdot T_{Fems4exc} \cdot K_{exc-irs}(D_{block}) \quad (3.3-50)$$

The blocking spot will also block part of the bio-emission rays as shown below:

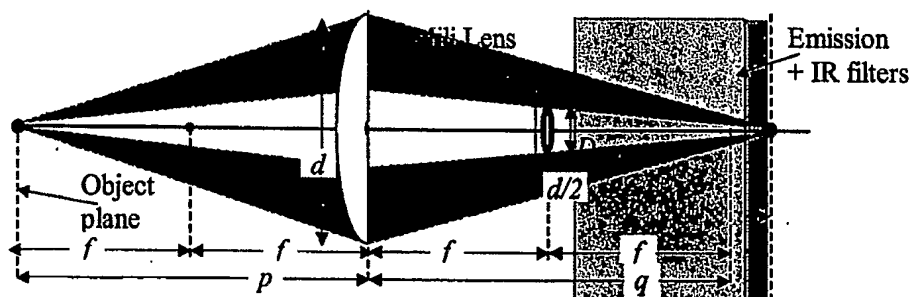


Figure 3.3-28: The Emission Rays Blocking

The emission transmission approximation is:

$$K_{ems-trs} = 1 - \left(\frac{D_{block}}{d/2} \right)^2 \quad (3.3-51)$$

And the resulted bio-emission reaching the detector calculated according to:

$$I_{ems-max-m-lens-blocking-det} = I_{ems-max-m-lens-det} \cdot K_{ems-trs} \cdot K_{mirror}(D_{block}) \quad (3.3-52)$$

The K_{mirror} is a coefficient indicating the excitation rays refraction efficiency. The coefficient is in range $K_{mirror}(D_{block}) < 2$, depends on the mirror diameter and refraction feature.

3.3.7 Performance Comparison Of The Optical Setups

Three types of optical setups were presented in previous sections. The last, based on the mLens, has additional derivatives improving the performance. We would like to compare between the optical systems.

3.3.7.1 The Theory

The sensitivity to the bio-emission is the main requirement from the electro-optical system. The bio-emission is proportional to the biochemical reaction intensity expressed by the n_{GFP} parameter. The minimal sensitivity is defined as ability to extract signal masked in signal uncertainty. The signal uncertainty assembled from a variety of factors listed at the "Section 3.8.1: Bio-Fluorescence Signal Uncertainties".

The signal uncertainty will be marked as I_{unc-px} . The precise signal uncertainty analysis hasn't been done yet. It's an issue for the advanced research. However will assume that uncertainty is proportional to the unfiltered excitation intensity sensed by the detectors pixel:

$$I_{unc-px} = Un2B \cdot I_{exc-px} \cdot QE_{exc} \quad (3.3-53)$$

The sensed bio-emission must be $S2Un$ times stronger that the signal uncertainty:

$$I_{ems-px} \cdot QE_{ems} \geq S2Un \cdot I_{unc-px} \quad (3.3-54)$$

The bio-emission intensity is proportional to the n_{GFP} , therefore we have:

$$\{ I_{ems-px} = I_{ems-max-px} \cdot n_{GFP} \} \& \{ R_{ems/exc} = R_{ems-max/exc} \cdot n_{GFP} \} \quad (3.3-55)$$

Combining the equations (3.3-53), (3.3-54) and (3.3-55) we will get:

$$\frac{I_{ems-max-px} \cdot QE_{ems}}{I_{exc-px} \cdot QE_{exc}} \cdot n_{GFP} \geq S2Un \cdot Un2B \quad (3.3-56)$$

Following the equation (3.3-48) and (3.3-55) we got:

$$R_{ems-max/exc} \cdot n_{GFP} = S2Un \cdot Un2B \quad (3.3-57)$$

Where $R_{ems-max/exc}$ is a constant that depends on the optical setup. Therefore the minimal optical system sensitivity to the bio-chemical reaction is expressed by:

$$n_{GFP-min} = \frac{S2Un \cdot Un2B}{R_{ems-max/exc}} \quad (3.3-58)$$

We will require the signal to uncertainty: $S2Un = 2$ and will assume that uncertainty to unfiltered excitation intensity is: $Un2B = 0.5$. The $R_{ems-max/exc}$ will be calculated to the each optical setup according to formulas received in the previous sections. Lets compare the optical systems minimal sensitivities.

3.3.7.2 The Lens free, V-Lens And mLens Based Optical Systems

The spectrum equivalent parameters are presented at the "Section 3.3.5.1". They are concentrated in the table below:

Table 3.3-1: Spectrum Equivalent Parameters

Kind	Description	Variable	Value
Fixed	ExEms Quantum efficiency	EmQE	0.43
Fixed	Emission Filter Transmission 4 Excitation	TFems4exc	1.80E-05
Fixed	Emission Filter Transmission 4 Emission	TFems4ems	5.62E-01
Fixed	Detector QE superposition 4 Emission	QEems	0.35
Fixed	Detector QE superposition 4 Excitation	QEexc	0.30
Fixed	Transmission Of Medium 4 Excitation	Texc	0.99
Fixed	Transmission Of Medium 4 Emission	Tems	0.99

We will compare the optical system sensitivities for different reaction chambers geometries represented by the H – heights & W – diameter cylindrical dimensions.

Table 3.3-2: Optical Systems Minimal Sensitivities Comparison

Worksheet	W	H	nGFPmin			
			no lens	lens	lens (f2/d4)	lens (f1/d4)
h2-w1-fX-d2	1.00	2.00	12.95%	0.21%	5.26%	1.89%
h1-w1-fX-d2	1.00	1.00	21.59%	0.35%	9.18%	3.00%
h0.5-w1-fX-d2	1.00	0.50	38.70%	0.69%	16.97%	5.21%

Analyzing the results, the following conclusions could be done: (i) reaction chamber height has almost linear influence on the sensitivity; (ii) the best sensitivity is for

configuration with video lens. It x30 higher than mLens and x100 higher than without lens based case; (iii) the mLens with focal distance of 1mm provides x3 more sensitivity than that with focal distance of 2mm.

3.3.7.3 The mLens Based Optical Systems With Spatial Filter

The spatial filter for the excitation rays has been presented at the "Section 3.3.6.3.3" It could be used in case that the emission filters thickness is less than focal length of the mLens. The spatial filter efficiency depends on the diameter of the blocking spot. Therefore the blocking spot diameter has influence on the minimal sensitivity of the mLens based system. The comparison of the sensitivities for the different diameters of the blocking spots concentrated in the table below:

Table 3.3-3: Sensitivity Comparison For The mLens Based System With Spatial Filter

Blocking Spot Diameter (mm)	Excitation Filter Transmittance (%)	Emission Filter Transmittance (%)	Focal Length (mm)	nGFPmin (%)
0.05	99.90%	99.75%	1.00	5.26%
0.10	98.00%	99.00%	1.01	5.20%
0.20	90.00%	96.00%	1.07	4.93%
0.40	40.00%	84.00%	2.10	2.50%
0.50	10.00%	75.00%	7.50	0.70%
0.60	2.00%	64.00%	32.00	0.16%
0.70	0.50%	51.00%	102.00	0.05%
0.80	0.05%	36.00%	720.00	0.007%
0.90	0.01%	19.00%	3800.00	0.001%
0.99	0.00%	1.99%	1990.00	0.003%

Notes: (1) Currently this coefficient is estimated. Will be investigated at the advanced research stage.

According to the estimated results, the blocking point of 0.6mm diameter provides better performance than Video-lens based optical system. The spatial filtering method could dramatically improve the sensitivity of the electro-optical system. Therefore the spatial filtering is the issue for advanced research.

3.4 Temperature Control

The integrated system includes three modules requiring temperature control for stable biological signal generation and measurement. Currently, the integrated system is designed to work under laboratory conditions with ambient temperature in range of +20°C to +30°C. The modules and the temperature control requirements are presented in the table below:

Table 3.4-1: The Modules Requiring Temperature Control In The Integrated System

#	Module	Temperature Control Requirement	Max ΔT
1	Image Sensor	Stable temperature regulated in the range of -15 to +25°C	- 45°C/+5°C
2	LED assembly	Stable temperature regulated in the range of +15 to +25°C	- 10°C/+5°C
3	Bio-house	Stable temperature regulated in the range of +15 to +35°C	-10°C/ +15°C

The thermoelectric cooler (TEC) was selected as core component providing the temperature control solution. We use a Peltier type TEC that uses semiconductor heat pumps [29]. The TEC has "cold" and "hot" surfaces, while the "cold" side coupled to the target module and "hot" to the heat sink.

In order to select the TEC and the heat sink we define the cooling requirements based on heat generated. There are active and passive heat loads. Calculations are presented for both transient and steady states. The TEC and heat sink selection process for IBIS4 CMOS Image Sensor is demonstrated below for steady state cooling requirement of $\Delta T = 45^\circ\text{C}$.

3.4.1 Selection Of TEC & Heat Sink For IBIS4 CMOS IS Cooling

The IBIS4 CMOS image sensor has the following heat dissipation parameters:

Table 3.4-2: The IBIS4 CMOS IS Thermal Related Coefficients

Parameter	Description	Value	Units
Active Load	The power dissipation of the IBIS4	0.5	W
Device Dimensions	The ceramic package dimensions $L \times W \times H$	24x24x2	mm.
Density	The ceramic package density (approximate)	2500	Kg/m ³
Specific Heat	Parameter of the ceramic package	975	J/kg*K
Ins. thickness	The thickness of the insulator	2	Mm
Ins. thermal cond.	The thermal conductivity of the insulator	0.2	W/m*K

The AZTEC simulation software was used for the calculation of the total heat power removal. The parameters concentrated in the table above were substituted into the "Power Dissipation Worksheet". The total heat power Q_c was calculated as shown on the figure below.

The screenshot shows the "Power Dissipation Worksheet" window. It contains several sections for inputting device and cooling parameters:

- Select Configuration:** Four diagrams showing different cooling scenarios: Volume Cooling (Passive Load in Insulating Container), Volume Cooling (Active Load in Insulating Container), Device Cooling (Insulated Device or Cold Plate), and Device Cooling (Uninsulated Device or Cold Plate). The "Device Cooling (Insulated Device or Cold Plate)" option is selected.
- Device Dimensions:**
 - Shape: ☒ Box, ☐ Cylinder
 - Length: 24 (mm)
 - Width (W): 24 (mm)
 - Height (H): 2 (mm)
- Cooling Requirements:**
 - Ambient Temp (Ta): 30 (°C)
 - Active Temp (Tg): -15 (°C)
 - Active Load (Watt x Area): 0.5 (W)
 - Time to cool from Ta to Td: 180 (sec)
- Insulation Properties:**
 - Thickness (t): 2 (mm)
 - Other Insulation: (dropdown menu)
 - Thermal Conductivity: 0.2 (W/m-K)
- Device Properties:**
 - Other Material: (dropdown menu)
 - Density: 2500 (kg/m³)
 - Specific Heat: 975 (J/kg-K)
- Requirement for Heat Pumped from Cold Side:**
 - Passive Heat Load (Watts): 1.41
 - Active Heat Load (Watts): 0.50
 - Steady State Heat Load @ Tc (Watts): 1.91
 - Qc Requirement (Watts): 1.91
 - Surface Area (sq cm): 22.4
 - Device Volume (cu cm): 1.2
 - Transient Heat Load (Watts): 0.70

Buttons at the bottom include "Clear Requirements", "Print", and "Return to TEC Selection".

Figure 3.4-1: Calculation Of Cold Side Heat Pumping Parameters

The total simulated heat load was $Q_c = 1.91\text{W}$. We assume $Q_c \sim 2\text{W}$ for further calculations. We assume that the TEC hot side temperature is $T_h = 35^\circ\text{C}$ and the maximum cooling temperature of -15°C therefore $\Delta T = 50^\circ\text{C}$. For a one stage TEC type the maximal temperature difference between hot and cold sides is about 64°C . This number was reasonable and therefore one stage TEC type is selected.

The Melcore Inc. CP1.0-63-06 TEC was selected¹⁰ with the following parameters: $I_{TEC-max} = 3A$, $V_{TEC-max} = 7.62V$, $Q_{TEC-max} = 12.7W$.

The calculated maximum TEC input power is 10.1W. The power dissipated into the heat sink coupled to the hot side of the TEC is the sum of the total heat load and the input power of the TEC: $Q_{HS} = 1.91 + 10.1 = 12.1W$. The heat sink resistance (HSR^{11}) is:

$$HSR = (T_h - T_a) / Q_{HS} \quad (3.4-1)$$

For our case the $T_h = 35^\circ C$, $T_a = 30^\circ C$, so $HSR = (35-30)/5.18 = 0.97[^\circ C/W]$. The standard Pentium4 CPU cooler¹² SP420B8 by Spire-Coolers [30] was selected with $HSR = 0.33[^\circ C/W]$. The margin in HSR insures the cooling system performance.

3.4.2 Selection Of The Cooling Configuration For Bio-House & LED Assembly

The maximal cooling requirement for the bio-house and LED assembly is $10^\circ C$, so low power TEC and simple heat sink without ventilator will be selected. The TEC mounting will be done from the side and not from the bottom as in case of Image Sensor. Therefore the possibility for the two TECs per cooling unit will be considered. This will create the symmetry in temperature distribution over the cooled modules.

¹⁰ The procedure for the selection of the appropriate TEC module will be described in the TAU-WTA development manual document.

¹¹ Measure of the ability of the sink to dissipate the applied heat

¹² Heat sink with ventilator

3.5 Electronics

The electronics of the integrated system supports all the functions modules. It provides communication with a personal computer (PC), activation of the excitation light and the photoluminescence quantification device, the activation of the liquid pumping mechanism and the control of the defined temperature. It also provides a possibility to process the bio-signals and to run risk assessment algorithms, and to interface the user through a keyboard and a display. The electronics card block diagram is in the figure below:

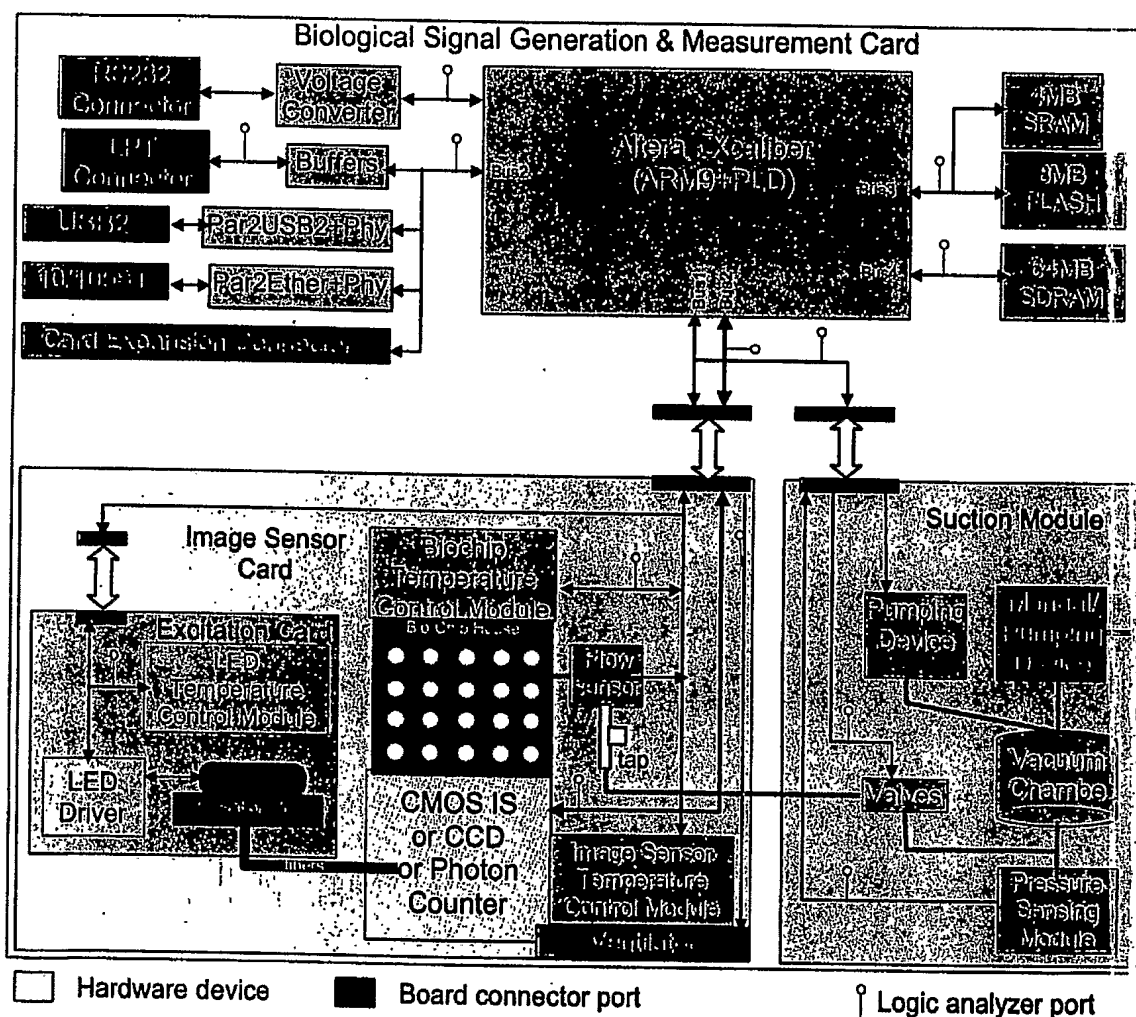


Figure 3.5-1: The Block Diagram Of The Electronics Card

The electronics card performs the following functions:

- Suction of the tested water from the sample ports of the biochip into the reaction chambers. The suction implemented on the "Suction Module". The suction module allows pumping of water with nL precision. For details refer to the "Section 3.2.5.1". The pumping activation and control electronics are described in the "Section 3.5.1".
- Temperature control for: (i) the biochip – provides a stable temperature around 25°C. This is for stabilizing the biological activity; (ii) light sensing device – a possibility to download temperature for the delta of 40°C. This allows reducing dramatically the dark current of the detector; (iii) the excitation light generation module – provides stable temperature around 25°C. This is stabilizing the emission of the excitation power.
- Activation of the excitation light and regulation of the intensity (refer to the section 3.3.3.2)
- Biological signal quantification using the following detectors: (i) IBIS4 CMOS Image Sensor by Fill-Factory. Refer to the "Section 3.3.4.1: Light Quantification Using IBIS4 CMOS IS By Fill Factory"; (ii) KAF0261 Full Frame CCD by KODAK; (iii) H7155 Photon Counting Head by Hamamatsu. Inc. (Japan)
- Communication with the PC using the following options: (i) LPT Port – main option; (ii) USB2 port – for future support; (iii) Ethernet port – for future support.
- Connectors for keypad, LCD, touch-pad expansion, not used pins of FPGA, Logic analyzer connection for the debugging.
- ARM9 microprocessor – implemented inside the Xcaliber device by Altera Inc.. Will be used for the future developments of: (1) on card bio-signal processing, (2) risk assessment management, (3) user interfacing.

3.5.1 The Suction Activation And Control Electronics

The mechanical part of the suction module is described in Figure 3.2-5: External Pumping Scheme. The electronics presented below activates and controls the suction:

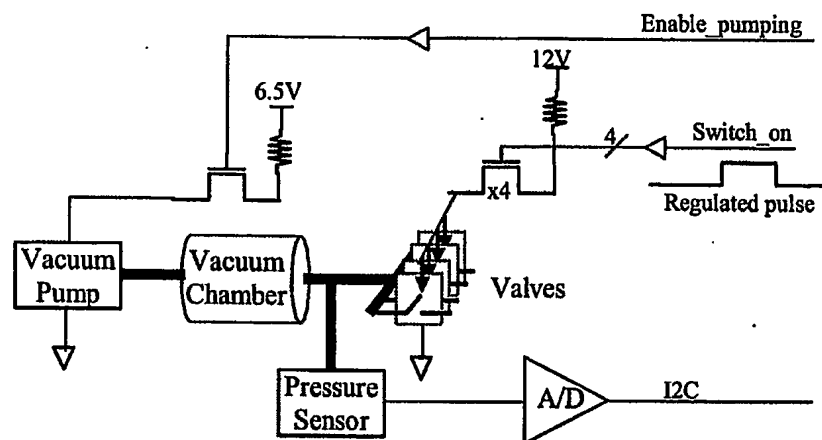


Figure 3.5-2: Electronics For The Suction Activation And Control

The vacuum pump generates the negative pressure¹³ in the vacuum chamber. The negative pressure pumping process occurs when “*Enable_pumping*” signal is in logic state ‘1’. The negative pressure in the vacuum chamber is digitally controlled. The pressure is sampled once per second and compared to the set value. When “pressure” < “set” condition is TRUE the “*Enable_pumping*” pushed to ‘0’ and vacuum pump stops the operation. The negative pressure is retained in the vacuum chamber, until valves activation.

The valves response time is 5ms. The activation is done by supply of 12V through MOS transistor gate. The MOS transistor gate is opened during the pulse applied through “*Switch_on*” signal. The pulse width is configurable with resolution of 5ms. This allows regulating the liquid suction with nL precision.

¹³ Referenced to ambient pressure

3.5.2 Temperature Control Electronics

The temperature control electronics is used for biological and electro-optical activity stabilization and optimization. The circuit is based on a Peltier Thermoelectric Cooler (TEC) that was used in our integrated system. The temperature control is based on the analog negative feedback as shown on the figure below:

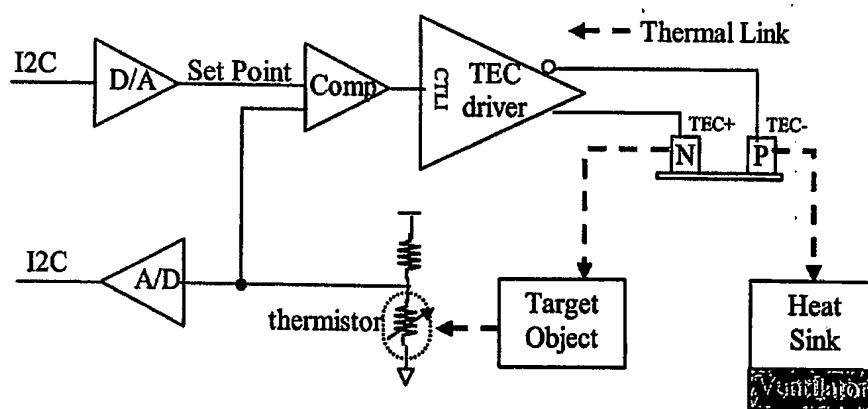


Figure 3.5-3: The Temperature Control Circuit Schematics

There are three temperature control circuits in the system: (1) LED temperature stabilization, (2) bio-house temperature stabilization and the third (3) image sensor cooling and/or temperature stabilization. In case of cooling the “hot side” of TEC is heated. The heat sink with ventilator is required to dissipate the TECs “hot side” heat.

The TEC is driven by MAX1968 chip by MAXIM[31]. The MAX1968 chip is highly integrated and cost-effective, high-efficiency, switch-mode driver. The TEC driver consist of two switching buck regulators that operate together to directly control TEC current. This configuration creates a differential voltage across the TEC, allowing bi-directional TEC current for controlled cooling and heating. The voltage at “CTLI” input directly sets the TEC current. An external thermal-control loop is used to compare the voltage at the thermistor to a set-point signal. The set point voltage is regulated through D/A. If the set-point voltage is different from the thermistor voltage, the error-correcting signal is sent to the “CTLI” input.

In addition to the analog feedback, used for the stable temperature control, the digital feedback is also implemented. The A/D converter is used to translate the voltage on the thermistor. The digitized thermistor voltage corresponds to some temperature level. The

sampled temperature controlled to the set temperature at the defined time intervals. If the temperatures are different than the analog thermal-control loop operation is failed and technician intervention required.

3.5.3 The LEDs Driver

LED driver is based on the MAX6957 chip by MAXIM [32]. The MAX6957 chip allows driving 16 LEDs independently. The external register R_{SET} allows setting the global current. Programming the MAX6957 chip through SPI interface allows defining of one of 16 intensity levels for each LED. The current driven to each LED is:

$$I_{LED} = \left(\left(\frac{936[V]}{R_{SET}} \right) / 16 \right) \cdot level \quad (3.5-1)$$

The R_{SET} resistor minimal value is 31.2K, so that the maximum segment current is 30mA. In order to make global maximal current configurable, the R_{SET} is variable. It is combined from 31.2K resistor and quad 100K I2C-potentiometer with equivalent resistance of 400K. The number of resistance levels is 1024. This allows regulating the global current between 2-30mA.

Each LED provides excitation for one functional group of the reaction chambers (refer to the "Section 3.2.7: The Reaction Chambers Functionality on the page 21). It is done by conduction of the optical fibers from LED¹⁴ harbor port to the reaction chambers harbors as shown on the Figure 3.6-1.

3.5.4 Light Quantification Devices Control And Data Acquisition

The electronics card support the three kinds of the light quantification devices. They are IBIS4 CMOS Image Sensor by Fill-Factory, KAF6021 CCD by KODAK and H7155 Photon counting head. The IBIS4 CMOS Image Sensor is partly described in the "Section 3.3.4.1".

The KAF6021 CCD and H7155 Photon counting head are not documented in that work. They will be used for very low light intensity biological signal quantification. That is the issue for the advanced researching of the luminescence reporters based biosensors.

3.5.5 PC Communication

The PC is used as host and the daughter card is used as slave. The host controls the daughter card and receives back the status and data. Currently the host \leftrightarrow daughter card

¹⁴ The excitation filter located between them

communication performed through the parallel¹⁵ port. The communication through parallel interface is limited to one full resolution frame of 1 Mega-pixel per 5 seconds. In order to improve the bandwidth the USB2 & Ethernet 10/100BT options were prepared on the daughter card. The implementation of USB2 and 10/100BT protocols will be done on the advance development stage.

In addition the Ethernet 10/100BT interface will allow activation of the daughter card through local area network.

3.5.6 Expansion Connector

The expansion connector provides possibility to upgrade the integrated system with keypad and LCD monitor. In that case the integrated system will get the Personal Digital Assistant (PDA) functionality. The additional communication devices like bluetooth, IrDA, etc are could be supported through the expansion connector too.

3.5.7 The Xcaliber Integrated ARM9 and Programmable Logic Device

The combined Programmable Logic Device (PLD) with ARM9 RISC microprocessor is used in the electronics card. Both devices are incorporated into Xcaliber chip by Altera. This allows System On Chip (SOC) emulation. The firmware developed in PLD and ARM9 core could be converted to ASIC on the advanced stage of the system development.

The firmware developed for the PLD part of Xcaliber device provides control of all functional modules: PC interface, Suction activation, LED activation, Temperature control and finally Light quantification devices support.

¹⁵ LPT port

3.6 Mechanical Design And Integration

The integrated system includes various electro-optical, mechanical, fluidics and other modules. In order to make it robust and compact special mechanical packaging sub-modules have been developed. Here is a list of the mechanical sub-modules (See Figure 3.6-1):

- Excitation – housing for super bright 5mm LEDs, excitation filter and optical fibers harboring
- “Bio”-house – insertion of the biochip into light non-transparent environment, connection to the external suction ports, harboring the second side of the excitation fibers, optical path to the light sensing module
- Light Sensing – optical path from the bio-house to the light sensors, micro-Lens array housing and the housing for the emission filter

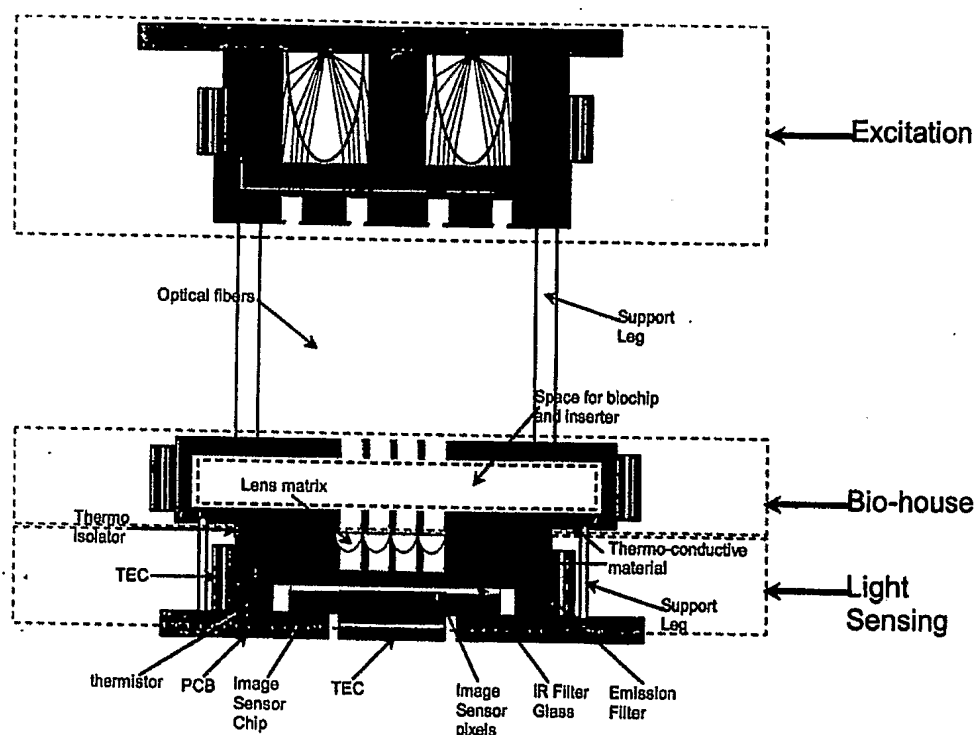


Figure 3.6-1: Excitation, Bio-House And Light Sensing Mechanical Modules Schematics

Additional two mechanical sub-modules are currently under development:

- External Suction Activation – assembly of negative pressure generation pump, vacuum chamber, valves manifold, tubes to the external suction ports. The schematics of this module shown on the Figure 3.2-5: External Pumping Scheme.

- Packaging – mechanical chassis for electronics card and mechanical sub-modules mounting, box for external protection

The assembly of the integrated system mechanics could be done according to the drawings presented below:

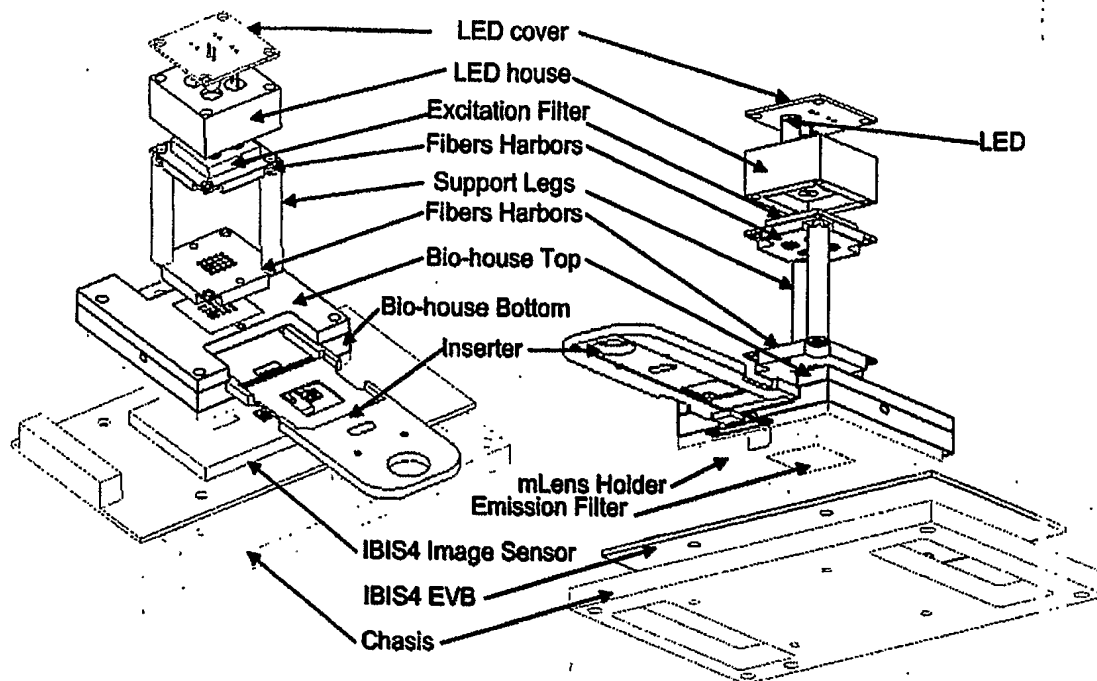


Figure 3.6-2: The Integrated System Electro-Opto Mechanical Assembly Scheme

3.7 The Software And Algorithms

A specially dedicated software was prepared at Tel-Aviv University to manage the integrated system. The software includes the Graphical User Interface (GUI), drivers for the hardware units control, tools for the biological data presentation and analysis.

Two algorithms for data processing were conceived. The algorithm for slow biological signal compression is presented in the "Sub-Section 3.7.2". The algorithm for the detection of known chemical concentration is presented in the "Sub-Section 3.7.3".

3.7.1 Graphical User Interface (GUI)

The GUI provides convenient environment for the integrated system operation. In this work the GUI for TAU-TMS GUI that currently is described. The GUI for TAU-WTA integrated system will have some additions and changes. The GUI main window shown on the figure below:

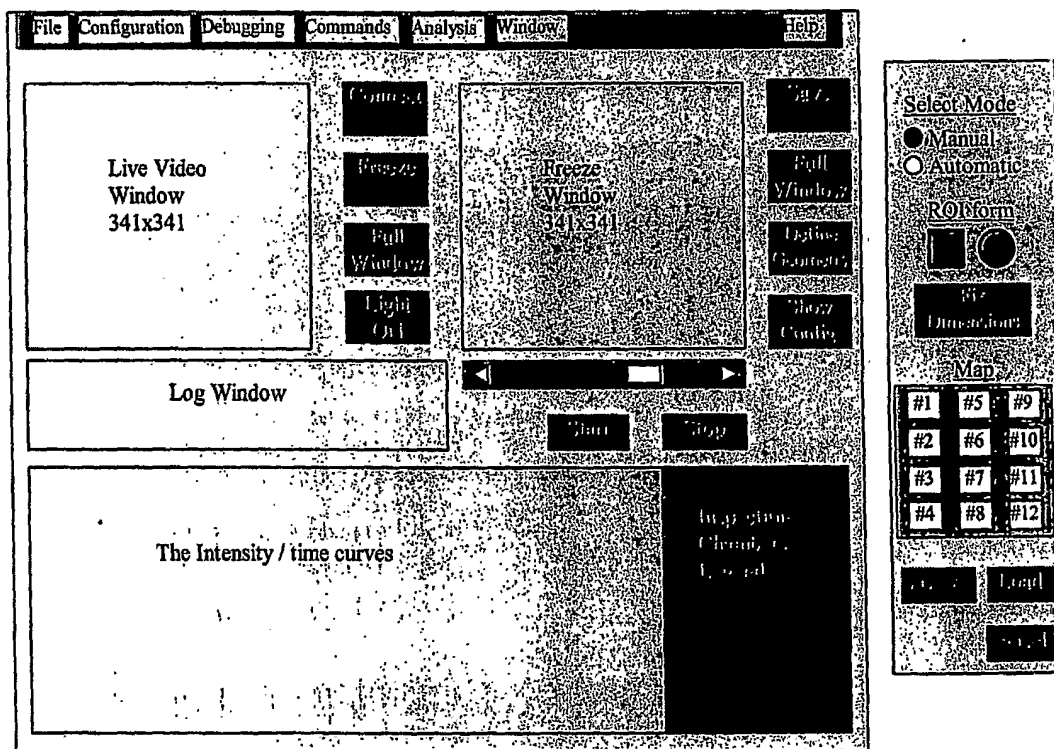


Figure 3.7-1: The Main GUI Window

The GUI main window includes the following objects:

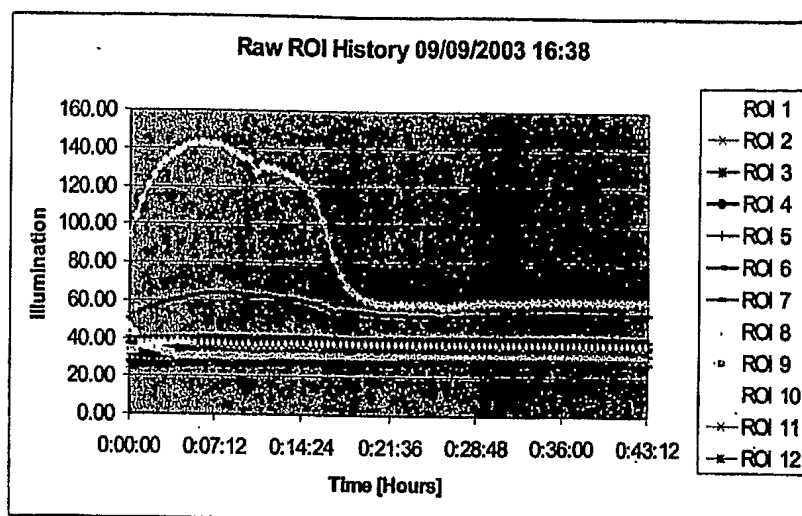
- The "Live Video" Window monitoring the events inside the reaction chambers

- The "Freeze Window" displaying the captured frames. The geometry of the reaction chambers is defined in the freeze window. The marked reaction chambers in the freeze window are named as "Region Of Interest" (ROI). The quantified emission results are displayed in corresponding ROIs. The scrolling possibility allows going over the captured frames during the experiment.
- The quantified results for each reaction chamber are displayed on the graph object as "Intensity / time curves".
- The menu of the GUI allows: (1) setting the configuration of the integrated system modules (2) save the results, and (3) load the previous experiment results for playback or demonstration.

For more information please use to TAU-TMS operational manual¹⁶.

The ASCII results of the kinetics experiment are saved into the excel file. The conditions of the integrated system operation are saved too. The ASCII data used to create the chart displaying kinetics of the bio-signal as shown on the figure below:

¹⁶ Will be prepared in the future.



	Biosensor	Biosensor concentration	Toxicant	Toxicant concentration
ROI 1	Rec-A	0.00E+00	Water	0.00E+00
ROI 2	Rec-A	0.00E+00	Water	0.00E+00
ROI 3	Rec-A	0.00E+00	Water	0.00E+00
ROI 4	Rec-A	0.00E+00	Water	0.00E+00
ROI 5	Rec-A	1.00E+08	NA	10ppm
ROI 6	Rec-A	1.00E+08	NA	10ppm
ROI 7	Rec-A	1.00E+08	NA	10ppm
ROI 8	Rec-A	1.00E+08	NA	10ppm
ROI 9	Rec-A	1.00E+08	NA	20ppm
ROI 10	Rec-A	1.00E+08	NA	20ppm
ROI 11	Rec-A	1.00E+08	NA	20ppm
ROI 12	Rec-A	1.00E+08	NA	20ppm

Figure 3.7-2: A Chart With Biological Signal Kinetics And ROI Contents

The chart supports the presentation of data in a way that shows the biological signal kinetics. Each curve's data is shown on the legend at the bottom part of the picture. The legend includes the following information: (1) biosensor type and its concentration, (2) target material and its concentration.

3.7.2 Slow Biological Signal Compression Algorithm

Usually, the slow physiological signals contribute additional information at higher frequencies. For example, the high frequency ECG techniques provides advanced heart diagnostics.

In case of our biological signal the high frequency information is screened by the signal uncertainty factors. Therefore, only slow biological signal could be processed. In this work,

an algorithm for slow biological signal is suggested. The algorithm is based on a continuous conversion of the measured data to simple polynomial approximation.

. This could be useful in the following cases:

- Reducing in some orders the memory required for the experimental data archiving.
- Provides reduced data quantity for the neuron network and fuzzy logic algorithms for signal analysis. That could increase significantly the learning process of the algorithms.
- Allows fast results presentation.

The suggested algorithm for slow biological signal compression is part of the integrated system operation software. The algorithm modules are marked by the yellow color on the drawings below:

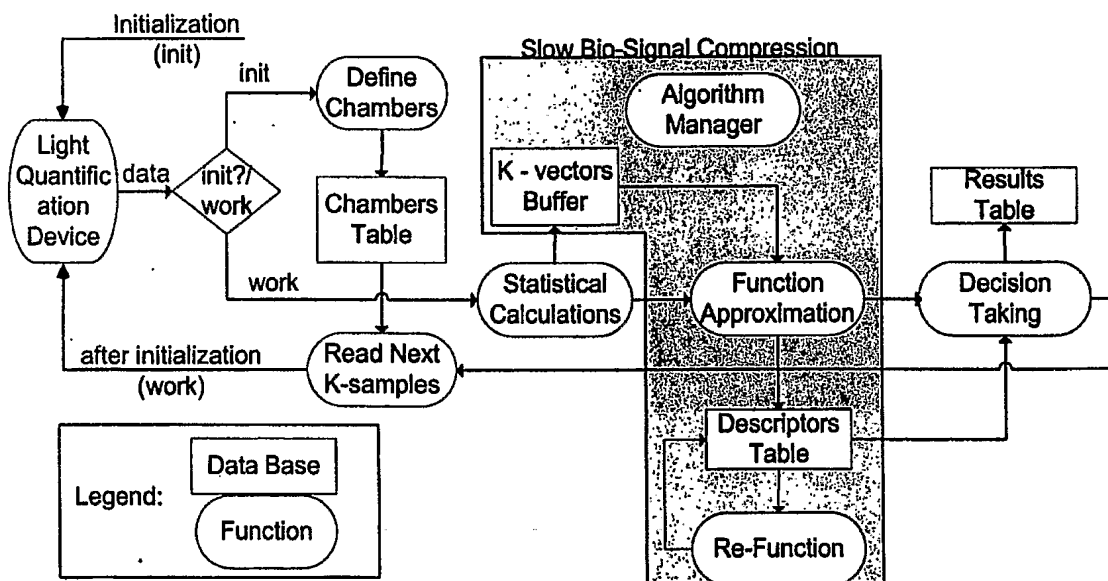


Figure 3.7-3: The Modules Of The Slow Biological Signal Compression Algorithm (Filled By Yellow)

At the initialization stage the ambient light illuminates the reaction chambers of the biochip. CMOS Image Sensor or CCD captures the picture with the biochip. For each reaction chamber the corresponding "Region Of Interest" (ROI) is defined by user or by contour recognition algorithm. After the suction of the tested liquid into the reaction chamber the biochemical reaction is occurs. The kinetics experiment is started.

The system running in loop, sampling the optical biological signal emitted from the reaction chambers. The statistical calculations¹⁷ for each ROI are performed. After collection of the K-samples the "K-samples vector" is created. The K-samples vector used as input to the "Function Approximation" module of the algorithm.

The further explanation will be done on the single reaction chamber. The example of biological signal kinetics displayed as curve on the following figure:

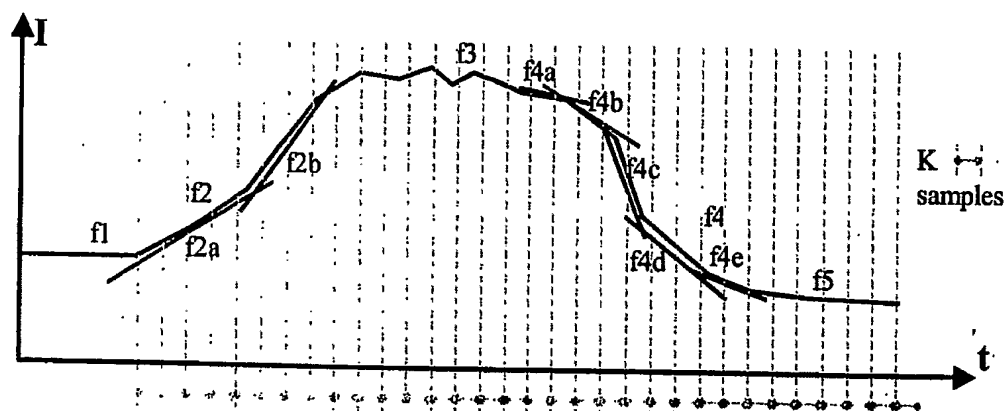


Figure 3.7-4: The Processing Tools For Slow Biological Signal Curve

Each curve fraction between the dashed lines is the K-samples vector. The sampling frequency is adapted to allow curve fraction approximated by linear function $f(t) = a \cdot t + b$. The "Function Approximation Module" transfers each curve fraction to the linear function. This function corresponding to the specific curve fraction is named "Function Descriptor". The result is stored in the "Descriptors Table" database. For each curve the row in the table is allocated and named as "Detector#X". The structure of the descriptors table database is shown on the figure below:

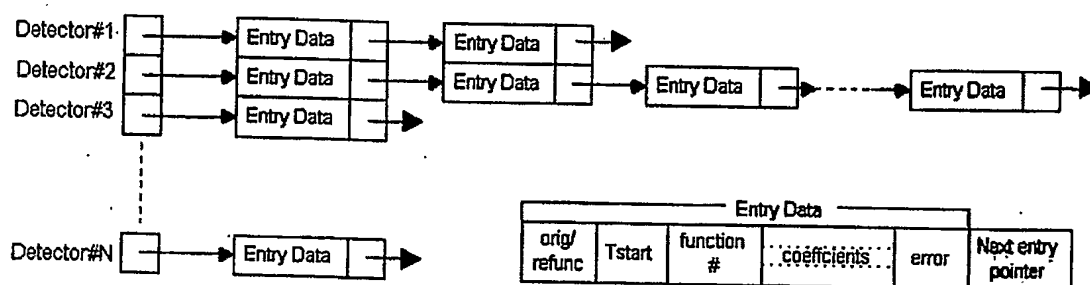


Figure 3.7-5: Function Descriptors Table Data Base

¹⁷ The simplest statistical calculation is averaging of all pixels inside the ROI

After the linear approximation of the K-samples vector the results is stored as "Entry Data" linked structure as described on the figure above. The entry data is marked as "orig" (original). The entry data structures are linked into the linked list. The "Algorithm Manager" module activates the "Re-function module" that reduces the number of sequential entry data structures to one. For example on the Figure 3.7-4 the first four sequential K-samples vectors are re-functioned to f_{2a} . The f_{2a} function descriptor is registered as single Entry Data structure in the functions table database. It marked as "refunc"(re-functioned).

The same process is done for the next five K-sample vectors. The re-functioned Entry Data structure describes f_{2b} linear function is created in the descriptors table database.

The "algorithm manager" activates the "re-function module" again. Both structures that represent f_{2a} and f_{2b} are reorganized by structure represent parabolic function¹⁸ f_2 .

The "re-function module" would be able to generate complex functions that are listed in the table below.

Table 3.7-1: The Functions That Could Be Generated By Re-function Module

#	Function	Formula	Coefficients number
F1	Poynomic	$f(t) = \sum a_N \cdot t^N$	N+1
F2	Exponential	$f(t) = \sum a_N \cdot e^{t \cdot b_N}$	2N+1
F3	Periodic	$f(t) = \sum a_N \cdot \cos(b_N t + \varphi_N)$	3N
F4	Sync	$f(t) = (1/t) \cdot \sum a_N \cdot \cos(b_N t + \varphi_N)$	3N

The representation by additional functions is possible. The best functions for such compression and decision taking technique are issues for the advanced research.

¹⁸ $f(t) = a \cdot t^2 + b \cdot t + c$

3.7.3 The Simple Algorithm For Known Chemical Concentration Calculation

The development of algorithms for toxicity detection is out of scope of this work. However the simple algorithm for detection of known chemical concentration is suggested.

The reaction chambers could be joined according to functional groups. For the algorithm the F.Groups of kind#2 and kind#3 are required (refer to the section 3.2.7: The Reaction Chambers Functionality).

The preliminary information regarding the "Peak Signal Concentration" (PSC) is required for the algorithm. The experiments configured according to F.Group of kind#2 are used for PSC detection. The expected experimental results are shown on the figure below.

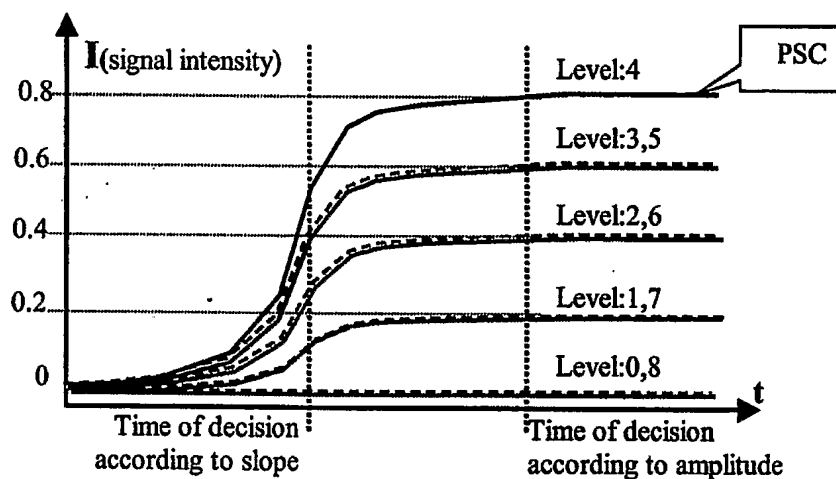


Figure 3.7-6: Biochemical Reaction Amplitude Versus Toxicant Concentration

The levels numbered from 0 to 8 indicate the chemical concentrations. The lowest concentration corresponds to the level#0 and the highest to the level#8.

Using the functional group of kind#3 the concentration could be calculated. The wrapper of the calculation algorithm presented on the Figure 3.7-7. The readout received from the non-induced biosensors is subtracted from three other readouts. The "Reference Signal" used as PSC curve. The "Under Test Signal" is used as unknown concentration curve. The "High/Low Concentration Indicator Signal" determines if the concentration is above or below the PSC.

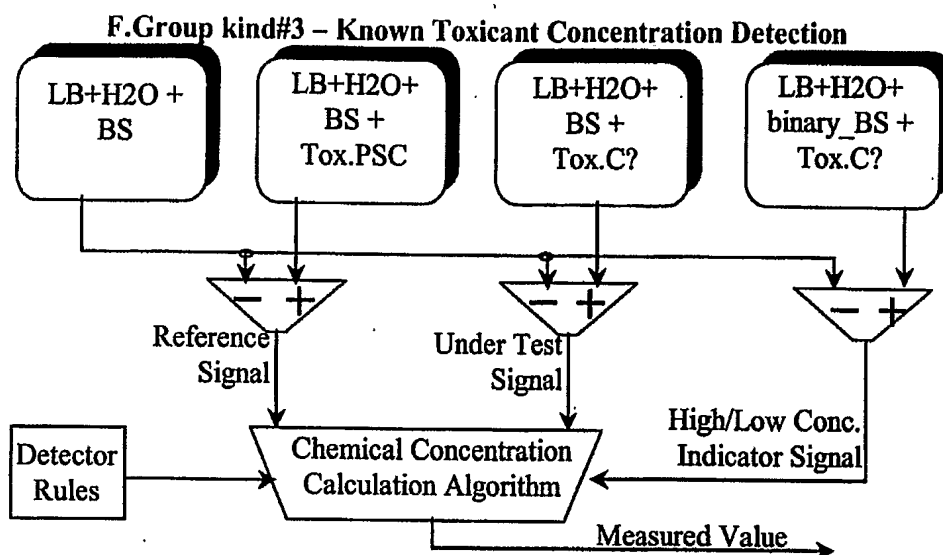


Figure 3.7-7: The Wrapper Of The Chemical Concentration Calculation Algorithm

The “Chemical Concentration Calculation Algorithm” presented on the wrapper scheme above is implemented as mathematical module: The mathematical implementation presented on the figure below:

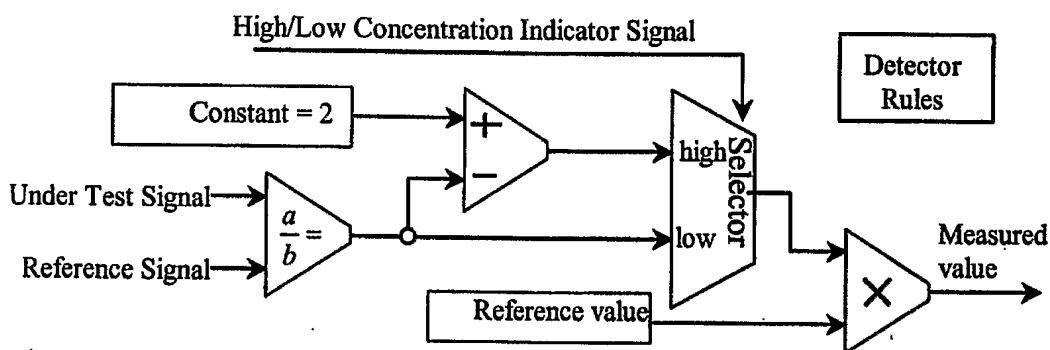


Figure 3.7-8: The Core Of The Chemical Concentration Calculation Algorithm

In practice, we have to develop more algorithms for detecting unknown chemicals and concentrations. It can be done using our process, although this is a very complicated task. It requires a panel of different biosensor that currently under development. Performing thousands of experiments on a stable integrated system is required as well. Once the conditions will allow gathering required amount of biological data the algorithms would be developed.

3.8 The Calibration Of The Integrated System

The biological signal magnitude (n_{GFP}) has been introduced in "Section 3.3.5.3". Later, in Section 4.1" it will be linked to the definition of the **biological signal**. The method for the calculation of the biological signal (n_{GFP} magnitude) from the real measurements will be described in the "Section 4.2: Biological Signal Quantification". Inaccurate n_{GFP} calculation will cause false results in water analysis. In order to avoid, or at least to reduce the false results, we have to calibrate the integrated system. The calibration of integrated system minimizes the signal uncertainties.

Measurement and calculation of the bio-signal uncertainties is a part of the integrated system calibration. Knowing integrated system signal uncertainties allows estimation of the false results probabilities.

3.8.1 Bio-Fluorescence Signal Uncertainties Mapping

The detailed calculation of the biological signal from the real measurements will be presented in the "Section 4.2". However the calculation precision is limited by the uncertainties sources. The uncertainties are having biological, electro-optical and mechanical origins. They are listed below:

- **Biological:** (a) intensity fluctuations from the protein molecules; (b) variations in the number of emitting molecules; (c) uncertainty in the number of emitting cells; (d) variations in the GFP molecules generation; (e) dried bacteria viability after resuscitation.
- **Electro-Optical:** (a) Excitation energy intensity variability; (b) excitation and emission filters area uniformity; (c) light sensing device: area uniformity and sensitivity variability.
- **Mechanical:** (a) biochip sealing optical transmission uniformity; (b) reaction chambers dimensions deviations; (c) deviation in amount of desiccated bacteria in reaction chamber; (d) deviation in injected liquid under test into the reaction chamber.

The n_{GFP} uncertainty analysis is a very complicated issue and hasn't been done yet. This is the issue for the advanced research.

The biological and electro-optical signal uncertainty factors are strongly depends on the temperature fluctuations. Therefore the temperature control mechanisms were introduced into the TAU-WTA integrated system.

3.8.2 Excitation Light Preparation Procedure For TAU-WTA Integrated System

The excitation light is supplied to the reaction chambers using the optical fibers as shown on the Figure 3.6-1. Two optical fibers types could be used in the system: (a) optical fiber with 1mm diameter per reaction chamber, (b) batch of 8x256um fibers per reaction chamber. As was already described in the "Section 3.3.3.2" there are 4 super bright 5mm LEDs in the system. Each LED supplies the excitation light for 9 optical fiber harbors. The reason is to allow selection of 5¹⁹ harbors from 9 with closest intensities. The 4 excess harbors are optically blocked.

The excitation light calibration procedure includes two stages. The first is selection of 4 LEDs with the closest optical power. The second stage is to select 5 harbors for each LED providing the closest intensities. The procedure is done using the optical power meter. The optical fiber is fixed in front of optical power meter head. The second side of the optical fiber is inserted into the harbor under test.

The measurements of the intensities are registered in the database. The measurements are done for each one of 16 intensity levels driven by the MAX6957 chip (refer to the "Section 3.5.3: The LEDs Driver"). The results are stored in database like in the Table 4.3-2. The reaction chambers are numbered from A1 to D4 as shown on the Figure 3.2-9. The chambers for excitation optical power reference are numbered as A0 – D0. The measured excitation intensities will be referenced as: $P_{fiber-A0-L1} - P_{fiber-D4-L16}$, where L1 – L16 are indicates the level of driven current to the LED by the MAX6957 chip.

¹⁹ The five-excitation fibers are used per functional group - 4 for reaction chambers and fifth for excitation intensity reference. For more details refer to the "section 3.2.7-The Reaction Chambers Functionality".

3.8.3 The TAU-WTA Calibration Procedure For The Biological Experiment

The calculation of bio-signal from the experimental measurements will be presented at the "Section 4.2.1". In this section we will discuss the calibration procedures required for the method shown there. The method express the biological activity by the equation (4.2-10)

$$\text{which is } n_{GFP} = \left(\frac{QO_{LB-H2O-GFP-DC} - QO_{LB-H2O-DC}}{T_{int} \cdot P_{fiber}} \right) \cdot \left(\frac{1}{K_{bs-px}} \cdot \frac{(6e4/2^{bits})}{QE \cdot FF} \right).$$

This equation is valid for $QO_{LB-H2O-DC}$. The $QO_{LB-H2O-DC}$ is quantified output received from reaction chamber filled with "Luria Bertani" Nutrient medium²⁰ (LB) and water. It must be measured under the same excitation power (P_{fiber}) as for the $QO_{LB-H2O-GFP-DC}$. The $QO_{LB-H2O-GFP-DC}$ is reaction chamber filled with LB, water and biosensors.

There are two ways to acquire $QO_{LB-H2O-DC}$:

- Method-1: Pre-experiment measurement with reaction chambers filled by water and LB only. The same reaction chambers will be filled by water + LB + biosensors during experiments.
- Method-2: One of the S. Groups (or 4 reaction chambers) allocated to be filled by water and LB only. It would be used for calculation of the unfiltered excitation optical power and LB emission during the experiments.

Method-1 has the advantage that all the reaction chambers could be utilized for the experiment. However, pre-experimental measurement is required for quantification of the LB medium contribution for photoluminescence.

In case of method-2 the pre-experimental measurement is not required. However, each fiber emits different excitation power. The excitation optical power supplied to the reference reaction chamber could be different from that with the biosensor. Therefore, the derived expression (4.2-10) is not accurate for that case and correction factors for the evaluation of quantified water + LB quantified measurements are required.

Here is the way the correction factors could be applied. The reaction chambers were numbered at the Section 3.2.7 on the Figure 3.2-9. The indexes *A1* and *A2* will be used. The reaction chamber corresponding to *A1* will be filled by water + LB, and *A2* by water +LB + Biosensors.

²⁰ Nutrient that has fluorescent properties

The $QO_{A1-LB-H2O-DC}$ depends from the excitation optical power (P_{fiber}) and the dark current (I_{DC}). It is proportional to:

$$QO_{A1-LB-H2O-DC} \propto K_1 \cdot I_{DC} + P_{fiber-A1} \cdot (T_{Fem4exc} + K_2 \cdot A_{LB}) \quad (3.8-1)$$

While A_{LB} is absorption of the excitation rays by the LB medium, K_1 and K_2 are constants and $T_{Fem4exc}$ is a transmission of the emission filter for the excitation spectrum (refer to the "Section 3.3.5.1: Optical Parameters Calculation". The dark current contribution could be eliminated by the double readout technique mentioned at the "Section: 3.8.4.2". Therefore we receive the dependency just from the excitation optical power (P_{fiber}):

$$QO_{A1-LB-H2O} \propto P_{fiber-A1} \cdot (T_{Fem4exc} + K_2 \cdot A_{LB}) \quad (3.8-2)$$

The readout from the reaction chamber filled with water, LB and the biosensors could be eliminated from the dark current contribution too. It is proportional to:

$$QO_{A2-LB-H2O-GFP} \propto P_{fiber-A2} \cdot (T_{Fem4exc} + K_2 \cdot A_{LB} + K_3 \cdot A_{GFP}) \quad (3.8-3)$$

While A_{GFP} is the excitation rays absorption by the GFP molecules of the biosensors. In order to get the quantified emission intensity QI_{GFP} contributed by the GFP molecules we can perform the following manipulation:

$$QI_{GFP} = QO_{A2-LB-H2O-GFP} - \left(\frac{P_{fiber-A2}}{P_{fiber-A1}} \right) \cdot QO_{A1-LB-H2O} \propto P_{fiber-A2} \cdot K_3 \cdot A_{GFP} \quad (3.8-4)$$

Two corrections are required in order to implement equation (4.2-10) for method-2:

- The elimination of the dark current contribution to the quantified outputs.
- Multiplying of the quantified output, as received from the reaction chamber filled by water + LB (indexed as A1), by the correction factor: $P_{fiber-A2}/P_{fiber-A1}$

Therefore, the corrected bio-signal calculation using method-2 is presented by the following equation:

$$n_{GFP} = \left(\frac{QO_{A2-LB-H2O-GFP} - \left(\frac{P_{fiber-A2}}{P_{fiber-A1}} \right) \cdot QO_{A1-LB-H2O}}{\tau \cdot P_{fiber-A2}} \right) \cdot \left(\frac{1}{K_{bs-pr}} \cdot \frac{(6e4/2^{bits})}{QE \cdot FF} \right) \quad (3.8-5)$$

For the description of the coefficients refer to Section 4.2.1.

Two methods were shown for the TAU-WTA integrated system calibration for the biological experiment conduction. The evaluation of the methods would be done after the completion of the TAU-WTA integrated system debugging.

3.8.4 Temperature Stability

As was mentioned in Section 3.8.1 the temperature variations are influenced by the precision of the bio-signal calculation. The temperature depends on (a) the excitation light generation device (LED), (b) the biological activity, and (c) the light quantification device.

The influence of the temperature fluctuations on the LED and light quantification device was evaluated experimentally and the results are described in the following sections.

3.8.4.1 The LED Emission Intensity Versus Temperature

The LED emission optical power versus temperature was measured using the following accessories: SMT LED, heating blower, Optical Power Meter, and a Thermometer. The LED tester, through Ampere-meter connected in series, supplied the current to the LED. The LED environment was heated to 90°C and the optical power and temperature were measured at one-second intervals. The result is presented on the on chart below:

The current remained constant at 10mA during all the experiment. From the chart Figure 3.8-1 we can see that for each 10°C change-in the LED temperature the optical emission decreases by ~50uW, or 2.5%. It's a typical LED behavior [33]. The conclusion is that stable temperature supply is important to mount stable excitation power.

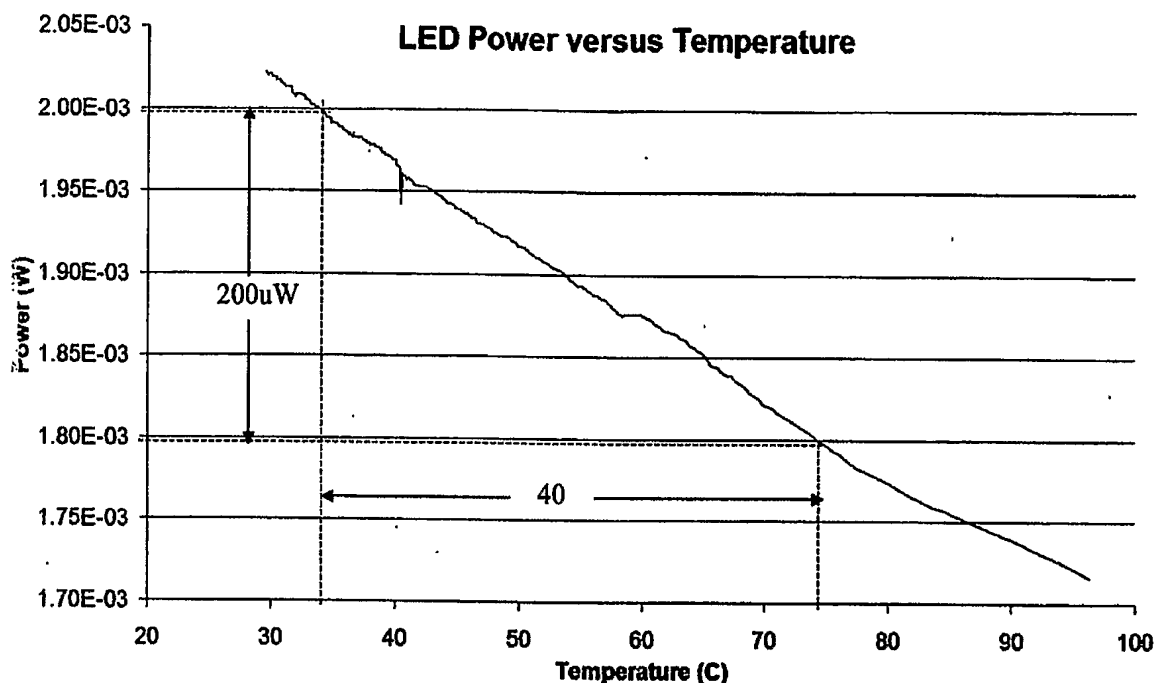


Figure 3.8-1: LED Optical Intensity Versus Temperature

3.8.4.2 Image Sensor Temperature sensitivity

The CMOS image sensor is used in the integrated system as the light quantification device. For a certain photon flux Image Sensor output depends on the temperature. One reason is that device leakage, hence dark current, is doubled every +8°C.

In order to measure the dark current versus temperature we use the ACS-1394 camera by PVS Inc. The camera consists of an ACS-1024 CMOS Image Sensor made by PVS Inc., a FPGA circuitry and a Fire Wire Interface that connects the camera to the PC through a Fire-Wire Interface and is used in the TAU-TMS²¹. The camera block diagram is described on the figure below:

²¹ First integrated system developed by TAU

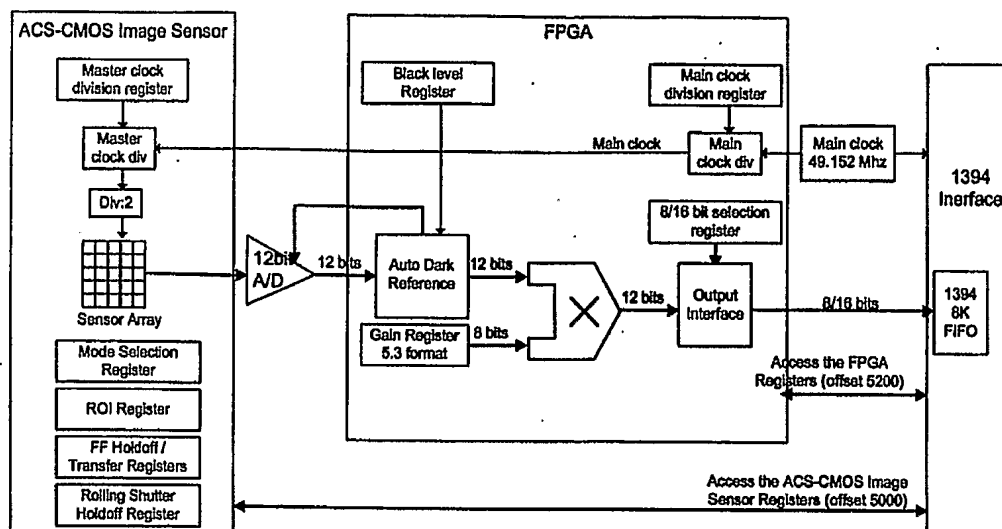


Figure 3.8-2: An ACS-1394 Camera Used In the TAU-TMS Integrated System

The camera was encapsulated by a metallic enclosure. The heat removal aspect was not taken into consideration in the mechanical design of the camera. For the room temperature of 20°C the temperature on the image sensor was stable at about²² 50°C. This doubles the dark current about by 16 times.

The dark current and the camera sensitivity dependency versus temperature were characterized experimentally. A thermometer was attached to the camera package from the outside. The thermal coupling wasn't ideal so the thermometer showed just the trend in the temperature. Initially we tested the camera at room temperature of 20°C. The experiment started 15 minutes after powering on of the camera. Each 30 seconds the frame was captured in the dark and then immediately after switching LED on. This technique named "Double Readout". The double readout enables to compensate the dark current variations. For the integration time of 2 seconds the acquired results are presented on the figure below:

²² Was not measured from inside but calculated according pixel saturation time caused by dark current

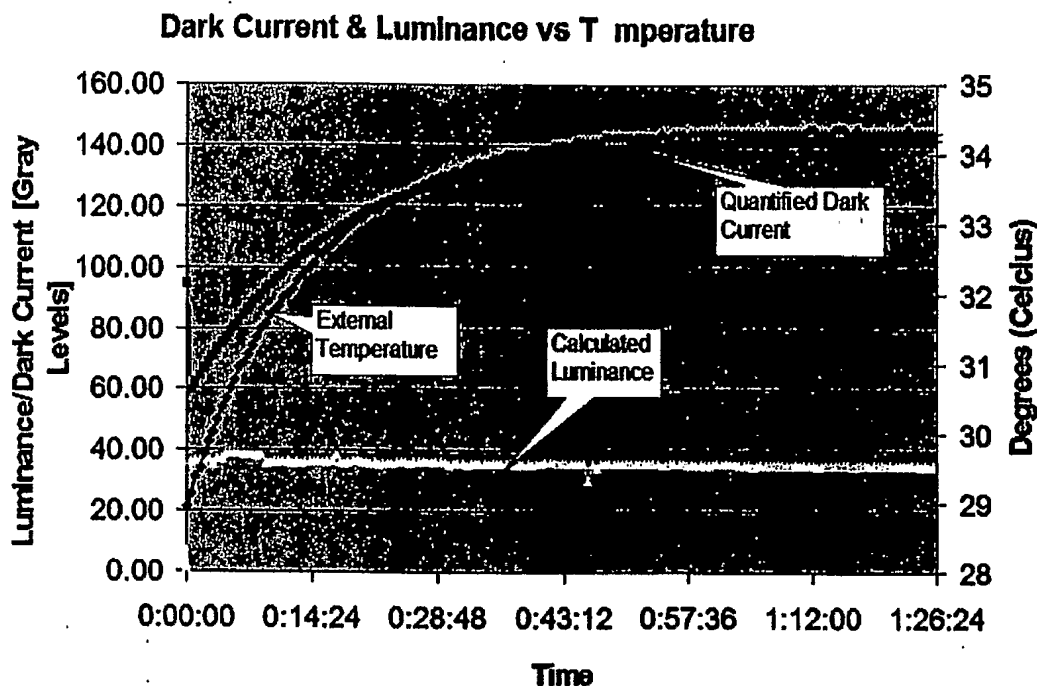


Figure 3.8-3: ACS-1394 Camera Dark Readout After Power On

On the graph we see: (1) quantified dark current sample – pink curve, (2) external temperature – blue curve and (3) subtraction of dark current sample from quantified LED-illuminated sample – yellow curve.

We got the following conclusions from the experiment:

- The temperature increase of the CMOS Image Sensor raising the dark current as was expected.
- The double sampling solves the temperature variations problem. The contribution of the dark current is eliminated; therefore calculated luminance curve is constant.
- The cooling of the Image Sensor is important in case of long integration time. Otherwise the dark current reduces the dynamic range of the illumination measurement. We could see on the graph that half of dynamic range (140/256 gray levels) is wasted for quantified dark current.

4 Biological Characterizations

4.1 Biological Signal Definition

The integrated system engineering aspects were described in the previous section. They are based on the biophysical model that is presented in Section 3.3.5: Modeling Of The Bio-Florescence Electro-Optical System.

The main parameters of the biophysical model are the dimensions of whole cell biosensor and its concentration. The biosensor dimensions are known. The concentration can be modified for optimal biological activity. The biological activity was determined as optimum for the concentration of $1e8[b/mL]$.

Note that one of the main goals of the "Integrated System Research" presented at the end of Section 1.1: The Research Objectives. The integrated system must provide the biological signals input to the water analysis algorithms. Therefore we have to provide the firm definition for the biological signal.

As was already mentioned before, the biochemical reaction occurs following the interaction between the biosensor and chemical. This reaction induces the Green Florescent Proteins (GFP) molecules that are spreads inside the biosensor. The GFP molecule that absorbs photon at a wavelength of 470nm – blue light, emits other photon at a wavelength of 510nm – green light. The green light is measured by electro-optical system. The result indicates the degree of the blue light absorption, which depends on saturation of whole cell biosensor by GFP molecules. The biosensor saturation by GFP molecules indicates the degree of biochemical reaction efficiency.

The logical linkage from the previous paragraph could be finished by to the following conclusion. Measuring²³ the green light emitted by GFP molecules allows us to grade the reaction efficiency. The graded reaction efficiency will be named the "Bio-Signal".

The bio-signal is depends on number of factors. There are two kinds of factors. (i) The first kind includes the type and concentration of the whole cell biosensor, nutrients in the liquid medium, and the temperature. Those factors are configurable and thus named "Bio-Signal Configurable Factors" (BSCF). (ii) The second type includes time, tested chemical and its concentration. Those factors are variable and thus called "Bio-Signal Variable Factors" (BSVF). The change of bio-signal intensity over the time is named as "Kinetics".

²³ More precise to say is calculating. The reason is that emission contributed by the GFP molecules is extracted from the integrated signal quantified by the light-sensing device. The method for such calculation is presented at the "Section 4.2.1".

The general description of whole cell based biosensor operation was already presented at the "Section 3.1". The significant part of the design considerations was based on typical bio-signal. The typical bio-signal was characterized using general representatives of the biosensors and chemicals. The general biosensors representative is *E.coli* bacteria – *Rec-a* strain. It interacts with general chemical representative - Nalidixic Acid (NA). The set of experiments presented in the table below was performed to make general bio-signal characterization.

Table 4.1-1: The Bio-Signal Characterization Experiments

#	Experiment	Goals	Equipment	Detailed Description
1	Biological Signal Characterization	The typical characterization of the bio-signal is important for considerations of the integrated system design.	Victor2 by Wallac	4.2.2
2	Emission – Excitation Dependency	Proof of assumption that emission intensity has linear dependence from the excitation intensity	Halogen Lamp based setup	4.3
3	Kinetics experiments on the TAU-TMS	Testing sensitivity of the TAU-TMS-ver1 experimental system to interaction between E-coli and inducer (in fresh and resuscitated conditions)	TAU-TMS-ver1	4.4
4	Biocompatible Glues research	Finding biochip sealing glues friendly for the biological activity of E-coli	Victor2 by Wallac	4.5
5	Minimal Human Cells concentration	Finding minimal concentration of HU.EF1:EG4 human cells for sensitive measurements on TAU-TMS-ver1	TAU-TMS-ver1	4.6

4.2 Biological Signal Quantification

The mechanism for bio-fluorescence generation and measurement was generally described at the "Section 3.1: The Integrated System Overview". Now let's see in details how we can quantify the bio-signal.

4.2.1 Bio-Signal Quantification on TAU-WTA Integrated System

Until now two integrated systems were developed at the Tel-Aviv University. The first one, titled TAU-TMS (Toxicity Measurement System) was developed at the early research stage. A number of different experiments were performed on it. They are described at the "Sections 4.4: Kinetics Experiments On The TAU-TMS" and "Section 4.6: The Human Cells Emission Intensity As Function Of The Concentration".

The second integrated system named TAU-WTA (Water Toxicity Analysis) is under development now. The electro-optical and biochip related modules are already produced and currently under debugging.

Let's describe how the biological signal can be quantified using the TAU-WTA integrated system. In TAU-WTA biochip there are 16 reaction chambers that could be divided to 4 functional groups. The excitation energy is supplied through optical fiber. The IBIS4 CMOS image sensor by Fill-Factor is used as light sensing and quantification device.

The light-sensing device quantifies all visible light energy sensed by it. The quantified energy will be named "Integrated Signal". In our case there are three light energy sources quantified to the integrated signal. This process is schematically presented below:

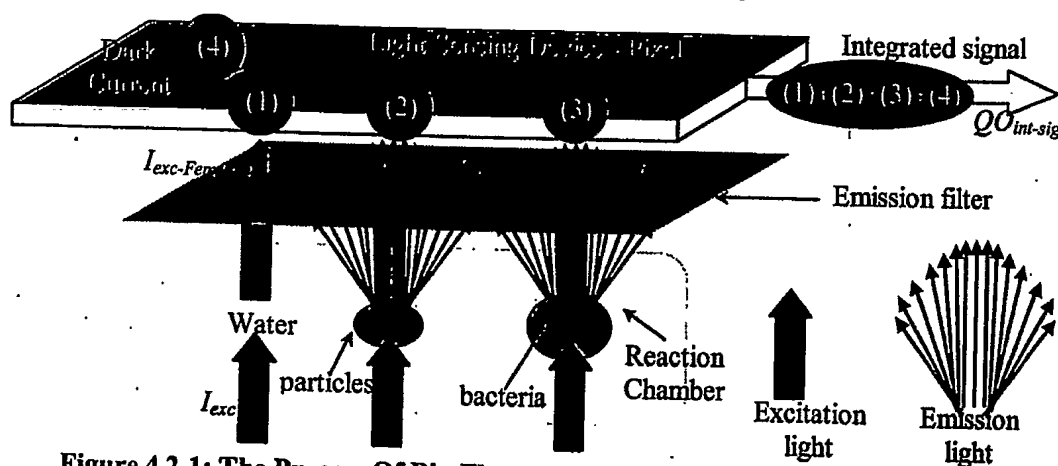


Figure 4.2-1: The Process Of Bio-Fluorescence Integrated Signal Formation

As could be seen from the figure above, there are the following light sources quantified by the pixel to the quantified integrated signal $QO_{int-sig}$:

- (1) Unfiltered excitation intensity $I_{exc-Fem4exc}$ – the emission filter attenuates the excitation energy I_{exc} in 4 orders but can't eliminate it completely.
- (2) In order to support the biological activity the whole cell biosensors are placed into nutrient medium named LB. This medium has fluorescent properties too. Its emission intensity contribution to the integrated signal signed as I_{LB} .
- (3) The emission intensity contributed by GFP molecules signed as I_{GFP} .
- (4) The I_{DC} is the dark current of the light quantification device contributing to the integrated signal.

Our goal is to evaluate the biochemical reaction efficiency, which is equal to the bio-signal (refer to Section 4.1 titled Biological Signal Definition). The biochemical reaction efficiency is already defined as n_{GFP} in the "Section 3.3.5.3". The variable I_{exc-i} is excitation intensity in [photon/sec] units in layer i , and I_{ems-i} is photons emitted by GFP molecules located in layer i . The dependency of emission from excitation in the layer i , is expressed by (3.3-28), (3.3-27) and (3.3-24). As was mentioned in the "Section 3.3.5.3" just a little portion from I_{ems-i} intensity is reaching the pixel of light quantification device. The portion depends on the optical setup between them. For the matter of the discussion lets use the electro-optical setup described in the "Section 3.3.6.3: The Matrix Of mLenses". The emission intensity that reaches the pixel of the light quantification device expressed by (3.3-45) and (3.3-44). Assembly of all above equations expresses emission reaches the light quantification device as:

$$I_{ems-mLens-det} = \sum_{i=1}^{i=N_{layers}} \left(A_{GFP-max} \cdot I_{exc-i} \cdot n_{GFP} \cdot T_{ems}(H_{2l}) \cdot \frac{\Omega_{affi}}{4\pi} \cdot T_{mlens} \cdot T_{Fems4ems} \right) \quad (4.2-1)$$

The excitation source intensity expressed by (3.3-22). Each level of reaction chamber attenuates the source intensity. The intensity at level i is expressed by (3.3-26). Now we can express the excitation at level i as:

$$I_{exc-i} = \left(\frac{P_{fiber}}{E_{ph}(470nm)} \right) \cdot T_{exc}^{i-1}(\Delta h) = P_{fiber} \cdot \left(\frac{T_{exc}^{i-1}(\Delta h)}{E_{ph}(470nm)} \right) \quad (4.2-2)$$

Now we can express the intensity emitted by GFP molecules as function of biophysical reaction efficiency and excitation power in [W] units:

$$\begin{aligned}
I_{ems-mlens-det} &= \\
&= \sum_{i=1}^{i=N_{layers}} \left(A_{GFP-max} \cdot P_{fiber} \cdot \left(\frac{T_{exc}^{i-1}(\Delta h)}{E_{ph}(470nm)} \right) \cdot n_{GFP} \cdot T_{ems}(H_{2l}) \cdot \frac{\Omega_{af\beta}}{4\pi} \cdot T_{mlens} \cdot T_{Fems4ems} \right) = \\
&= n_{GFP} \cdot P_{fiber} \cdot \underbrace{\sum_{i=1}^{i=N_{layers}} \left(A_{GFP-max} \cdot \left(\frac{T_{exc}^{i-1}(\Delta h)}{E_{ph}(470nm)} \right) \cdot T_{ems}(H_{2l}) \cdot \frac{\Omega_{af\beta}}{4\pi} \cdot T_{mlens} \cdot T_{Fems4ems} \right)}_{K_{bs-exc-ems-optics-mlens}}
\end{aligned} \tag{4.2-3}$$

The $K_{bs-exc-ems-optics-mlens}$ is a constant coefficient that depends on reaction chamber geometry; biosensors concentration; filters and medium transmission; mLens based optics geometry and photon energy at wavelength of 470nm. Now we can get the simple expression regarding emission intensity that achieves the light quantification device:

$$I_{ems-mlens-det} = n_{GFP} \cdot P_{fiber} \cdot K_{bs-exc-ems-optics-mlens} \tag{4.2-4}$$

The emission intensity projected on the detector is spreads over area $S_{ems-det}$. The area of the light quantification pixel is S_{px} . Following the (3.3-34) the GFP molecules emission intensity projected on the pixel is:

$$I_{ems-mlens-px} = n_{GFP} \cdot P_{fiber} \cdot K_{bs-exc-ems-optics-mlens} \cdot (S_{px} / S_{ems-det}) = n_{GFP} \cdot P_{fiber} \cdot K_{bs-px} \tag{4.2-5}$$

The K_{bs-px} is coefficient fitting between the excitation energy and bio-emission intensity projected on the pixel of light quantification device. It expressed as following:

$$K_{bs-px} = \frac{S_{px}}{S_{ems-det}} \cdot \sum_{i=1}^{i=N_{layers}} \left(A_{GFP-max} \cdot \left(\frac{T_{exc}^{i-1}(\Delta h)}{E_{ph}(470nm)} \right) \cdot T_{ems}(H_{2l}) \cdot \frac{\Omega_{af\beta}}{4\pi} \cdot T_{mlens} \cdot T_{Fems4ems} \right) \tag{4.2-6}$$

Lets remember that the light intensities are measured in [photon/sec] units. In the TAU-WTA integrated system the CMOS Image Sensor is used as light quantification device. The relationship between quantified output (QO) of the Image Sensor and photon units expressed

$$\text{by the equation (3.3-3): } N_{ph}(T_{int}) = \frac{6e4 \cdot ((QO(T_{int}) - QO_{DC-e-}(T_{int})) / 2^{bits})}{QE \cdot FF}$$

The dark current quantification is done in complete darkness. In our integrated system simple switching off of the excitation light used for that.

The quantified integrated signal $QO_{int-sig}$ includes the contribution of intensity emitted by GFP molecules, LB and unfiltered excitation light. Lets assume that we have a way to separate the contributions. The separated, quantified GFP molecules emission will be signed as QI_{GFP} . Combining between (4.2-5) and (3.3-3) we are receive equation allowing us to grade the bio-signal for the integration time T_{int} :

$$n_{GFP} \cdot P_{fiber} \cdot K_{bs-px} \cdot T_{int} = \frac{6e4 \cdot (QI_{GFP}/2^{bits})}{QE \cdot FF} \quad (4.2-7)$$

Now, finally, we can grade the biochemical reaction of to get bio-signal amplitude by:

$$n_{GFP} = QI_{GFP} \cdot \left(\frac{1}{T_{int} \cdot P_{fiber}} \right) \cdot \left(\frac{1}{K_{bs-px}} \cdot \frac{(6e4/2^{bits})}{QE \cdot FF} \right) \quad (4.2-8)$$

The last thing that left to do is to show how to separate the QI_{GFP} from $QO_{int-sig}$. In the Section 3.2.7: The Reaction Chambers Functionality the logical division of the reaction chamber to functional groups was presented. We select "F.Group type#1: Biological Signal Stability Testing". The quantified integrated signal received from the reaction chamber named "LB+H2O" is includes just factors (1), (2) and (4) – refer to the "Figure 4.2-1: The Process Of Bio-Fluorescence Integrated Signal Formation". This signal will be marked as $QO_{LB-H2O-DC}$. The quantified integrated signal received from the reaction chamber named "LB+H2O+BS+Tox" is named as $QO_{LB-H2O-GFP-DC}$. The biochemical reaction is occurs in this reaction chamber, therefore all four factors are contributes to the integrated signal. The quantified emission intensity of the GFP molecules could be found by simple subtraction:

$$QI_{GFP} = QO_{LB-H2O-GFP-DC} - QO_{LB-H2O-DC} \quad (4.2-9)$$

The final equation for bio-signal amplitude calculation is:

$$n_{GFP} = \left(\frac{QO_{LB-H2O-GFP-DC} - QO_{LB-H2O-DC}}{T_{int} \cdot P_{fiber}} \right) \cdot \left(\frac{1}{K_{bs-px}} \cdot \frac{(6e4/2^{bits})}{QE \cdot FF} \right) \quad (4.2-10)$$

The precision of this equation is the issue for the advanced research.

4.2.2 Bio-Signal Characterization Using Victor-2 Fluoremeter

The characterization of the bio-signal is important for considerations of the integrated system design. The best way to characterize the bio-signal is to use standard and stable equipment. The experiments were performed on a industrial fluoremeter named Victor-2 by Wallac Inc.. In this section the kinetics experiment is described. The experiment was configured to allow separation between light sources. The methodology for separation was already described in previous section.

The experiment was performed at the following conditions: (a) biosensor – E-coli-REC-A bacteria, (b) bacteria concentration $1e8[b/mL]$, (c) the tested liquid volume is 100uL. The 12x8 micro-title plate was used as reaction chambers array. The reaction chambers were filled with contents according to the following setup:

- The first row - 8 empty reaction chambers for excitation background measurement

- The second row - 8 reaction chamber filled by LB
- The third row - reaction chambers filled by LB, bacteria and NA under the following concentrations: 0ppm, 0.15ppm, 0.31ppm, 0.62ppm, 1.25ppm, 2.5ppm, 5ppm, 10ppm

We got 8 columns with 3 reaction chambers in each. We can note that looking on the column of 3 reaction chambers we will get "F.Group kind#1". And looking on the third row - "F.Group kind#2" is formed (refer to the Section 3.2.7 for explanations). The configuration described on the figure below:

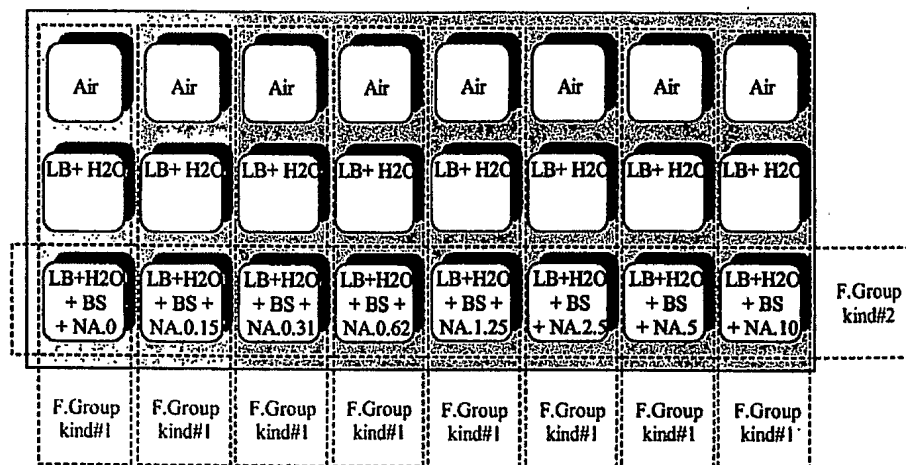


Figure 4.2-2: The Victor2 Kinetics Experiment Setup

The following results were received

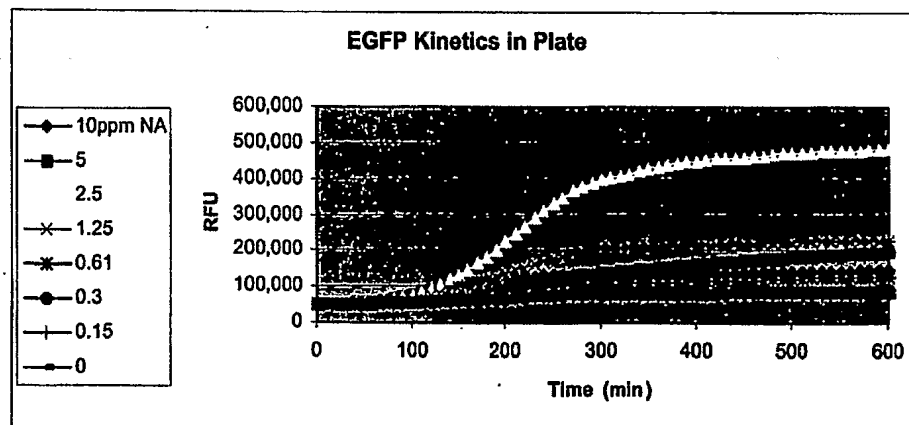


Figure 4.2-3: The Kinetics Of E-Coli-REC-A ⇌ NA interaction In LB Medium

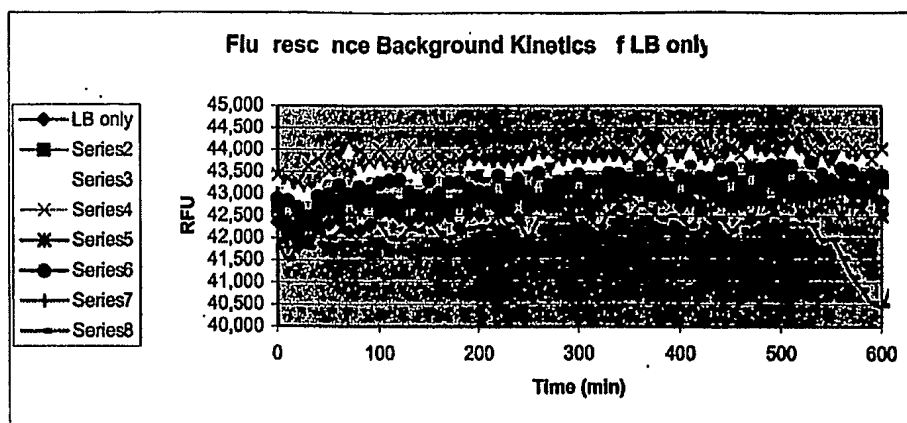


Figure 4.2-4: The Kinetics Of LB Medium Fluorescence

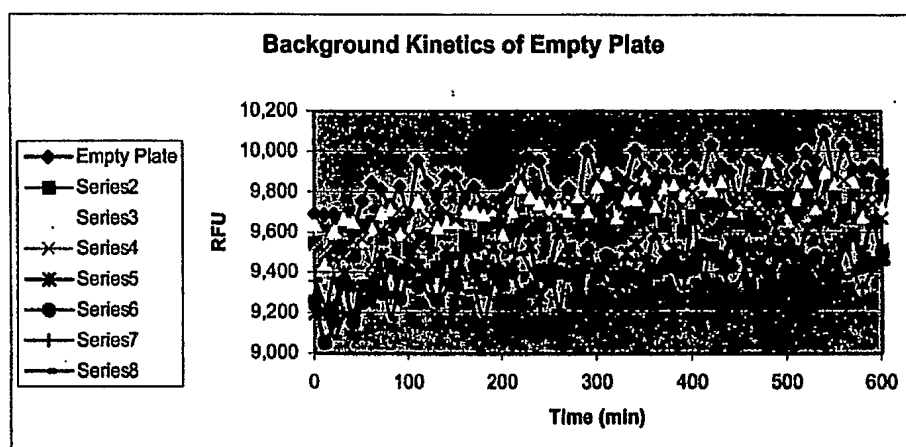


Figure 4.2-5: The Kinetics Of Excitation Background

Lets start the results analysis. The Victor2 electro-optical system is unknown, therefore the method used in the "Section 4.2.1: Bio-Signal Quantification on TAU-WTA Integrated System" couldn't be used. However other kind of biological signal gradation could be done.

First lets separate the light sources. The Victor2 in fluorescence measurement mode quantifies the light in Relative Fluorescence Units (RFU). The unfiltered excitation energy kinetics presented on the Figure 4.2-5: The Kinetics Of Excitation Background. Let's assign the curves as $QO_{iExc}(t)$. The average $QO_{Exc} = 9,578$ RFU and maximal uncertainty is $QU_{Exc} = 525$ RFU.

The interesting issue is the estimation of the fluorescence strength of the nutrient medium of LB kind. Lets assign the kinetics of LB fluorescence as $QI_{LB}(t)$. The curves of the LB fluorescence with unfiltered excitation background are assigned as $QO_{iExc+LB}(t)$. The LB fluorescence could be calculation by simple subtraction:

$$QI_{LB}(t) = QO_{iExc+LB}(t) - QO_{Exc} \quad (4.2-11)$$

The average of LB fluorescence is $QI_{LB} = 33,457$ RFU and maximal uncertainty is $QU_{LB} = 3,054$ RFU. The maximal uncertainty was received by summation of excitation and LB only uncertainty around average result. The assumption that LB uncertainty is proportional to the excitation intensity will be used.

The QO_{Exc+LB} is the average measured among the $QO_{iExc+LB}(t)$ curves. The value is 43,035 RFU and the uncertainty is $QU_{Exc+LB} = 2,529$ RFU. The quantified intensity contributed by GFP molecules is also calculated by subtraction:

$$QI_{GFP}(t) = QO_{iExc+LB+GFP}(t) - QO_{Exc+LB} \quad (4.2-12)$$

Now the curves could be analyzed. First let's analyze the biochemical reaction at the beginning as function of NA concentration.

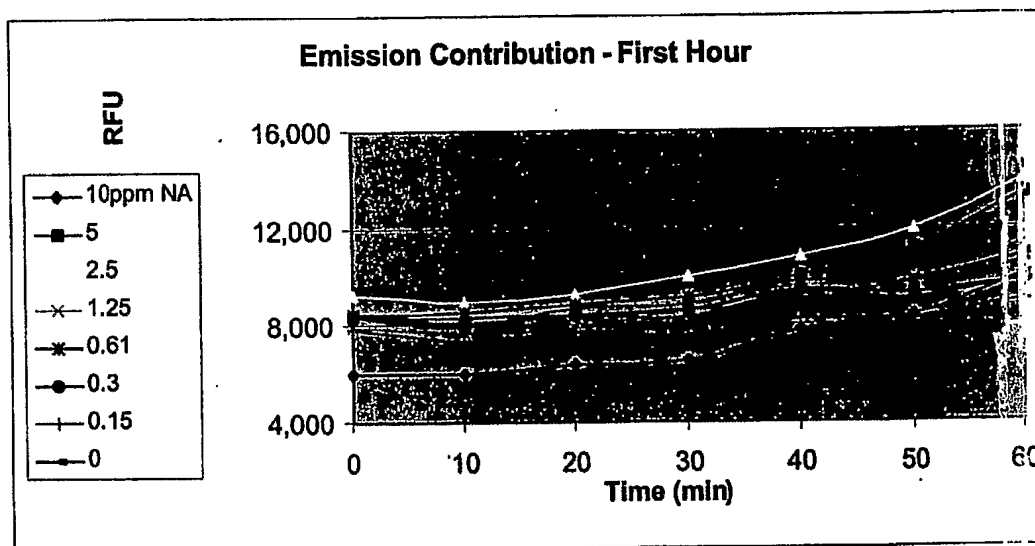


Figure 4.2-6: The Kinetics Of Biochemical Reaction At The First Hour

At the beginning of the experiment, the $Time = 0$, there is biochemical reaction is still not occurred. Therefore the same quantified outputs must be accrued. However the uncertainty between the average $QI_{GFP}(0) = 8,098$ RFU is $QU_{GFP}(0) = 4,606$ RFU. This uncertainty may grow for growing emission intensities, but this couldn't be measured in the current experiment. The trend of amplitude increase is starts after 20minutes. That trend is exists for all curves even for the reaction chamber without chemical.

From the information gathered during first hour, three conclusions could be done:

- The *E. Coli* - *rec-A* generates GFP molecules even without reaction induced by chemicals. This called "basalic activity". The intensity emitted by them named "basalic value".
- The biochemical reaction is the same for any concentration of NA less than 10ppm during the first hour. Therefore there decision regarding water contents couldn't be done for current setup.
- The ratio of uncertainty of the biochemical reaction to the excitation background is $QU_{GFP}/QO_{Exc} = 4,606/9,578 \approx 0.5$.

The acceptable test duration is 2-3 hours. Lets see what's happens during minutes 60-150.

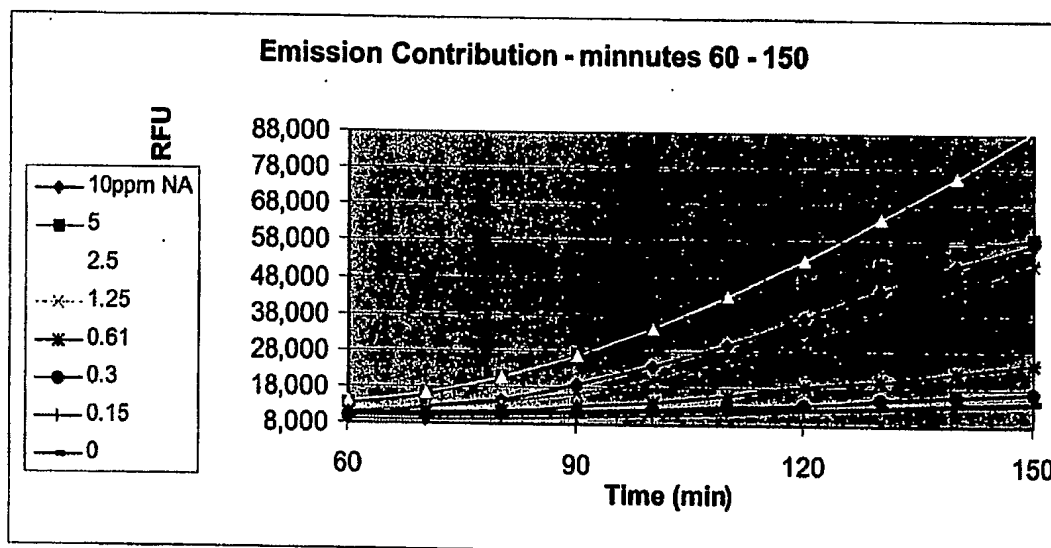


Figure 4.2-7: The Kinetics Of Biochemical Reaction During Period Of 60-150 minutes

As we could see the strongest biochemical reaction occurred under 2.5ppm NA concentration. For 5ppm the reaction was suppressed after 100min. For 10ppm the reaction was suppressed from the beginning. The reaction is linear to NA concentration between 0.61-2.5ppm. This is noticeable by looking on three curves: 0.61ppm, 1.25ppm and 2.5ppm. The biochemical reaction under the concentration below 0.3ppm is hard to distinguish from the basalic activity.

The biological activity during period of 60-150 minutes could be summarized by the following conclusions:

- The reaction could be divided into the following regions:
 - Basalic – for low NA concentrations

- Linear – for medium NA concentrations
- Suppressed – for high NA concentrations
- The binary biosensor is necessary to distinguish between linear and suppressed ranges
- The calculation of NA concentration could be done according the amplitudes comparison after 2hours. In order to get better resolution regarding suppressed range, the kinetics data should be analyzed (compare 10ppm and 5ppm to see that).

The results are proves that model for the known chemical concentration detection presented in the “Section 3.7.3” is valid. In order to utilize the model much more data must be collected for statistics.

The experiment was performed during 10hours. Although 10hours duration is not acceptable for real time water toxicity detection, there is a lot of useful information for the research. The kinetics of the emission contributed by GFP molecules described on chart below:

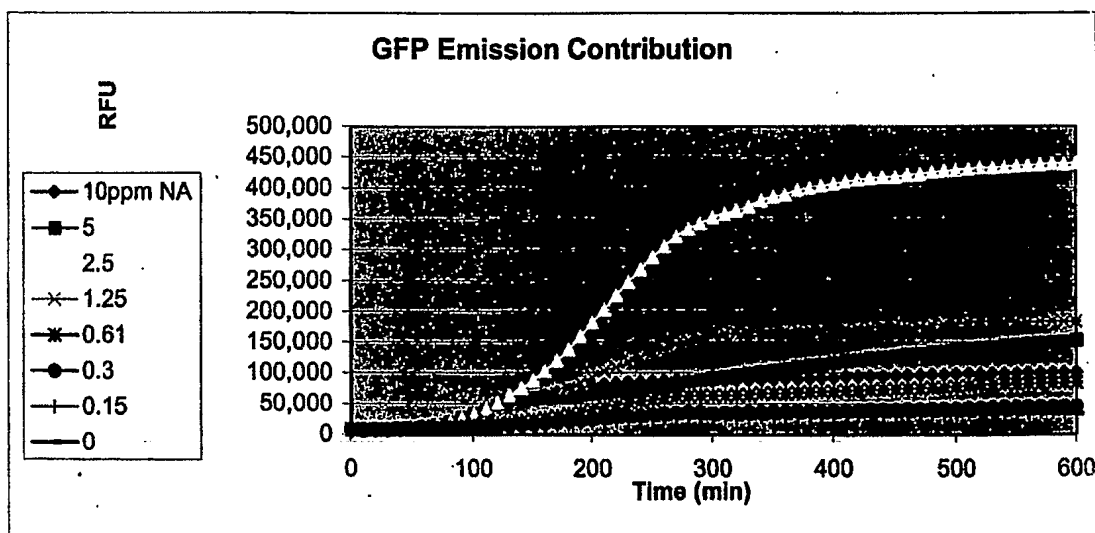


Figure 4.2-8: The Kinetics Of Biochemical Reaction During Period Of 10 Hours

It seems that 2.5ppm NA concentration is optimal condition for the biochemical reaction. According to its curve looks that the saturation of whole cell biosensors by GFP molecules corresponds to the RFU of 500,000. If 500,000 RFU is equivalent to $n_{GFP} = 1$, we can represent the curves as amplitude of bio-signals $n_{iGFP}(t)$:

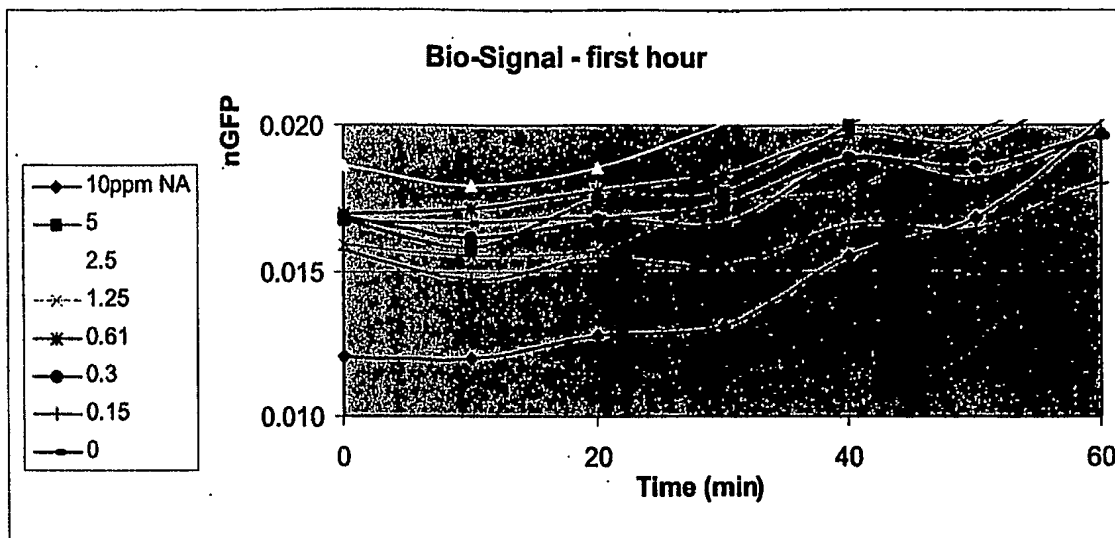


Figure 4.2-9: The Bio-Signal Amplitude Kinetics, $n_{GFP}(t)$, During The First Hour

We could see that there is a basic saturation of 1.5% of the biosensor by GFP molecules. This 1.5% saturation occurs during whole cell biosensor producing.

For the time acceptable for water analysis the bio-signal kinetics presented on the chart below:

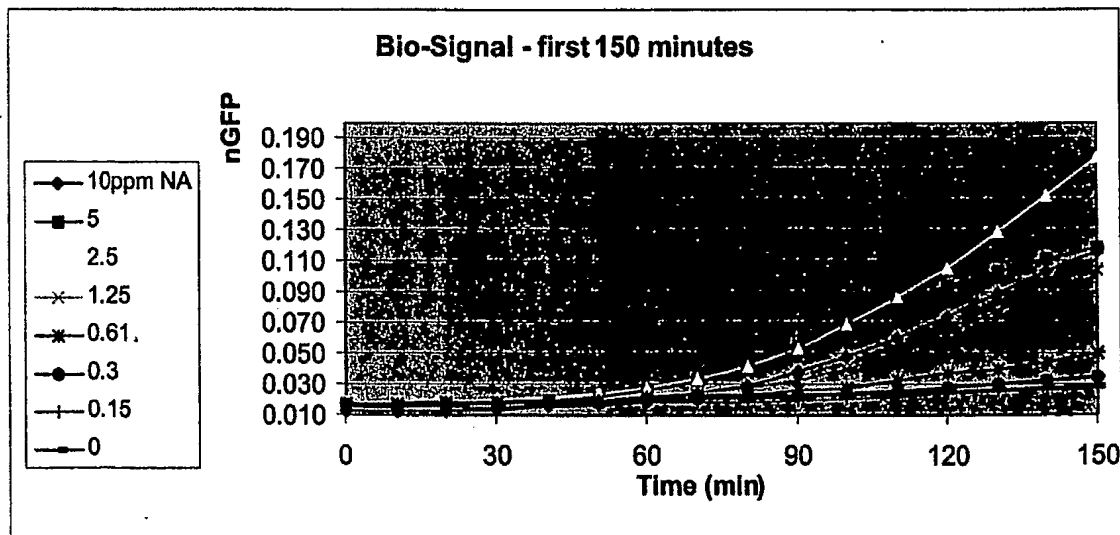


Figure 4.2-10: The Bio-Signal Amplitude Kinetics, $n_{GFP}(t)$, During The First 150 Minutes

Analyzing the two above charts the following conclusions could be done:

- High basalic activity of the biosensors reducing sensitivity of the integrated system

- The mLens based integrated system will be able to detect bio-signal among noise just an hour after test start. Please refer to **Table 3.3-2** in **Section 3.3.7.2: The Lens free, V-Lens And mLens Based Optical Systems.**

4.3 Emission – Excitation Dependency

The fluorescence effect is based on the molecular absorption. The fluorescence absorption is an interaction between the molecules in the ground state with excitation photon. The interaction promotes an electron to high-energy molecular orbital. Part of the electron energy is wasted on the orbital due to molecular vibration process. Then the transition of the electron back to the ground state of the energy is occurs. During that transition the emission of photon is take place. The Beer-Lambert law expresses the molecular absorption:

$$A_{mol} = \epsilon \cdot c \cdot l \quad (4.3-1)$$

The ϵ is a molar absorption coefficient ($M^{-1}cm^{-1}$ units), c is a concentration of absorbing species (M units) and l is a path-length traversed by the light (cm units).

As could be seen from the Beer-Lambert law, the absorption is generally independent of excitation light intensity. However for high intensity laser irradiation the law could be not valid[34].

In our integrated system LED illumination is used as excitation light source. The LED intensity much lower than that of the laser and the emission is not coherent. The emission to excitation intensity dependency is expected to be linear. The expectation was proved by two experiments described in consequent sub-sections.

4.3.1 The Halogen Lamp Based Excitation / Emission Intensity Experiment

This first experiment was preformed on the early stage of the research. The halogen lamp was used as excitation source. The experimental setup is schematically presented below:

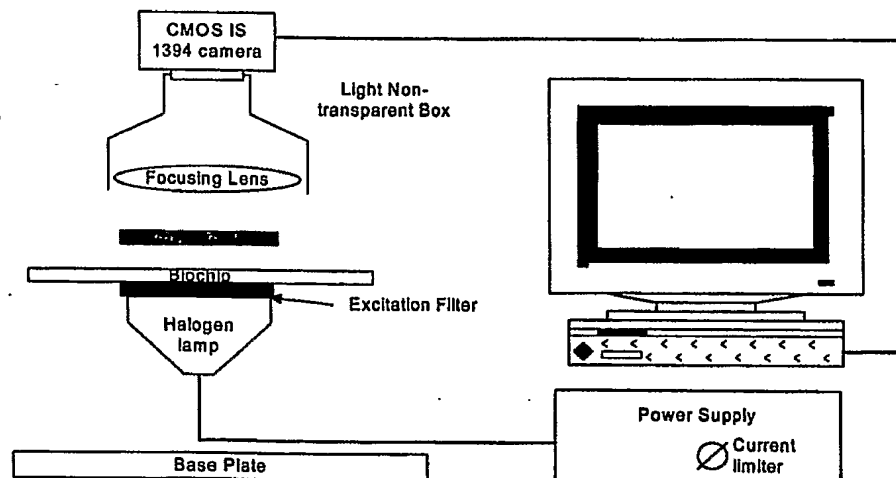


Figure 4.3-1: Halogen Lamp Based Setup For Emission-Excitation Dependency Experiment

The halogen lamp received the power from the laboratory power supplier. The laboratory power supplier we used has ability to limit current. The maximum current that can be supplied is 6A. The halogen lamp has a wide emission spectrum. In order to get the required excitation light spectrum the excitation filter was used. The optical power measured with the optical power meter as function of the current supplied to the halogen lamp presented on the figure below:

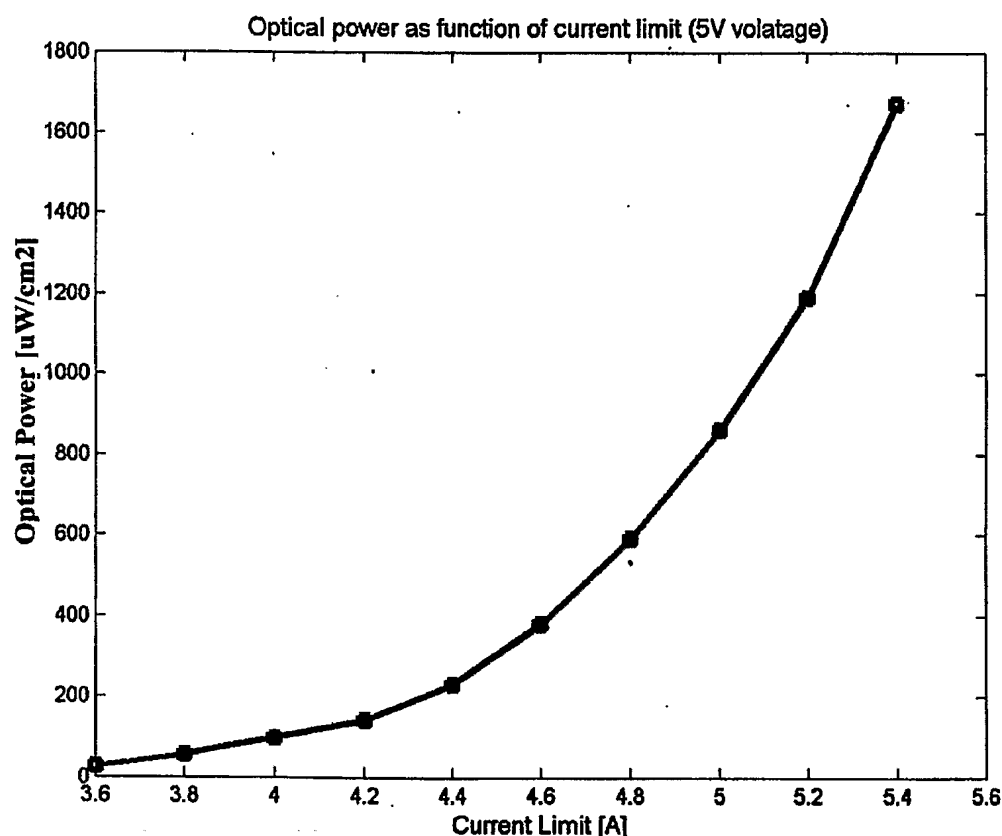


Figure 4.3-2: Excitation Power As Function Of Current Supplied To The Halogen Lamp

From the graph above we could see that the excitation light optical power is tunable in range of: 20-1,700 [$\mu\text{W}/\text{cm}^2$]. The biochip was placed immediately after the excitation filter. The volume of the reaction chambers of the biochip is 2 μL . The induced *E. Coli* – rec-A based biosensors, 1×10^9 [b/mL] concentration, were placed into the reaction chamber.

Emission filter was mounted between the video lens of the camera and the biochip. The camera transferred the sampled pictures to the personal computer (PC). The pictures were processed in Matlab tool. The ACS-1394 camera by PVS was used. It was operated under the following conditions: Mode: Rolling Shutter, Quasi CDS; Resolution: 1024x1024; ClkFreq:

3Mhz \Leftrightarrow div8; Exposure clock: MC/4; Black level reference: 0xa0, which equal to gray level 10.

Two reaction chambers we used on the biochip. The induced solution with the biosensors was placed into the first. The second was left empty and used for measurement of the excitation intensity that wasn't filtered by the emission filter.

The experiment was operated for 5 levels of the excitation intensities. The picture was captured for each excitation intensity level. For visual inspection of the results the pictures were combined into the picture presented on the figure below:

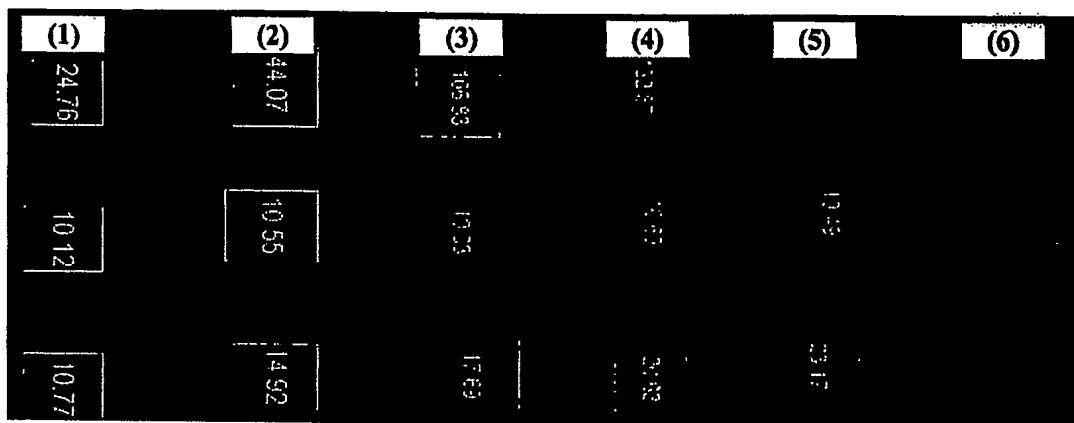


Figure 4.3-3: Combined Picture From: (1-5) Reaction Chambers Captures Under Different Excitation Intensities, (6) Reaction Chamber Captured Under Ambient Light.

The combined picture includes three rows. The first on includes the emission and unfiltered excitation under different excitation intensities. The second row used for dark current quantification. We can note that the same value was received independently of the excitation intensity. The third row is the quantified intensity of the unfiltered excitation light intensity. The last column from the right is used as reference of reaction chambers location and dimensions. The results were processed and displayed in the table below:

Measurement	1	2	3	4	5
Amperes	4.0	4.5	4.8	5.0	5.4
Optical Power [uW/cm2]	98.0	300.0	590.0	860.0	1670.0
Under Test Value	24.8	44.1	106.8	132.9	250.8
Background Value	10.8	14.9	17.7	20.6	23.2
Emission Value	14.0	29.2	89.1	112.2	227.6

Table 4.3-1: The Halogen Lamp Based Emission/Excitation Experiment Results Processing

The graphical representation of the results is shown below:

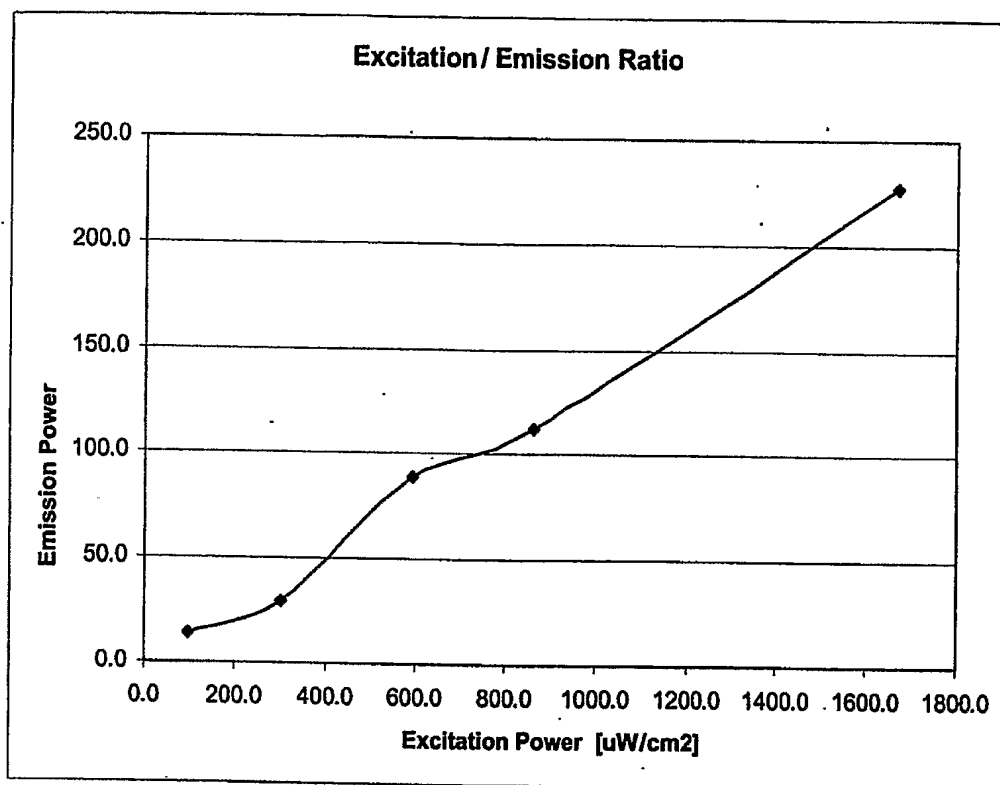


Figure 4.3-4: The Halogen Lamp Based Emission/Excitation Experiment

The received curve is almost straight line. The line is not completely straight due to not precise methodology testing. The conclusion is that the emission intensity has linear dependence from the excitation intensity. This dependence is for wide range of the excitation power. By this experiment linear dependence was for the range of 0-2[W/cm²].

4.3.2 The Excitation / Emission Intensity Experiment Performed On TAU-TMS

The experiment was repeated on the TAU-TMS. The excitation part of TAU-TMS electro-optical structure presented in the "Section 3.3.3.1: Matrix Of SMT LEDs". The excitation part included 12 LEDs. The number of the reaction chambers is 12 too. Each LED corresponds to one of the 12 reaction chambers. Each LED could be activated individually for 16 intensity levels.

For the experiment the reaction chamber#6 was used. The volume of 1.5uL of induced solution with biosensors was injected. The solution was under concentration of 1e9[b/mL]. The PVS image sensor was operated under the following conditions: Mode: Rolling Shutter, Quasi CDS; Resolution: 1024x1024; ClkFreq: 6Mhz ==> div4; Exposure clock: MC/4; Black level reference: 0xa0, which equal to gray level 10.

First the Optical Power Meter measured the power of each LED. The measurements were done for each one of 16 levels. The 30mA current was supplied for LED for the intensity level 16. For other levels the current supply is proportional. The results are presented in the table below:

Table 4.3-2: Mapping of TAU-TMS LEDs Intensities Versus Level

LED Intensity Measured By OPM [uW] - wide filter												
Level	1	2	3	4	5	6	7	8	9	10	11	12
1	16	15	16	16	14	17	15	16	12	16	16	14
2	32	32	33	32	29	33	31	32	24	31	32	29
3	47	46	48	47	42	48	45	48	36	46	48	43
4	62	60	62	62	55	63	59	62	47	60	62	56
5	76	74	76	75	68	76	73	76	58	72	75	69
6	89	87	88	88	80	89	85	89	68	85	87	81
7	101	99	100	100	91	101	97	101	77	96	99	93
8	113	111	112	112	102	113	109	113	86	107	111	104
9	124	122	123	124	113	125	120	125	94	118	121	115
10	135	133	133	135	123	136	131	136	102	128	132	125
11	146	143	143	145	132	146	141	147	110	138	141	135
12	156	154	153	156	142	156	151	156	117	147	151	144
13	165	163	162	166	151	165	160	166	124	155	160	153
14	175	171	171	175	159	174	169	175	130	164	168	162
15	185	180	179	184	168	183	178	184	137	171	177	170
16	193	189	189	193	176	191	187	192	143	179	184	178

The LED#6 was the single LED between the 12 LEDs that was activated. It was activated for every consecutive intensity level [1:16]. The 14 pictures were captured that corresponds to the levels 1:9,11:15. The pictures for the levels 10 and 16 were missed. The results were processed and presented in the table below:

Table 4.3-3: Processing Of The Emission / Excitation Ratio Experiment Results

Level	Excitation Intensity [uW/cm2]	Cam ra Readout [GL]	Neighbor Background [GL]	Excitation Backgorund [GL]	Emlssion [GL]
1	17	22.2	4.6	10.12	12.08
2	33	42.4	5.6	12.32	30.08
3	48	60.6	6.5	14.3	46.3
4	63	77.9	7.4	16.28	61.62
5	76	94.2	8.4	18.48	75.72
6	89	109.5	9.3	20.46	89.04
7	101	123.8	10.1	22.22	101.58
8	113	137.3	10.8	23.76	113.54
9	125	150.7	11.7	25.74	124.96
10	138	163	12.7	27.72	135.28
11	146	174.8	13.1	28.82	145.98
12	156	185.2	13.7	30.14	155.06
13	165	194.8	14.4	31.68	163.12
14	174	203.8	15	33	170.8
15	183	210.8	15.4	33.88	176.92

The excitation background was calculated by multiplication by factor x2 of the readout from reaction chamber#5. The emission was calculated by subtraction of excitation background from readout of reaction chamber#6.

The captured pictures are presented on the Figure 4.3-5 below. The picture colors were inverted to negative for better situation illustration.

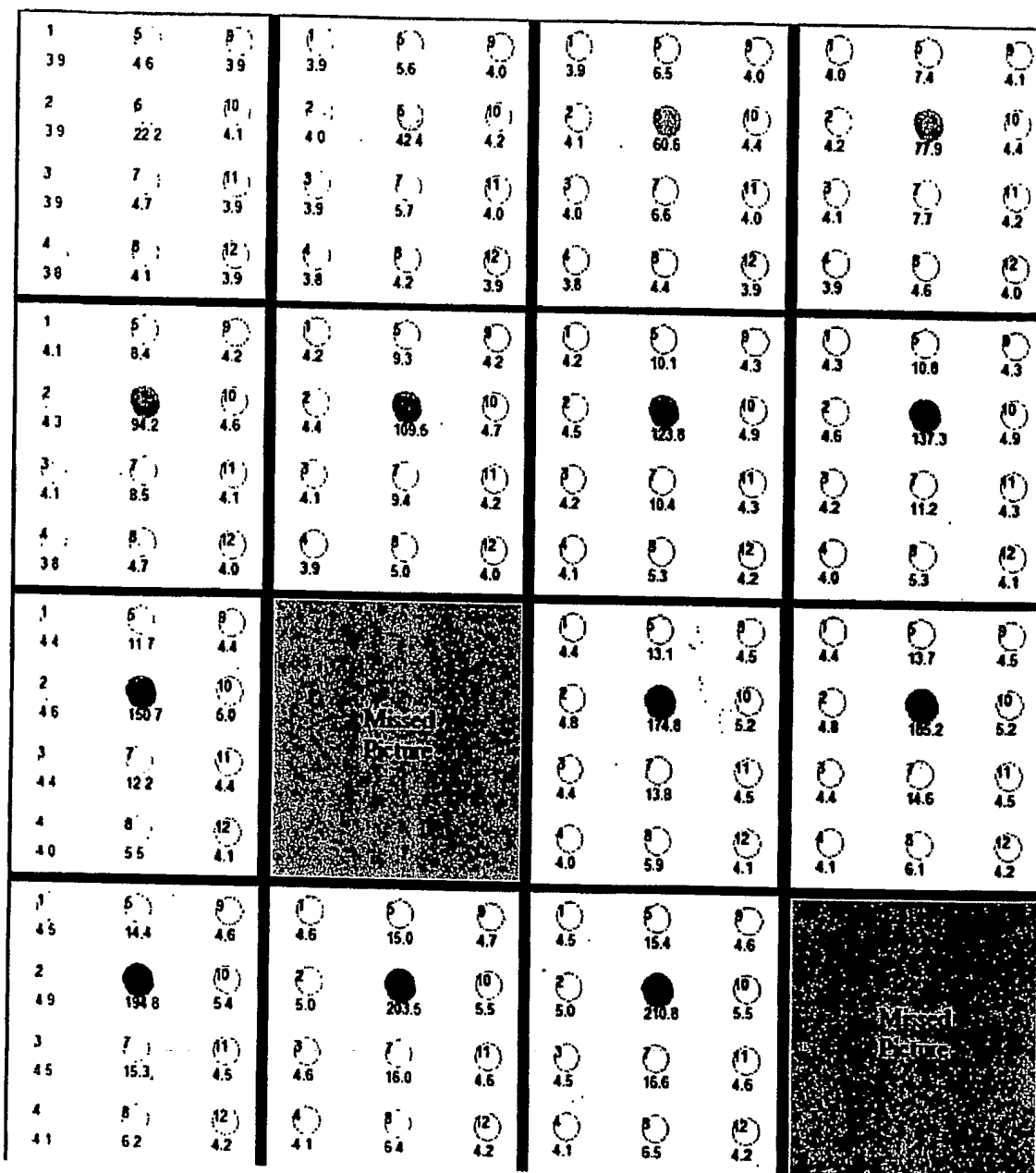


Figure 4.3-5: The 14 Pictures Captured During Emission / Excitation Experiment on TAU-TMS

The result for picture#10 was interpolated. The processed results were presented on the chart below:

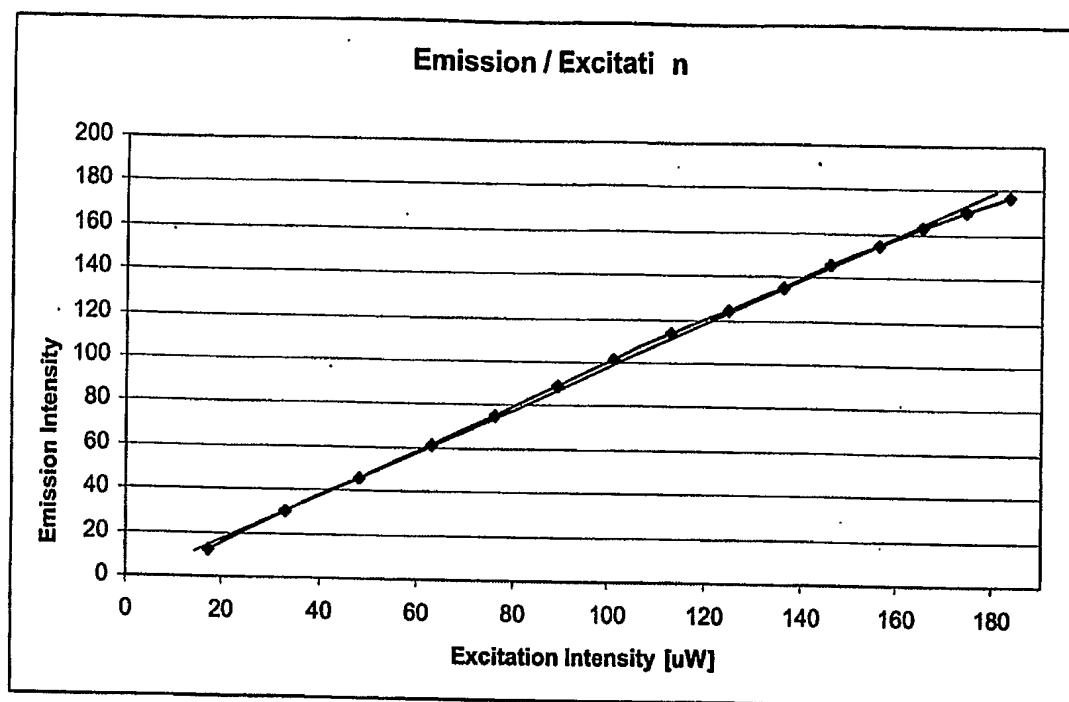


Figure 4.3-6: The Emission Versus Excitation Intensity Linearity.

The blue line is present the real results, while the red line shows the straight line. From the chart above we could see that there is a linear dependency between the excitation and emission.

4.3.3 Emission / Excitation Dependency - Summary And Conclusion

From the two experiments we got that the emission has a linear dependency from the excitation intensity. This important conclusion because the assumption based on it was used many times in this work.

In the integrated system each reaction chamber receives own excitation light source. The intensities of the excitation light sources are not the same. Although the special efforts were done to get the equal excitation light intensities, the variance is still about 20%. The linear dependency between the emission and excitation intensities allows us to make correction for the real emission intensity calculation.

4.4 Kinetics Experiments On The TAU-TMS

After TAU-TMS was completed a number of biological experiments were performed on it. The main goal was to check ability of TAU-TMS to supply the stable bio-signal. The evaluation of the bio-signal uncertainty was important too.

Two types of the kinetics experiments were performed. The fresh biosensors were used for the first type. For the second type dried biosensors were resuscitated and used.

4.4.1 Fresh Biosensors Kinetics Experiments On The TAU-TMS

The biological activity is acquired by working with the fresh biosensors. The fresh biosensors are grown in optimal conditions. Once they are ready, they immediately used for the experiment.

Kiwi chip, described in the "Section 3.2.4" was used for the experiment. All twelve reaction chamber were used under the following conditions: (2 repetitions) x (2 biosensors E-coli - rec-A quantities: 1.5×10^6 , 1.5×10^5 [bacteria/1uL]) x (3 NA concentrations: 0, 5, 10ppm). The experiment duration was 5 hours. The kinetics results are presented on the charts below:

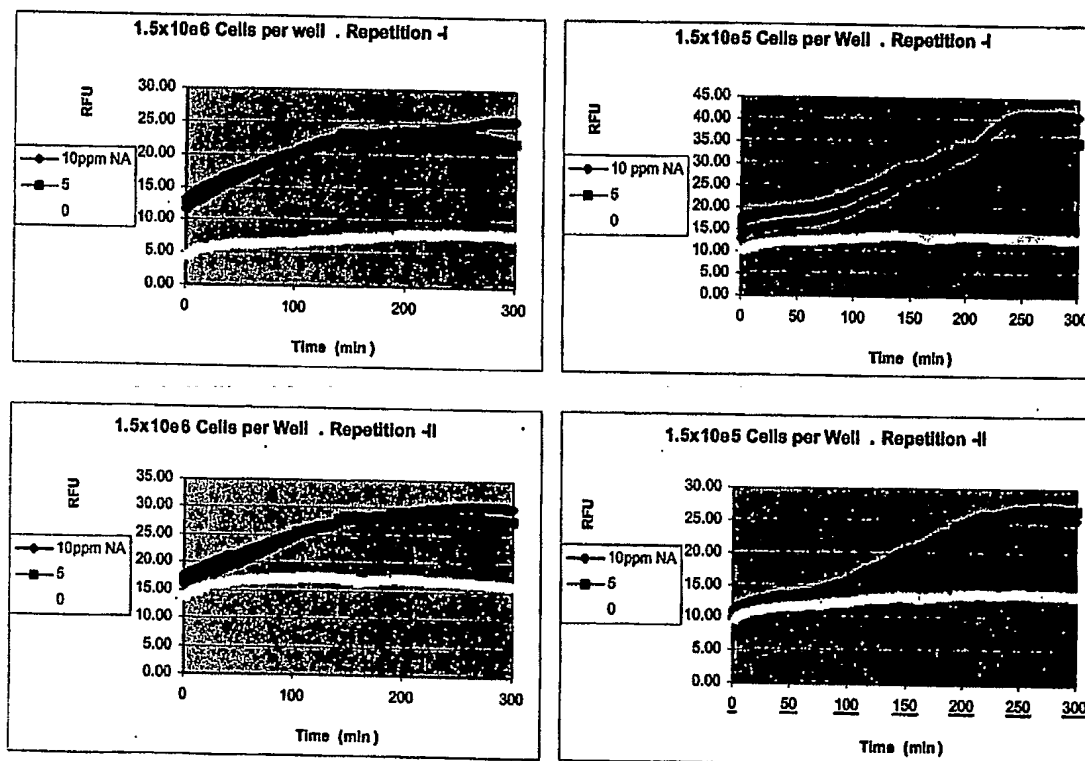


Figure 4.4-1: The Kinetics Experiment With The Fresh Biosensors

From the graphs above we could see that experiment was successful. The expected results were acquired. The stronger emission was registered for $1.5e5$ [b/RC] \Leftrightarrow $1.5e8$ [b/mL]. The biochemical reaction wasn't occurred for zero NA concentration. The significant biochemical reaction was acquired for 5ppm and 10ppm NA.

4.4.2 Dried Biosensors Kinetics Experiments On The TAU-TMS

The viability of the resuscitated biosensors is about 20%. Therefore the bio-signal is too weak to be sensed by TAU-TMS. The weak bio-signal is masked inside the signal uncertainty. In order to decrease the signal uncertainty the TAU-WTA integrated system has been designed. The biochip and electro-optics related modules are currently under debugging. It will be used for biological experiments soon. This is the issue for the further research.

4.5 The Biocompatible Glues Research

There are a few techniques for sealing of the biochip. The techniques included: plasma fusion, ethanol bonding, ultra sonic fusion, simple gluing, etc. The glue residuals could be found in the reaction chamber. The residual could depress the biochemical reaction.

The kinetics experiment was performed to find the biocompatible glue. The cast glues were added to the biochemical solution. The following glues were tested: Epoxy, Super-Glue, Transparent Plastic, Control – no glue. The kinetics of the reactions was registered. The results are presented below:

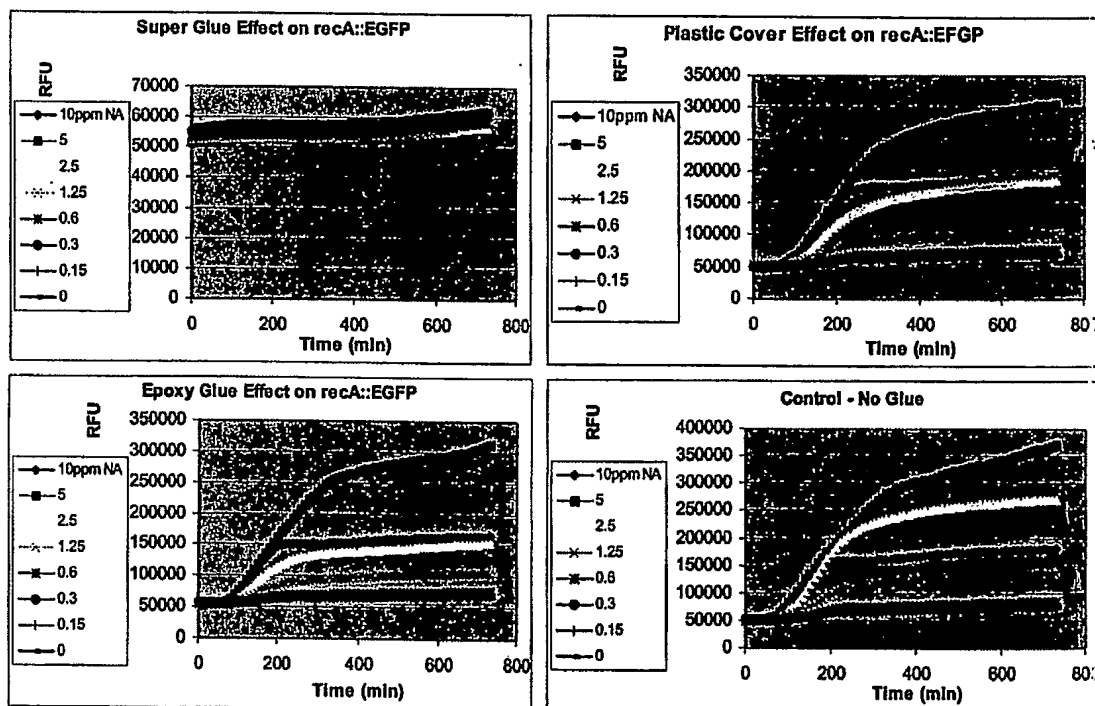


Figure 4.5-1: Influence Of The Glues On The Biochemical Reaction

From the results above we can see that the reaction wasn't occurred in presence of the super glue. The value 55,000 RFU that was registered is the result of nutrients fluorescence. Apparently the biosensors died at the beginning. The epoxy glue and transparent plastic are hasn't influenced on the biochemical reaction.

Currently the transparent plastics are used for the biochip sealing. More glues will be investigated if will be necessary. There is a possibility that glue will be used for the fusion between layer3 and layer2 of the EPMFC-ver4 biochip – refer to the "Section 3.2.5.3". The glues and sealing techniques is the issue for the further researching.

4.6 The Human Cells Emission Intensity As Function Of The Concentration

Using the human cells as the whole cell based biosensors is a very important part of the research. The human cells are much more complex than the bacteria. Therefore much more efforts are applied to get the working biosensors. On the other side the human cells are expected to be much sensitive to the toxicants than the bacteria.

The research and development of the human cell based biosensors is performed in the Israeli Ministry Of Health (MOH). The human cells based biosensor that was tested is marked as *HU.EF1:EG4*. The goal of the performed experiment was to find the minimal cells concentration required to get measurable bio-signal on the TAU-TMS.

The human cells were grown on the 2x2mm surface of the Kiwi chip reaction chambers. Actually the cells were grown on the bottom covering glass. The following concentrations were prepared: 500, 750, 1000, 1500 cells/well. Four Kiwi biochips were used correspondingly to the concentrations. All 12 reaction chambers of the Kiwi Chip were utilized with the same content. The cells were already induced, therefore single picture capture was done for each concentration. The picture of the emission received from biochip with 1500 cells/well presented below:

4	8	12
112.9	108.5	23.8
3	7	11
36.2	116.5	132.6
2	6	10
93.9	93.8	29.3
1	5	9
75.1	69.6	62.7

Figure 4.6-1: Emission From Human Cells - 1500 cells/well

We could see that not for all wells the reaction occurred. For example the signal wasn't acquired from the wells: 3,10 and 12. The strong emission was registered from the wells: 2,4,7,8 and 11.

The average value of all wells for specific concentration is calculated. The resulted average values for each concentration are compared. The wells without signal were not considered in the average value calculation. The unfiltered excitation light (backlight) was quantified too. It was subtracted from the emission signal during results processing.

For the 1500 cell/well concentration the results processing shown in the table below:

Table 4.6-1: Human Cells – 1500 cell/well results processing

Reaction Chamber	Backlight	Signal + Backlight	Signal	Good Result	
1	31.2	75.1	43.9	1	43.9
2	50.3	93.9	43.6	1	43.6
3	24.4	36.2	11.8	0	0
4	25.9	112.9	87	1	87
5	32.7	59.6	26.9	1	26.9
6	27	93.8	66.8	1	66.8
7	23.9	116.5	92.6	1	92.6
8	24.5	108.9	84.4	1	84.4
9	28.3	62.7	34.4	1	34.4
10	30.6	29.3	-1.3	0	0
11	27.2	132.6	105.4	1	105.4
12	17.5	23.8	6.3	0	0
				9	585
				Average 65.00	

The column "Good Result" indicates if the well was considered in the average value calculation. The "Signal" column is calculated by subtraction of the "Backlight" from "Signal + Backlight". The results of the same processing for the rest of concentration are presented on the chart below:

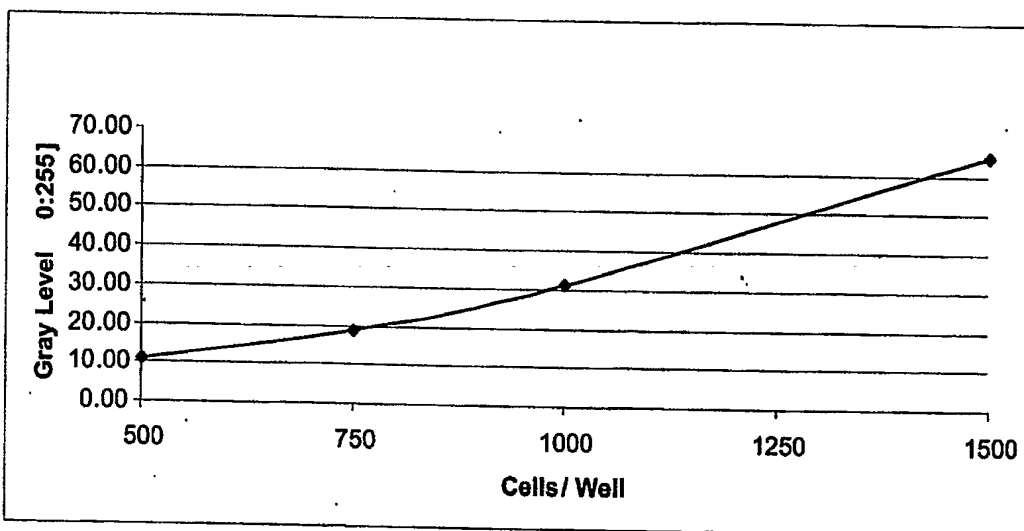


Figure 4.6-2: Emission Intensity As Function Of Human Cells Concentration

We got almost linear dependence of the emission intensity from cells concentration. The conclusion is that for higher concentration of the human cells, the integrated system more sensitive.

In contradictory to the bacteria the biological activity of the human cells is raised when cell are close to each other. Filling the full volume of the reaction chamber by the human cells could increase dramatically the sensitivity of the integrated system.

4.6.1 Increasing Integrated System Sensitivity By Growing Cells On The Beads

The human cells could be grown just on the surface. In order to fill the reaction chamber volume with the human cell, beads solution was suggested. The method described on the figure below:

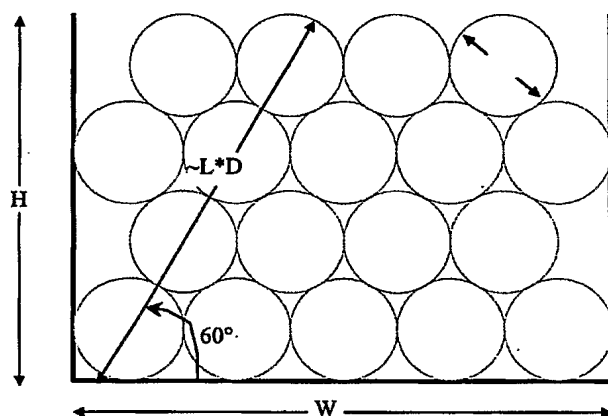


Figure 4.6-3: Human Cell Grown On The Beads Fills The Reaction Chamber Volume

The increase in signal amplitude is expected to be proportional to the surface area. The calculations presented below:

The number of bid layers L: $N \cdot D = \frac{H}{\sin(60^\circ)}$, therefore

$$L = \frac{H}{D \cdot \sin(60^\circ)} \quad (4.6-1)$$

Now we interested to find the total number of beads inside the reaction chamber. The number of beads in the single even level is:

$$N_{\text{even}} = \left(\frac{W}{D}\right)^2 \quad (4.6-2)$$

In the odd level will include the following number of beads:

$$N_{\text{even}} = \left(\frac{W}{D} - 1\right)^2 \quad (4.6-3)$$

Therefore the total number of beads is:

$$N_{total} = 0.5 \cdot L \cdot (N_{even} + N_{odd}) \quad (4.6-4)$$

The surface area of the single bead is

$$S_{bead} = 4\pi \cdot (D/2)^2 \quad (4.6-5)$$

And the total surface area is:

$$S_{total} = S_{bead} \cdot N_{total} \quad (4.6-6)$$

The ratio between the surface areas of the mono-layer to the beads is:

$$R = S_{total} / W^2 \quad (4.6-7)$$

The example of such calculation is presented below:

Reaction Chamber			Bead		
Width	W	1 mm	Diameter	D	0.1 mm
Thickness	H	1 mm	Surface	Sb	0.0314 mm ²
Layers number	L	11	Ntotal		995.5
Neven		100	Stotal		31.275 mm ²
Nodd		81	Sbid/S		31.275

For the reaction chamber with dimension of 1x1x1mm and beads with diameter of 100um the increase of x31 in sensitivity could be achieved. This is the issue for the advanced research.

5 Discussions

In Section 3 we presented in details the investigation of the integrated system. All the engineering aspects including mechanics (Section 3.6), electronics (Section 3.5) and software (Section 3.7) were successfully realized. The temperature control design in Section 3.4 is currently under implementation. It expected to add stabilization factors to the biological signal acquisition and increase the light quantification device sensitivity.

The TAU-TMS integrated system was completely implemented and found appropriate for working with fresh bacteria (Section 4.4). The TAU-WTA integrated system, which is successor of the TAU-TMS, is currently under implementation and debugging. We are envisaging that it will improve in order of magnitude the sensitivity to the biological signal and will allow working with the biosensors rehydrated from dormant state.

A great progress must be notified with the biochip investigation. The IPMFC technology was evaluated and characterized (Section 3.2.4.1). The EPMFC technology has been evaluated too. We have found that the "serial channels" topology, implemented in the EPMFC-ver3 design, guaranteeing equal liquid pumping into each reaction chamber. We implemented pneumatics module allowing pumping liquid with 100nL resolution. The conceptual design for the EPMFC-ver4 biochip presented in the Section 3.2.5.3 fulfilling the biochip micro-fluidics requirements presented at the beginning of the Section 3.2.1. Future implementation of the EPMFC-ver4 chip will provide solution for on chip biochemical reaction initialization. This will finalize the biochip functional configuration requirements.

The GFP based optical reporters of the biosensors were experimentally characterized (Section **Error! Reference source not found.**). Following the spectral features of the optical reporters excitation and emission filters were selected correspondingly (Section 3.3.2).

The light generation technologies were investigated (Appendix-A). The "Light Emitting Device" (LED) was selected as most suitable technology. The matrix of discrete LEDs was implemented in the TAU-TMS integrated system (Section 3.3.3.1). The disadvantages of the discrete LEDs were analyzed in the same section. The 5mm LED with the optical fibers solution was implemented in frame of the TAU-WTA integrated system design (Section 3.3.3.2). It allowed to reduce the reaction chambers pitch for EPMFC-ver3 biochip and to utilize better excitation energy.

The photometry technologies were mapped in Appendix-B. The CMOS Image Sensor devices were selected for light sensing and quantification. Two CMOS image sensors are have been used in the research (Sections **Error! Reference source not found.**). The

methodology for utilization of the CMOS Image Sensor as photometry device was presented in Section 3.3.4.1.

In Section 3.3.5 the model of the bio-fluorescence electro-optical system was introduced. It allows us to make the integrated system performance estimation before implementation of the biochip reaction chambers geometry, optics and electro-optics and to save a lot of unnecessary efforts. The bio-emission cross-talks, which is an important parameter too, hasn't been yet analyzed in the model, therefore beehive structure eliminating cross-talks was implemented in the optical-mechanical setup. The miniaturization of the integrated system has been achieved by mLens based optical setup implementation (Section 3.3.6.3). The addition of the spatial filter, presented in Section 3.3.6.3.3, expected to increase the sensitivity of the electro-optical system in some extra orders of magnitude. The optical setups without lens, with video-lens and array of mLens were presented in Section 3.3.6 and compared in Section **Error! Reference source not found.**

The methodology for the calibration of the integrated system is introduced in Section 3.8. It will be evaluated after completion of the TAU-WTA integrated system electro-optical part debugging. The stability of the light emission and sensing as function of temperature was characterized in Section 3.8.4.2.

The "Biological Signal" was firmly defined in Section 4.1 as efficiency of the biochemical reaction, which is equivalent to percentage of the whole cell based saturation by GFP molecules. The methodology for the calculation of the bio-signal amplitude was presented in the Section 4.2. The bio-signal amplitude is an obligatory input to the water contents analysis algorithms that currently under development. The Section 4.2.2 described methodology for calculation of the bio-signal amplitude for data received from the Victor-2 industrial fluorometer.

Various biological characterizations were performed during the research. Part of them were presented in the Section 4. We convinced that bio-emission intensity is proportional to the excitation (Section 4.3). The TAU-TMS integrated system was evaluated as compatible to work with fresh biosensors, however not sensitive enough to work with the rehydrated biosensors (Section 4.4). The basic research of biocompatible adhesives was done and presented in Section 4.5. In addition to cooperation with biologist from HUJI, the experiments with human cells prepared at Israeli ministry of health were performed. The concentration of the human cells in order to get measurable biological signal was done (Section 4.6). The method to increase in order of magnitude the biological signal received from the human cells was suggested in Section 4.6.1.

6 Summary And Conclusions

The title of the research described in that book is "Whole' Cell Based Acute Toxicity Detection Integrated System". It's obvious that this is a very multi-disciplinary research. The performance of the integrated system depends on the long list of aspects like: biology, chemistry, heat transfer, electronics, optics, electro-optics, u-fluidics, material processing, mathematics, and software and may be more. All of those aspects were considered in that research.

Although all aspects were considered in the research, not all were deeply investigated. The aspects that were not deeply investigated are out of scope of my research work. However the improvement of the integrated system must be continued. This improvement will allow detection of smaller concentrations and also will expand the list of detectable chemicals.

The aspects that were not deeply investigated were mentioned as "issues for advanced researching" in this book. They are concentrated at the table below:

Table 4.6-1: The Issues For Advanced Research

#	The Issue For Advanced Research	Description and Motivation	The Section in which it was Mentioned
1	Excitation Light Spatial Filtering	Blocking the unfiltered excitation rays. Improves significantly sensitivity of electro-optical system. The expensive fluorescent filters set may be not necessary.	3.3.6.3.2
2	Bio-Signal Uncertainty Analysis	The precise estimation of the uncertainties. This will allow prioritizing the required improvements. The improvement in performance of the integrated system could be estimated for each uncertainty reduces.	3.8.1
3	Bio-Signal Precision Analysis	Bio-signal calculation based on assumptions regarding biosensor dimensions, symmetry, concentration and absorptions. The precise researching of above factors will allow precise bio-signal quantification. That will allow to compare bio-signal received from different biosensors	4.2.1
4	Slow Bio-Signal Compression Algorithm	Allows significantly reduce amount of data necessary to archive the test history. Can accelerate the water analysis algorithms. Can reduce the hardware resources requirements	3.7.2
5	Algorithms for chemical and their concentration	The panel of biosensors, stable integrated system and high sensitivity will allow that.	3.7.3

	detection		
6	External Pumping Mechanism Precision	The trend of the research is to scale down the reaction chamber dimensions. In order to allow that the external mechanism for the liquid pumping must have a high pumping resolution.	3.2.5.1
7	EPMFC-ver4 Design	Complete solution for all requests from the biochip	3.2.5.3
8	Biochips high quantity production technology	Production of medium quantity of the biochips for massive experimental data acquisition. Mass production for the potential products	3.2.6
9	Rehydrated Biosensors Kinetics Experiments on TAU-WTA	Evaluation of TAU-WTA integrated system sensitivity to the bio-signal emitted by the rehydrated biosensors. High sensitivity will allow to TAU-WTA to become commercial device for Water Analysis	4.4.2
10	Biocompatible Glues	To find biocompatible glues for biochips sealing and fabrication	4.5
11	Growing human cells on the beads	Filling the volume of the reaction chamber with the human cells by beads. This increase the sensitivity of the integrated system	4.6.1
12	CCD and Photon Counting Head	Advanced research for the very low light bioluminescence intensities quantification	3.5.4
13	Nutrient medium optical characterization	Investigating nutrients medium with low without fluorescent ingredients	4.2.2
14	Interference type filters attenuation versus incident angle	The exact characterization of the attenuation efficiency versus angle is important in consideration of the electro-optical setup design. E.g for specification of excitation light and emission collecting optics	3.3.2
15	Image Sensor Noise Analysis	Knowing the noise sources will allow to reduce them and increase the sensitivity of the integrated system	Appendix-C
16	Measurement of the bio-fluorescence electro-optical system model parameters	Precise simulation of the integrated system setup before manufacturing.	3.3.5
17	Bio-emission cross-talks characterization	Estimation of the trade-off between the electro-optical system sensitivity and the bio-emission cross-talks	4

The goal of this work has been achieved. We have a working integrated system TAU-TMS allowing us to get measurable bio-signal resulted from interaction between the biosensors and chemicals. The TAU-WTA integrated system is currently under debugging and expected to provide significant improvement in sensitivity and uniformity of the results.

The methods for the biological signal quantification are presented in this work (Section 4.2), therefore the research on water analysis algorithms could be started.

The deep investigation of the issues presented at the Table 4.6-1 is a real challenge, which is necessary to achieve in order to commercialize the integrated system.

7 References

1. Frances S. Ligler, J.P.G., Chris A. Rowe-Taitt, and James P. Dodson, *Array biosensors for simultaneous detection of multiple analytes*. SPIE, 2001. 4252.
2. Richard B. Thompson, H.-H.Z., Badri P. Maliwal, and Carol A. Fierke, *Real Time Quantitation of Cu(II) by Fluorescence-Based Biosensing Approach*, in SPIE. 2001.
3. Belkin S., *Microbial whole-cell sensing systems of enviromental pollutants*. Current Opinion in Microbiology, 2003. 6: p. 206 - 212.
4. Johan HJ Leveau , S.E.L., *Bioreporters in microbial ecology*. Current Opinion in Microbiology, 2002. 5: p. 259 - 265.
5. Michael L. Simpson, G.S.S., Greg Patterson. David E. Nivens, Eric K. Bolton, James M. Rochelle, James C. Arnott, Bruce M. Applegate, Steven Ripp, Michael A. Guillorn, *An integrated CMOS microluminometer for low-level luiminiscence sensing in the bioluminiscent bioreporter integrated circuit*. Sensors and Actuators B, 2001. 72: p. 134-140.
6. Tai Hyun Park, M.L.S., *Integration of Cell Culture and Microfabrication Technology*. Biotechnology Progress, 2003. 19: p. 243-253.
7. Jerome Rajan Premkumar, O.L., Rachel Rosen, and Shimshon Belkin, *Encapsulation of Luminous Recombinant E. coli in Sol-Gel Silicate Films*. Advanced Materials, 2001. 23: p. 1773 - 1775.
8. Toshiba, Toshiba Announces New High Sensitivity Biosensor with Optical Sensing Technology. http://www.toshiba.co.jp/about/press/2003_03/pr1901.htm. 2003.
9. PointsourceTechnologies, Vigilant X-3TM Microbiometer. <http://www.pointsourcetech.com/products.htm>. 2003.
10. CHEMetrics, Portable analyzers of cyanide in water. <http://www.chemetrics.com/>.
11. LaMotte, Portable analyzers of cyanide in water. <http://www.lamotte.com/>.

12. Orbeco-Hellige, Portable analyzers of cyanide in water. <http://www.orbeco.com/>.
13. Thermo-Orion, T.E.C.-f., Portable analyzers of cyanide in water. http://www.thermo.com/eThermo/CDA/BU_Home/BU_Homepage/0,1285,161,00.html.
14. SilverlakeResearch, Drinking Water Test Kits. <http://www.watersafetestkits.com/>.
15. UniversalDetectionTechnology, Anthrax 'Smoke Detector'. <http://www.udetection.com>.
16. Kinoshita, R.K., *Optimize Your System With The Right Filter Set*. Biophotonics International, 2002. November 2002: p. 46.
17. Hogan, H., *Picturing the perfect CMOS*. Photonics Spectra, 2003. June 2003: p. 88.
18. Boas, G., *Micro-LEDs enable lab-on-chip technology*. Biophotonics International, 2003. June 2003: p. 27.
19. Evan Thrush, O.L., Ke Wang, Mark A. Wistey, James S. Harris Jr., Stephen J. Smith, Integrated semiconductor fluorescent detection system for biochip and biomedical applications. <http://snow.stanford.edu/~ethrush/>.
20. Lamontagne, N.D., *Flashing fluorescence improves detection*. Biophotonics International, 2003. April 2003: p. 26.
21. Epstein, J., *Optical Fibers Test DNA*. Photonics Spectra, 2003. April 2003: p. 41.
22. Dr. Enrico G. Picozza, D.S.M.F., *The workhouse of Proteomics*. Biophotonics International, 2003. June 2003: p. 40 - 45.
23. Robinson, K., *Near Infrared fluorescent system images the heart*. Biophotonics International, 2002. December 2002: p. 55.
24. Kaplan; Shay (Givat Elah, I.S.A.H., IL), *Apparatus, and method for propelling fluids*. 2002: United States.
25. Mikrotechnik, The Machine For Hot Embosing. <http://www.jo-mikrotechnik.com/page.php?2/8/3>.
26. EpitexIncorporation, SMT470 High Performance Blue color TOP LED. <http://www.epitex.com/html/SMT470.htm>.
27. FillFactory, FillFactory's High Fill Factor N-Well Pixel® (US Patent 6,225,670). http://www.fillfactory.com/htm/technology/htm/high_fill.htm.

28. FillFactory, Dual Slope Dynamic Range Expansion.
<http://www.fillfactory.com/htm/technology/htm/dual-slope.htm>.
29. Marlow, Introduction to Thermoelectric Cooling.
http://www.marlow.com/TechnicalInfo/introduction_to_thermoelectric_co.htm.
30. SpireCoolers, Socket 478 Cooling kit.
<http://www.spirecoolers.com/asp/fcc.asp?ProdID=123>.
31. MaximSemiconductor, MAX1968, MAX1969 Power Drivers for Peltier TEC Modules. http://www.maxim-ic.com/quick_view2.cfm/qv_pk/3377/ln/en.
32. MaximSemiconductor, MAX6957- 4-Wire-Interfaced, 2.5V to 5.5V, 20-Port and 28-Port LED Display Driver and I/O Expander. http://www.maxim-ic.com/quick_view2.cfm?qv_pk=3365.
33. Lumitron, Precision subminiature solid state and incandescent illuminating devices. <http://www.lumitroncorp.com/LED%20Application%20Notes.htm>.
34. Redmond, R.W., Introduction To Fluorescence and Photophysics, in Handbook Of Biomedical Fluorescence. 2003. p. 2-3.

Appendices

Appendix-A The Light Emitting Devices Comparison

Individual Excitation Light Source For Matrix Of Reaction Chambers

#	Excitation Light Device	Intensity	Rays Dispersion	Relevant Spectrum	Dimensions	Conclusion
1	Laser	Very high (*****)	Parallel (*****)	488,470nm (*****)	Too large (*)	Can't be used due to dimensions
2	VCSEL	Very high (*****)	Parallel (*****)	Red, UV (*)	Medium (***)	470nm still wasn't developed, so can't be used
3	Packaged LED die (SMT LED)	High enough (***)	$2\theta_{1/2} = 110^\circ$ (*)	Peak 470nm (*****)	Medium (***)	Excitation energy couldn't be utilized effectively
4	Super Bright (SB) LED	High (****)	$2\theta_{1/2} = 15^\circ$ (***)	Peak 470nm (*****)	Large (**)	Could be applied just for matrix with large pitch
5	SB LED + optical fibers	High enough (***)	$2\theta_{1/2} = 5^\circ$ (****)	Peak 470nm (*****)	Compact (****)	Could be applied for matrix with fine pitch
6	uLED chip + lens matrix	High enough (***)	Parallel (*****)	Peak 470nm (*****)	Very Compact (*****)	The best solution but requiring custom design

Area Excitation Light Source For Matrix Of Reaction Chambers

#	Excitation Light Device	Intensity	Rays Dispersion	Relevant Spectrum	Uniformity	Conclusion
7	Electroluminescent Sheet	Very low (*)	Diffusive (*)	White light (**)	(*****)	Can't be used due to too low intensity and diffusive light
8	Halogen Lamp	Very high (*****)	$2\theta_{1/2} = 100^\circ$ (*)	White light (**)	(**)	Could be used but has uniformity and heating problem
9	Optical Fiber net	Medium (**)	$2\theta_{1/2} = 50^\circ$ (**)	Depends on LED	(****)	Precise custom design required.

	light distributor		(**)			
--	-------------------	--	------	--	--	--

Appendix-B Photometry Technologies Comparison

#	Light Sensing Device	Sensitivity. Required - (**)	Compactness. Required - (****)	Price per matrix. Required - (\$\$)	Conclusion
1	PIN Photodiodes	(***)	(**)	(\$\$)	Could be used for medium-dense RC matrix
2	Avalanche Photodiodes	(****)	(***)	(\$\$\$)	Couldn't be used for non-dense RC matrix
3	Photomultiplier	Medium (****)	(*)	(\$\$\$\$)	Possible with optical fiber and serial readout
4	CMOS IS	(**)	(****)	(\$)	Best solution
5	CCD	(***)	(****)	(\$\$-\$\$\$)	Possible but expensive

Appendix-C Minimal Light Intensity For The IBIS4 CMOS Image Sensor

For the $F_{DC} = 50\%$ the maximal integration time is 28.4[sec]. For $bits = 8bit$ the number of quantization levels is 256, while the $QO_{DC_e} = 128$. The 15% of the dark current non-uniformity contributes uncertainty of $QO_{uncertainty} = 18$. For minimal signal to noise requirement of 3 the signal must be at least $18 \times 3 = 54$ and $QO = 128 + 54 = 182$. For the $QE \cdot FF = 30\%$ the integrated signal characterized by $4.2e4$ [photons] or 1,485[photons/sec]. The signal uncertainty is 1/3 that is 495[photons/sec].

Multiple sampling of the signal followed by averaging could reduce the signal uncertainty. Really the noise analysis is much more complicated issue, but wouldn't be covered in this research.

Appendix-D Abbreviations List

Abbr.	Description	Abbr.	Description
TAU	Tel-Aviv University	LB	Luria Bertani
HUJI	Hebrew University Of Jerusalem	NA	Nalidixic Acid
WTA	Water Toxicity Analysis	BSCF	Bio-Signal Constant Factors
TMS	Toxicity Measurement System	BSVF	Bio-Signal Variable Factors
IPMFC	Integrated Pumps Micro Fluidic Chip	RMS	Root Mean Square
EPMFC	Externally Pumped Micro Fluidic Chip	RFU	Relative Florescence Units
SP	Simple Chip	ROI	Region Of Interest
BSG&M	Biological Signal Generation & Measurement		
GFP	Green Fluorescent Protein		
E. Coli	Escherichia Coli		
CNC			
PVS	Photonics Vision System Inc.		
OCM	Optical Center of Mass		
TEC	Thermo Electric Cooler		
PC	Personal Computer		
PSC	Peak Signal Concentration		

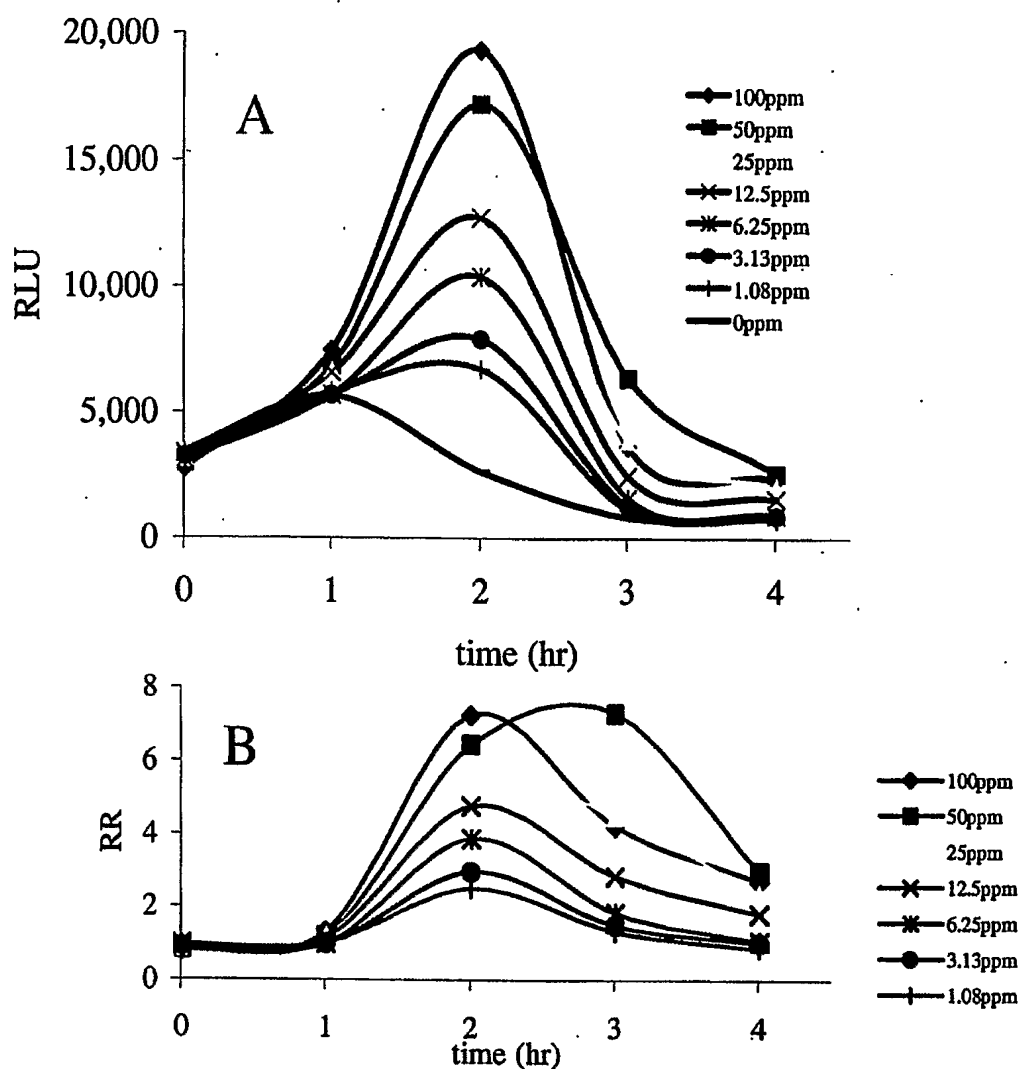


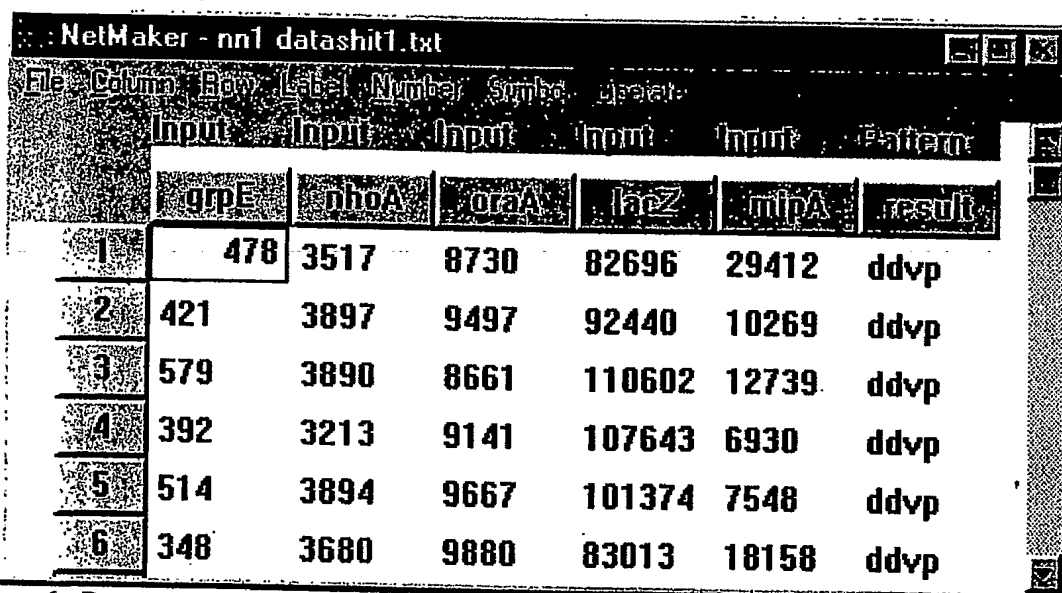
Figure 5 – Response of *oraA::luxCDABE* to nitrogen mustard as an example to the responses exhibited during the screening. Both RLU intensity (A) and response ratio (B) were examined in order to select the appropriate promoters.

2.4.1. Data preparation

To examine the nn detection potential I have entered RLU values produced by five members of the biosensor panel (*grpE*, *lacZ*, *mipA*, *oraA*, and *nhoA*) in response to sterile LB and the five model toxicants, which have elicited adequate responses (DDVP, ethyl parathion, paraquat, potassium cyanide, and nitrogen mustard). The input values were based on the RLU values measured from the panel after 30, 60, and 120 minutes as response to the C_{max} of the different toxicants. In this case I chose to simplify the data by ignoring the time dimension as well as the toxicant concentration. Thus I have produced three separate nn systems for 30, 60, and 120 minutes. As outputs I chose to enter the name of the toxicant, i.e. "DDVP".

The data introduced to the nn had to be arranged in advance in such way that the nn can recognize the data appropriately. The data were arranged in a table and introduced to the NetMaker software (BrainMaker, California Scientific Software) as illustrated in Figure 6. The NetMaker software was used for the preparation of the nn. Using this software I have gathered the data and created training and testing files. In total, 240 "facts" were entered into the NetMaker file for each nn system.

A fourth nn system based on the same data source was set as well. However, in this system I have used data collected during the first 30 minutes (8 RLU readings), thus taking into account the time dimension. This system will be referred to as "time course nn".



	grpE	nhoA	oraA	lacZ	mipA	result
1	478	3517	8730	82696	29412	ddvp
2	421	3897	9497	92440	10269	ddvp
3	579	3890	8661	110602	12739	ddvp
4	392	3213	9141	107643	6930	ddvp
5	514	3894	9667	101374	7548	ddvp
6	348	3680	9880	83013	18158	ddvp

Figure 6 - Data preparation for the nn system in the NetMaker format. The input values were based on the RLU values measured from the panel after 30, 60, and 120 minutes as response to the C_{max} of the different toxicants. The data, which was introduced to the nn had to be arranged in advance in such way that the nn can recognize the data appropriately. The data was arranged in a table and introduced to the NetMaker software. As outputs I chose to enter the name of the toxicant i.e. "DDVP".

data were gathered from experiments which took place in a 96-well microtiter plate while the nn training data was collected from experiments in a 384-well plates.

Running of the time course system was carried out using the average RLU values collected during the first 8 RLU readings (30 minutes).

2.4.5 Toxicant identification

2.4.5.1 Self-testing results

As described in section 3.4.3 the nn tests itself with 10% of the data used for the training. The four nn systems were tested with 24 facts producing the following results:

- 120 minutes nn: 24 of the 24 facts were correctly analyzed.
- 60 minutes nn: 19 of the 24 facts were correctly analyzed
- 30 minutes nn: 22 of the 24 facts were correctly analyzed.
- Time course nn: 24 of the 24 facts were correctly analyzed.

2.4.5.2 Running the nn

As described above, the nn was introduced with average RLU values collected from 40 repetitions of the panel members in response to five different toxicants and sterile LB at a given time (Figure 7). The resulting DP values are detailed in Table 6 and illustrated in the BrainMaker software format in Figure 8. In Table 6 the left column represents the actual toxicant present in the sample while the top row represents the output values produced by the nn as a result of the data introduction to the network. The right column represents the false negative values. These are the probabilities that a poisoned sample is considered a safe one. In the same way, the bottom row represents the false positive values, indicating the probability of a safe sample to be poisoned.

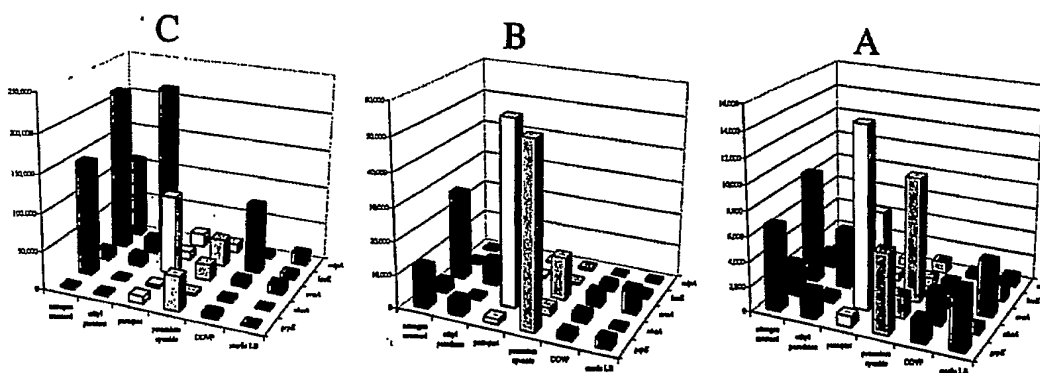


Figure 7 – RLU values used for the running of the three nn systems. The nn was introduced with average RLU values collected from 40 repetitions of the panel members in response to five different toxicants and sterile LB 30, 60, and 120 minutes following exposure (A, B, and C respectively).

0.0003 to 0.0113 indicating that the nn false alarm rate will be potentially very low. More importantly, the false negative rate ranges from 0.0003 to 0.0008. Any similarity between the two organo phosphates was not found though the DP for DDVP when ethyl parathion was actually present, was relatively high (0.0884). This may be due to the limited number of toxicants, which the nn was trained to detect. Another observation is that the distinction of potassium cyanide is relatively poor. The DP for potassium cyanide when DDVP was present was 0.3604 however the reciprocal value was 0.0003 indicating that the nn does not distinct potassium cyanide very well rather than DDVP.

When comparing between the three nns, it is not clear which one produces the best results. This question will be addressed in the discussion.

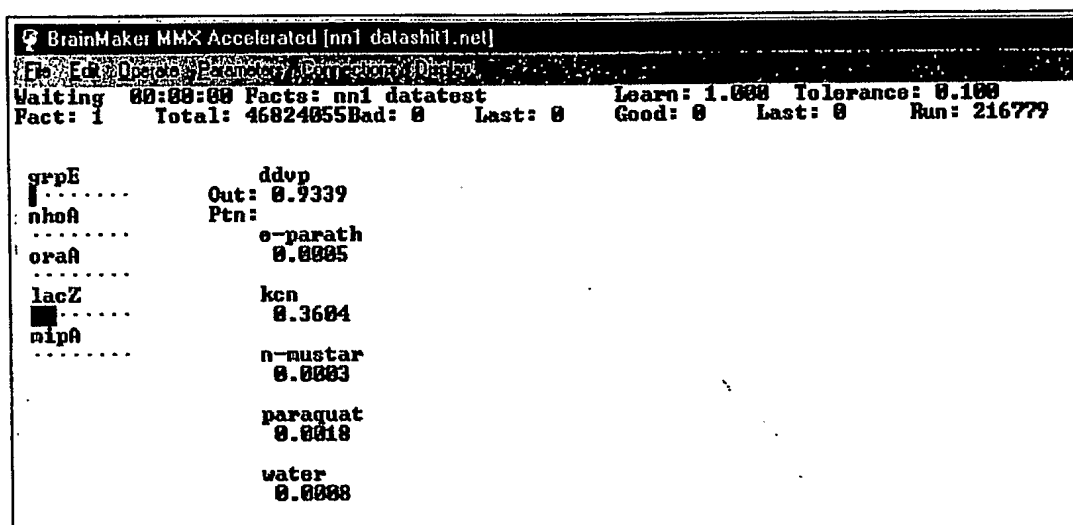


Figure 8 - The resulting DP values as detailed in the BrainMaker software format. The left side of the screen details the input data of the five promoters. The next column to the right shows the output values to each compound. These are the probabilities according to the trained nn system for the presence of each compound in the sample. In this case the nn detected the presence of DDVP in the sample based on the 120 minutes system.

2.4.5.3 nn responses to different toxicant concentrations

The first step of the nn running was with data collected as a response to the same toxicant concentration as the nn was trained with. In this section we have tested the nn with RLU values collected from the panel in response to lower toxicant concentrations. The nn outputs are illustrated in Figure 9 A, B, and C representing the 30, 60 and 120 minutes nns respectively. The graphs describe the nn DP values versus the toxicant concentration. In general, we can see that the DP dependence on toxicants concentrations decreases with time. In other words, the nn, which were trained with "late" data found it difficult to detect low toxicant concentrations. The reasons for this will be discussed later.

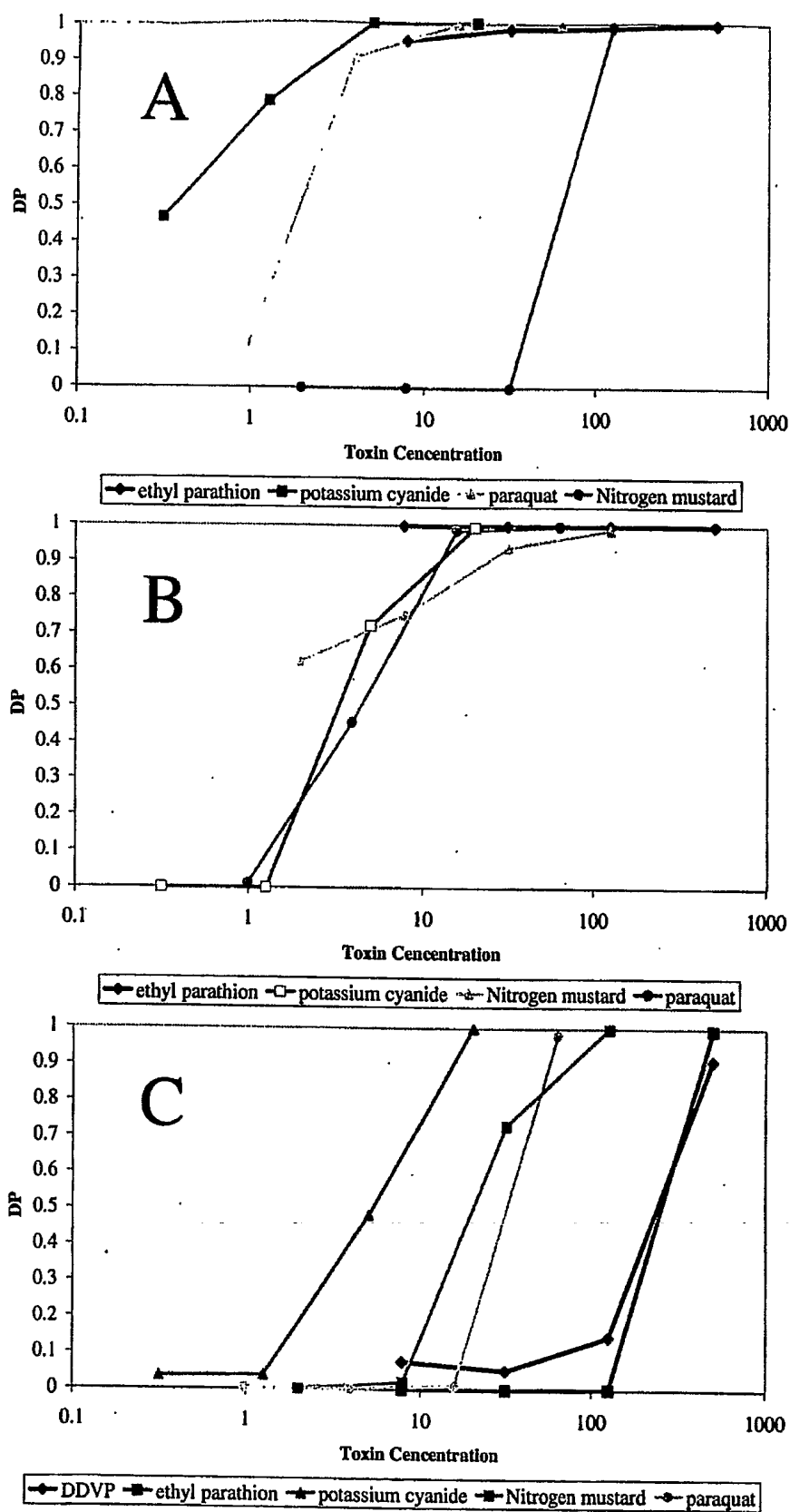


Figure 9 – Testing the nn with RLU values collected from the panel in response to lower toxicant concentrations. The graphs describe the nn DP values versus the toxicant concentration produced by the 30 (A), 60 (B) and 120 (C) minutes nns.

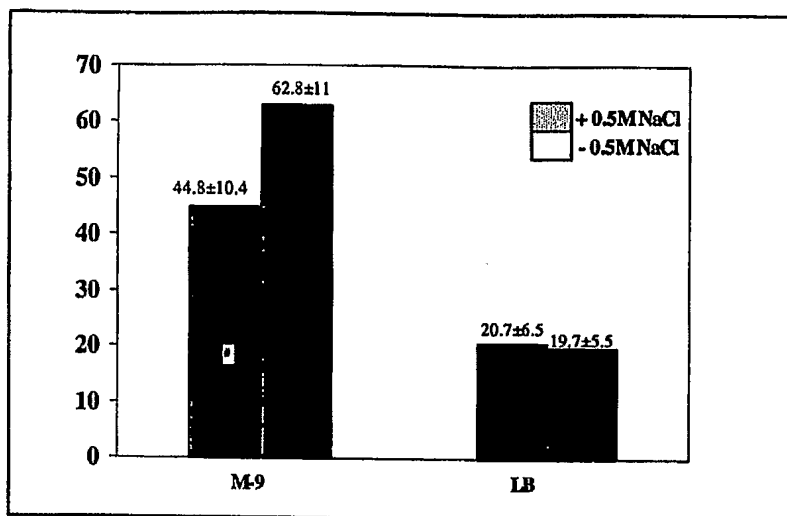


Fig. 10. Survival of *E. coli* MG1655 grown in LB or M-9 with/out 0.5 M NaCl immediately after Freeze-drying

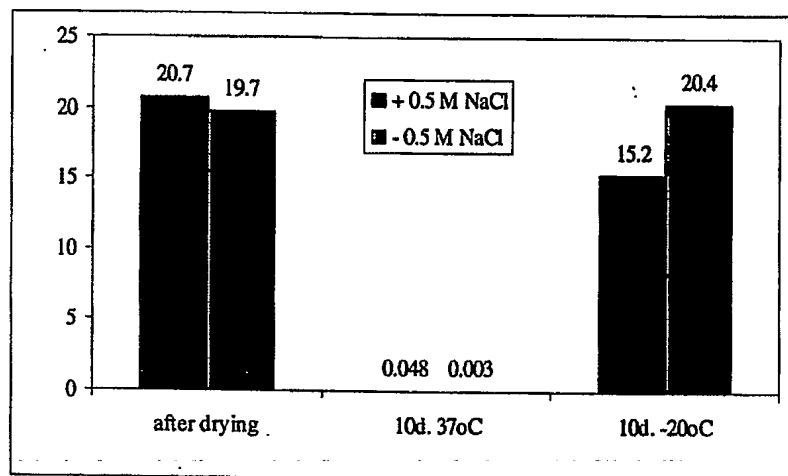


Fig. 11. Survival of *E. coli* MG1655 grown in LB +/- 0.5 M NaCl immediately after freeze-drying and after storage at different temperatures

2.5.3.2. High temperature drying protocol

This protocol was derived from scientific papers and patent by Tunnacliffe et al (US Patent No. 6,468,782. Title- "Methods for preserving prokaryotic cells and compositions obtained thereby") and V. Bronshtein (US patent No. 6,509,146,

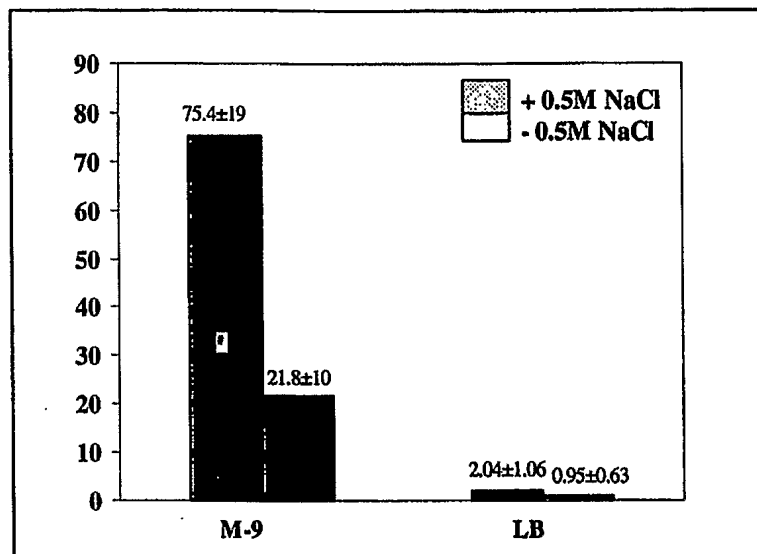


Fig. 12. Survival of *E. coli* MG1655 grown in LB or M-9 with/out 0.5 M NaCl immediately after High Temp Drying

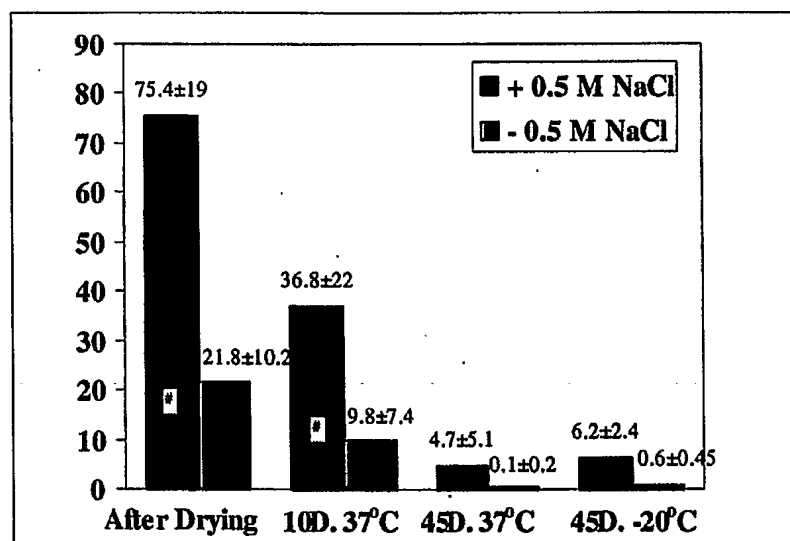


Fig. 13. Survival rates and stability of *E. coli* MG1655 grown in M-9 +/- 0.5 M NaCl immediately after High Temp. Drying and after storage at different temperatures

Recently, a number of experiments, which included a secondary drying step in both freeze-drying and HTD protocols, were conducted. The preliminary results indicated that while the immediate survival rates were similar to ones obtained earlier, the long-term stability upon storage at 37°C for 7-10 days seemed to

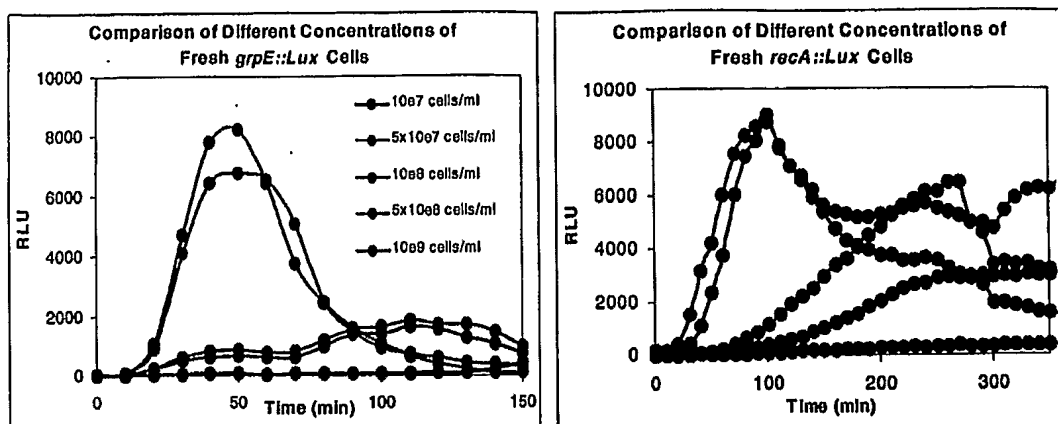


Fig. 14. Fresh Cells *recA::Lux* and *grpE::Lux* induction in different Cell concentrations. Sample volume: 1 μ L.

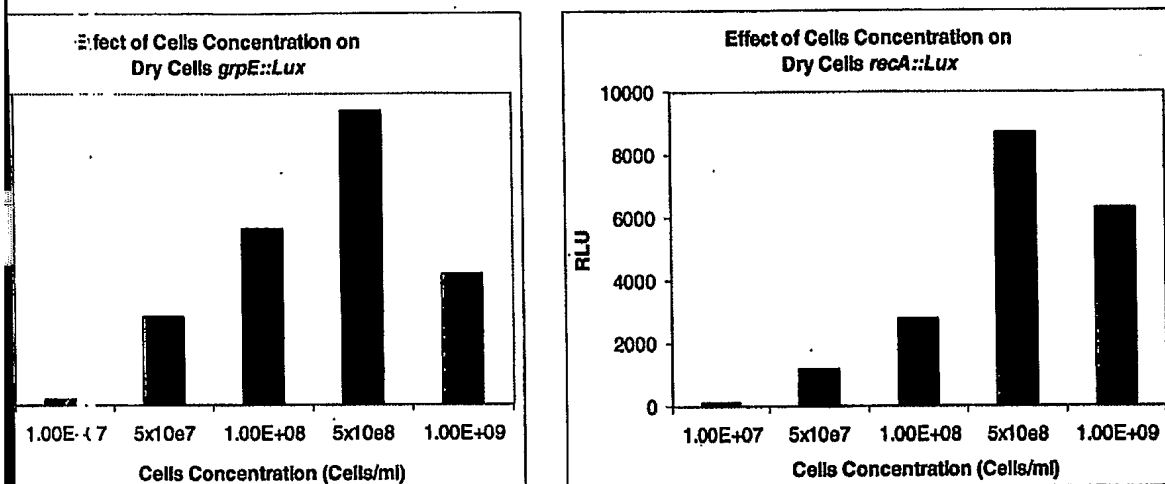


Fig. 15. Dry Cells *recA::Lux* and *grpE::Lux* Induction in Different Cells concentrations and in volume of 1 μ L.

Fig. 16. Reten

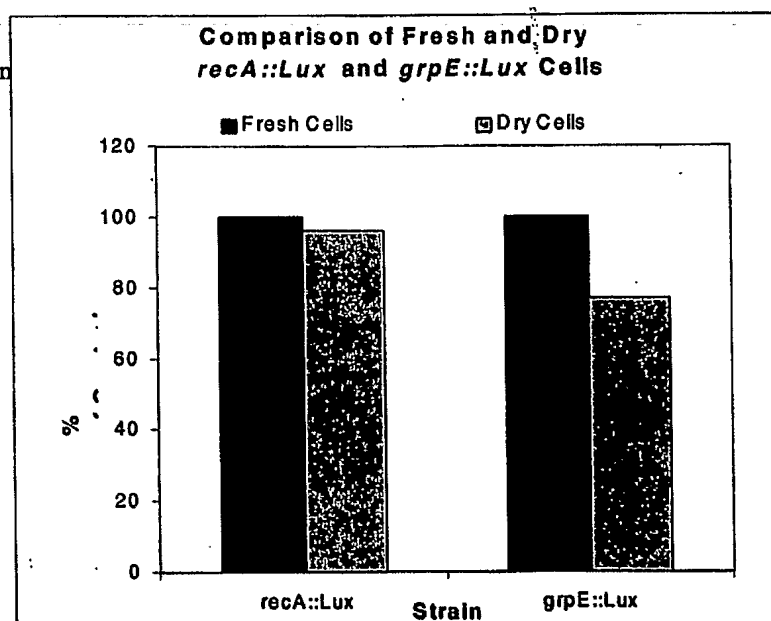


Figure 17 depicts the results of an experiment in which a single cell concentration was used (5×10^8 cells/ml), in different volumes. The differences were not high, but it appears that for this cell concentration a volume of 0.6 μ L seemed preferable.

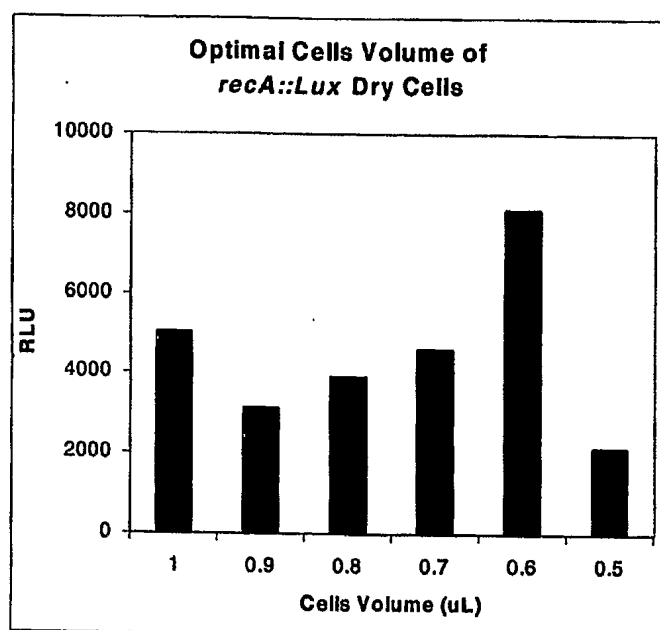


Fig. 17. Dry cells *recA::Lux* induction in different volumes. Cell concentration: 5×10^8 cells/ml.

Using 0.5 μ L as a constant volume, the data in Fig. 18 reflect the effects of different cell concentrations. For both fresh and dry *recA::Lux* cells, best induction occurred at the highest cell concentration tested, 10^9 cells/ml (5×10^5 cells/cavity). In Figure 19, a five-fold higher cell density was tested as well, indicating a lowered activity but an earlier signal development.

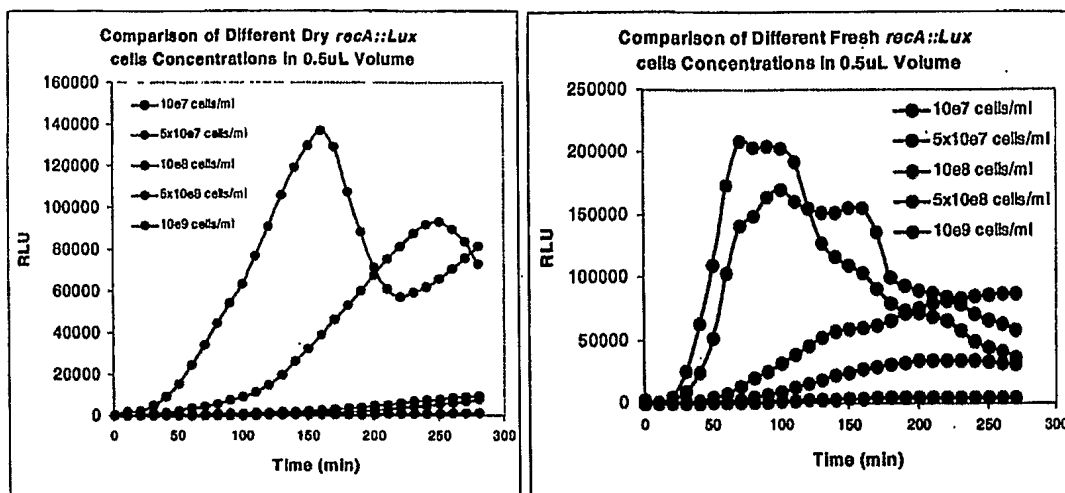


Fig. 18. Dry cells *recA::Lux* induction in different cell concentrations. Volume: 0.5 μ L.

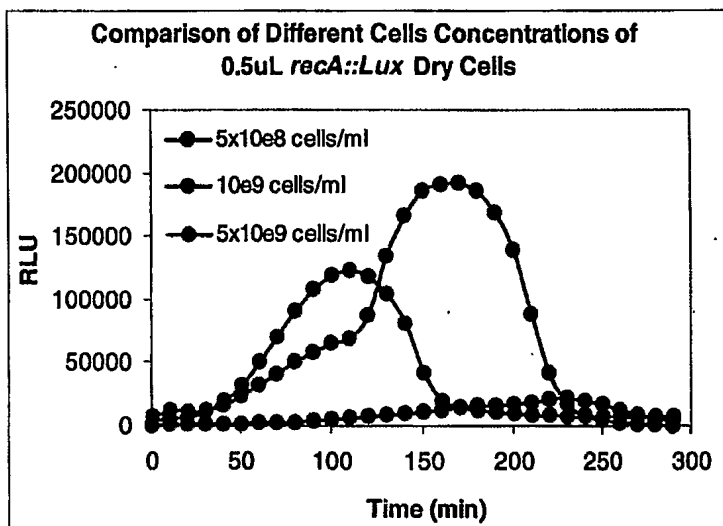


Fig. 19. Dry cells *recA::Lux* induction in different cell concentrations. Volume: 0.5 μ L.

In all the experiments described above, activity data were of cells shortly following the lyophilization procedure. Comparison of residual activity following prolonged storage is depicted in Figure 20, for cells pre-grown in rich (LB) or minimal (M9) media. After 2 weeks of storage, approx. 20% of the activity was retained in cells maintained at -20°C and 5-15 % at 4°C . Growth in M9 appeared to have some beneficial effect.

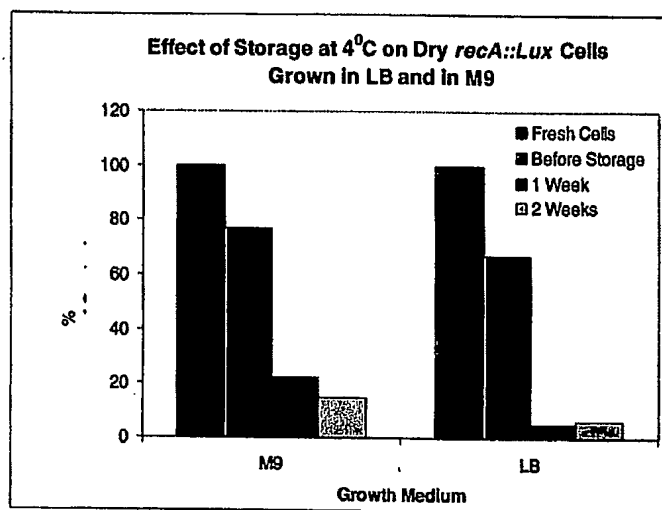
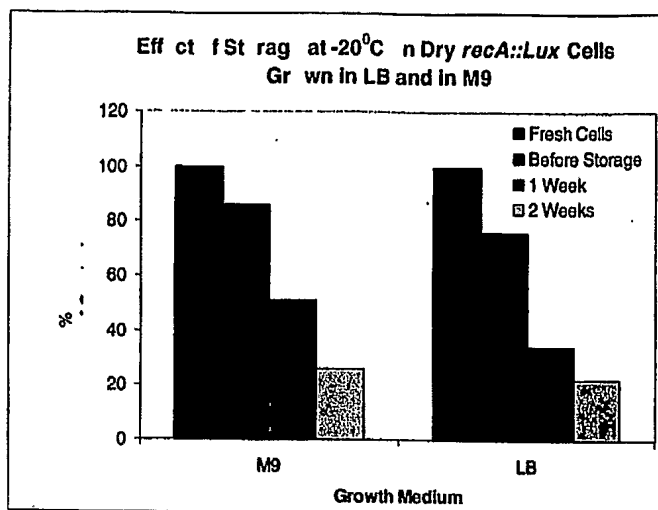


Fig. 20. Residual activity of *recA::lux* cells following storage at -20 °C and 4 °C (bottom).

25. Mbeunkui F, Richaud C., Etienne AL, Schmid RD, Bachmann TT: **Bioavailable nitrate detection in water by an immobilized luminescent cyanobacterial reporter strain.** *Appl Microbiol Biotechnol* 2002, **60**:306-312.
35. Polyak, B, Bassis E, Novodvoretz A, Belkin S, Marks RS: **Bioluminescent whole cell optical fiber sensor to genotoxics: system optimization.** *Sensors & Actuators B-chem* 2001, **74**:18-26.
36. Rajan Premkumar JR, Rosen R, Belkin S, Lev O.: **Sol-gel luminescence biosensors: encapsulation of recombinant *E. coli* reporters in thick silicate films.** *Anal Chim Acta* 2002, **462**:11-23.
37. Biran I, Walt DR: **Optical imaging fiber-based single live cell arrays: a high-density cell assay platform.** *Anal Chem* 2002, **74**:3046-3054.
38. Bolton EK, Sayler GS, Nivens DE, Rochelle JM, Ripp S, Simpson ML: **Integrated CMOS photodetectors and signal processing for very low-level chemical sensing with the bioluminescent bioreporter integrated circuit.** *Sens Actuator B-Chem* 2002, **85**:179-185.

Other references

3. Andersen, J. B., C. Sternberg, L. K. Poulsen, S. P. Bjorn, M. Givskov, and S. Molin. 1998. New unstable variants of Green fluorescent protein for studies of transient gene expression in bacteria. *Appl. Environ. Microbiol* 64:2240-2246.
5. Baldwin, T. O., J. A. Christopher, F. M. Raushel, J. F. Sincliar, M. M. Ziegles, A. J. Fisher, and I. Rayment. 1995. *Curr. Opin. Struct. Biol* 5:798-809.
6. Belkin, S. 2003. Microbial whole-cell sensing systems of environmental pollutants. *Current Opinion in Chemical Biology* in press.
9. Ben-Israel, O. 1998. The use of the microbial *lux* system for elucidation of anti bacterial activity of toxic agents in water. Ph.D. Technion, Haifa.
10. Ben-Israel, O., H. Ben-Israel, and S. Ulitzur. 1998. Identification and quantification of Toxic Chemicals by Use of *Escherichia coli* Carrying *lux* Genes Fused to Stress Promoters. *Appl. Environ. Microbiol* 64:4346-4352.
11. Billard, P., and M. S. DuBow. 1998. *Clin. Biochem* 31:1-14.

15. Chalfie, M., Y. Tu, G. Euskirchen, W. W. Ward, and D.C. Prasher. 1994. Green Fluorescent Protein as a marker for gene expression. *Science* 263:802-805.
16. Cormack, P. C., R. H. Valdivia, and S. Falkow. 1996. FACS-optimized mutants of green fluorescent protein (GFP). *Gene* 173:33-38.
18. Daunert, S., G. Barrett, J. S. Feliciano, R. S. Shetty, S. Shrestha, and W. Smith-Spencer. 2000. Genetically Engineered Whole-Cell Sensing Systems: Coupling Biological Recognition with Reporter Genes. *Chem. Rev* 100:2705-2738.
20. Dvorak, J. 1991. Best of 1990: BrainMaker Professional, Version 1.5. PC Magazine.
21. Engebrecht, J., K. Nealson, and M. Silverman. 1983. Bacterial bioluminescence: Isolation and genetic analysis of functions from *Vibrio fischeri*. *Cell* 32:773-781.
23. Fisher, A. J., F. M. Raushel, T. O. Baldwin, and I. Rayment. 1995. *Biochemistry* 34:6581-6586.
24. Fisher, A. J., T. B. Thompson, J. B. Thoden, T. O. Baldwin, and I. Rament. 1996. *Biol. Chem* 271:21956-21968.
27. Hakkila, K., M. Maksimow, M. Karp, and M. Virta. 2002. Reporter Genes *luxFF*, *luxCDABE*, *gfp*, and *dsred* Have Different Characteristics in Whole-Cell Bacterial Sensors. *Anal. Biochem* 301:235-242.
28. Hansen, L. H., and S. J. Sorensen. 2001. The Use of Whole-Cell Biosensors to Detect and Quantify Compounds or Conditions Affecting Biological Systems. *Microb. Ecol* 42:483-494.
33. Kohler, S., S. Belkin, and R. D. Schmid. 2000. Reporter gene bioassays in environmental analysis. *Anal. Chem* 366:769-779.
35. Leveau, J. H., and S. E. Lindow. 2002. Bioreporter in microbial ecology. *Current Opinion in Microbiology* 5:259-265.
37. Meighen, E. A. 1992. *Encyclo. Microbiol* 1:309-319.
38. Meighen, E. A. 1994. Genetic of bacterial bioluminescence. *Annu. Rev. Genet* 28:117-139.
39. Meighen, E. A. 1991. Molecular biology of bacterial bioluminescence. *Microbiol. Rev* 55:123-142.

40. Meighen, E. A., and P. V. Dunlap. 1993. Physiological, biochemical and genetic control of bacterial bioluminescence. *Adv. Microb. Phys* 34:1-67.
44. Naylor, L. H. 1999. *Biochem. Pharmacol* 58:749-757.
45. Phillips, G. N. 1997. *Curr. Opin. Struct. Biol* 7:821-827.
51. Rosenberg, R. 2002. Accurate high-throughput measurement of *E. coli* promoter activity. Msc. Weizmann Institute of Science, Rehovot.
52. S.G.Boxser. 1996. Another green revolution. *Nature* 383:484-485.
53. Sagi, E., N. Hever, R. Rosen, A. J. Bartolome, J.R.Premkumar, R. Ulber, O. Lev, T.S.Scheper, and S. Belkin. 2003. Fluorescence and bioluminescence reporter functions in genetically modified bacterial sensor strains. *Sensors & Actuators B-chem* in press.
54. Southward, C. M., and M. G. Surette. 2002. The dynamic microbe: green fluorescent protein brings bacteria to light. *Mol. Microbiol* 45:1191-1196.
57. Stewart, G. S. A. B., and P. Williams. 1992. *lux* genes and the applications of bacterial bioluminescence. *J. Gen. Microb* 138:1289-1300.
58. Toxnet.com, posting date. [Online.]
59. Tu, S. C., and H. I. X. Mager. 1995. Biochemistry of bacterial bioluminescence. *Photochem. Photobiol* 62:615-624.
62. VanDyk, T. K. 2002. Lighting the way: Genome - Wide. Bioluminescent Gene Expression Analysis. *ASM News* 68:222-230.
63. VanDyk, T. K. 2001. LuxArray, a High-Density, Genomwide Transcription Analysis of *Escherichia coli* Using Bioluminescent Reporter Strains. *Journal of Bacteriology* 183:5496-5505.
64. VanDyk, T. K., W. R. Majarian, K. B. Konstantinov, R. M. Young, P. S. Dhurjati, and R. A. LaRossa. 1994. Rapid and sensitive pollutant detection by induction of heat shock gene-bioluminescence gene fusions. *Appl. Environ. Microbiol* 60:1414-1420.
66. Walker, G. C. 1996. The SOS response of *Escherichia coli*, p. 1400-1411. In Umbarger (ed.), *Escherichia coli* and *Salmonella typhimurium*: Cellular and Molecular Biology, 2 ed. ASM Press, Washington DC.
69. Wilson, T., and J. W. Hastings. 1998. *Annu. Rev. Cell. Dev. Biol* 14:197-230.
71. Zimmer, M. 2002. Green fluorescent protein (GFP), Application, Structure and Related Photophysical Behavior. *Chem. Rev* 102:759-781.

A BACTERIAL PANEL FOR TOXICITY DETECTION

1. Overview: microbial whole-cell sensing systems

1.1 General approaches to monitoring the presence of chemicals

There are two general approaches to the monitoring of chemicals in the environment. The traditional one is based on chemical or physical analysis: it allows highly accurate and sensitive determination of the exact composition of any sample, it is essential for regulatory purposes, and is necessary for understanding the causes of the pollution and the means for its potential remediation. However, a complete array of analytical instrumentation necessary for such exhaustive analysis is complex, costly, and requires specialized laboratories. In addition, such methodologies fail to provide data as to the bioavailability of pollutants, their effects on living systems, and their synergistic/antagonistic behavior in mixtures. As a partial response to these needs, a complementary approach is based on the use of living systems in a variety of environmentally oriented bioassays.

Numerous biological systems have been used for such purposes, ranging from live organism assays such as fish toxicity tests to others based on sub-cellular components or enzymes. All of them share the same characteristic: they test the effect of the target chemical(s) rather than identify it. A special position among the test organisms utilized for such purposes is held by unicellular microorganisms, bacteria in particular. Their large population sizes, rapid growth rates, low costs and facile maintenance often make them a lucrative option for pollution monitoring.

1.2 Common toxicity bioassays

The aim of toxicity bioassays is to provide the most relevant information regarding the potential toxicity to humans of tested samples. Hence, the closer a test organism is phylogenetically to human beings, the higher the likelihood of it providing relevant toxicological data. Nonetheless, utilization of complex organisms in toxicity bioassays presents difficulties and limitations in terms of culturing, reproducibility and maintenance necessitating to balance the complexity of the organism / assay, and the relevance of the obtained toxicological information. There also ethical and economical considerations that limit the scope of whole-organism assays.

Know water toxicity bioassays make use of whole organisms (fish, crustaceans, oysters, tadpoles, earthworms, plants etc.), isolated tissues & whole-cells of eukaryotic organisms (human, fish, algae), prokaryotic organisms (native or genetically-engineered gram negative bacteria, etc.), and isolated sub-cellular components (enzymes, sub-mitochondrial particles, antibodies, DNA/RNA). The latter are usually of a more selective nature and do not necessarily provide a representation of general bio-toxicity.

Toxicity bioassays may be classified by the bioreporting elements which are utilized (eukaryotic or prokaryotic organisms, whole cells and tissues, cellular isolates, ..), bioreporters responses (for example: behavioral, physiological, metabolic changes), end-points (acute or chronic), application strategy (batch or on-line) etc. The following list attempts to summarize most commonly used assays, either commercially available or under development.

Whole organism-based bioassays make use of a variety of organisms. Toxicity to these organisms is assessed by evaluating changes in behavioral patterns, physiological activities, reproducibility or ultimately in the viability of bioreporter populations. These parameters may be continuously monitored by a variety of high-tech data acquisition systems and evaluated by sophisticated computational algorithms. Non-typical behavioral / physiological states may be considered as indicative of potential toxicity which, pending verification, may be discerned as a true toxic situation.

The organisms, which are used in water toxicity monitoring may be classified by their trophic levels. These include fish, crustaceans, algae, oysters, etc. The following are a few examples of currently available technologies:

1. Fish:

- a. The new bbe fish toximeter (http://www.bbe-moldaenke.de/english/produkte_e.html)
- b. The new combined bbe fish and Daphnia toximeter (http://www.bbe-moldaenke.de/english/produkte_e.html)
- c. Real time fish biomonitor-USACEHR
(http://usacehr.detrack.army.mil/acam/Methods/Fish_Bio/default.asp)
- d. Bio-Sensor – automated and continuous water quality monitor
<http://bmi@biomon.com/biosenso.html>
- e. BehavioQuant® fish toxicity monitor
<http://www.bafg.de/html/projekte/biomonitore/index.htm>

2. Daphnia, mussels-clamps, and algae:

- i. Daphnia, mussels-clamps, and algae toximeters (bbe) (http://www.bbe-moldaenke.de/english/produkte_e.html)
- ii. Super IQ Toxicity Test kit, Artoxkit M™, CerioFast™, Daphnia magna, Daphnia pulex, Daphnia IQ test, Daphtoxkit F™, Thamnotoxkit™, Thamnocephalus plat (http://www.aquasurvey.com/Services/Screening_Tests/screening_tests.html,
http://www.biohidrica.cl/Assay_Thamnotoxkit.htm)
- iii. Musselmonitor (http://www.musselmonitor.nl/01_engels/01_starteng.htm)

Eukaryotic whole-cell based bioassays make use of intact cells or tissues that originate from a variety of organisms. Changes in the activity of cells such as electric currents, pigment arrangement, translocation of cellular moieties are monitored and serve as toxicity indicators.

The following are a few examples of currently available and under development technologies:

1. The FluoroTox system (Cellomics-<http://www.cellomics.com/>)
2. Neuron based biosensor – electric pulse signals (NRL)
3. Fish chromatophors – color pattern signals of fish chromatophors (OSU)
4. DARPA projects (Cellomics, Neuron cells on solid state electronics {Cornell}, mammalian olfactory system (odorants) {Harvard}, vascularized tissue sensors {MIT}, detection system for biological agents (toxins) {Promega corporation}, brain based hybrid device cultured brain slices {Univ. Of California}, Hybrid biological-electronic biosensors, cultured neural tissues, debilitation of cognitive functions-multichip module {Univ. Southern California})
5. Induction of MFO (mixed Function Oxidases) *in vitro* (hepatocytes from fish, rats, chickens, .).

Whole-cell bacterial based bioassays follow and monitor metabolic activity of bacteria, which serves as indicators of toxicity. A partial representation of technologies, which use native – non-engineered bacteria is presented in the following paragraph.

- i. Microtox – use of naturally luminescent marine bacteria for toxicity determination (<http://www.azurenv.com/mtox.htm>)

- ii. Toxichromotest- EBPI-Canada: sensitive *E.coli* strain in which toxicity inhibits β -galactosidase, which upon reaction on a chromogenic substrate produces a measurable color (<http://www.ebpi-kits.com/toxichromotest.htm>)
- iii. Mutatox – for the determination of genotoxicity using a native dark variant of luminescent marine bacterium (<http://www.azurenv.com/mtox.htm>)
- iv. ToxAlert {Merck} – toxicity determination using luminescent marine bacteria
- v. Toxscreen bioassay – Checklight, toxicity determination by marine luminescent bacteria (<http://www.water-technology.net/contractors/monitoring/checklight/>)
- vi. ATP-tox system – measures the effect of toxicity on bacterial growth and luciferase activity by measuring luminescence of cell extracts. The bacterial cells may be of several types such as *E. coli* and *Salmonella*.
- vii. *Bacillus subtilis* rec assay – estimates the mutagenicity of samples by their affects on viability of rec-defective strains of *Bacillus subtilis*
- viii. Ames test – getotoxicity determination – determination of genotoxicity by reversion of inability to synthesize histidine.
- ix. On-line TOX – toxicity determination by immobilized marine bacteria (http://w210.ub.uni-tuebingen.de/dbt/volltexte/2001/308/pdf/Buettner_114_pic.PDF)

It is worthwhile to note that while the majority of technologies are suited to perform batch measurements under laboratory conditions, only a few are field-orientated and a just handful are available as on-line monitors, a valuable and sought-after application.

The on-line technologies include all of the fish based monitors, some of the daphnia, mussels-clamps, and algal test, the MICROTOX –OS monitor that is based on the AZUR bioreporter technology and was developed by Siemens, the IUT On-line TOX, and the on-line version of the Toxscreen bioassay by Checklite.

BioPhysico-chemical toxicity bioassays

These assays make use of cell-free biological active entities that originate from living cells, and include the following:

1. **Immunoassays:** Designed for the detection of specific agents like pesticides & contaminants {Millipore, Ohmicron, ..}, some are field- portable kits (plates, electrodes).

2. **Enzymatic assays:** Enzymes are intensively used for many diagnostic applications including environmental monitoring. In these applications enzymes such as AchE, organophosphate hydrolase are fabricated and immobilized on appliances or materials such as electrodes, chips arrays etc. Changes in enzymatic activity (usually its decrease) are measured (potentiometric, color, ...), and may be indicative of the presence of toxicity.
3. Instrumentation based on enzymatic reaction of horse reddish peroxidase to produce luminescence, EcloxM-probably specific to selected agents {Severn Trent-mil spec}.

As mentioned above, the micro-size bioreporter (whole cell or cell free materials) may be immobilized on varying surfaces and appliances, hence bearing the ability to be used in arrays, which ultimately may present a high thru-put, highly effective means for toxicity monitoring.

1.3 Genetically engineered microorganisms as biosensors

An additional attractive characteristic in the use of bacteria is that they can be "tailored" to respond by a detectable signal to pre-specified changes in their environmental conditions. Several recent reviews have addressed different aspects of the use of such genetically engineered microorganisms as bioreporters (S1-S6, 6).

In all cases, the principle is the same: the fusion of two genetic elements, one of them acting as the sensing element and the other as a reporter.

Choice of sensing element: in most cases a promoter of a gene belonging to suitable stress response system is selected. The specificity and spectrum of the response depend upon the choice of promoter.

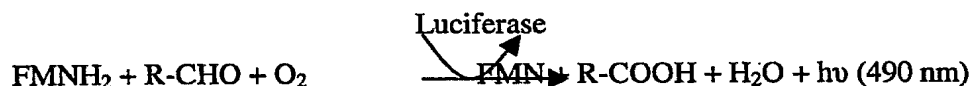
Choice of reporting element: there are several available options for a molecular reporter system. In the present project, we have concentrated either on bacterial bioluminescence (*lux*) genes or a green fluorescent protein (gfp) gene.

Using similar approaches, bacterial strains have been developed for assaying genotoxicity, rather than "regular" toxicity. In these cases, the promoters serving as the sensing elements were selected from among DNA repair operons such as the SOS system, and the reporters were either bacterial *lux*, *β -gal* (S4) or *gfp* (S17, S18). A more developed yeast-based (*Saccharomyces cerevisiae*) system for genotoxicity assessment is being continuously improved upon by Walmsley and coworkers (S19).

1.3.1 Bacterial bioluminescence

Bioluminescence appears in many groups of organisms such as insects, algae, dinoflagellates, fungi, jellyfish, clams, shrimp, squid, fish and bacteria (18). Bioluminescence was studied thoroughly both genetically and biochemically and bioluminescence genes were cloned into organisms which are not naturally luminescent. Luciferase is a generic name for any enzyme that catalyzes a light-emitting reaction (5, 18). The different luminescent organisms differ in the luciferase structure and activity, as well as in its substrate (33, 40). Luminescent bacteria are facultatively aerobic gram negative rods mostly found in the marine environment. These have been classified into three genera: *Vibrio*, *Photobacterium* and *Photorhabdus* (39). They appear as free-living cells, or symbionts. Amongst them the species *Vibrio fischeri*, *Vibrio harveyi*, *Photobacterium phosphoreum*, *Photobacterium leiognathi* and *Photorhabdus luminescens* (57, 59). Only the latter is a non-marine organism.

Luciferase acts as a mixed function oxidase, which catalyzes the oxidation of a reduced flavin mononucleotide (FMNH₂) and a long chain aldehyde to FMN and a corresponding fatty acid in the presence of molecular oxygen. This reaction produces 490 nm light emission (62):



The bacterial luciferase is a heterodimeric protein built of α and β subunits. The α and β subunits amino acid sequence differ within bacterial species by up to 45% and 55%, respectively (11, 37). The α subunit (41 kDa) is in charge of light emission, enzyme's affinity and turn-over number. It has been suggested that the enzyme's catalytic site lies in the α subunit (23, 24, 69). The β subunit (37 kDa) is assumed to involve FMN interaction (40). The natural bacterial luciferase substrate is an aldehyde tetradecanal, synthesized by an heterotetrameric enzymatic complex (500 kDa) called Fatty Acid Reductase (FAR)(50). This enzymatic complex consists of four reductase, synthetase and transferase subunits.

The most studied bacterial luminescence system is that of *Vibrio fischeri* (27). It is encoded by the *lux* system, which is a seven-gene system divided into two operons transcribed in opposite directions (Figure 1). Between the two operons is the regulation site.

The right operon includes the *luxA* and *luxB* genes, encoding for the synthesis of the α and β luciferase subunits respectively. The genes *luxC*, *luxD* and *luxE*, encoding for the reductase, synthetase and transferase FAR subunits respectively, are positioned in the right operon as well (62). The gene *luxI* is stationed upstream to the *luxC* and encodes the LuxI protein, an autoinducer synthetase.

The left operon consists of *luxR*, which encodes for the synthesis of the LuxR protein. It interacts with the autoinducer to form a regulatory complex for the *lux* operon gene induction regulation (21, 38, 39). When used as a reporter system, *luxR* and *luxI* are removed, and the *lux* operon's expression is regulated by the promoter fused upstream to the *luxC* gene.

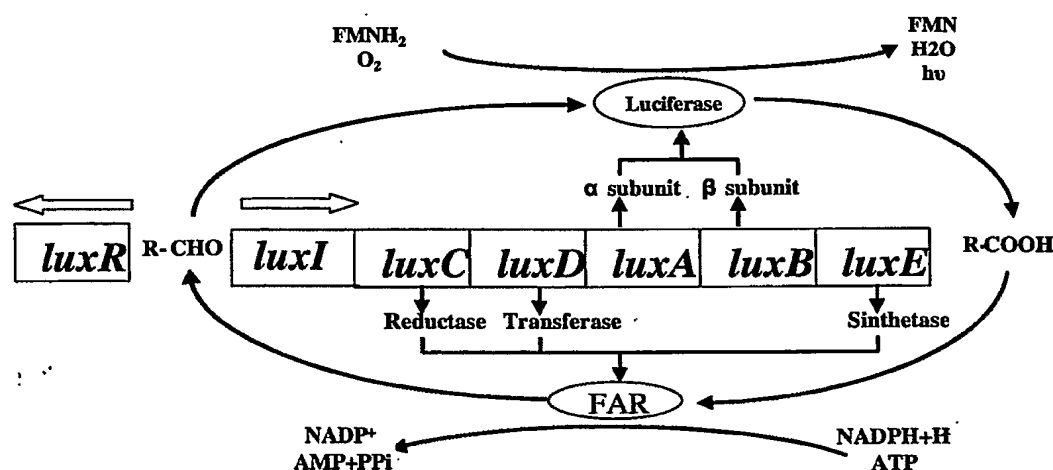


Figure 1 – Regulation of the *luxCDABE* operon of *Vibrio fischeri*.

1.3.2 Green fluorescent protein

GFP is a photoprotein which has been isolated and cloned from the jellyfish *Aequorea aequorea* better known as *Aequorea victoria* (Figure 2D). In the last decade there has been an extensive use of the GFP, which currently has 22 variants available. As a reporter, the GFP has several advantages. It is autofluorescent, and therefore no addition of cofactors or substrates is required (44). The GFP is a highly stable protein, and some variants have half-lives of more than 24 hours (3). It remains stable even in extreme pH and is resistant to photobleaching (71). It is not involved in cell metabolism, and thus remains fluorescent in non viable cells (15, 27). Bacteria containing GFP can be detected at a single cell level using techniques such as epifluorescence microscopy or flow cytometry (28, 35). GFP acts as an accessory protein to aequorin or luciferase by shifting the blue bioluminescence produced by these proteins into green fluorescence emission (45). Excitation of the GFP is maximal at 395

1.3.3 Selecting the appropriate promoter

There are two general strategies for selecting the appropriate promoter for the design of a bacterial reporter strain.

One of them is based upon pre-existing knowledge: the selection of known promoters, previously shown to be induced by the target chemicals.

The other approach is based upon the screening of a large number of genes, in search for the ones induced in the presence of the target chemicals. In this approach, pre-knowledge of the nature of the gene and its promoter is not required. The only important outcome at the screening stage is that the gene is induced by the target chemicals. A detailed study of the characteristics of the response can then follow.

Such a screening can be carried out using two different types of analytical tools: DNA arrays and promoter fusion libraries. In the present project we have adapted the second type, using two libraries (both in *E. coli*, with *E. coli* promoters): a *lux* fusion library obtained from Dupont and a *gfp* fusion library from the Weizmann Institute.

1.3.3.1 The *E. coli luxCDABE* promoter fusion library

The library was obtained from Dr. Tina Van Dyk of the DuPont Company. It contains 689 different promoters upstream of the *luxCDABE* inserted into pDEW201 plasmid and transduced into *E. coli* strain DPD1675. 27% of the *E. coli* genome is represented in this library including most of the stress response systems (62). The *luxCDABE* genes used in this library were from the terrestrial bacterium *Photorhabdus luminescens*. During the experiments each construct was exposed to seven toxicants at seven concentrations as well as to a control sample.

1.3.3.2 The *E. coli* GFP library

The GFP library was obtained from Dr. Uri Alon of The Weizmann Institute of Science generously supplied the library (51). It contains 189 *E. coli* strains harboring low copy plasmids with different promoters upstream to the GFP coding sequence. The library was exposed to several toxicants in order to locate the responding promoters.

1.3.4 Use of genetically engineered bacteria for toxicity monitoring

As mentioned above, genetically-engineered bacteria may be used for toxicity / genotoxicity assessments. While some bacterial constructs may be used as indicators of

specific agents or selected groups of toxic substances (heavy metals, DNA damaging agents), others may be used as indicators of general toxicity / genotoxicity.

Several genetically-engineered based toxicity/genotoxicity monitoring systems are commercially available or under development:

1. Vitotox – ThermoLab sys. - Use of genetically engineered *Salmonella typhimurium* harboring a *recN::lux* fusion for genotoxicity determination and a *pri::lux* fusion as indicator of cytotoxicity and internal control. The development of luminescence is monitored and acts as a measure of genotoxicity and cytotoxicity. (http://www.thermo.com/eThermo/CDA/Products/Product_Detail/1,1075,12903-116-X-116-13985,00.html)
2. umuC assay - Use of genetically engineered *Salmonella typhimurium* harboring a *umuC::lacZ* fusion for genotoxicity determination. Upon genotoxic damages the *umuC* gene is activated producing β -galactosidase, which upon reaction with a chromogenic substrate produces a measurable color.
3. MetPLATE & MetPAD – Activation of β -galactosidase by the presence of heavy metals, which upon reaction with a chromogenic substrate produces a measurable color (http://www.biohidrica.cl/Assay_MetPlate.htm)
4. SOS chromotest – Special *E. coli* strain which contains a *sfiA::lacZ* fusion hence the expression of β -galactosidase is under the regulation of the SOS response i.e. assesses genotoxicity. Determination of post exposure β -galactosidase activity is achieved by its interaction with a chromogenic substrate that produces a measurable color. Constitutive Alkaline phosphatase activity serves as a monitor of bactericidal effects (http://www.biohidrica.cl/Assay_SOSchromotest.htm).

1.4 Biosensors and whole-cell biosensors

A biosensor is an instrument that couples a biological entity to a hardware system for various detection applications. Normally, the advantage in using a biological component lies in the extremely high specificity of biological molecules. Thus, successful biosensors have been based on the specific interactions between enzymes and their substrates, the recognition between antibodies and antigens, accessibility of specific target molecules to their receptors, or the high affinity of

nucleic acids strands to their complementary sequences. In all of these, the focus is on the specificity endowed by the unique bio-recognition of two molecules.

A completely different analytical approach calls for the biological entity in question to be not a molecule but rather a live, intact cell. While a lot of the specificity described above may be lost, it is more than compensated for by the fact that by monitoring such an activity we are able to detect, by very simple means, very complex series of reactions that can exist only in an intact, functioning cell. Global parameters such as bioavailability, toxicity, or genotoxicity cannot be probed with molecular recognition or chemical analysis; they can only be assayed by using whole cells.

In the present project we have set out to define a whole-cell reporter panel, based on genetically engineered *E. coli* strains, that would compose the biological part of a whole-cell, biochip biosensor system.

1.5 The panel approach

Regardless of how well a microbial sensor strain is designed and engineered, it is unreasonable to expect that a single strain will be able to cover the whole range of toxicants that need to be detected in a broad spectrum toxicity detection system. One of the possible solutions is to put together a panel of sensor strain that, together, will provide the desired detection range.

This idea has been put forward several times in the past, including by Belkin (S14) and others (9, 10). Similar panels have recently been shown to sensitively respond to important environmental pollutants such as dioxins (S15) and endocrine disruptors (S16). In these and many similar studies, the reporter system of choice was a microbial bioluminescence operon (*luxCDABE*).

The panel approach has also been utilized at least in one commercial product that we are aware of, for the purpose of in vitro toxicology by gene expression profiling technologies. As we understand it, the company involved, Xenometrics, is now a part of "Discovery Partners International" (<http://www.discoverypartners.com/index.html>).

1.6 Interpretation of the panel's responses

As pointed out above, the reporters panel will be composed of different bacterial strains that, together, will cover a broad spectrum of toxic responses. For this purpose, the

spectra covered by the different strains should be complementary, but also with a significant degree of overlap.

When such a panel is exposed to a toxic sample, three types of information can be gained from the response:

- i) The **occurrence** of a signal will indicate that the sample is toxic
- ii) The **intensity** of the signal will be a measure of the degree of toxicity
- iii) The **pattern** of the response (which strains are "turned on", and by how much) will reflect the nature of the toxic effect of the sample.

The analysis of part (c) above is the most complicated, but is an integral part of the proposed concept. We have demonstrated the feasibility of this concept by using a commercially available "Neural Network" (nn) software (BrainMaker, California Scientific Software). The nn software is named after the human brain cells that perform intelligent operations, and it can be trained by repeated presentation of examples, which include both inputs and outputs. In our case the input is the reporting system's signal intensity (e.g. luminescence, fluorescence) while the output will be the toxicant identity. Nns, just like people, learn by example and repetition. At a fundamental level, all nns learn associations. When the network sees particular input data, it responds with particular output data. The software is based on a large-scale statistical analysis of the input data, which is amended following each training session to the desired accuracy (20). When the nn is being trained, it is presented with many input-output pairs of data. These input-output pairs are called "facts". Following training, the nn can be tested with data that was not introduced to it before and only then the nn can run with real data.

Every responsive promoter produces a unique response pattern to different toxicants. These fingerprints can be characterized in three dimensions (intensity, time and toxicant concentration). If the nn can identify the response pattern of each promoter to each toxicant it may be able to detect the toxicant present in the sample according to the panel's response.

1.7 Immobilization and integration of bacterial cells into biosensors

In the microbiological environment, the term "biosensor" or "microbial biosensor" is often used to describe just the responsive microbial strain. In biosensor literature, however, it is claimed that in order to be considered a true biosensor the biological entity needs to be integrated into the appropriate hardware, as indicated in the definition provided in the beginning of this review. While the isolated bacterial strain may serve as an excellent reagent in the laboratory, in order to be taken outside its boundaries it needs to be incorporated into a

device that will allow storage and maintenance of the live cells, access to the sample and signal capture. Several recent reports offer some potential incorporation solutions including alginate attachment onto optic fiber tips (S35), agar immobilization at the bottom of microtiter plate wells (S25) and encapsulation in sol gel matrices (S36). In the latter report, encapsulated luminescent bacteria maintained full activity at 4 °C for over 3 months. A different approach, that of random embedding of individual fluorescent *E. coli* and *Saccharomyces cerevisiae* cells into a high-density microwell array etched at the distal edge of an optical imaging fiber was reported by Biran and Walt (S37). The location and fluorescence of each individual cell was monitored using an optical decoding system, based upon the specific "signature" of each cell type. A chip-based system was developed by Simpson and coworkers, who used a CMOS (complementary metal-oxide semiconductor) imager for very low-level detection of the bioluminescent signal of a *Pseudomonas fluorescence* strain induced by naphthalene or salicylate (S38). Their device, termed bioluminescent bioreporter integrated circuit (BIBIC), is probably the first integrated whole-cell biochip.

A different tack towards the production of a whole-cell biochip is pursued in the present project, in which bioluminescent or fluorescent *E. coli* sensor cells are maintained in mm-size cavities on a silicon or plastic chip.

2. Methodology and main results

2.1 The model toxicants used

Seven model toxicants listed in Table 1 were selected as representatives of the different toxicants groups and were chosen according to their toxicity and other characteristics unique to their group.

Table 1- The seven model toxicants, their molecular formula, mechanism of action and the LD₅₀ values calculated for an oral exposure to rats according to (58).

Toxicant	Molecular formula	Mechanism of action	LD ₅₀ (mg/kg)
Ethyl Parathion	C ₁₀ H ₁₄ NO ₃ PS	AChE Inhibition	2
Dichlorvos	C ₄ H ₇ Cl ₂ O ₄ P	AChE Inhibition	56
Potassium Cyanide		Reacts with Iron in Mitochondrial Cytochrome Oxidase	6.5
Nitrogen Mustard	C ₅ H ₁₁ Cl ₂ N	Alkylation by Beta-Carbons (DNA cross-linking and cleavage)	10
Paraquat	C ₁₂ H ₁₄ N ₂	Depletion of cellular NADPH	150
Methomyl	C ₅ H ₁₀ N ₂ O ₂ S	AChE Inhibition	17
Botulinum Toxicant A		Irreversible binding to motoneuron junction (presynaptic)	0.1

2.2 Promoter screening

The *E. coli luxCDABE* library was the major screening tool for the promoter search. During this step more than 200,000 luminescence reading were carried out in order to locate the best responding and suitable promoters for the biosensor panel.

2.2.1 Bacterial strains and plasmids

The library was provided by Dr. Tina Van Dyk at DuPont. It contains 689 different promoters upstream of the *luxCDABE* operon fused into the pDEW201 plasmid (Figure 3) and transformed to *E. coli* strain DPD1675 (63). 27% of the *E. coli* genome is represented in this library including most of the stress response systems (62). The *luxCDABE* genes used in this library originated from the terrestrial bacterium *Photorhabdus luminescens*. In addition one strain containing the *grpE* promoter upstream to the *luxCDABE* operon of *Vibrio fischeri* was tested at 30 °C (64).

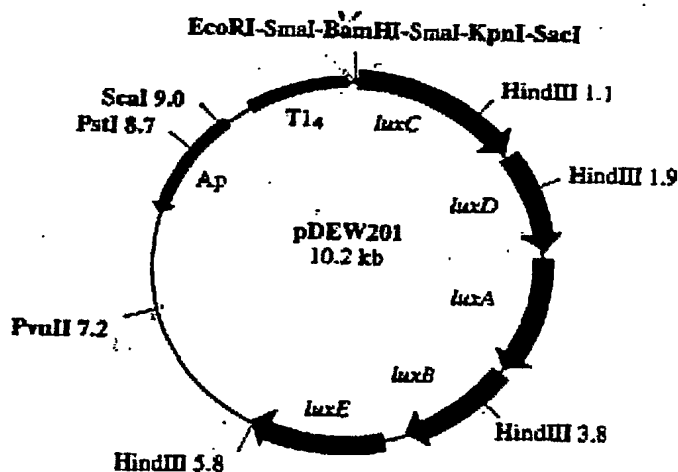


Figure 3 - pDEW201 plasmid containing the *luxCDABE* operon from the terrestrial bacterium *Photorhabdus luminescens*. This plasmid was used for the *luxCDABE* library construction. By inserting 689 different *E. coli* promoters upstream to the *luxCDABE* operon followed by transformation into *E. coli* RFM443 strain DPD1675 (63).

2.2.2 Bacteria storage

The library is kept in 96-well microtiter plates (Costar. USA), at -80 °C (Revco LegaciTM. USA), in 20% glycerol solution (Frutarom LTD. Israel). The library is being restored every three months by growing each strain overnight in LB with 100 µg ampicillin/ml (Sigma. USA) in a 96-well 2 ml microtiter plate (Costar. USA), at 37 °C, 200

rpm (YIH DER LM-530 incubator), followed by re-suspension in glycerol to a final concentration of 20%.

2.2.3 Cell growth and exposure to toxicants

During the experiment each strain was exposed to seven toxicants at seven concentrations as well as to a control sample.

Growth: Each strain was grown for 20 hours in 1 ml LB with 100 µg ampicillin/ml (Sigma. USA) followed by x100 dilution into a final volume of 1 ml LB for two hours in a 96-well 2 ml microtiter plate (Costar. USA), at 37 °C, 200 rpm (YIH DER LM-530 incubator).

Exposure to toxicants: Bacteria were then transferred into a 384-well microtiter plate (Costar. USA) containing double dilutions of the toxicant in LB in such a manner that each strain was exposed to seven different concentrations of the toxicant as well as to a control containing LB only.

2.2.4 Luminescence measurement and data analysis

Luminescence was measured during 4-6 hours in 1-1.5 hour intervals using VICTOR² Wallac 1420 luminometer (Turku, Finland). Luminescence is represented by Relative Luminescence Units (RLU). The responses were characterized using several parameters:

A. Luminescence, (RLU).

II. Response Ratio (RR_L) was calculated as the ratio between the luminescence measured from the induced well (RLU_i) divided by the luminescence measured from the control well (RLU_c):

$$RR_L = RLU_i / RLU_c$$

III. RR_{max} - Maximal RR_L obtained during the course of exposure.

IV. C_{max} - toxicant concentration that produced the RR_{max}

Another analysis that took place was the RR_{max} distribution amongst the whole *luxCDABE* library. This was done in order to examine the screening procedure's efficiency to differentiate responding from non-responding promoters. Promoters were divided according to their RR_{max} into the following groups:

Non - responsive – $0 < RR_{max} < 2$

Low - responsive – $2 < RR_{max} < 3$

Medium - responsive – $3 < RR_{max} < 5$

Highly - responsive – $5 < RR_{\max} < 10$

Very highly - responsive – $10 < RR_{\max}$

RR_{\max} distribution that will show a high proportion of responding promoters will imply that the screening protocol, does not answer the screening's objectives. However, a high Non – responding combined with a low very high – responding proportions will imply on a good screening procedure.

2.2.5 Characterization of the luminescent bacterial panel

In the first step following the completion of the screening, strains which responded to the toxicants were isolated and retested to verify their response. Then a series of experiments took place to characterize the responses of the selected promoters. This provided information as to the response rate, sensitivity, specificity and toxic concentrations of the toxicants as well as the determination of operation parameters of the biosensors. These experiments were carried out in a 40 repetitions format in order to increase the characterization's significance (Figure 4A).

Further experiments using other toxicants were carried out as well. These took place in a white 96-well microtiter plate as explained in section 3.5.

2.2.6 Bacteria isolation and storage

The selected bacteria were grown overnight in 10 ml LB with 100 µg ampicillin/ml (Sigma. USA) at 37 °C, 200 rpm (YIH DER LM-530 incubator). Then, the cultures were mixed with 10 ml glycerol 40% (Frutarom LTD. Israel) to a final glycerol concentration of 20%. 50 µl portions of the mixture were divided to a 200 µl sterile 1.5 ml eppendorf tube (Elcam Plastic. Israel) and kept in –80 °C (Revco Legaci™. USA).

2.2.8 Cell growth and exposure to toxicants

Growth: 5 µl of the stored bacteria were inoculated for 16 hours in 1 ml LB with 100 µg ampicillin/ml (Sigma. USA) followed by x100 dilution into a final volume of 1 ml LB for two hours in a 96-well 2 ml microtiter plate (Costar. USA), 37 °C, 200 rpm (YIH DER LM-530 incubator).

Exposure to toxicants: Bacteria were then transferred into a 384-well microtiter plate (Costar. USA) containing 4 quadruple dilutions of the toxicant in LB and a clean LB as a control. Each strain that was selected to the panel was exposed to all of the model toxicants.

Additional toxicants: Following the completion of the panel's characterization in response to the model toxicants, the panel was exposed to other toxicants, which are listed in Table 2. The experiments took place in a white, 96-well microtiter plate (Costar. USA) in a duplicates. Each strain was exposed to a series of seven double dilutions of the toxicant and a control of sterile LB.

Table 2 – Additional toxicants used in this study

Toxicant	Manufacturer
2 Chlorophenol	Sigma. USA
2,6 Dichlorophenol	Sigma. USA
2,4,5 Trichlorophenol	Sigma. USA
Saxitoxicant	Sigma. USA
Tetrodotoxin	Sigma. USA
Cholchicin	Sigma. USA
Phosdrin	Sigma. USA

2.3 Measurements and data analysis

Luminescence was measured for 2 hours in 4.8 min intervals using VICTOR² Wallac luminometer (Turku, Finland). Average luminescence from the 40 repetitions and standard deviations were calculated using Microsoft Excel.

The parameters that were calculated are listed below and illustrated in Figures 4.B, C, and D. These were selected in order to examine each strain responses as well as the whole panel's function ability. The selected parameters will provide information on the response's intensity (RR_{max} , ΔL_{max}) as well as sensitivity (C_{max} , EC_{200}) and response rate (t_{max} , t_{200}).

1. RR_{max} – Maximal Response Ratio = RLU_i / RLU_c
2. ΔL_{max} [RLU] – Maximal Response Differential = $RLU_i - RLU_c$
3. C_{max} [mg/l] – Toxicant Concentration at ΔL_{max} and RR_{max}
4. t_{max} [min] – Time to reach RR_{max} and ΔL_{max}
5. EC_{200} [mg/l] – Toxicant concentration at $(RLU_i - RLU_c) / RLU_c = 1$ (using C_{max})
6. t_{200} [min] – Time at $(RLU_i - RLU_c) / RLU_c = 1$ (using C_{max})
7. TDC – Target Detection Concentration [mg/l]– LD_{50} (mg/kg) x 70 kg / 2 L

Where LD_{50} refers to oral exposure in rats.

nm with a minor peak at 475 nm. Maximal emission occurs at 509 nm with a small shoulder at 540 nm (Figure 2C) (18).

The molecular weight of the GFP is 27 kDa and it is built of 238 amino acids organized in an 11 β -sheets units, forming a 30 Å diameter and 40 Å length β -barrel or β -can cylinder (Figure 2A). The chromophore is a three amino acids α -helix, located in the β -barrel. Its location protects the chromophore from unregulated oxidation which adds to its high stability (Figure 2B) (66, 71). Fluorescence occurs following a post-translation cyclization of the three amino acids (Ser65-Tyr66-Gly67) in the presence of molecular oxygen. Fluorescence depends on the chromophore-protein interaction and when located in a different protein, the chromophore will not produce fluorescence (52).

Studies comparing the GFP with other reporting genes have concluded that the GFP is slower and less sensitive than luciferases-based reporting systems (6, 27, 53).

The GFP mutant used in this research, Enhanced GFP (EGFP), has two targeted mutations. A replacement of Ser65 with a Gly, and Ser72 with Ala. The EGFP mutant shows 100-fold fluorescence than the wild type, its ripening time shortens to 30 min and the protein's folding can occur at 37 °C. It undergoes excitation at 488 nm and the emission maximum is at 507 nm (16).

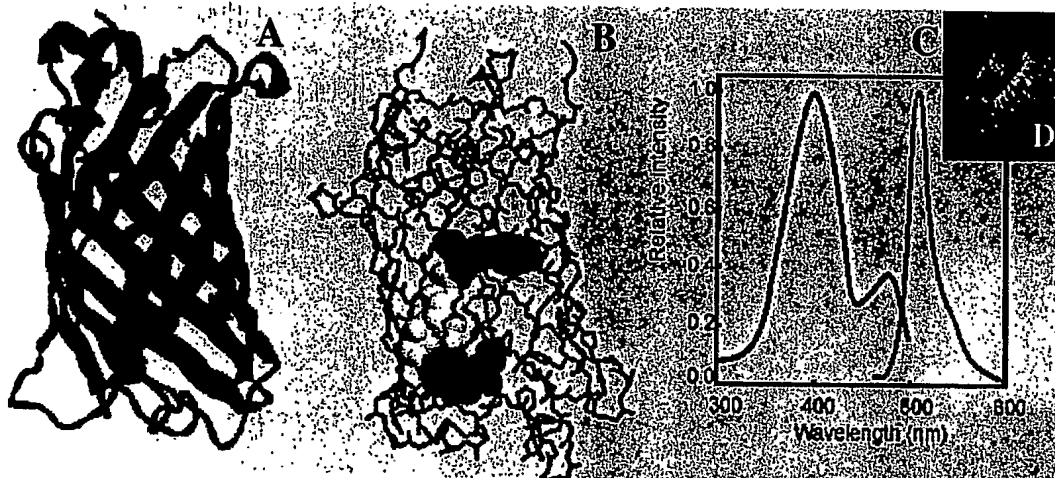


Figure 2 – The Green fluorescent protein from the jellyfish *Aequorea victoria* (D)(71). The GFP is 27 kDa and it is built of 238 amino acids organized in an 11 β -sheets units, forming a 30 Å diameter and 40 Å length β -barrel or β -can cylinder (A)(71). The chromophore is a three amino acids α -helix, located in the β -barrel. Its location protects the chromophore from unregulated oxidation which adds to its high stability (B)(66). Excitation of the GFP is maximal at 395 nm with a minor peak at 475 nm. Maximal emission occurs at 509 nm with a small shoulder at 540 nm (C)(18).

2.3.1 *E. coli luxCDABE* library screening

As mentioned above, throughout the screening, response ratios as well as the absolute RLU values were analyzed for each promoter against all toxicants. Measurements were taken during 4-6 hours every 1-1.5 hour (Figure 5). High responses due to a sudden drop in the control RLU or ones, which did not show a concentration-dependent responses were ignored. The distribution of the responses among the library members is summarized in Table 3. Promoters which produced the highest response ratios, were isolated and retested. These are detailed in Table 4 as well as the RR_{max} and C_{max} .

2.3.2 RR_{max} distribution

Analysis of the RR_{max} distribution amongst the whole library was carried out as explained in section 3.1.6 and presented in Table 6. The results show that most of the promoters did not respond and a small number of promoters produced a high response ratio. Paraquat was found to be the strongest inducer, to which 4% of the promoters produced a response ratio higher than 10. Potassium cyanide, ethyl parathion, nitrogen mustard and DDVP induced less than 1% of the promoters to RR_{max} higher than 10, though a fair number of promoters produced detectable responses to these toxicants. Exposure to methomyl produced very poor responses from a very limited number of promoters. Retesting of these promoters as well as examination of lower and higher methomyl concentrations showed even poorer results. Exposure to Botulinum Toxin A (B-tox) did not produce any response thus no continued use of this toxicant was made in this research.

Table 3 – RR_{max} distribution amongst the *E. coli luxCDABE* library. *E. coli* strains harboring 679 different promoters were exposed to seven model toxicants in seven concentration. Response ratio distribution was analyzed in order to examine the screening procedure's efficiency. High responses were induced by paraquat. Potassium cyanide, ethyl parathion, nitrogen mustard and DDVP induced lower but detectable responses. Exposure to methomyl produced very low responses. B-tox exposure did not produce any responses. Average values do not include the B-tox.

Toxicant	$0 < RR_{max} < 2$	$2 < RR_{max} < 3$	$3 < RR_{max} < 5$	$5 < RR_{max} < 10$	$10 < RR_{max}$
Ethyl Parathion	89.6%	6.3%	2.1%	1.7%	0.4%
DDVP	91.7%	5.7%	2.0%	0.4%	0.1%
Potassium Cyanide	62.9%	24.3%	9.4%	2.7%	0.7%
Nitrogen Mustard	84.5%	9.5%	4.1%	1.6%	0.3%
Paraquat	71.1%	13.7%	7.5%	3.7%	4.0%
Methomyl	90.1%	7.1%	2.0%	0.7%	0.1%
Botulinum Toxin A	100%	-	-	-	-
Average	81.7%	11.1%	4.5%	1.8%	0.9%

2.3.3 Promoter selection

The library screening aim was to select a limited number of bacterial strains, which could respond to a wide variety of toxicants. Following the screening, the selected promoters were isolated and retested in order to ensure that the responses observed in the screening step were authentic. The next step in the selection process was the cross examination of their responses to different toxicants in order to make sure that the biosensor panel would cover as wide range as possible of toxicants.

At the end of this process six promoters were selected for the present panel. These were: *lacZ*, *grpE*, *fiu*, *nhoA*, *oraA*, and *mipA*. It is highly likely that additional studies will lead to the expansion of the panel and/or to the replacement of some of its members.

2.3.4 Characterization of the selected panel's responses

40 repetitions were carried out. This allowed the characterization of the selected panel's responses to the model toxicants as well as to others. The results are summarized in Table 5 showing only the significant responses to the different toxicants.

A quick look at the results shows that several promoters responded to the same toxicant, such as *nhoA*, *lacZ*, and *fiu* to paraquat, or *grpE*, *lacZ*, and *fiu* to potassium cyanide. However, to some of the toxicants only one member of the panel produced a response (DDVP, Phosdrin and Cholchicin). Furthermore, the characterization results indicate that different response patterns are being produced by the panel members in response to the different toxicants.

Table 4- Promoters which produced the highest response ratios during the screening. From that list of promoters, six were selected for the biosensor panel. These were: *lacZ*, *grpE*, *fiu*, *nhoA*, *oraA*, and *mipA*.

Toxicant	Promoter	RR _{max}	C _{max} (mg/l)	Toxicant	Promoter	RR _{max}	C _{max} (mg/l)
Ethyl Parathion	<i>MipA</i>	20	500	Nitrogen Mustard	<i>oraA</i>	6	31
	<i>LacAYZ</i>	8	500		<i>recA</i>	6	250
DDVP	<i>GrpE</i>	7	125	Paraquat	<i>nhoA</i>	34	500
	<i>Fiu</i>	5	500		<i>lacAYZ</i>	28	500
Potassium Cyanide	<i>LacAYZ</i>	19	20	Methomyl	<i>otsAB</i>	3	2000
	<i>MalPQ</i>	9	20		<i>yciD</i>	2	2000

Table 5 – Characterization summary of the responses of the 6 promoters selected for the biosensor panel based on the 40 repetitions experiments. The tested toxicants were paraquat, potassium cyanide, the three organophosphates (ethyl paration, DDVP and phosdrin), the carbamate metham sodium and the chemical warfare agent nitrogen mustard. Responses were characterized according to the maximal response ratio and differential (RR_{max} and ΔL_{max} respectively), the concentration and time in which the former values were obtained (C_{max} and t_{max} respectively), the theoretical toxicant concentration and response duration needed to induce a two fold response ratio (EC_{200} and t_{200} respectively).

Toxicant	Promoter	RR_{max}	ΔL_{max}	$C_{max}(mg/l)$	$t_{max}(min)$	TDC(mg/l)	$EC_{200}(mg/L)$	$t_{200}(min)$
Model toxicants								
Paraquat	<i>nhoA</i>	50.2	146,344	62.5	96/110	5,250	0.43	21
	<i>lacZ</i>	13.0	253,421	32.5	123/132	5,250	9.0	85
	<i>fiu</i>	16.9	29,591	250	120/60	5,250	9.8	42
Potassium Cyanide	<i>grpE</i>	15.4	60,587	20	96/78	230	1.0	26
	<i>lacZ</i>	13.8	43,108	20	100/132	230	4.0	70
	<i>fiu</i>	5.2	7,509	20	120/120	230	0.2	85
E-Parathion	<i>lacZ</i>	4.7	47,776	125	132/132	70	13.0	120
	<i>mipA</i>	20.2	196,600	500	87/110	70	79.0	60
DDVP	<i>grpE</i>	5.9	5,290	125	132/132	1,960	32.5	41
N-Mustard	<i>oraA</i>	7.8	90,770	125	110/110	350	6.1	52
	<i>fiu</i>	4.6	7,258	125	120/120	350	11.0	80
Additional toxicants								
2,4,5-Trichlorophenol	<i>grpE</i>	22.1	54,432	31	90/90	2,960	1.0	21
	<i>lacZ</i>	16.1	74,832	31	120/120	2,960	0.8	95
	<i>fiu</i>	11.7	33,697	31	30/120	2,960	1.2	39
2,6-Dichlorophenol	<i>grpE</i>	19.5	47,877	31	90/90	6,550	1.2	29
	<i>fiu</i>	4.4	25,553	125	30/120	6,550	16.0	31
2-Chlorophenol	<i>grpE</i>	18.7	33,345	250	90/90	12,110	2.8	32
	<i>fiu</i>	5.8	11,971	500	90/120	12,110	3.4	80
Colchicine	<i>fiu</i>	4.0	1,924	45	120/120	203	14.3	85
Phosdrin	<i>lacZ</i>	3.7	12,900	180	120/120	170	38.3	110
Metham Sodium	<i>lacZ</i>	6.5	30,468	180	120/120	28,700	20.0	90
	<i>mipA</i>	5.9	27,745	180	120/120	28,700	18.0	100

2.4. Toxicant recognition using neuronal network software

There are several steps in the formation of nn. First the data must be edited in the appropriate way and introduced to the nn. Then the nn must be trained and tested before being used with unknown data. In this section I will describe the nn preparation, while in the Results section I will describe the nn testing results as well as the outputs after being introduced with unknown data.

To design the nn for toxicant detection we have used the data collected from the characterization experiments. I chose to introduce the network only with the RLU values and not with other parameters such as response ratio etc. The rationale behind this approach was that the nn is expected to analyze the data by itself according to its mathematical functions. Any manipulation on the data could interfere with the data processing by the nn. The formation of the nn took place in the following steps:

2.4.2. Training the Neuronal Network

Following preparation, the data were exported to the nn software for training. During training, the nn is presented with the input as well as output data, which is entered over and over again until the nn output matches the entered data output of all facts or until it was stopped. Each cycle is called a "run". This step can take up to several days depending on the computer system used. However, the important parameter to look for when nn is training is the number of "runs" completed, and the ratio between "good" and "bad" facts (20). A good fact is defined as a fact by which the nn was able to correctly produce an output during the training, while a bad fact is a fact, which was not correctly analyzed by the nn. The training of this nn was stopped after more than 215,000 runs, followed by testing the nn. Training of the time course system was completed after about 5 seconds and was stopped automatically by the software.

2.4.3. Testing the Neuronal Network

Before actually using the nn with real unknown data, it is necessary to test the nn performance. This is done as an integral step of the nn preparation. By default, while creating the data files the nn creates a test file, which contains 10 % of the entered facts. These are "hidden" from the nn during the training step and are used only for the purpose of testing the nn. Testing was done in a single step mode. Thus, of the 240 facts entered, 24 were used for the testing when each one was tested individually. The output produced by the nn gets a value on a scale between 0 and 1 when 1 represents 100 % probability for the toxicant's presence in the sample. This value will be referred to as detection probability or DP.

2.4.4. Running the Neuronal Network

This is the final and most important step of the process and its results are detailed in section 3.4. Although the nn tests itself using unknown data, I have decided to test the nn with another data source. I have entered the average RLU values of the 40 repetitions of each panel member 30, 60 and 120 minutes after exposure.

The nn's were also introduced to RLU values collected from the panel in response to lower toxicant concentrations, in order to test its ability to identify low toxicant concentrations. Two more tests were carried out in order to examine the nn abilities. The first was with data collected from the freeze-dried bacteria in response to paraquat exposure, the second was with data collected from the panel in response to methomyl and 2,4,5 trichlorophenol. Both sets of

From Table 6 we can see that the 30 minutes nn was able to successfully identify 5 of the six tested materials but failed to detect the DDVP. However, it did not respond to it as if it was a safe sample. The DP values for the detected compounds were higher than 99%. The false positive rate did not exceed 0.0064 and was usually very low. The false negative rate was low as well ranging from 0.0003 to 0.0362 (the latter value was given to the DDVP sample).

From the 60 minutes nn output it seems that the nn was able to identify most of the toxicants. Nevertheless, the nn misjudged the DDVP to be sterile LB. That was probably due to the fact that the response of the panel to DDVP after 60 minutes is not significant enough. This will be discussed further in the discussion. No similarities were found between the two organo-phosphates. The false positive rate was generally low though the safe sample had 29% probability to be ethyl parathion. Other than that the nn was able to detect the sterile LB as a safe sample. The false negative rate was usually very low (between 0.0003 to 0.0032) yet the DDVP was mistaken to be a safe sample.

Table 6 – The output values produced by the three Neuronal Networks. The values describe the probability (on a 0 to 1 scale) for the presence of the suspected toxicant in the sample based on the RLU values entered. The rows represent the actual toxicant in the sample while the columns represent the output values produced by the network. The table includes the output data by the 30, 60 and 120 minutes neuronal networks. The bottom row of each neuronal network, describing the output of sterile LB actually represents the false positive probability let alone the last column. On the other hand the last column actually represents the false negative probability.

Actual	Output	DDVP	Ethyl Parathion	Potassium Cyanide	Nitrogen Mustard	Paraquat	Sterile LB
30 min nn							
DDVP		0.0003	0.3269	0.0010	0.0003	0.0042	0.0362
Ethyl Parathion		0.0003	0.9939	0.0008	0.0003	0.0022	0.0013
Potassium Cyanide		0.0020	0.0015	0.9996	0.0005	0.0003	0.0120
Nitrogen Mustard		0.0003	0.0003	0.0191	0.9900	0.0069	0.0013
Paraquat		0.0003	0.0003	0.0003	0.0005	0.9976	0.0003
Sterile LB		0.0003	0.0003	0.0064	0.0025	0.0003	0.9974
60 min nn							
DDVP		0.0406	0.0003	0.0005	0.0003	0.0003	0.9932
Ethyl Parathion		0.0003	0.9993	0.0557	0.2342	0.0027	0.0003
Potassium Cyanide		0.0284	0.0005	0.9944	0.0132	0.0003	0.0032
Nitrogen Mustard		0.0044	0.0003	0.0039	0.9886	0.0047	0.0003
Paraquat		0.0005	0.0003	0.0003	0.0047	0.9983	0.0003
Sterile LB		0.0008	0.2906	0.0152	0.0003	0.0003	0.9950
120 min nn							
DDVP		0.9339	0.0005	0.3604	0.0003	0.0018	0.0008
Ethyl Parathion		0.0884	0.9961	0.0088	0.0003	0.0003	0.0003
Potassium Cyanide		0.0003	0.0003	0.9998	0.0003	0.0003	0.0003
Nitrogen Mustard		0.0003	0.0003	0.1829	0.9998	0.0003	0.0003
Paraquat		0.0301	0.0003	0.0003	0.0003	0.9834	0.0003
Sterile LB		0.0025	0.0003	0.0113	0.0005	0.0013	0.9971

From a quick look at the 120 minutes nn outputs it is obvious that the nn could detect with a very high accuracy the different toxicants. The lowest DP values was 0.9339 for the detection of DDVP while others were higher than 0.98. The false positive rate ranges from

In general, the only toxicant that was detected at low concentration was ethyl parathion (only in the 30 and 60 minutes systems). The systems were not able to detect any other low concentration toxicants.

2.4.5.4 Running of the time course nn system

This nn system was tested with data collected from the panel in response to the same toxicant concentration as the 30, 60, and 120 minutes systems. The output DP values are detailed in Table 7. The results indicate that the system can detect after already 30 minutes low concentrations of DDVP, ethyl parathion, potassium cyanide, and paraquat. The system failed to detect low nitrogen mustard concentrations, but was able to identify it at C_{\max} .

The system successfully identified the sterile LB with a DP value of 0.9986 and a false positive rate of 0.0003 to 0.0049. The false negative rate ranged from 0.0003 to 0.0108 (in response to potassium cyanide).

Table 7 – DP values produced by the time course system. The nn was tested with data collected from the panel in response to low toxicant concentrations. Though the training of the nn was done with data collected in response to the C_{\max} only, the system was able to detect in most cases lower toxicant concentrations after only 30 minutes.

Toxicant dilution	DDVP	ethyl parathion	potassium cyanide	nitrogen mustard	paraquat
1	0.9900	0.9976	0.9937	0.9605	0.9964
1/4	0.9842	0.9956	0.9932	0.2615	0.9961
1/16	0.9812	0.9954	0.9661	0.0225	0.9114
1/64	0.9803	0.9944	0.9427	0.0130	0.0533

2.5 Stabilization of bacterial cells: freeze-drying and room temperature drying

In order to study basic aspects of drying and their affect on the short and long-term viability, activity and storage stability of dried bacteria, experiments were run under bulk conditions i.e. in lyophilization vials (8 ml) with an average drying volume of 200 μ l.

Several experimental variables were evaluated; all were based on scientific papers and patents already published:

1. Growth media and bacterial preconditioning by growth media supplements
2. Drying formulations
3. Drying protocols
4. Storage temperature

2.5.1 Growth media and preconditioning of bacteria

2.5.1.1. Growth media

The first step in the preparation of bacteria to stabilization processes is their cultivation to a desired cell density / growth stage. In our experiments, early log phase was chosen as it promotes optimal sensitivity and activity of our bioreporters. Bacteria were grown in two growth media; Luria Bertani (LB) and M-9, in the presence or absence of high concentrations (0.5M) of NaCl (as will be discussed later).

- Luria Bertani is a rich, non-defined medium, which contains many complex organic substances. Under such rich growth conditions, bacteria can import simple as well as complex elements that are available in the growth medium. LB medium is capable of supporting rapid growth of many bacterial strains including our bioreporters.
- M-9 medium is a defined minimal medium, which contains simple-basic ingredient. (NH_4 , glucose, phosphate, sulfate, ..). Under such growth conditions bacteria are driven to auto-synthesize many of the needed elements to maintain growth. Not all *E.coli* strains can grow in this medium and even those that do, show a slower growth rate when compared to growth in LB.

2.5.1.2 Preconditioning of bacteria

Bacterial adaptation to high osmotic pressure (high osmolality - typically but not confined to high salt concentrations) is a multi-stage process that involves the activation of varying cellular stress responses.

The goal of such an adaptive response is to equilibrate the osmotic pressures inside and outside the cell in order to maintain homeostasis. This may be achieved by increasing the intracellular content of solutes (often referred to as compatible solutes) either by auto-synthesis or by active import from the surrounding matrix. Such compatible solutes can be accumulated in high concentrations with minimal interference to cellular metabolism. Glycine-betaine, proline, hydroxyectoine and trehalose are a few examples of compatible solutes.

It is well documented that accumulation of compatible solutes, especially trehalose may provide enhanced resistance to stresses like freezing or drying. Varying strategies are being applied to stimulate intracellular synthesis and accumulations of compatible solutes. For example, (a) bacteria can be grown under conditions that promote the synthesis and accumulation of compatible solutes, (b) sugars may be intentionally loaded into cells, (c) sugars, which enter the cells via natural transport system may be modified and rendered non-metabolizable hence promoting their accumulation and (d) bacteria may be genetically engineered to produce excess amounts of compatible solutes like trehalose.

Based on literature references (scientific and patents), which presented high survival rates and a good long-term stability of bacteria grown in high salinity M-9 or other minimal media we decided to evaluate the effects of growth in regular & high salinity growth media on our bioreporters. Such growth conditions are thought to stimulate the auto-synthesis and accumulation of compatible solutes. High salinity (HS) growth media (LB and M-9) were obtained by adding NaCl to a final concentration of 0.5M.

It soon became apparent that high survival rates were obtained with bacteria grown in M-9 medium (rather than LB) and that in some instances, growth in HS M-9 provided even better results (as will be discussed later).

It would seem plausible to speculate that when grown in M-9 medium, bacteria are forced to activate synthetic pathways that are not necessarily activated or are activated

to a lesser extent when grown in LB, and that this physiological state may confer some resistance to the stresses exerted during the stabilization process.

Furthermore, when grown in HS M-9, bacteria need to activate adaptation responses to the high osmolarity, and to auto-synthesize, rather than import, ingredients such as compatible solutes to cope with the osmotic stress, as no such importable materials are available in the surrounding minimal medium. On the other hand, with LB (which contains yeast extract), bacteria can import (and probably prefer to do so) compatible solutes and other ingredients from the surrounding medium while minimizing their own resource activation and utilization.

Therefore, it is possible that auto-synthesis of compatible solutes and other metabolites, which occur upon growth in regular and HS M-9 (in comparison to LB) is the factor, which promotes the increased resistance to the stabilization processes.

During the course of the experiments we became aware of a problem associated with the activity of bacteria grown in saline M-9 (which gave the best results in terms of survivability and stability). It became apparent that growth under high salinity affected the luminescence reporter system and some of our promoters (which were slightly activated) resulting in decreased sensitivity. The activation of some of our bioreporter promoters by the applied growth conditions may be a part of the natural bacterial response to the deliberate osmotic stress that is imposed in order to improve their resistance to the stabilization processes.

This fundamental problem needs to be addressed, possibly by finding other suitable growth media or by altering the ones that we now use. We are planning to explore the effects of adding varying osmoprotectants (ectoine, hydroxyectoine, non-metabolizable glucose, ..) to the currently used high-osmolarity or regular M-9 growth media.

2.5.2. Drying formulations:

Drying formulations have a pronounced/critical effect on the stabilization process and the resulting products (as will be discussed in more details elsewhere). Drying formulations can be obtained commercially or be developed (tailor made) to specific applications by expert companies. It seems that some of the know-how is protected by patents or maintained as commercial secrets within these companies.

We have evaluated two drying formulations, both of which were suggested in previous publications. While one formulation originated from a freeze-drying protocol, the other originated from a protocol describing drying under high temperatures and reduced pressure (H.T.D), achieving vitrification; as will be mentioned later.

The differences between the freeze-drying and HTD promote variations in the drying formulations. Nevertheless, we have crossed checked the HTD formulation in a freeze-drying process and it seems that at least for freeze-drying, the HTD formulation gave similar results.

Drying formulations may contain bulking agents, cryoprotectants, lyoprotectants etc. Sugars, especially reducing ones like trehalose, are abundantly used in stabilization processes such as freeze-drying, air-drying and HTD. The beneficial effects of some sugars in stabilization processes are of two main categories:

- i. Direct interaction with biological entities – interaction with cellular membranes and proteins and possibly anti-oxidant action
- ii. Bulk characteristics – Intra and extra cellular formation of stable glass matrixes, which minimizes ice crystal formation and halts all chemical reaction hence promoting stability.

According to the literature, maximal protections against freezing/drying damages are obtained when sugars are present both inside and outside the cells. While extra-cellular addition of sugars is easily achievable, intracellular accumulation of sugars is harder to achieve. Ways to increase the synthesis and accumulate of compatible sugars were mentioned previously.

2.5.3 Drying protocols:

Obviously, drying protocols are at the heart of drying processes. The development and application of drying protocols is far from being trivial. Although they may be based on trial and error, basic science is involved in these processes and its thorough understanding will make the difference between witchcraft-drying and sound, efficient and economic processes (a review of these subjects may be presented elsewhere).

There is a need to emphasize that other drying methods are currently available or being developed for example; air drying, spray drying, column drying etc. Although some are not applicable for drying sensitive biologicals, others may be optional / alternatives to conventional stabilization processes.

Basically, two drying protocols were evaluated; a freeze-drying protocol and a high temperature drying protocol. When so doing we followed the procedures as were presented in the relevant papers and patents.

The basic characteristics of the two protocols are as follows:

- i. In a freeze-drying process, samples are pre-frozen to the extent of complete freezing (complete freezing may be achieved at varying temperatures depending on many parameters or may not be practically achievable at all!). In high temperature drying processes samples are not frozen, on the contrary, attempts are made to avoid any freezing of the samples.
- ii. In freeze-drying processes vacuum is applied after samples have been frozen. The reduced pressure causes the ice crystals to sublime from the samples promoting their drying. Samples are best kept frozen until a low-enough water content is obtained. With HTD protocols, vacuum is applied to samples that are held at higher than zero temperatures (typically 20-30°C), water then boils and is removed quickly leaving the samples in a glassy foamed state.
- iii. Upon conclusion of the primary drying step, which removed the bulk water (mentioned above) a secondary drying step is performed (which removes adsorbed water) with both drying protocols. The aim of this step is to obtain the desired low water content in order to provide optimal performance in terms of long-term stability and functionality of dried

samples. Typically, drier samples are more stable, although a too-low residual water content might be detrimental. The secondary drying step involves an increase in sample temperatures (10-60°C) which drives-off most of the remaining water.

Assessment of the pros and cons of the two processes as presented in the literature shows that in recent years, attempts are made to develop higher temperature drying protocols / techniques for the following reasons:

1. Avoidance of freezing damages
2. HTD protocols are faster and more economic processes
3. Stability of HTD products tends to be higher, especially under non-refrigerated conditions. As there is growing demand (market) for storage under environmental conditions (rather than freezing or refrigeration), HTD processes seem to be more attractive.

2.5.3.1 Freeze-drying protocol

A simple drying protocol, which did not include a secondary drying step, was used. The drying formulation consisted of a 12% trehalose solution (chosen because it was mentioned in several papers). Typically, 300 µl aliquots of the bacterial-formulation mix were placed into 8 ml lyophilization vials. The vials were placed on the pre-cooled shelf of the lyophilizer (-40°C), let to equilibrate and freeze for ca. 90 min followed by vacuum application (ca. 30 mTorr). The drying process was carried out with a shelf temperature of -40°C for ca. 18 hours. Vials were then capped under vacuum and stored at 37°C (representative of accelerated aging processes) or -20°C (a conventional storage temperature).

Viability and activity of dried bacteria were assessed before and immediately after drying and at pre-determined storage time intervals. The residual moisture of dried samples was checked once and were found to be in the range of 10-12%.

Survival rates immediately after drying (depending on growth media) were 10-60% (see Figure 10) and survival rates upon storage of ca. 10 days at 37°C ranged 0.01-0.2% (rather low – see Figure 11). The high ranges survival rates were obtained with bacteria grown in M-9.

6,537,666, 5,766,520, 6,306,345). Additional patents that refer to such a stabilization of materials are (5,149,653, 6,426,210, RE37,872 etc.)

Tunnacliffe's patent describes a commercially available process named Q-T4 for the stabilization of biological materials (a company in England that developed the process has shut down its operation but the technology might be available by license?). Bronshtein has also developed a few technologies that were sold (according to him) to pharmaceutical companies in the USA.

The basic principle of this technique is to dry samples at ambient temperatures under reduced pressure. This in fact causes samples to boil and rapidly lose a large amount of their water. Usually, viscosity enhancers, which promote high viscosity to the samples are added, hence, upon boiling, foams are produced. The formation of foams provides a large surface area, which further accelerates sample drying. Usually, care is given to avoid freezing of samples that may occur by evaporative cooling upon boiling.

The resulting material is a stable foam containing the biologicals. This foam can be further processed.

A drying protocol, which did not include a secondary drying step, was typically used. The drying formulation consisted of a 38% trehalose and 1.5% of Polyvinyl-Pyrrolidone (PVP), which serves as a viscosity enhancer and cake strengthener (this formulation was used in some of Tunnacliffe's papers).

Typically, 200 μ l aliquots of the bacterial-formulation mix were placed into 8 ml lyophilization vials. The vials were placed on the pre-warmed shelf of the lyophilizer (+30°C), let to equilibrate and then vacuum was applied (ca. 30 mTorr). The drying process was carried out with a shelf temperature of +30°C for ca. 18 hours. Vials were then capped under vacuum and stored at 37°C or -20°C.

Viability and activity of dried bacteria were assessed at pre-determined time intervals. The residual moisture of dried samples was checked once and the results were in the range of 9-10%.

Survival rates immediately after drying (depending on growth media) were 1.0-70% (see Figure 12) and survival rates upon storage of ca. 10 days at 37°C ranged 0.5-40% (see Figure 13). The high-range survival rates were obtained with bacteria grown in M-9 media

improve. Unfortunately, long-term storage of 30 days at 37°C resulted in a significant loss of viability and was still considered unsatisfactory.

In addition to the experiments reported above, a series of experiments is planned in which matrixes of varying cryoprotectants and compatible solutes will be assessed for their protective abilities in both drying protocols and upon storage. These experiments will be performed in 96 or 384 well plates and will allow rapid screening and fast data gathering that might present improved formulations for bacterial stabilization.

Comments from Rami Peahzur:

1. With respect to growth media, some modifications (nothing I can think of right now) may be performed that might be later be defined as novel.
2. Some patents refer only to increasing intracellular trehalose (by varying means) contents as a means for improving survival of bacteria. If we were to find other mechanisms / substances that might be used to improve survival of bacteria (for example that are activated/synthesized in regular or high osmolarity M-9, that were both shown to provide enhanced survival relative to LB) we might have something novel. (over-production of rpos, novel stress genes?, gentic engineering?)
3. As for drying formulations, I have already mentioned that drying and freeze-drying formulations are commercially available and are probably patented. It might be possible for us to develop formulations but I do not think that we will be able to develop anything that is novel and different from ones which are already available.
4. Based on our current know-how and what has been published, I do not see much room for developing novel stabilization processes.

2.6 Stabilization of bacterial cells – immobilization in polymers

Immobilization is a process in which materials with a desired activity (such as enzymes and live cells) are immobilized onto substrates by a variety of immobilization agents / techniques. Typically, this process provides a mechanically stable form of the active material, which can then molded / manipulated and used in a

variety of industrial, diagnostic and research applications. Immobilized products may be found in the chemical industry (traditional process, fine chemicals, ..), in diagnostic applications, in bioremediation –biotransformation applications etc.

The immobilization processes should not affect the activity of immobilized active materials and be compatible with foreseen applications.

Biocatalysts can be whole cells or isolated enzymes and can be immobilized by a variety of process such as adsorption, ionic binding, covalent attachment, cross-linking and entrapment and micro-encapsulation. The later two may be regarded as mild immobilization methods as they do not involve modification or binding of the biocatalysts.

Typically, immobilization of biocatalysts is performed in aqueous solutions by materials that are capable of transformation from a liquid water-soluble state into a stable solid state, which will typically remain stable upon re-hydration.

Several mechanisms in which immobilization materials revert from a liquid state to a stable solid state are known. These include temperature shifts that are usually, but not confined to cooling, for materials such as agar / agarose, gelatin and poloxamers.

Cross-linking may be achieved by cationic ions (typically Ca^{++}) for substances such as alginates, carrageenan, polyacrilamides, PVA, or by other reactions, which promote polymerization such as Sol-Gel.

Cross-linking / coalescence may also be achieved by drying as is the case of latexes and by photodynamic action of UV or visible light such as the case for PVA-SBQ. Novel, non-aqueous deposition techniques make use of lasers (NRL).

Immobilization of aqueous solutions may be performed by several procedures according to the choice of immobilization materials and the desired applications.

The gel method in which sheets of varying sizes may be obtained includes melting of the gel, mixing with the biocatalyst, cooling in appropriate molds and than processing as desired.

The droplet method produces spherical beads of varying sizes and includes a drop wise extrusion of the immobilizing –biocatalyst solution into a solidifying solution (such as CaCl_2), the immobilization agents solidifies entrapping the biocatalyst. Some of these substances such as alginate may be reversely de-stabilized by the presence of monovalent ions (such as Na^+).

The emulsion method is a high-tech method, which relies on the formation of emulsions of the immobilizer–biocatalyst solutions and non-reactive oils. These are

warmed and mixed in a way as to generate droplets of required sizes and geleation occurs upon cooling of the oil.

The immobilization process that will be applied for our applications will need to be compatible with mass production of the biochip production technology. Preferably, it will be modulated to be a part of the biochip fabrication process in which the layered structures are formed.

Currently it would seem that suitable technologies will rely dry deposition such as the use of lasers or wet deposition processes such as "ink-jet" type technologies, both can be manipulated to be part of the biochip production process.

2.7 On-chip lyophilization & revival

The previous two sections summarize our efforts in preservation of cells for long-term stable storage. As mentioned, the procedures employed were based on available literature with no apparent significant modifications.

The present section is different in that it describes a procedure that has not been previously reported. While the drying techniques used are not different from those previously outlined, in this case we are talking about

- i) Lyophilization of extremely small volumes (0.5-2 μ l)
- ii) Lyophilization "on-chip": the entire process is carried out after placing the cells in the chip cavity.
- iii) To simulate drying in a cavity-like volume, most experiments were carried out in 1536-well microtiter plates.

In general, the activity of *Lux*-including strains was tested in final volume of 1 μ L or less per well, in 1536-well microtiter plate. Only 1 of 4 wells was used, and activity was measured in Victor² Luminometer, in 384 wells designated program. In most lyophilization experiments 12% Trehalose was used as osmo-cryoprotectant.

2.7.1 Methods

Single colonies of *E. coli* strains DPD2794 or TV1061, containing *recA::Lux* or *grpE::Lux* plasmid fusions, respectively, were inoculated in liquid LB-Kan medium for overnight growth at 37°C. These cultures were diluted 1:300 in fresh LB medium without antibiotics in final volume of 50ml, and allowed to grow at 30°C to the early logarithmic growth phase at a turbidity of $OD_{600nm}=0.1$, which is equivalent to 10^7 cells/ml. The cultures were then concentrated by centrifugation and resuspended to the desired concentration either in 12% trehalose for lyophilization, or in LB for fresh cell induction. Lyophilization, as well as induction, of cell suspensions took place in opaque white 1536-well microtiter plates (Costar).

The microtiter plate containing cell suspensions was lyophilized in an Advantage, Virtis Lyophilizer for overnight in a vacuum of 20mTorr, at -40°C shelf-temperature. Prior to vacuum application bacteria were frozen by ramping the shelf temperature from 0°C to -40°C at a rate of $0.23^{\circ}C \cdot min^{-1}$. Aliquots of tested compounds diluted in LB were added to the lyophilized bacteria-containing microtiter plate and induction was followed by measuring luminescence in a Wallac Victor² luminometer.

2.7.2 Main results

As demonstrated in Fig. 14, optimal induction for fresh *recA::Lux* cells, as well as for *grpE::Lux* cells, is obtained in cells concentrations of 5×10^8 and 10^9 cells/ml. Optimal induction for dry cells of both types is obtained in cells concentrations of 5×10^8 cells/ml (Fig. 15). This cell concentration, in a volume of 1 μ L, implies the use of 5×10^5 cells/well.

A comparison of the activity of the dry vs. the fresh cell reveals that a relatively small fraction of the activity was lost upon drying: 96% and 76% were maintained for the *recA::Lux* and *grpE::Lux* cells, respectively (Fig. 16).

REFERENCES

S-numbered References

1. Daunert S, Barret G, Feliciano JS, Shetty RS, Shrestha S, Smith-Spencer W: **Genetically engineered whole-cell sensing systems: coupling biological recognition with reporter genes.** *Chem Rev* 2000, **100**: 2705-2738.
2. Hansen LH, Sørensen SJ: **The use of whole-cell biosensors to detect and quantify compounds or conditions affecting biological systems.** *Microb Ecol* 2001, **42**:483-494.
3. Keane A, Phoenix P, Ghoshal S, Lau PCK: **Exposing culprit organic pollutants: a review.** *J Microbiol Meth* 2002, **49**:103-119.
4. Kohler S, Belkin S, Schmid RD: **Reporter gene bioassays in environmental analysis.** *Fresenius J Anal Chem* 2000, **366**:769-779.
5. D'Souza SF: **Microbial biosensors.** *Biosens. Bioelec.* 2001, **16**: 337-353.
6. Belkin S: **Microbial whole-cell sensing systems of environmental pollutants.** *Curr. Opinion Microbiol.* 2003. **6**: 2060212.
14. Belkin S, Smulski, DR, Dadon S, Vollmer AC, Van Dyk TK, LaRossa RA: **A panel of stress-responsive luminous bacteria for toxicity detection.** *Wat Res* 1997, **31**: 3009-3016.
15. Min J, Pham CH, Gu MB: **Specific responses of bacterial cells to dioxins.** *Environ Toxicol Chem* 2003, **22**:233-238.
16. Gu MB, Min J, Kim EJ: **Toxicity monitoring and classification of endocrine disrupting chemicals (EDCs) using recombinant bioluminescent bacteria.** *Chemosphere* 2002, **46**:289-294.
17. Sagi E, Hever N, Rosen R, Bartolome AJ, Premkumar JR, Ulber R, Lev O, Scheper T, S. Belkin: **Fluorescence and bioluminescence reporter functions in genetically modified bacterial sensor strains.** *Sens Actuator B-Chem* 2003, in press.
18. Kostrzynska M, Leung KT, Lee H, Trevors JT: **Green fluorescent protein-based biosensor for detecting SOS-inducing activity of genotoxic compounds.** *J Microbiol Methods* 2002, **48**:43-51.
19. Knight AV, Goddard NJ, Billinton N, Cahill PA, Walmsley RM: **Fluorescence polarization discriminates green fluorescent protein from interfering autofluorescence in a microplate assay for genotoxicity.** *J Biochem Biophys Methods* 2002, **51**:165-177.

WHAT IS CLAIMED IS:

1. A method of detecting presence or absence of a substance in a sample, the method comprising:

(a) providing a plurality of cells, each cell of said plurality of cells being capable of unique expression of at least one reporter gene, whereas said plurality of cells generate a unique expression profile upon exposure to the substance; and

(b) subjecting said plurality of cells to the sample and recording an expression profile from said plurality of cells to thereby detect presence or absence of the substance in the sample.

2. The method of claim 1, wherein each cell is genetically modified such that an expression of said reporter gene is directed by a different promoter sequence in each cell.

3. The method of claim 1, wherein the substance is a toxic substance and the sample is an air or water sample.

4. The method of claim 1, wherein the substance is a biomolecule and the sample is a biological sample.

5. A device for detecting presence or absence of a substance in a sample, the device comprising:

(a) a support for supporting a plurality of cells, each cell of said plurality of cells being capable of unique expression of at least one reporter gene, whereas said plurality of cells generate a unique expression profile upon exposure to the substance; and

(b) a detector for detecting expression of said at least one reporter gene from said plurality of cells.

6. The device of claim 1, wherein said support is configured as a multiwell plate, whereas each well includes a culture of a specific cell of said plurality of cells.

7. A system for detecting presence or absence of a substance in a sample, the system comprising:

(a) a device including:

(i) a support for supporting a plurality of cells, each cell of said plurality of cells being capable of unique expression of at least one reporter gene, whereas said plurality of cells generate a unique expression profile upon exposure to the substance; and

(ii) a detector for detecting expression of said at least one reporter gene in said plurality of cells; and

(b) a processing unit for obtaining and processing data representing said expression detected by said detector to thereby provide information relating to the presence or absence of the substance in the sample.

WHOLE CELL BASED TOXICITY DETECTION INTEGRATED SYSTEM

Abstract

After the September-11 events the modern world is living under a permanent threat of possible terrorists attacks. One of the most harmful terrorists acts could be water reservoirs poisoning. This fear is especially actual for western countries like the USA and Israel. Although there is still no firm governments regulations regarding on line water acute toxicity monitoring, the issue is very important and special devices to divert such terror should be investigated.

There is a growing awareness all over the world to the quality of food and drinks that consumed daily. Therefore, it is very desirable to have a reliable monitor of food and drinks quality. Such device will improve the consumer's confidence and prevent potential short and long-term disasters.

Today, there is a substantial gap between the needs and capabilities in detection methods and devices of potential water poisoning. The gap is derived from the inability to obtain a sufficiently sensitive early warning upon the occurrence of such events. On the other hand, the food and drinks quality-monitoring systems do not exists for the consumer and governmental markets.

The "Water Toxicity Analysis" (WTA) integrated system is currently under investigation in Tel-Aviv University (TAU) – Physical Electronics Department in collaboration with biologists from the Hebrew University Of Jerusalem (HUJI) – Environmental Sciences Department. The integrated system is based on the genetically engineered whole cell based biosensors embedded into the biochip. The biosensors are engineered to emit a fluorescent signal in the presence of general or pre-determined classes of toxicants. The fluorescent signal is quantified by the integrated system and the quantified results are used for the water toxicity analysis algorithms. The duration of the water toxicity analysis on the TAU-WTA integrated system is in the range of minutes to hours.

Currently the study is preformed toward acute water toxicity detection. After the successful completion of that stage the research will be continued on the developing of the integrated system for drink and food quality analysis.